FTD-HC-23-544-70

[redacted]

AD 726581

FOREIGN TECHNOLOGY DIVISION

AIRCRAFT ELECTRIFICATION IN CLOUDS AND PRECIPITATION

by

I. M. Imyanitov

Distribution of this document is unlimited. It may be released to the Clearinghouse, Department of Commerce, for sale to the general public.

266

EDITED TRANSLATION

AIRCRAFT ELECTRIFICATION IN CLOUDS AND PRECIPITATION

By: I. M. Imyanitov

English pages: 254

Source: Elektrizatsiya Samoletov v Oblakakh i Osadkakh 1970, pp. 1-211

Translated under: F33657-71-D-0057

UR/0000-70-000-000

THIS TRANSLATION IS A RENDITION OF THE ORIGINAL FOREIGN TEXT WITHOUT ANY ANALYTICAL OR EDITORIAL COMMENT. STATEMENTS OR THEORIES ADVOCATED OR IMPLIED ARE THOSE OF THE SOURCE AND DO NOT NECESSARILY REFLECT THE POSITION OR OPINION OF THE FOREIGN TECHNOLOGY DIVISION.	PREPARED BY: TRANSLATION DIVISION FOREIGN TECHNOLOGY DIVISION WP-AFB, OHIO.

UNCLASSIFIED

Security Classification

DOCUMENT CONTROL DATA - R & D

(Security classification of title, body of abstract and indexing annotation must be entered when the overall report is classified)

ORIGINATING ACTIVITY (Corporate author) Foreign Technology Division Air Force Systems Command U. S. Air Force	2a. REPORT SECURITY CLASSIFICATION UNCLASSIFIED 2b. GROUP

REPORT TITLE

AIRCRAFT ELECTRIFICATION IN CLOUDS AND PRECIPITATION

DESCRIPTIVE NOTES (Type of report and inclusive dates)

Translation

AUTHOR(S) (First name, middle initial, last name)

Imyanitov, I. M.

REPORT DATE	7a. TOTAL NO. OF PAGES	7b. NO. OF REFS
1970	254	123

8a. CONTRACT OR GRANT NO. F33657-71-D-0057 b. PROJECT NO. c. d.	9a. ORIGINATOR'S REPORT NUMBER(S) FTD-HC-23-544-70 9b. OTHER REPORT NO(S) (Any other numbers that may be assigned this report)

10. DISTRIBUTION STATEMENT

Distribution of this document is unlimited. It may be released to the Clearinghouse, Department of Commerce, for sale to the general public.

11. SUPPLEMENTARY NOTES	12. SPONSORING MILITARY ACTIVITY Foreign Technology Division Wright-Patterson AFB, Ohio

13. ABSTRACT

When flying in the clouds or during rainfall there may appear corona or even sparks on the surface of the airplane. As a result, strong statics develop, which increase the probability of hitting the airplane by lightning. In some cases, the aerodynamics of the airplane may be subjected to changes. The electrification of the airplane may distort the results of micro-physical observation of the clouds, particularly the measurement of the atmospheric electricity. This volume is the first attempt to cover the subject in all meteorological aspects. An analysis is given of the static electrification of bodies in streams of particles. The relationship between electrification of the airplane and cloud parameters is discussed. Experimental data on electrification in different meteorological conditions are given. The book is designed for meteorologists, specialists in aviation and in electricity who deal with the problem of static electrification, also for post-graduates who specialize in hydrometeorology, airplane design and in physics.

DD FORM 1 NOV 65 1473

UNCLASSIFIED

Security Classification

UNCLASSIFIED
Security Classification

14. KEY WORDS	LINK A		LINK B		LINK C	
	ROLE	WT	ROLE	WT	ROLE	WT
Aircraft Static Electricity Aircraft Design Hydrometerorology						

UNCLASSIFIED
Security Classification

И. М. ИМЯНИТОВ

ЭЛЕКТРИЗАЦИЯ САМОЛЕТОВ В ОБЛАКАХ И ОСАДКАХ

ГИДРОМЕТЕОРОЛОГИЧЕСКОЕ ИЗДАТЕЛЬСТВО
ЛЕНИНГРАД • 1970

TABLE OF CONTENTS

PAGE

INTRODUCTION

The study of static electrification has a curious history. The first sources of electricity, discovered back in the seventh century B.C., were in today's terms static electricity generators. Amber — electron in Greek — becomes luminous when rubbed with wool or fur and gave its name to the new form of energy and the science associated with it — electricity. And yet the nature of static electrification has received far less study than the nature of the processes in chemical current sources or electromagnetic generators, even in the latest electrodynamic and magnetodynamic modifications. The little attention devoted to the nature or even the very phenomena of static electrification is usually associated, first of all, with the relatively cool relationship of the other sciences and technologies to this problem and, second, with the difficulty involved in the study of the static electrification phenomena. "In our preoccupation with the dramatic developments in the numerous fields of modern physics ...we tend to forget our profound ignorance of some of the longest-known phenomena of physics. Among these are... static electrification," wrote one of the foremost investigators in this field, L. Loeb, in 1957 in his book "Static Electrification". The introduction of the term "triboelectricity" (or frictional electricity) really did not clarify anything about the nature of static electricity, since the quantitative and qualitative relationships which arise in the process of rubbing two bodies together remained completely mysterious. "It is not unusual," wrote P. S. H. Henry in 1953, "to encounter two pieces of material which are apparently identical in all respects and can be highly charged under identical conditions, but are found to be charged with electricity of opposite signs."

The reason for this great variability of the magnitude and even the sign of static electrification is that this electrification depends on the properties of the surface — on minute traces of contamination or the quality of the finish. Even a monatomic impurity film on the surface is sufficient to alter the static electrification characteristics.

The ever-changing twentieth century with its constant generation of new fields of engineering, continuous and rapid increase of travel speeds and material machining speeds, use of new synthetic materials, and ventures into new regions of space have forced the engineers to return to the problem of static electrification. The static electrification phenomena are having an increasing effect on production technology, communications, and flight vehicle operating conditions.

The static electrification which develops during flight in clouds and precipitation has had a very significant effect on aircraft flight.

Summarizing the results of the major studies in this field, R. Gunn, an outstanding American investigator, noted in 1946 that in certain regions of the United States the annual military aircraft losses resulting from interference created by static electricity amounted to more than 1% of the total number of airplanes. The intensity of static electrification grows as the square or even the cube of the flight vehicle speed, increases markedly with increasing cloud density and with increase of the precipitation intensity from the clouds; yet the basic trends in airplane design and operation are toward progressive increase of the speed, particularly with the introduction of jet engines and the trend toward all-weather flight operations.

While in 1946 airplanes were charged to a potential of 300-400,000 volts and their charging currents did not exceed a few hundred microamperes, i.e., the power of the airplane electrostatic interference generator reached several tens of watts, today these parameters amount to 1-1.5 million volts, 10 mA and 10 kW. In this coneection, we recall that the stability and reliability of radio communication with the airplane, the quality of the on-board radio navigation equipment operation, and the probability of lightning striking the airplane depends to a considerable degree on the magnitude of the airplane's electric charge. It is not surprising that the static electrification problem has been termed the static hazard problem and is drawing increasing attention from airplane designers, radio communication equipment designers, operational personnel, and meteorologists. For the latter, this problem is also important in that the static electrification phenomena have a marked effect on the results of atmospheric electricity measurements and many microphysical measurements in clouds and precipitation. Cases are known in which the results of studies of cloud and precipitation electricity carried out over several years have been found to be completely incorrect because of failure to account for the effect of static electricity on the experimental results.

At the present time, static electrification is studied basically as a source of interference with the normal operation of aircraft, in meteorological measurements, and so on. However, there is no doubt that many effects associated with static electrification are useful. Study of the static electrification of bodies moving in clouds and precipitation is the key to understanding the processes of intensive electrification of water droplets and hailstones, and this means the particle interaction conditions and, thus, the processes of precipitation formation in electrified clouds.

The success in solving the problems of actively affecting the electric state of clouds and electrical influence on the development of clouds and precipitation is closely associated with the studies of static electrification of airplanes and cloud particles. The static electrification processes together with the intense ionization of the air at the surface of the airplane have a marked effect on the aerodynamic characteristics of the airplane and can, in particular, play the role of a "lubricant" to reduce significantly the in-flight aerodynamic drag.

The static hazard problem for airplanes is a complex problem and its solution involves both the study of the effect of meteorological conditions on airplane electrification and the solution of specific problems of radio communication, high-voltage engineering, and so on. The objective of the present work was to study the connection between the airplane charge and the currents flowing to the airplane, the connection with meteorological characteristics of the atmosphere, and also to clarify the nature of airplane electrification. This formulation of the task is a result of the fact that the characteristics being considered are purely electrical parameters, which must form the basis of the modeling experiments or calculations. On the other hand, the large number of airplane types and the variety of radio equipment used make it impossible to solve with sufficient generality the problem of the concrete interference which develops on a given airplane under given conditions with the use of some specific apparatus. Therefore, we have limited ourselves to simply presenting the methodology for solving concrete problems.

Many general static electrification problems can be explained on the basis of the study of airplane static electrification. From this viewpoint, the book may be useful to readers involved with the theory and application of static electrification.

In this book, we examine the electrification conditions during flights at speeds less than the speed of sound.

The book is based to a considerable degree on the results of investigations at the laboratory of free atmospheric electrification of the Main Geophysical Observatory im. A. I. Voyekov, where the author works.

Various laboratory personnel have participated actively in designing the equipment for the measurements, in the experiments themselves, and in the discussion and analysis of the measurement results: Chief Engineer B. F. Evteyev; Senior Scientific Associate Ya. M. Shvarts; Candidate of Tech. Sci. Ye. V. Chubarina, Candidate of Phys. and Math. Sci; Junior Scientific Associate V. V. Mikhaylovskaya; and Engineers S. I. Andreyeva, N. P. Ziganov, N. T. Markchev, and Yu. F. Ponomarev.

The acquisition of the required data involved extensive flight investigations. Many of the studies were made on airplanes of the State Scientific and Research Institute for Civil Aviation. Airplane commanders V. K. Klyaus, A. A. Krestenko, V. K. Kuz'menko, S. D. Popov, and A. N. Lebedev and their flight crews carried out measurements under the most difficult weather conditions. The success of the flight tests was due in considerable measure to the continued participation of V. S. Aleksandrov, Chief Engineer of GOSNIIGA (State Scientific Research Institute of Civil Aviation). The organization of the test program owes much to the initiative and interest of M. M. Kulik, Deputy Minister of Civil Aviation, and R. V. Sakach, Deputy Director of GOSNIIGA.

The author wishes to thank sincerely all the personnel listed above and feels it his duty to note that this book could not have appeared without their invaluable assistance.

BLANK PAGE

CHAPTER 1

PROBLEMS ASSOCIATED WITH STATIC ELECTRIFICATION OF AIRPLANES AND OTHER FLIGHT VEHICLES

About 50 years ago it was noted that St. Elmo's fire — a luminous corona discharge in a strong electric field — occurs not only on the tops of ship masts, church spires, and lightning rod points, but also at the tips of airplane wings, propellers, and the antennas of airplanes flying in clouds. Electrical sparks sometimes flash across the cockpit windows with a strong crackling noise. Disruption of radio communication by interference was frequently observed back in the early nineteen twenties during flights in clouds by airplanes equipped with radio receivers. Although these flights were infrequent — the pilots tried to keep as far as possible from clouds and precipitation — the researchers attempted to discover the nature of these phenomena and particularly the interference. By analogy with ground-level St. Elmo's fire, the luminosity was explained by the presence in the clouds of strong electric fields. Findeisen advanced the hypothesis that radio interference is the result of microdischarges which occur in clouds during collisions of charged particles. However, it was noted that this interference (termed static) occurs after the airplane enters the cloud and is not noted during flight near clouds. Therefore, Morgan [1] suggested the idea that the interference is created as the result of variations of the antenna potential which occur during contact with charged cloud particles. This theory made it possible to explain, in particular, the then known fact that interference is less during reception on a shielded loop than during reception on an unshielded antenna.

The rapid development of aviation and radio communication and navigation equipment led to the situation in which flights in clouds became routine operations rather than infrequent events, particularly in military aviation. However, even during World War II the pilot of an airplane entering clouds could not determine where the cloud was more or less dense, where the cloud was less hazardous, and in what parts of the cloud the danger was the greatest. Some aircraft found themselves in dangerous conditions and at the same time lost their communications and the radio navigation instruments, particularly the radio compasses, could not be trusted. This situation not infrequently led to accidents. In certain regions of the United States the annual military airplane losses due to interference created by static electricity amounted to more than 1% of the total airplane fleet [4]. Hucke [3] was one of the first to make a detailed study of the sources of this interference. He installed points on the sharp extremities of the airplane and measured the current flowing through these points. It was noted that during flight in clouds, a corona current flows through the points,and radio static interference occurs when this corona appears. Hucke suggested that the corona current arises as a result of electrical charging of the airplane as a whole. This assumption was later confirmed by several studies, in particular the fundamental investigation conducted during the war years under the leadership of R. Gunn [4-8].

It was later found that the effect of the airplane's electrical charge is not limited to the generation of radio interference.

Studies of the conditions under which airplanes are struck by lightning, conducted by the present author [9] and by Fitzgerald [10], showed that under certain conditions the probability of lightning striking the airplane is associated with the effect of the airplane on the lightning. Here, the airplane's electrical charge plays an essential role

Both the electrical charge of the flight or lifting vehicle as a whole and the electrical charge of individual parts of the instruments may have a significant effect on the results of atmospheric electricity measurements in the free atmosphere. Probe charging may have an effect on the results of microphysical measurements. We note also that electrical charging of airplanes may have an effect on their aerodynamic characteristics. The variation of the charge distribution over the airplane surface as it approaches the ground may be used to determine airplane flight altitude, and so on.

Without considering, for the time being, the reason behind the origin of the electrical charge of airplanes, let us examine some questions which arise in connection with the existence of this charge.

§ 1. Effect of Charging of Flight Vehicles and Measuring Devices on the Results of Meteorological Measurements

The appearance of an electrical charge on airplanes or other flight vehicles carrying atmospheric electricity measuring equipment, and also the currents flowing to these vehicles, may have a significant effect on the accuracy of the measurement of both the atmospheric electricity elements and the microphysical characteristics of clouds. Moreover, there are often cases in which the measurement errors owing to the effect of the charge are so large that measurements become impossible. Let us examine in greater detail the effect of electrical charging on the measurement of the individual elements. For simplicity we assume that the measurements are being made on an all-metal airplane

Atmospheric electric field intensity measurements. Assume a conducting uncharged body is introduced into the uniform electrical field of intenisty E which is being measured. The field intensity E_i at the individual points i of the body will be completely defined by the field intensity E and the body geometry

$$E_i = k_i E, \tag{1.1}$$

where k_i is a coefficient defined by the body shape. Thus, by measuring the field intensity E_i at the body surface and knowing the coefficient k_i we can determine the magnitude of the atmospheric field intensity.

If there is an electrical charge Q on the body, then the field intensity E_i at the point i will be the sum of the field intensities created by the field being measured and the body charge

$$E_i = k_i E + p_i Q. \tag{1.2}$$

where p_i is a coefficient defined by the body shape.

We recall that the connection between the field intensity E_i at any point of the airplane surface and the surface charge density σ_i is given by the relation

$$E_i = 4\pi\sigma_i.$$

It is obvious that the field intensity measurement error in this case is

$$\delta = \frac{p_i Q}{k_i E}, \tag{1.3}$$

and, if the value of δ exceeds an acceptable magnitude, measurement is impossible.

Measurements of the external field intensity can be made with relatively large body charges by making measurements at two points of the body [11].

On a charged conducting body at diametrically opposed points A and B (Figure 1.1) the field intensity in the case of the indicated field direction will be, respectively,

$$E_A = k_A E - p_A Q,$$
$$E_B = -k_B E - p_B Q. \quad (1.4)$$

For example, for a sphere $|p_A| = |p_B| = \frac{1}{r^2}$, and if the points A and B are taken on a diameter directed along the line of intensity of the field being measured, then $k_A = k_B = 3$.

After suitable transformations of (1.4) we obtain

$$E = AE_A + BE_B,$$
$$Q = CE_A - DE_B, \quad (1.5)$$

where $A = f_1(k_A, k_B, p_A, p_B)$, $B = f_2(k_A, k_B, p_A, p_B)$, $C = f_3(k_A, k_B, p_A, p_B)$, $D = f_4(k_A, k_B, p_A, p_B)$.

For example, for a sphere of radius r

$$E = \frac{E_A + E_B}{6}, \quad Q = \frac{r^2}{2}(E_A - E_B).$$

Thus, by measuring simultaneously the field intensity at two points of the airplane surface, we can determine the magnitude of the atmospheric electric field intensity and the magnitude of the airplane charge.

In this case, the error δ_{2_E} in the measurement of the atmospheric field intensity introduced by the airplane charge Q will be

$$\delta_{2_E} = \delta_{1_E} \frac{E_Q}{E_E} = \delta_{1_E} \frac{pQ}{E_E}, \quad (1.6)$$

where δ_{1_E} is the error in the measurement of the atmospheric field intensity in the absence of the charge, and E_Q and E_E are the average intensities of the field created at the measurement points by the electrical charge and the atmospheric field. We note also that the measurement of the airplane's self-charge in the presence of the external field is also associated with additional measurement errors.

The error δ_{2_Q} in the measurement of the magnitude of the airplane's self-charge Q introduced by the external field will be

$$\delta_{2Q}=\delta_{1Q}\frac{E_E}{E_Q}. \tag{1.7}$$

where δ_{1Q} is the measurement error in the absence of the external field.

The overall error in the measurement of the external field intensity is

$$\delta_E=\delta_{1E}+\delta_{2E}=\delta_{1E}\left(1+\frac{E_Q}{E_E}\right). \tag{1.8}$$

and the error in the self-charge measurement is

$$\delta_Q=\delta_{1Q}+\delta_{2Q}=\delta_{1Q}\left(1+\frac{E_E}{E_Q}\right). \tag{1.9}$$

It is convenient to write these equations in the form

$$\delta_E=\delta_{1E}\left(1+\frac{V_{Q_A}+V_{Q_B}}{V_{E_A}+V_{E_B}}\right). \tag{1.10}$$

$$\delta_Q=\delta_{1Q}\left(1+\frac{V_{E_A}+V_{E_B}}{V_{Q_A}+V_{Q_B}}\right). \tag{1.11}$$

where V_{E_A}, V_{E_B}, V_{Q_A} and V_{Q_B} are the voltages developed at the output of sensors located at the points A and B (assuming the coefficients relating the output signal with the input signal are linear) owing to the external field and the airplane's self-charge, respectively.

It follows from (1.8) and (1.9) or (1.10) and (1.11) that if the self-charge field exceeds the atmospheric charge field by, say, a factor of 1, 10, or 100, then for a field intensity measurement error of δ_{1E} the overall measurement error will be $2\delta_{1E}$, $11\delta_{1E}$ and $101\delta_{1E}$, repectively. In the case of high measurement accuracy $\delta_{1E}\approx 1\%$ it becomes impossible to make measurements with $E_Q>100E_E$, and the technique in question (in the form being discussed) can serve basically only for the elimination of questionable cases during data analysis. However, we must bear in mind that there are techniques (differential measurement methods and the method using feedback to suppress the noise signal) which permit measurements to be made even with $E_Q \gg (1000 \div 10000) E_E$ [9].

For such low ratios of the useful signal to the interference signal, the measurement accuracy will be determined primarily by the accuracy of the determination of the field deformation coefficients k_A, k_B, p_A and p_B (see [1.4]). In a medium which is not perturbed by the presence of a body, an increase of the accuracy of the determination of these coefficients can be achieved by the use of models which reproduce the original exactly, by the use of advanced techniques for measuring the distribution of the field intensity or potential (the electrolytic bath technique, for example). In a medium in which the presence of a body disrupts the charge distribution in the medium, there is no advantage in increasing either the equipment accuracy or the accuracy of the determination of the field deformation coefficients (within the framework of the technique being discussed) in comparison with the measurement accuracy which is defined by the field created as a result of the medium charge redistribution. The question of the magnitude of the disturbance introduced by the metering body must be posed anew in each specific research problem, since the disturbance depends both on the probe properties and the characteristics of the medium. We shall examine somewhat later the problem of the effect of the airplane and probes on the magnitude of the electrical field in a clear atmosphere, in clouds, and in precipitation.

We should also note that the coefficients k_A, k_B, p_A and p_B change as the airplane approaches the ground; therefore, measurements at altitudes less than 10-15 fuselage diameters either cannot be made with the indicated precision or the values of these coefficients must be determined for each measurement altitude.

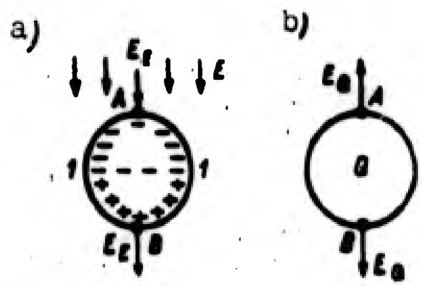

Figure 1.1. Method for measuring the charge of an isolated body.

a) sphere in electrical field;
b) charged sphere.

<u>Disruptions of the charge distribution in the atmosphere created by the probing body and their effect on the accuracy of the measurement of the ion spectrum, conductivity, atmospheric electric field intensity, and airplane</u> self-charge. The appearance of an airplane or other body in the atmosphere leads to a redistribution in the vicinity of the body of the electrical charges under the influence of the intrinsic electrical charge of the body and as a result of the action of the external electrical field. This charge redistribution — the electrode effect — leads to the appearance of a space charge layer near the body, in which the ion spectrum is different from the spectrum in the free atmosphere, and whose electrical field affects the results of the self-charge field and atmospheric field measurements.

The properties of the medium can also change significantly with the occurrence of corona discharges at individual points of the body. Corona or even spark breakdown occurs when the field intensity at individual points of a body reaches the breakdown value, that is, when the body charge or the external field intensity reach certain critical values. Under the influence of the discharges, the conductivity, ion concentration, and so on, may change by many orders of magnitude in comparison with their values in the atmosphere. We shall return to this question in subsequent chapters, but in the present section we shall discuss only the electrode effect.

The size of the electrode effect region and also the magnitude of the change of the ion concentration, space charge, and conductivity in this region increase with increase of the body electrical charge $\underline{Q}$ and ion mobility $\underline{K}$, while they decrease with increase of the airplane motion velocity $\underline{w}$. It is obvious that the concentration of the ions having the same sign as that of the body charge will be reduced and that the concentration of the ions of opposite sign will be increased somewhat at the walls of the sounding body in comparison with their values in the free atmosphere.

Let us examine the trajectory of an air ion near a charged body T, traveling with the velocity w (Figure 1.2), neglecting the additional field created by displacement of the ions under the influence of the body.

The ion velocity components along the x, y z axes, respectively, will be

$$\frac{dx}{dt}=w_x+KE_x,$$
$$\frac{dy}{dt}=w_y+KE_y,$$
$$\frac{dz}{dt}=w_z+KE_z. \qquad (1.12)$$

where K is the ion mobility, w_x, w_y w_z are the freestream air velocity components along the corresponding axes, and E_x, E_y E_z are the intensity components of the field created by the charged body.

For the solution of the quasisteady equation we can obtain from (1.12)

$$\frac{dy}{dx}=\frac{w_y+KE_y}{w_x+KE_x},$$
$$\frac{dz}{dx}=\frac{w_z+KE_z}{w_x+KE_x}. \qquad (1.13)$$

With the aid of (1.13), we can calculate the individual ion trajectories, and after performing the corresponding summation for the ions of different mobilities and for the ions located at different distances y and z from the x-axis, we can determine the values of the ion concentration, conductivity, and space charge at any distance from the body and thereby account for the perturbation of these elements. The solution of (1.13) for bodies of complex form cannot be expressed by a simple analytic expression and in actual cases is found either

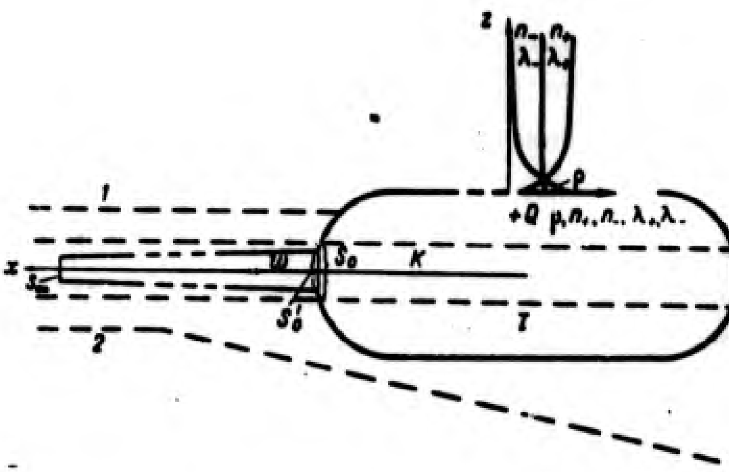

Figure 1.2. Electrode effect about a body T carrying the charge +Q and traveling with the velocity w.

1) and 2) trajectories of negatively and positively charged ions. The upper part of the figure shows the distributions of the concentrations of the n_+ and n_- ions, polar conductivities λ_+ and λ_-, and the space charge ρ at the walls of the body.

by modeling [12] or is calculated by one of the approximate techniques.

In order to reduce measurement errors, the ion concentration and conductivity measurements should be made by either extending the instrument sensor beyond the limit of the disturbed layer or locating it on the body axis of symmetry along the flight axis (see Figure 1.2). In the latter case, for $Q = 0$, ions whose trajectories at infinity pass through the area S_∞ will enter the inlet port of area S_0. The relationship between the dimensions of the area S_0' (it is obvious that $S_0' \leq S_0$) crossed by the ions whose trajectories cross S_∞ and the body charge and size is again given by (1.13). Knowing the relationship between S_0' and S_∞, we can derive the relationship between the ion concentration $n_{\pm\infty}$ or the conductivity $\lambda_{\pm\infty}$ in the zone which is not perturbed by the body and their measured values [13, 14].

Assuming the ion stream to be incompressible, we can write

$$w_0 S_0' n_0' = w_\infty S_\infty n_\infty, \tag{1.14}$$

where the subscript ∞ denotes values of the corresponding elements in the zone which is not perturbed by the body, and the subscript 0 denotes the values of these elements near the body. It follows from (1.14) that

$$\frac{\lambda_0}{\lambda_\infty} = \frac{n_0}{n_\infty} = \frac{w_\infty S_\infty}{w_0 S_0}, \tag{1.15}$$

since the ion velocity at an infinite distance from the body is independent of the body charge.

If E_n is the normal component of the electric field at the point of entry of the air stream into the ion probe, w_0 is the airstream velocity at the point of entry into the probe, and w_Q is the ion velocity under the influence of the airplane charge, then the number of ions with mobility K which enter the probe is given by the relations [14]:

$$n_1 = n_\infty \int_{S_0} w_0 dS - n_\infty \int_{S_0} w_Q dS = n_\infty \left(\int_{S_0} w_0 dS - K \int_{S_0} E_n dS \right) \tag{1.16}$$

and

$$n_2 = n_\infty \left(\int_{S_0} w_0 dS + K \int_{S_0} E_n dS \right), \tag{1.17}$$

where n_1 is the number of trapped ions repelled by the field and n_2 is the number of ions of the opposite sign. It can be shown that an increase of the number of ions n_2 does not affect the accuracy of the ion concentration and conductivity measurements, since these "excess" ions settle on the probe walls as a result of "sagging" of the field inside the probe tube [14].

The number of ions n_1 entering the probe will diminish with an increase of the intensity of the field proportional to the airplane charge, which leads to a reduction of the measured ion concentration and conductivity in comparison with the true values. The errors of the ion concentration δ_n and conductivity δ_λ measurement associated with the effect of the airplane charge are given by the following relations which follow from (1.16)

$$\delta_n = \frac{K\int\limits_{S_0} E_n\,dS}{\int\limits_{S_0} w\,dS} = \frac{Kp_0QS_0}{\int\limits_{S_0} w\,dS},$$

$$\delta_\lambda = \frac{\bar{K}p_0QS_0}{\int\limits_{S_0} w\,dS}, \qquad (1.18)$$

where p_0 is the coupling factor between the field intensity and Q, and $\bar{K}$ is the average mobility of the ions which create the conductivity. We recall that $\lambda = e\sum_i n_i K_i$ where e is the ion charge. In the case in which the freestream velocity is constant across the probe section and equal to $\bar{w}_0$, (1.18) can be written in the simplified form

$$\delta_n = \frac{Kp_0Q}{\bar{w}_0},$$

$$\delta_\lambda = \frac{\bar{K}p_0Q}{\bar{w}_0}. \qquad (1.19)$$

If we recall that the field intensity, at the surface of bodies of similar shape, from a given charge is inversely proportional to the body area, and that $w_0 = \Theta_0 w$, where Θ_0 in the first approximation is inversely proportional to the projected frontal area, then, as noted previously, the measurement error introduced by the charge Q is larger, the larger the charge, and it is smaller, the higher the airplane speed.

For more precise estimates of the errors it is necessary to take into account the geometry of the sounding body. For bodies of very simple shapes this accounting may be made in analytic form. The solution of (1.13) and (1.15) in the first approximation yields [13]

$$\frac{n_{0\pm}}{n_{\infty\pm}} = 1 - b\frac{Kp_0Q}{w_0}$$

and

$$\frac{\lambda_{0\pm}}{\lambda_{\infty\pm}}=1-b\frac{Kp_0Q}{w_0}; \qquad (1.20)$$

for a body T of spherical form

$$b=2\frac{R_0^2}{r_0^2}\left(1-\sqrt{1-\frac{r_0^2}{R_0^2}}\right).$$

where R_0 is the sphere radius, and r_0 is the probe radius.

For a body T of elongated cylindrical form traveling along its axis

$$b=\frac{R_0}{r_0}\left(\arcsin\frac{r_0}{R_0}\right).$$

The measurement errors δ introduced by the charge of the sounding body into the ion concentration and conductivity measurements will be, respectively

$$\delta_n=\frac{n_{0\pm}-n_{\infty\pm}}{n_{\infty\pm}}=-b\frac{Kp_0Q}{w_0}=-b\frac{Kp_0Q}{\Theta_a w},$$

$$\delta_\lambda=\frac{\lambda_{0\pm}-\lambda_{\infty\pm}}{\lambda_{\infty\pm}}=-b\frac{\bar{K}p_0Q}{w_0}=-b\frac{\bar{K}p_0Q}{\Theta_a w}. \qquad (1.21)$$

For small r_0/R the Equations (1.2) for both the sphere and the cylinder may be written in the form

$$\frac{n_{0\pm}}{n_{\infty\pm}}=1-\frac{Kp_0Q}{w_0}$$

and

$$\frac{\lambda_{\pm}}{\lambda_{\infty\pm}}=1-\frac{\bar{K}p_0Q}{w_0}.$$

In this case, the corresponding measurement errors will be

$$\delta_n = -\frac{K p_0 Q}{w_0} = -\frac{K p_0 Q}{\theta_0 w},$$
$$\delta_\lambda = -\frac{\bar{K} p_0 Q}{w_0} = -\frac{\bar{K} p_0 Q}{\theta_0 w}. \tag{1.22}$$

Similar expressions for the measurement errors can also be obtained for charged bodies having the form of an ellipsoid of revolution, elongated in the flow direction, and for an elliptical cylinder [13].

These errors in the conductivity and ion concentration measurement can be reduced if the probe is mounted in an undisturbed flow zone, and p_0 should be small. Usually, these conditions are contradictory. Therefore, the measurement error introduced by the charge may be very large and may reach 100%. Moreover, the error in the measurement of the ratio of the polar conductivities may amount to thousands or tens of thousands of percent.

Figure 1.3 shows the effect of the airplane charge on the measurement of the electrical conductivity of the air. With a field intensity near the fuselage greater than 2-4,000 V/m, conductivity measurements become impossible.

Let us examine the influence of the electrode effect on the measurements of the space charge. By definition, the space charge is

$$\rho = e(N_1 - N_2), \tag{1.23}$$

where e is the ion charge, and N_1 and N_2 are the concentrations of the positive and negative ions of all mobilities. In accordance with (1.16) and (1.17), N_1 and N_2 ions enter the probe opening (see Figure 1.2) under the influence of the airplane charge.

Since the space charge ρ is calculated on the basis of the magnitude of the charge q entering the probe per unit time, using the formula

$$\rho = \frac{q}{w_0 S_0},$$

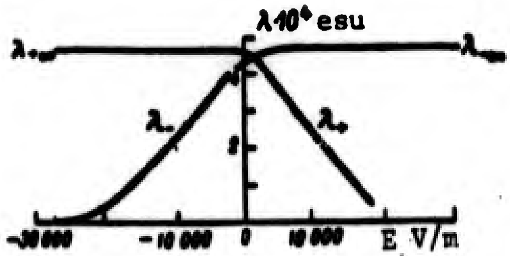

Figure 1.3. Air conductivity measurement error induced by airplane charge.

$\lambda_{+\infty}$ and $\lambda_{-\infty}$ are the true values of the air conductivity, λ_+ and λ_- are the measured values of the air conductivity. Measurements were made on an airplane flying at a speed of about 300 km/hr. The sensor was a tube mounted from the airplane nose and having a length of about one meter and diameter 10 cm [4]. The abscissa axis is the field intensity created by the airplane charge at the center of the fuselage.

then, using (1.23), (1.16), (1.17), we can write

$$\rho = e\left[\frac{\left(\sum_i n_{1_i} - \sum_j n_{2_j}\right)\int_{S_0} w_0\,dS}{\int_{S_0} w\,dS} + \frac{\left(\sum_i n_{1_i}K_{1_i} + \sum_j n_{2_j}K_{2_j}\right)\int_{S_0} E\,dS}{\int_{S_0} w\,dS}\right]. \tag{1.24}$$

where n_{1_i} and n_{2_j} are the concentrations of the positive and negative ions with the mobilities K_{1_i} and K_{2_j}.

The space charge measurement error $\delta\rho$ introduced by the charge of the sounding body will be

$$\delta\rho = -\frac{\sum_i n_{1_i}K_{1_i} + \sum_j n_{2_j}K_{2_j}}{\sum_i n_{1_i} - \sum_j n_{2_j}}\,\frac{\bar{p}_0 Q}{\bar{w}_0}, \tag{1.25}$$

if we set $\int_{S_0} w_0\,dS = \bar{w}_0 S_0$ and $\int_{S_0} E\,dS = \bar{p}_0 Q S_0$.

If the space charge is created by light ions, the measurement error is always large and may exceed hundreds or thousands of percent.

The additional field intensity introduced by the electrode effect at the airplane surface in the clear atmosphere is small. If the perturbed layer thickness is much less than the body dimensions, the maximal perturbed layer thickness d (see Figure 1.2) can be found from the formula d = kEt, where t is the time for the body to travel a distance equal to the dimensions of the perturbed zone. The charge of a unit column of the perturbed layer is $q_n = \rho d$ and the corresponding field intensity jump is

$$\Delta E = 4\pi q_n = 4\pi\rho d = \bar{e}\bar{n}\bar{K}Et = e\bar{n}\bar{K}E\frac{L}{w} = e\bar{n}\bar{K}L\frac{\bar{p}Q}{w}, \tag{1.26}$$

where $\underline{L}$ is the body length, and $\underline{p}$ is the average value of the coefficient $\underline{p}_0$.

For a body having the length $\underline{L} = 20$ m and traveling with the velocity $\underline{w} = 50$ m/sec in an atmosphere with ion concentration $\bar{n} = 1000\ 1/\text{cm}^3$ having the average mobility $\underline{K} = 2 \cdot 10^{-4}$ m^2/V·sec with an average field intensity $\underline{E} = 10{,}000$ V/m at the walls of the body, the maximal perturbed layer thickness (at the level of the body trailing edge) does not exceed 160 cm, the additional field intensity ΔE introduced by the space charge layer will not be more than 3 V/m, i.e., three orders of magnitude less than the primary field intensity. The error introduced by the additional field can reach a significant magnitude only for very slowly moving bodies.

Influence of airplane charging and currents to airplanes during flight in clouds and precipitation on the results of measurement of atmospheric electricity elements and the microphysical characteristics of clouds. Airplane flight in clouds and precipitation is accompanied not only by intense charging of the airplane but also by charging of the particles with which the airplane and the meteorological metering equipment collide. Let us examine the primary effects on the measurement results in this case.

Without dwelling on the reasons for charging of the airplane (this will be done in subsequent chapters) we simply note that, after collision of particles with the airplane and their separation from the airplane surface, the particles are charged with electricity of one sign, and the airplane is charged with electricity of the opposite sign. In this case, the magnitude of the charge acquired by the particles is much greater than the charge which existed on them prior to contact with the airplane. The primary charged particle stream rebounds from the airplane upon striking its frontal parts.

Let us examine how the stream of charged particles separating from the airplane affects the accuracy of the measurement of the airplane charge and the atmospheric electrostatic field. It is obvious that if the airplane charging current owing to the aerosol particles is $\underline{I}_{ch}$, then the current charging the aerosol particles as they separate from the airplane is $-I_{ch}$. If a constant aerosol particle stream with velocity w relative to the body and concentration n strikes the sounding body T having the length l and thickness h in the directions perpendicular to the air stream, and if each of the particles of radius r acquires the charge q_r, then the current transported by these particles after separation is $-I_{ch}=lhwnq_r$, assuming that the particles pass over the body T with the velocity which they had prior to impact. Behind the points O, located somewhere near the midsection of the body, the stream of particles which have separated from the surface of the sounding body does not change in magnitude. The total electrical charge q of the aerosol particles located in a perpendicular (with respect to the velocity vector) column of unit cross section also remains constant behind the points O. Then, neglecting edge effects, we can find

$$-I_{\text{зар}}=lhwnq_r=2qlw,$$

if the particle flux is symmetric, and

$$-I_{\text{зар}}=q_1lw+q_2lw, \tag{1.27}$$

if the particle fluxes above and below the body are not equal and the charges above and below the body equal q_1 and q_2, respectively.

If we neglect the change of the individual particle field with distance from the body along the normal to its surface, then the intensity created by the particle flux at the body surface is $\Delta E=4\pi q$ behind the points O and somewhat less in the regions closer to the nose part of the body. If the thickness of different sections of the sounding body is different while the material of the body surface is the same, then in the first approximation we can consider that the magnitudes of the charge q are distributed in proportion to the thicknesses h of the different body sections. For example, for an airplane the charged particle flux above the fuselage may exceed by several times the flux above the wings and, correspondingly, the charge q_f of this flux above the fuselage is greater than the charge q_K of the flux above the wings by a factor of $\frac{h_f}{h_K}$. Then, for an airplane the

Formula (1.27) may be written in the form

$$-I_{\text{зар}} = \bar{q}_{\text{к}} l_{\text{к}} w + \bar{q}_{\text{ф}} l_{\text{ф}} w,$$

where $\bar{q}_K$ and $\bar{q}_f$ are the average charges of a unit aerosol column above the wings and fuselage, and l_K and l_f are the wing length and fuselage width.

Since $\bar{q}_{\text{к}} \approx \bar{q}_f \frac{h_{\text{к}}}{h_f}$, then

$$-I_{\text{зар}} = q_{\text{ф}}\left(\frac{h_{\text{к}}}{h_{\text{ф}}} l_{\text{к}} + l_{\text{ф}}\right) w,$$

or

$$\Delta E_{\text{ф}} = 4\pi q_{\text{ф}} = -\frac{4\pi I_{\text{зар}}}{w\left(\frac{h_{\text{к}}}{h_{\text{ф}}} l_{\text{к}} + l_{\text{ф}}\right)}. \qquad (1.27')$$

This formula makes it possible to evaluate the additional field intensity created by the charged aerosol flux at the fuselage. In deriving the formula, we have omitted the fact that the current I_{ch} also flows to the engine nacelles, landing gear nacelles, antennas, and so on. Neglect of this fact leads to the situation in which the formula yields somewhat high values of ΔE. Contamination of the airplane surface may lead to the appearance of q_r which differ from the calculated values, but on the average, this formula yields reasonable values for the estimate of the quantity ΔE.

Usually, during flights in clouds, the overall current I_{ch} does not exceed 100 μA in the case of relatively strong charging of the airplane (when the charge field above the fuselage reaches several tens of kV/m). Let us estimate the order of magnitude of the error introduced by the charged aerosol flux into the measurements of the atmospheric field and the airplane charge. We assume that $w = 700$ km/h, $h_{\text{к}} = 50$ см, $l_{\text{к}} = 4\cdot 10^3$ см, $h_f = 300$ см, $l_f = 300$ см, then the field intensity from the particle charge at the fuselage is $\Delta E_f = 3000$ V/m and at the wings it is $\Delta E_{\text{к}} = 500$ V/m. We recall that the assumptions made in the derivation of the computational formula lead to obtaining values which are somewhat high. Moreover, the values of ΔE_{K} are presented on the assumption that the entire particle charge q is located on one side of the airplane. In actuality, after encountering the airplane, the aerosol particle flux splits into two relatively equal streams which pass above and below the airplane. Therefore, we must assume that at the point A and the point B of the airplane fuselage (see Figure 1.4) the additional field intensity does not exceed ±1000 V/m, and at the corresponding points of the wing the intensity does not exceed ±200 V/m. The ± signs mean that this additional field acts in different directions at the points A and B, just as the airplane charge field does. The errors in the determination of the external field and the ch ge which arise with the appearance of the charged aerosol layer depend on the relationship of q_1 and q_2 above the surface points A and B. It follows from (1.4) that in the case in question

$$\begin{aligned} E_A &= k_A E - p_A Q - 4\pi q_1, \\ E_B &= -k_B E - p_B Q - 4\pi q_2, \end{aligned} \tag{1.28}$$

hence, the calculated field intensity E_{ch} in the presence of the charged aerosol will differ from the true E, defined by (1.5) in the absence of the aerosol

$$E_q = E + \Delta E = E + 4\pi (Aq_1 - Bq_2).$$

i.e.,

$$\delta E_q = \frac{4\pi (Aq_1 - Bq_2)}{E}; \tag{1.29a}$$

similarly

$$\delta Q_q = \frac{4\pi (Cq_1 + Dq_2)}{Q}, \tag{1.29b}$$

where δE_q and δQ_q are the measurement relative errors of the corresponding quantities.

Let us evaluate the magnitudes of these errors for a specific airplane. For the Tu-104B $A \approx 0.7B$, therefore, the correction in determining the field intensity for $q_1 = q_2$ is about 30% of the

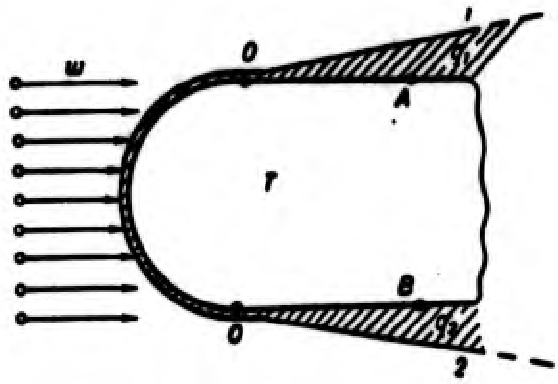

Figure 1.4. Distribution of charge q of aerosol particles near the airplane surface during flight through aerosols.

w is the aerosol particle velocity relative to the airplane; 1 and 2 are the boundaries of the stream of the particles which have acquired a charge after contact with the airplane.

intensity of the field created by the aerosol charge (for the example examined above, the correction is 100-200 V/m). The error in the charge determination may be quite large, and the field intensity from the aerosol charge may reach 2000 V/m (in the example considered above).

The error introduced by the charged aerosol layer into the measured values of E and Q will depend both on the characteristics of the clouds and precipitation and on the characteristics of the probe used and its flight regime. For example, the following values of the measurement error have been obtained for the Tu-104B airplane in different clouds.

We see from the table that when making measurements in clouds and precipitation, we should not expect high accuracy of the measurement of the armospheric field intensity or, particularly, of the measurement of the airplane charge, although in the majority of cases measurement precision which is quite adequate for geophysical

TABLE 1.1 INTENSITY OF ADDITIONAL FIELD CREATED BY CHARGED AEROSOL LAYER (Tu-104B AIRPLANE)

Form of cloud or precipitation	Cloud field intensity V/m		Airplane charge esu·10^{-3}		Current flowing to airplane μA		Intensity of additional field at fuselage ΔE V/m	
	average	maximal	average	maximal	average	maximal	average	maximal
Stratus	200	1 000	40	200	10	50	200	1 000
Cirrus	100	1 000	120	1500	100	1500	2 000	30 000
Thundercloud	50 000	200 000	500	7000	500	5000	10 000	100 000
Showers	10 000	50 000	100	2000	50	1500	1 000	30 000
Nimbostratus	1 000	20 000	200	2800	10	200	200	4 000

purposes is possible. Only in thunderclouds can the field intensity measurement error increase to 10,000-20,000 V/m and the airplane charge field measurement error at the measurement points to 50,000-100,000 V/m; it is true that in these cases both the external field and the airplane self-charge field reach values of ~100 000—200 000 V/m.

We must keep in mind that the error introduced by the aerosol layer can be reduced markedly by selection of the airplane type used for the research. The instrument sensors should be located near the wingtips in order to reduce this error.

Significant errors in the measurements in clouds and precipitation of the ion concentration, conductivity, space charge, particle charge, and so on may arise as a result of the charge currents created by the aerosol particles striking the electrodes of the measuring instruments.

If the metering instrument electrode has a sensor (metering electrode) with section area S and the useful signal current density is J_c, then the useful signal current $I_c = J_c S$ [11] when measuring the ion concentration, conductivity, and space charge. On the other hand, if the particles rebound from the entire receiver surface area, the interference current $I_n = SJ_n$ develops, and the measurement error in this case $\delta_r = \frac{I_n}{I_c} = \frac{J_n}{J_c}$ and may amount to thousands, tens of thousands, or even hundreds of thousands of percent during measurements in clouds, which excludes in principle any possibility of a measurement.

This error can be reduced significantly by making the electrode so that the useful signal is sensed by the entire electrode surface area, while the cloud particles can leave only along the perimeter of the instrument; in this case, the particles striking the inner parts of the electrode will be trapped by the electrode. In this case, the magnitude of the error is reduced. If the end surface of the electrode facing the stream has the form of a circle of radius R and if the instrument wall thickness is ΔR and the particle radius is r, then

$$\delta_r = \frac{2(\Delta R + r) J_n}{R J_c}.$$

In this case, the error may exceed thousands of percents. Without dwelling on the specific designs which permit reduction of this error [13, 15], we simply note that neglect of this error has been the reason for many research failures [16, 17].

In cloud particle spectrum measurements with the aid of an airplane we must remember that the particles which are charged during contact with the airplane, or the particles having a self-charge and flying past the charged airplane, travel along trajectories which differ from those calculated from aerodynamic considerations.

In the general case, the Equations (1.12) can be used to calculate the particle trajectories. We shall simply note here that if a particle travels a distance L along the fuselage, say, and the average field intensity from the airplane charge along its trajectory is E, then the deflection of the particle in this field will reach the following magnitude at the end of the path

$$\Delta z = w_E t = \frac{q_r \bar{E}}{6\pi r \eta} \frac{L}{v} = \frac{q_r \bar{p} Q}{6\pi r \eta} \frac{L}{v},$$

where w_E is the particle velocity component normal to the airplane surface (owing to the action of the airplane charge), t is the time for a particle of radius r to travel the distance L, η is the viscosity of the air; i.e., the particles may be deflected, creating marked distortions of the measured flow pattern. If the particle charges are high and are limited, let us assume, by the initiation of corona from the particles and $q_r = E_{th} r^2$, where E_{th} is the value of the field intensity at which the particles display corona, then the equation can be written in the form

$$\Delta z = \frac{E_{th} r \bar{p} Q L}{6\pi \eta v},$$

i.e., large particles may be deflected even more than small particles.

In absolute magnitude, the displacement Δz may reach several tens of centimeters.

The change of the particle trajectory under the influence of the airplane electric charge, together with the action of the electric field from the airplane charge on the water particle freezing conditions [18], may also have an influence on the airplane icing conditions.

§ 2. Influence of Airplane Electrification on Operating Conditions

Influence of electrical charging of airplanes on lightning strike conditions. The probability of airplane damage by lightning is very low if we evaluate this probability from purely "geometric" considerations, examining the situation in which an independently traveling lightning bolt strikes the airplane.

In fact, if the cloud volume is ω_0 and the "strike" volume is $\omega_1 = L_M S_c$, i.e., equal to the average length L_M of the primary lightning channel in the cloud multiplied by the airplane platform area S_c, then the probability P_T of lightning striking the airplane will be

$$P_T = \frac{L_M S_c n}{\omega_0} = \frac{\omega_1 n}{\omega_0}. \tag{1.30}$$

where n is the number of lightning discharges in the cloud during the time the airplane is in the cloud.

Denoting the lightning discharge repetition time interval in the given cloud by τ, the airplane characteristic dimension (length or wingspan) by l_c, the airplane speed by w, and neglecting the thickness of the lightning bolt channel in comparison with the airplane dimensions, we can write

$$P_T = \frac{L_M \pi l_c^2}{4\omega_0} \frac{d_0}{w\tau}, \tag{1.31}$$

where d_0 is the cloud length in the direction of airplane motion. Taking $\omega_0 = 10 \times 10 \times 10$ km^3, $L_M = 10$ km, $\tau = 10$ sec, l_c = 30 m and w = 500 km/hr, we find that $P_T < 10^{-4}$, i.e., a single direct primary lightning bolt strike on the airplane occurs for every 10,000 flights through thunderclouds.

In actuality the statistics on cases of direct lightning bolt strikes show a considerably higher strike probability. Several lightning strikes occur for less than a hundred random airplane flights through thunderclouds(1) in a period of a year. Consequently, the actual strike probability equals a few per hundred flights. What is the reason for the discrepancy between the theoretical and observed probabilities?

Footnote (1) appears on page 45

First of all, this discrepancy may be associated with the possibility that the crews of airplanes which enter thunderclouds may wisely consider it prudent not to report these flights through thunderheads in those cases when there is no damage. However, it is difficult to believe that in light of today's information on the weather situation it would be possible to conceal more than 50% of the entries into thunderheads.

Thus, in the temperate latitudes the actual lightning strike probability $P_{act} = 10^{-2}$. In fact, according to the data of Fitzgerald [24], who measured the number of lightning discharges in Florida which struck an airplane in active thunderclouds and the total number of lightning discharges occurring in the clouds during the time the airplane was in the cloud, the actual probability of lightning striking the airplanes is $P_{act} = 2 \cdot 10^{-2}$. We recall that in the tropics lightning discharges are more highly branched than in our latitudes.

Second, the disparity between P_T and P_{act} may be associated with the difference between the data used for the calculation and the conditions observed in real life. The values adopted for most of the quantities used for the estimate based on (1.31) understate the probability P_T in comparison with the true value. The linear horizontal dimensions of the thundercloud are usually greater than those used in the calculation by 2-3 times [18], the lightning repetition frequency in a single thundercloud usually does not exceed 3-4 discharges per minute. According to the data of Aiya [21], even in very active tropical frontal thunderstorms the maximal lightning discharge frequency does not exceed 25 strokes per minute, but these thunderstorms occupy an area of at least 10,000 km^2, i.e., the ratio $\frac{d_0}{w\tau}$ in (1.31) in these thunderstorms will also be less than the ratio we have used. The primary lightning channel length of 10 km (for the indicated cloud dimensions) corresponds approximately to the actual length. But in certain cases, the currents in the lightning branches are sufficiently high to cause damage to the airplane. It is not entirely clear how we should evaluate the length of a lightning discharge with such branchings in a cloud. If we use the data from photographs of lightning outside the cloud, then the lightning length may be increased by 2-3 times over that used in the calculation. With account for what we have said above about the underestimation of the role of the other parameters in (1.31), we can assume that the role of the cloud characteristics has been properly accounted for in our estimate of P_T (the estimate may even give a somewhat high value of P_T). The remaining possible assumptions are that the considerable discrepancy between the actual P_{act} and calculated P_T probabilities is associated either with incorrect account for the strike volume or with the possibility that the occurrence of lightning with the airplane in the cloud is not always a random event and may be associated with the influence of the airplane.

Let us examine what factors can lead to an increase of the strike volume.

Very frequently the assumption is made that lightning follows along the plume of the hot exhaust gases and the probability of lightning striking the airplane is increased, since the dimensions of the zone of "capture" of the lightning by the airplane increase. However, NACA data obtained prior to 1941 [22] show that of the 370 points of airplanes damaged by lightning, the exhausts and engines were never struck.

Following is a summary of lightning strike probabilities for modern airplanes, prepared in 1958 from NACA data [23]. The summary is based on an analysis of several hundred cases of lightning strikes on airplanes.

Radio antennas	27%
Wings	22% (half on the flaps)
Tailplane	21%
Fuselage	15% (12% on the nose, 3% at other points of the fuselage)
Propellers	7%
Radiocompass antenna	27%
Inspection panels	6%

It is clear from this summary that the exhaust gas jet has no effect on the lightning trajectory.

We must then assume that the airplane itself, like a lightning rod, leads to curvature of the lightning path and attracts the lightning discharge to the airplane itself. This may be associated either with the distortion of the cloud electric field by the airplane as a conducting metallic body or with the influence of the airplane's electric self-charge.

In the first case, the charges induced on the airplane by the external field disturb the cloud field. An estimate of the increase of the strike volume dimensions can be obtained on the basis of what is known about the action of a lightning rod. The action of the lightning rod, which is a grounded elongated semiellipsoid of revolution of height h, can be replaced by the action of an isolated ellipsoid of revolution of twice the height $2h$. The lightning rod intercepts more than 99% of the lightning strokes which pass within a distance less than h (the lightning rod protective cone) and part of the lightning strokes which pass at a distance less than $2h$. Assuming the airplane to be equivalent to a lightning rod, we must assume that lightning strokes passing at a distance $2l_c$ from the surface of the airplane may be intercepted by the airplane. It is obvious that the airplane can be approximated by an ellipsoid in the direction of maximal field magnification (along the wings) only very roughly, but in any case, this assumption leads to overestimation of the strike volume dimension. This overstatement will be even greater in the directions along the airplane fuselage and perpendicular to the plane of the wings. Then (1.31) may be written in the form

$$P_{\tau}=\frac{L_u \pi l^2_{\text{эф}}}{4\omega_0}\frac{d_0}{w\tau}. \qquad (1.32)$$

Assessment using (1.22) leads (for $l_{ef}=3l_c$) to a value of the strike probability $<10^{-3}$, which is also considerably less than the actual value.

We can assume that the airplane electrical charge affects the magnitude of the strike volume. Let us evaluate the action of this charge. This action may appear, first of all, as a change of the field along the lightning path and, second, as a change of the conditions for the initiation of the return discharge from the airplane surface.

The electric charge induced on the airplane by an external field of intensity E_a creates on the airplane the electric moment M, which causes along l_c at the distance R from the airplane the atmospheric electric field disturbance ΔE_g (Figure 1.5a)

$$\Delta E_g = \frac{M}{R^3} = \frac{\bar{k}E_a c l_c}{R^3}, \tag{1.33}$$

where $\bar{k}$ is a coefficient defined by the airplane construction and shows how the charge induced on the airplane is connected with the cloud field intensity; l_c is the airplane length in the corresponding direction (airplane length or wingspan); c is a coefficient which indicates in relative units the location of the centers of gravity of the airplane induced charges $c<1$. For modern passenger airplanes $c \approx 0.6-0.8$ [11].

The field disturbance ΔE_Q caused by the airplane self-charge Q is given by the expression (see Figure 1.5b)

$$\Delta E_Q \approx \frac{Q\bar{p}}{R^2}, \tag{1.34}$$

where $\bar{p}$ is a dimensionless coefficient which depends on the airplane construction. At large distances from the airplane $p = 1$, at small distances $p > 1$.

Thus, at some distance from the airplane we may find that (setting $c=\bar{p}=1$)

$$\frac{\Delta E_Q}{\Delta E_g} = \frac{R}{l_c}\frac{Q}{\bar{k}E_a} > 1. \tag{1.35}$$

We note that the data from our flights (Table 1.2) show, for example, that for the Tu-104 airplane in thunderclouds $\bar{p}Q>\bar{k}E_a$; in this case, it becomes obvious that the disturbance of the cloud electric field by the airplane charge acts at a considerably greater distance than the disturbance created by the airplane as a metallic body. Even if $\bar{p}Q=\bar{k}E_a$, at a distance $R=3l_c$ the field intensity from the charge will exceed by a factor of three the intensity from the induced charges, and at the distance l_c will be equal to the field intensity from the latter. Thus, we can assume that in the case of strong airplane charging $l_{ef}\approx 10l_c$, i.e., the value of the strike probability [see (1.32)] $P_T=10^{-2}$.

If the airplane acts as a charged lightning rod, the occurrence of a return discharge which intercepts the lightning may be facilitated by the fact that the field from the self-charge is superposed on the external field. The return discharge then occurs at greater distances from the lightning stroke, i.e., the dimensions of the strike volume are increased.

Assume there is no self-charge on the airplane, then the return discharge occurs at some point i for some $E_i=E_{cr\,i}$. On the other hand, the atmospheric field intensity created by the approaching lightning stroke, carrying in its forepart the charge Q_M at the distance R_1 from the lightning stroke, may be represented approximately in the form $E_a=\frac{Q_M}{R_1^2}$. Thus

$$E_{cr\,i}=k_iE_a=k_i\frac{Q_M}{R_1^2}. \tag{1.36}$$

If a lightning stroke approaches a charged airplane carrying the charge Q_c, then the return discharge again occurs for $E_i=E_{cr\,i}$, but now

$$E_{cr\,i}=E_E+E_Q=k_iE_a\mp p_iQ_c=k_i\frac{Q_M}{R_2^2}\mp p_iQ_c. \tag{1.37}$$

It follows from (1.36) and (1.37) that the distance R_2 at which the return discharge occurs on a charged airplane is connected with the distance R_1 at which the discharge occurs on an uncharged airplane

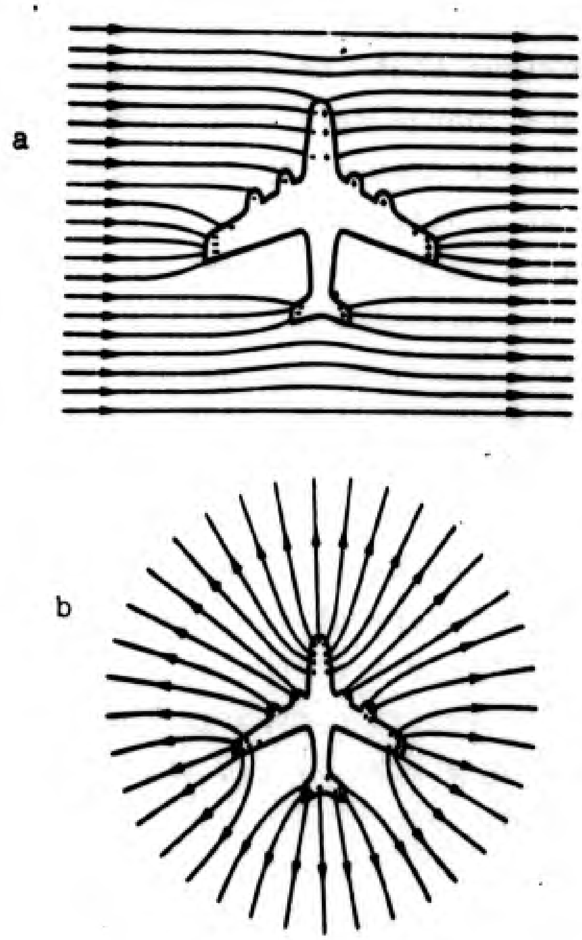

Figure 1.5. Electric field around airplane in flight (a) and electric field around charged airplane (b)

by the relation

$$R_2 = R_1 \sqrt{\frac{E_{\text{кр}i}}{E_{\text{кр}i} \mp p_i Q_c}} = R_1 \sqrt{\frac{k_i E_{\text{а.кр}}}{k_i E_{\text{а.кр}} \mp p_i Q_c}}, \qquad (1.38)$$

where $E_{a.cr}$ is the field intensity for which $E_{cr\,i}$ is reached. Equation (1.38) shows that the appearance of a charge on an airplane may either increase or decrease the probability of lightning striking the airplane, depending on the signs of the airplane and lightning charges. But for the calculation of the strike hazard, we must figure on the worst case, i.e., consider the increased probability. If we consider that the return discharge initiates with a field intensity $\sim 3\cdot 10^6$ V/m, then results of measurements of airplane charge in thunderclouds (Table 1.2) show that $R_2 = (2-3)R_1$, i.e., the airplane charge may further increase l_{ef} [see (1.32)] by 2 - 3 times l_{efQ} = (2 - 3) l_{ef} i.e., in the presence of a large airplane charge $P_1 \approx 10^{-2}$. With increase of the flight altitude, i.e., with reduction of the air pressure, E_{cr} decreases, therefore with increase of altitude the relative magnitude of R_2 and l_{efQ} must increase.

Let us examine the second assumption regarding the reasons for the discrepancy between the actual and theoretical probabilities of lightning strikes on airplanes, associated with the idea that the actual occurrence of the lightning in the cloud is caused by the presence of the airplane in the cloud.

We can assess the probability that the airplane acts as a sort of igniting electrode to cause the lightning stroke by referring to airplane lightning strike statistics. According to the NACA data collected prior to 1940, of the 169 cases of lightning striking airplanes, 50% of the strikes occurred in clouds in which lightning was not observed prior to the appearance of the airplanes [22]. The NACA statistics are based on pilot observations, but the U.S. pilots did not have any responsibility to avoid entry into thunderclouds, and therefore there is no basis to consider the information which they reported to the NACA to be in error. Therefore, we get the impression that it is the entry of the airplane into the cloud which causes the initiation of the lightning discharge, which then inevitably, rather than by accident, strikes the airplane. In civil aviation practice there have been many cases in which airplanes were struck by lightning in clouds in which there had been no prior observations of discharges, no extreme turbulence, none of the radar returns typical of thunderheads; in fact the clouds were described by the flight crews as being nimbostratus. However, further investigation of these cases disclosed that the crews of the airplanes which had been struck

TABLE 1.2. VALUES OF AVERAGE (E_{av}) AND MAXIMAL (E_{max}) INTENSITY OF ATMOSPHERIC ELECTRIC FIELD, AVERAGE AND MAXIMAL AIRPLANE CHARGE, AVERAGE AND MAXIMAL AIRPLANE POTENTIAL, AVERAGE AND MAXIMAL POWER OF ELECTRICAL NOISE SOURCE ON AIR-PLANE DURING FLIGHT IN THUNDERCLOUDS.

Date	Time, Hr-min	Flight altitude, m	Cloud top height, m	Number of lightning strokes/pass	Intensity, V/m av.	Intensity, V/m max.	Charge, esu av.	Charge, esu max.	Potential, V av.	Potential, V max.	Electrical noise source power, kW av.	Electrical noise source power, kW max.	Flight conditions	Observed radio noise
14/VIII 1961	14 35	10 000	10 200	2	50 000	100 000	$1\cdot10^6$	$4,2\cdot10^6$	$0,2\cdot10^5$	$8,4\cdot10^5$	0,15	3	Flight in developing thundercloud 7 km from core	Loss or radio communication at LF, MF, HF and at times (during charge increase) at VHF. Normal operation of radiocompass terminated
	15 04	10 000	>12 000	20/min.	100 000	200 000	$2\cdot10^6$	$6\cdot10^6$	$0,4\cdot10^6$	$1,2\cdot10^6$	0,6	5	Flight in same thundercloud in the core (mature cloud)	
	15 12	10 000	>12 000	5/min.	60 000	150 000	$3\cdot10^6$	$6\cdot10^6$	$0,6\cdot10^6$	$1,2\cdot10^6$	1,5	5	Flight in mature thundercloud 6 km from core	Loss of radio communication at LF, MF, HF and at times at VHF. Radiocompass inoperative
4/VII 1964	15 51	8 000	1 000	>5	900 000	305 000	$2,6\cdot10$	$7,8\cdot10^6$	$0,5\cdot10^6$	$1,5\cdot10^6$	1,0	8	In thundercloud (mature cloud)	
2/VII 1965	21 30	7 000	11 000	2—3/min.	70 000	100 000	$3\cdot10^6$	$7\cdot10^6$	$0,6\cdot10^6$	$1,4\cdot10^6$	1,5	7	In thundercloud 5 km from core (nighttime cloud)	Strong static at LF, MF, HF. Radiocompass inoperative
11/VIII 1965	17 00	1 200	600	none	10 000	30 000	$2\cdot10^5$	$3\cdot10^5$	$0,04\cdot10^6$	$0,06\cdot10^6$	0,006	0,015	In precipitation from squall cloud	

by lightning had noted severe radio reception interference and sparks on the cockpit windows, which indicated intense electrification of the airplanes which were struck by the lightning.

Data were presented in [25] on the conditions under which a DC-6 specially equipped for thunderstorm studies was struck by lightning (Table 1.3). The measurements were made in nine thunderstorms.

Strikes 1 and 2 occurred in the same thunderstorm cell, strike 3 occurred in another cloud. The conditions were similar in the two clouds. Both clouds were in the decaying stage. In all cases the strike occurred near the freezing isotherm; strong corona discharge was noted, which for the weak external fields was caused by the strong charging of the airplane. The strong corona discharge occurred about two seconds prior to the lightning strike on the airplane. We note that one lightning strike occurred in a zone of light turbulence, while another occurred in a moderate turbulence zone. Moreover the filled intensity in the cloud was not high (the last observation needs some checking, since the authors used a nonstandard measurement technique).

Let us examine in more detail the conditions under which the airplane can lead to the occurrence of lightning discharge in a cloud. For the development of a lightning discharge we must have: first, in a considerable volume of the cloud there must be an electric field with average intensity above the critical value required for supporting the discharge and, second, a sufficiently large region in which filed intensity extrema arise which are greater than that necessary for the occurrence of a discharge. If we assume that the cases of lightning strikes on airplanes are associated with the fact that the airplane played the role of this region, then we can understand both the cases of airplanes being struck by the first lightning discharge occurring in the clouds and also the cases of lightning strikes on airplanes in "quiet" clouds, frequently characterized as "nimbostratus."

TABLE 1.3. AIRPLANE LIGHTNING STRIKE CONDITIONS.

Measured element	Strike		
	1	2	3
Intensity component of atmospheric electric field, V/m			
-along wings E_x:			
before discharge	+3,000	0	-4,000
after discharge	1,000	+200	+2,500
-along fuselage E_y:			
before discharge	-1,500	0	0
after discharge	0	0	+4,000
-vertical E_z:			
before discharge	-16,000	-4,000	-27,000
after discharge	-5,000	+7,500	+23,000
Total field intensity before discharge $E=\sqrt{E_x^2+E_y^2+E_z^2}$	16,500	4,000	27,200
Flight altitude above sea level, m	4,870	4,870	5,340
Air temperature, °C	0	0	-2
Diameter of main thunderstorm cell, km	7	7	12
Cloud top altitude, m	9,000	9,000 (estimated value)	14,800
Airplane altitude above cloud base, m	12,000	12,000	1,800
Precipation	light rain, hail	heavy rain, hail	heavy rain, hail
Turbulence	light	severe	moderate
Airplane damage due to lightning	sm. hole in nose probe	sm. pinpoint hole and fused spot on wingtip probe	vertical antenna damage
Remarks	Entry into edge of sm. Cb. Audible corona discharge.	In strong downdraft. Audible corona discharge.	Audible corona discharge.

The light turbulence in quiet clouds does not prevent the accumulation of significant charges [26], and in fact high field intensities have been observed in individual nimbostratus clouds [27]. At the same time the light turbulence does not permit the development of nonhomogeneities with a field intensity sufficiently high to initiate a discharge. The airplane can play the role of such a nonhomogeneity. In order to prove this assertion we would have to compare the electrical characteristics of the airplane in the cloud and the characteristics of the nonhomogeneity capable of initiating a discharge. However, such a direct comparison cannot be made because of the lack of adequate information on the nonhomogeneities in question.

In order to evaluate the role of the airplane in the occurrence of a discharge in a cloud we can use the data of Newman [28], who conducted experiments on discharge initiation in clouds with the aid of a long wire carried aloft by a rocket. Newman indicates that raising a wire 300 meters long in two cases out of five led to the occurrence of a lightning stroke which followed the wire and vaporized it. Consequently, the wire in the cloud field as an initiating electrode created an electrical nonhomogeneity which was sufficient both with respect to the field intensity created and with respect to stored energy for the occurrence of a discharge. Comparing the disturbance introduced by the wire with the disturbance created by the charged airplane and comparing the stored energy of both systems, we can conclude that in thunderstorm clouds the airplane charge is sufficient (see Table 1.2) to initiate a discharge and thus to cause lightning to strike the airplane. Newman [28] also notes the necessity for rapid movement of the initiating electrode for the latter to be effective — this prevents the appearance of the electrode effect, the formation of a space charge which compensates by its field the electrode field.

It was noted in § 1 that high airplane speed prevents the formation of significant space charges around airplanes. Thus we can assume that the appearance of a charged airplane in a thunderhead or in a cloud in which the conditions are close to those in thunderclouds may in many cases lead to the initiation of a lightning discharge and to lightning striking the airplane. In fact, direct measurements in thunderclouds show that the airplane was usually strongly charged prior to the lightning discharge.

In [10] measurements were made of the external field intensity and the variation of the field intensity due to the airplane charge prior to a lightning strike (Table 1.4).

It is obvious that the field intensity at the airplane extremities exceeded the indicated values; thus the field variation due to the charge at the tips of the tailplane and wings could have been an order of magnitude greater than the values indicated. It was noted in [10] that in one of the two clouds investigated, which were in the decaying stage, three lightning strokes out of the three which occurred in the cloud struck the airplane, in the other cloud one of the two discharges which occurred struck the airplane. In active clouds the lightning strike probability was only 0.02.

Thus the probability of lightning striking the airplane depends to a considerable degree on the magnitude of the airplane charge. It should be remembered that thunderstorm discharges are one of the primary factors (according to Creedon [29], the primarily meteorological factor) leading to flight accidents.

Radio Interference on an Airplane due to the Effect of its Electric Charge. Several effects which influence the radio reception conditions aboard the airplane, the accuracy of the indications of the radio navigation equipment, and so on arise under the influence of the electric charge of the airplane and the currents flowing to the airplane.

These effects include:

1. Radio interference generated by processes as a result of which the airplane acquires a charge (these interferences occur, in particular, upon the appearance of microdischarges between the charged airplane and the cloud particles or precipitation particles located in the immediate vicinity of the airplane skin).

TABLE 1.4. DATA ON ELECTRICAL CHARACTERISTICS OF CLOUDS AND AIRPLANES DURING LIGHTNING STRIKE

Lightning strike number	Change of field intensity due to charging of airplane during discharge V/m	Change of horizontal component of external field, V/m	Change of vertical component of external field, V/m	Maximal current flowing to airplane, A
1	-197,000	-	-361,000	8700
2*	-151,000	+34,000	-173,000	2700
	+183,000	-174,000	-	-
3	+240,000	-15,000	-148,000	2800
4	-164,000	+294,000	-103,000	4600
5	-178,000	+350,000	+29,000	-
6*	+68,000	-36,000	-167,000	5800
	+164,000	+36,000	+150,000	-
	+205,000	-146,000	+67,000	-

NOTES: 1. Starred values relate to individual components of thundercloud discharges. 2. The table shows the actual values of the intensity created by the external field at the pickups. In order to obtain the true values of the external field components, we must divide the value of the horizontal component by 8.8 and the value of the vertical component by 1.1.

2. Radio interference associated with ionization of the medium under the influence of the charged airplane or with impact ionization of the air at high flight speeds. This effect may be associated, in particular, with variations in the radiowave propagation conditions.

3. Radio interference which occurs owing to the redistribution of the induced or self-charge over the airplane surface as a result of variation of the external conditions or the charge loss conditions. This form of interference increases particularly on the nonconducting regions of the airplane surface, with increase of the airplane flight velocities, and during flights in significantly nonuniform conditions.

4. Radio interference which occurs with the appearance of corona discharges at the extremities of the airplane as the self or induced charge densities on these regions increase to some critical values at which breakdown of the air layer adjacent to the airplane occurs.

Usually, the last factor is the primary source of radio interference.

The occurrence and existence of corona discharges, positive or negative, is accompanied by marked variations of the current and the appearance of radio emission. In the case of negative corona the amplitude, frequency, and steepness of the generated pulses — Trichel pulses [30] which occur in the presence of electro-negative gases — are determined by the rate of charge accumulation on the corona discharging point and by the dissipation time of the negative cloud charge near the corona point [31]. In the case of a positive corona, the amplitude and frequency of the current pulsations are determined by the appearance frequency and duration of the avalanch pulses and the streamer appearance frequency. Both of these processes depend on the potential of the corona point and the current flowing to the point, and also on the positive space charge concentration near the point and the time for the disappearance of this charge [31]. The magnitude of the radio interference generated depends on several factors, particularly on the magnitude of the airplane charge and the current flowing to the airplane and from the corona points, the flight altitude and speed, and the relative positioning of the corona point and the reception point, the length, radius of curvature, resistance, and material of the areas on which the corona arises, the polarization of the discharge radiation and the receiving antenna directional pattern, on the receiver frequency and passband. For the moment, we are interested in the fact that these interferences depend on the magnitude of the airplane charge, the time rate of charge variation, and the magnitude of the currents flowing to the airplane.

We see from Table 1.2 that for flights in thunderstorms the total power feeding the radiated interference source may reach the order of several kilowatts. We must keep in mind that the airplane radio receivers accept signals of power $\sim 10^{-10} - 10^{-12}$ W.

If we assume that the interference energy source power decreases linearly with increase of the frequency, then its energy at a frequency of 1 MHz will exceed the signal energy by 10^4 times, at a frequency of 10 MHz the factor will be 10^3, and at a frequency of 50 MHz the factor will be 500.

In fact, during flights in thunderclouds, this interference may lead to complete loss of radio communication at the long, medium, and short wavelengths, and even in the UHF band normal radio compass operation cannot be obtained, and so on. The antennas may be charged to potentials which are hazardous for the crew.

Effect of airplane charge on flight aerodynamics. If an ionized gas stream flows near a charged body, the resulting forces may affect the behavior of the boundary layer and thus the flight aerodynamics or the flow conditions around the instrument sensors.

From the Navier-Stokes equation for the stationary case [123]

$$\rho(\bar{w}\nabla)\bar{w} = -\nabla P + \eta\nabla^2\bar{w} + q_0\bar{E}$$

(where ρ is the density of the air, ΔP is the pressure differential, w is the air velocity, η is viscosity) it follows that a marked influence of the electrical forces on the flow past a body which is ionized by the stream will be noted if the last term in the equation is of the same order of magnitude or exceeds the other terms. Introducing the characteristic values of the velocity w and body length L, stream space charge density q_0, and field intensity E_0 at the body, we can write the condition for marked influence of the electrical force [123]

$$E_0 q_0 > \frac{\rho w^2}{L} \quad \text{or} \quad q_0 > \frac{\rho w^2}{L E_0} = \frac{\rho w^2}{L p Q}.$$

Under actual conditions encountered during flights in thunderclouds, the field intensity at the wing tips and stabilizer tips reaches values of $\sim 10-20$ kV/cm and the current flowing to the airplane is about 10 mA. If we assume that the primary corona discharge current occurs at the tips of the wings and tailplane, say over a distance equal to one tenth of the wing or tailplane lengths, then the actual density $q_0 = 1.5$ esu/cm^3; on the other hand, for $w = 100$ m/sec and $L = 10$ m values of $q_0 \approx 1$ esu/cm^3 are sufficient for the electrical forces to begin to have a marked effect on the air flow around the airplane, at least at the tips of the wings, tailplane, and fuselage.

If we charge the airplane artificially and locate corona discharge points along the leading edges of the wings and tailplane, then by using technically achievable values of the charging current and airplane potential we can reduce markedly the airplane drag or the aerodynamic resistance of the pickups which protrude from the airplane.

<u>Measurement of airplane height from data on the charge density distribution over the airplane</u>. We have noted previously that as a charged airplane approaches the ground the charge density distribution over the airplane surface changes as a result of the charges induced on the ground, i.e., the coefficients p change. The change of the coefficients increases as the ground is approached. These coefficient changes can be used to create an altimeter, whose basic characteristic will be increase of the measurement accuracy as the ground is approached [33].

The complete calculation of the change of the coefficients p for an airplane is a complex problem and must be repeated for each specific airplane type. It is usually advisable to replace the calculation of the airplane charging process by a calibration using a model or even the airplane itself. Let us examine the basic features of this method for measuring altitude, using a sphere as an example.

Assume a sphere of radius a carrying the charge +Q is located at the distance h from the surface of the Earth (Figure 1.6). In the first approximation, the distribution of the surface charge density on the sphere can be calculated if we examine the interaction of a conducting charged sphere with the image charge -Q located at the distance 2h from the sphere (see, for example, [34]). Q' is the magnitude of the charge induced in the sphere by the charge -Q.

The surface charge density on the sphere may be written in the form

$$\sigma=\sigma_Q+\Delta\sigma, \tag{1.39}$$

where $\sigma_Q=\frac{Q}{4\pi a^2}$ is the charge density on the isolated sphere, and $\Delta\sigma$ is the disturbance introduced by the proximity of the Earth.

Neglecting the action of the external field and the space charge around the charged sphere, and also considering only the interaction of the sphere with the single image charge, creating on the sphere the induced charge Q, we can write (see, for example, [34])

$$\Delta\sigma=\frac{a^2-(2h)^2}{4\pi aR^3}Q,$$

where R is the distance from the image charge to the corresponding point of the sphere. We note that if h = 2a the error in determining $\Delta\sigma$ resulting from neglecting the higher order reflection terms is $\approx 7\%$, while if h = 5a this error does not exceed 1%.

At the points A and B of the sphere with $\theta=0°$ and $\theta=180°$ the additional charge density $\Delta\sigma_i$ created by the charge Q will be

$$\Delta\sigma_A=\frac{a^2-(2h)^2}{4\pi a(2h+a)^3}Q, \tag{1.40a}$$

$$\Delta\sigma_B=\frac{a^2-2h^2}{4\pi a(2h-a)^3}Q; \tag{1.40b}$$

The difference of the field intensities E_A and E_B at the points A and B is

$$E_A - E_B \approx 3\frac{Q}{4h^2 - a^2}. \qquad (1.41a)$$

$$\frac{E_A - E_B}{E_A + E_B} = \frac{3a^2}{4h^2 + ha}. \qquad (1.41b)$$

Then, by altering the difference of the field intensities at the points A and B and determining in some way the charge Q we can find the height h from (1.41a); the height h can also be found by excluding the magnitude of the charge Q from the calculations (Formula 1.41b). The effect of the external field on the instrument indications can be eliminated either by measuring the field intensity on the body at two additional points, C and D, for example [33], or by charging the sphere to values such that the influence of the external field is less than the measurement error or, finally, by combining both methods. We see from Formulas (1.41a) and (1.41b) that the quantity $E_A - E_B$ increases sharply with reduction of h. In actuality, account for the higher-order electrical reflections yields a still sharper dependence of of $\frac{\partial(E_A - E_B)}{\partial h}$ on h at heights comparable with the body dimension $(h \approx a)$.

Figure 1.7 shows how the difference $E_A - E_B$ of the charged Li-2 airplane varies as it approaches the Earth (curve 1); E_A and E_B were measured by electrostatic fluxmeters located respectively above and below the fuselage. The figure shows clearly how steeply this difference increases with reduction of the height h. Figure 1.7 also shows for comparison the curve 2, calculated using (1.41a) for a sphere of radius 1.5 m.

It appears that altimeters based on this principle would also be convenient for measuring the height of flying-crane type helicopters.

<u>Effect of airplane charging on explosion hazard during inflight refueling</u>. If an airplane has the electrical charge Q and its electrical capacitance is C, then the electrical energy stored by the airplane is

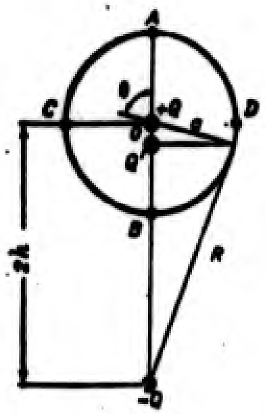

Figure 1.6. Schematic for calculating charge distribution on sphere.

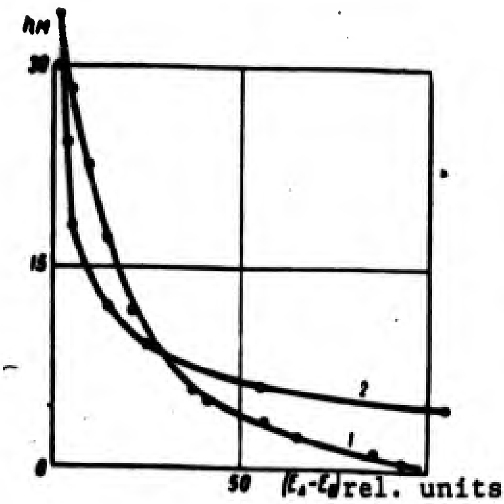

Figure 1.7. Change of field intensity distribution on charged bodies as they approach the Earth.

1) Li-2 airplane; 2) sphere

$$F_{s}=\frac{Q^{2}}{2C}.$$

In the first approximation, the capacitance of an airplane can be considered equal to 0.2-0.4 times the wingspan in centimeters [5] for passenger airplanes at subsonic speeds.

The energy stored by an airplane having the charge 10^{6} esu and wingspan ∿ 40 m (see Table 1.2) is equal to about 100 Joules, but we see from the table that this energy may reach ∿ 10^{4} Joules. If an electrical contact is formed between the charged airplane and another airplane, this power can be released in an electrical spark which arises as the contacting elements approach one another. Under unfavorable conditions (for example, if the contacting element is a refueling hose) the spark energy may cause ignition of the fuel.

Therefore, during inflight refueling, the airplane must of necessity be initially connected by means of a metallic cable before refueling is initiated. We must also bear in mind that as the fuel flows through the hose local electrical charges develop on the hose and in the fluid stream, which can also create an electrical spark. Therefore, the hose material and the refueling fuel-flow velocity must be such as to generate a sufficiently low electrical charge in the fluid.

Electrical charge on grounded helicopters. In many cases, a helicopter may be grounded, for example, when operating as a flying crane. If the helicopter is at the height h and has the maximal linear dimension l, and in the atmosphere there is an electrical field of intensity $\bar{E}$, then the helicopter will acquire in the field the bound charge (if we neglect terms of second-order smallness)

$$Q = mlh\bar{E},$$

where m is the coefficient connecting the helicopter dimensions with its electrical capacitance $C=ml$. The value of m is close to unity.

The electrical energy stored in the helicopter will be

$$F_{э} = \frac{Q^2}{2C} \approx \frac{mlh^2\bar{E}^2}{2}.$$

If the ground connection is broken for one reason or another and the electrical field changes in intensity, this energy can cause electrical injury to personnel.

FOOTNOTE

1. Footnote on page 24 — In accordance with the international classification, there is no differentiation of the Cb clouds into thunderstorm and squall. However, the modern techniques for identification of clouds make it possible to do this quite effectively. Therefore, in the following we shall differentiate between these two varieties.

CHAPTER II

AIRPLANE ELECTRICAL CHARGE IN CLOUDS AND PRECIPITATION

§ 1. Distribution of Self- and Induced Charges Over the Airplane Surface

Methods for measuring self- and induced charges. It was shown in Chapter 1 that by measuring the electric field intensity at two points of an airplane lying at the intersection of the corresponding neutral lines, we can determine one external field intensity vector component and the magnitude of the airplane's self-charge. By measuring the field intensity at two other points, located at the intersection of the neutral lines lying in two other planes, we can also measure the other components of the atmospheric field intensity [11, 69]. In certain cases, measurements are made at points other than the points of intersection of the neutral lines; however, this either requires an increase in the number of sensors [11], or reduces the measurement precision. Knowing the values of the atmospheric field intensity and the magnitude of the airplane's self-charge, we can determine both the induced charge and self-charge surface densities over the entire surface of the conducting, all-metal airplane, for example. However, we note that the construction of many all-metal airplanes includes surface segments made from nonconducting materials (radar antenna and communication antenna fairings, windshields, and so on); the magnitude of the charges on these areas correlates poorly with the magnitude of the charge on the conductive surface of the airplane. The area of such regions is usually small and the disturbances which they introduce are of a local nature. These disturbances may have a marked effect if the equipment used to measure the field intensity is located too close to the nonconducting components, and also during operation of radio equipment or instrumentation which have antennas and sensors located alongside the insulated segments.

The field intensity measurements are usually made with the aid of electrostatic fluxmeters, which either yield the values of the field intensity at selected points or provide directly the values of the field intensity components and the airplane's self-electric field components. Several studies have attempted to make measurements using collectors — devices which measure the atmospheric potential at some point [35 - 37]. Such measurements are very inaccurate. During flight in clouds and precipitation, the atmospheric potential at points lying near the airplane depends to a considerable degree, as was shown in Chapter 1, on the charge of the aerosol layer adjacent to the airplane. For a given airplane, the dimensions of this layer depend on the properties of the particles with which the airplane collides and on the flight speed and altitude. The potential values measured by the collector will vary as a function of the point of the aerosol layer where the collector is located; this introduces a very considerable error into the measurement results.

Distribution of the self- and induced charges over the surface of the airplane. The measurements of the distribution of the airplane's self- and induced charges are usually made on airplane models [11, 37]. The values of the coefficients p and k, which connect the field intensity at individual points with the magnitude of the airplane's charge and the external field intensity, are different for corresponding points of airplanes of different construction. At the

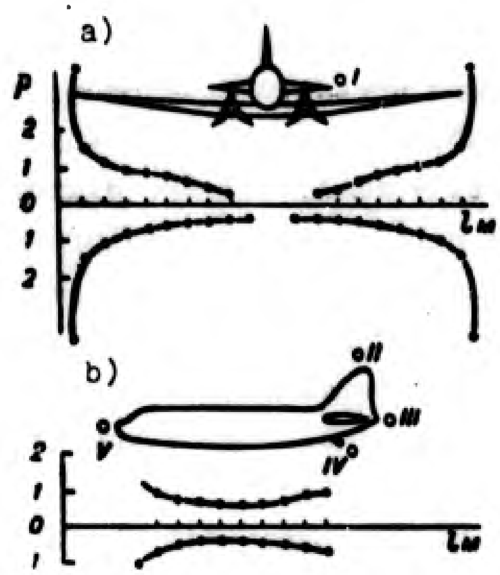

Figure 2.1. Distribution of self-charge over surface of Li-2 airplane. Circles denote points with large coefficients. p is expressed in V/m · esu I) p=3.7, II) p=3.2; III) p=2.4; IV) p=1.2; V) p=2.0.

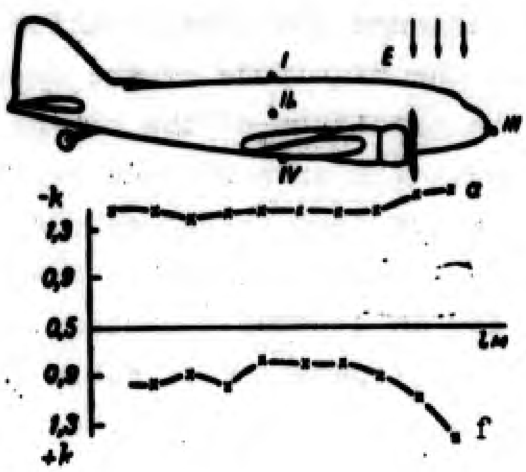

Figure 2.2. Distribution of induced charge over surface of Li-2 airplane in uniform vertical electric field.

I - upper pickup (k = 1.57);
II - side pickup (k = 0.46);
III - nose pickup (k = 1.42);
IV - bottom pickup (k = 0.82).

same time, the values of p and k do not differ markedly for points lying near the center-section for airplanes of similar types.

Figure 2.1 shows the distribution of the values of the coefficients p for the Li-2 airplane along the wings (a), and the fuselage (b) [38]. The upper halves of the figures show the value of p on the upper wing and fuselage surfaces; the lower halves show the value of p on the lower surfaces. The circles indicate the points where the charge density is particularly high. We see from the figures that the coefficients p may differ at individual points by nearly 20 times, i.e., the surface charge density at the wingtips may exceed the charge density at the wingroots by a factor of 20.

Figure 2.2 shows the distribution of the coefficients k along the plane of symmetry of an Li-2 airplane located in a vertical field [38]. Curve a relates to the upper part of the fuselage, curve b

is for the lower part of the fuselage. The Roman numerals denote the most convenient locations for the sensors measuring the vertical component of the external field intensity and the self-charge (I and IV), and for measuring the field components directed along the wings (II), and fuselage (III).

There may be a marked intensification of the field at individual points of the airplane surface. On the airplane tail-bumper and tip of the vertical fin (points IV and II in Figure 2.1), the vertical field component is intensified by 35 to 61 times, respectively. The field intensity at the wingtips is 58 times greater than the atmospheric field intensity component directed along the wings. At the airplane nose (point V in Figure 2.1), the field intensity exceeds by 14.5 times the external field intensity component directed along the fuselage.

The airplane construction does not always permit locating the sensors at the points of intersection of the neutral lines. In this case, the indications of the sensors measuring the field intensity components are affected not only by the corresponding component and the self-charge, but also by the other field components, which complicates the analysis of the results and increases the measurement error. The sensors are sometimes mounted at the points of maximal charge density, for example, at the wingtips [39], in order to increase the measurement accuracy in weak fields and for small charges. Figure (2.3) shows the distribution of the surface charge density in the presence of a self-charge on the IL-18 airplane, measured by Markchev and Evteyev. The nature of the charge distribution over the IL-18 is reminiscent in general, of the charge distribution on the Li-2 airplane, but the values of the coefficients, particularly at the extremities, are different.

In comparing the electrical charging of airplanes of different types, we must bear in mind that the ratio of the potentials of two airplanes carrying the same charges and having, in general, a similar

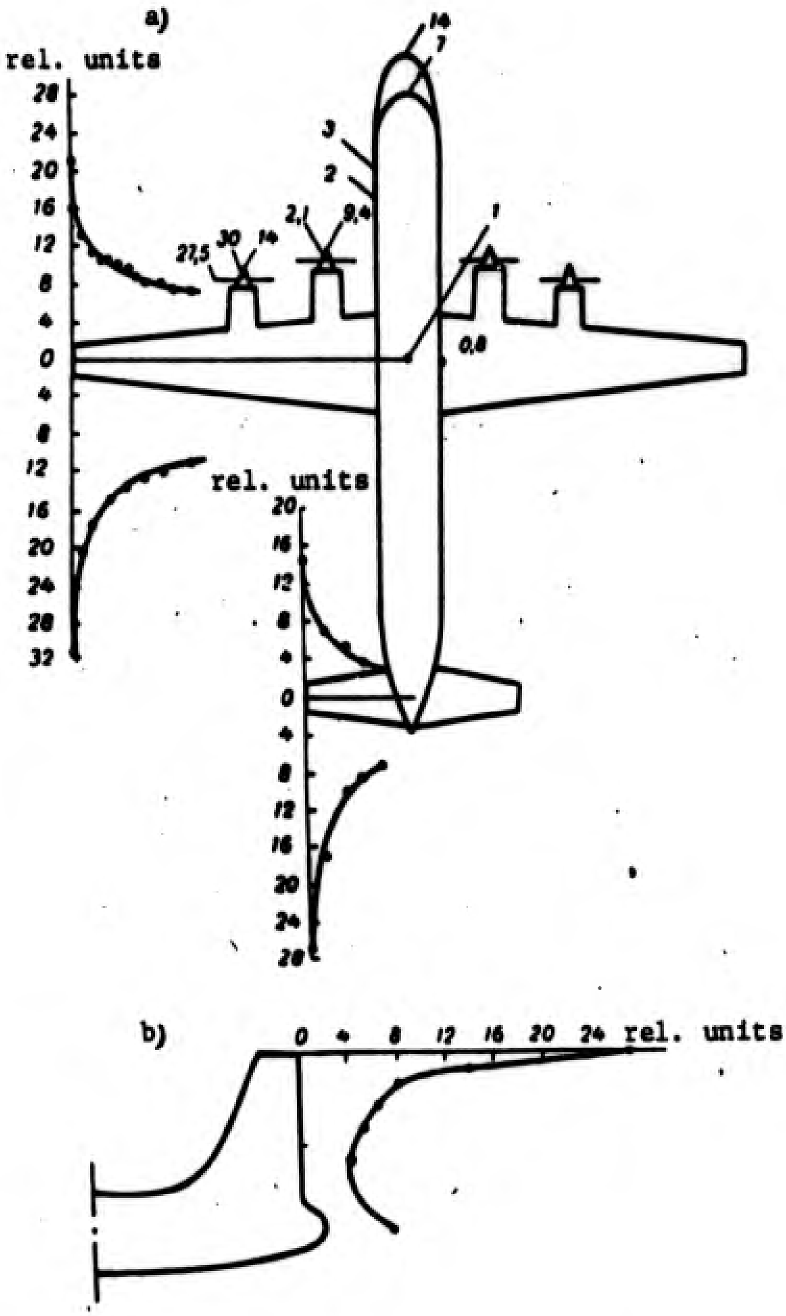

Figure 2.3. Distribution of self-charge over surface of IL-18 airplane. (a) along wings and tail; (b) along rudder. Numbers on figure are values of p at individual points of the airplane.

configuration is approximately the reciprocal of the ratio of the linear dimensions of the airplanes, while the ratio of the charge densities at similar points of these airplanes is the reciprocal of the ratio of the airplane surface areas [38].

The airplane charge field decays very slowly with distance. Figure 2.4 shows the distribution of the isopotential lines around an airplane which has some charge [35]. The airplane potential is taken as unity. Only at distances exceeding the airplane dimensions by 1 - 2 times can the field of the charged airplane be considered a point charge field.

The field intensity at any point of the airplane surface and in the vicinity of the airplane, and also the potentials of nearby atmospheric points, are determined by the magnitude $\underline{Q}$ of the airplane charge, the intensity of the external atmospheric field, and the airplane construction.

We shall examine the basic electrical characteristics of clouds and find how the magnitude of the airplane charge is related with the meteorological situation.

§ 2. Cloud Electrical Structure and Basic Electrical Parameters

In the clear atmosphere, there is always an electric field, whose intensity $\underline{E}_з$, at the earth's surface is about 100 V/m. The field intensity decreases approximately exponentially with altitude. This decrease is associated with the fact that the air conductivity λ, equal at the earth's surface on the average to $\lambda_e \approx 3 \cdot 10^{-14}$ 1/Ohm · m, increases nearly exponentially with altitude. In clear air at a given altitude[1], the values of λ in different regions of the

---

Footnote (1) appears on page 120.

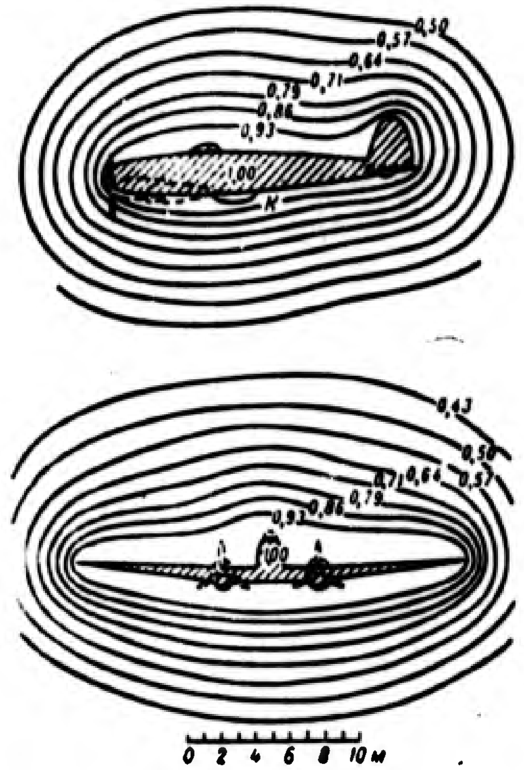

Figure 2.4. Distribution of isopotential lines in vicinity of charged airplane.

world differ by no more than $\pm 20\%$ [67], and the stationarity condition — the absence of charge accumulation in the atmosphere — requires that the conduction current density be constant as a function of altitude

$$i = \lambda_0 E_0 = \lambda_h E_h = (3 \div 4) \cdot 10^{-12}\ \mathrm{A/m^2}$$

where λ_h and E_h are the corresponding values of the conductivity and field intensity at the altitude h [40, 41, 27].

The appearance in the atmosphere of aerosol layers, particularly dust, clouds, precipitation and the like, alters markedly the electrical characteristics of the atmosphere: the conductivity changes, strong electric fields develop, large electrical currents begin to flow. Particularly, strong changes of the atmospheric electrical characteristics, having a stable nature as a function of time and appearing over extensive regions, are associated with clouds, precipitation, snowstorms, and the like.

Let us examine the basic electrical characteristics of clouds and precipitation.

The electrical structure of clouds is created as a result of the interaction of two basic groups of processes, one of which leads to electrification of the clouds, while the other tends to reduce the electrification. The cloud and precipitation particles (droplets, snowflakes, ice crystals) acquire electrical charges. If the cloud particles acquire a charge of one sign and the charge of the opposite sign remains in the air, then as a result of particle fall, macro-separation of the charges in space arises, and an electrical field is established, which exists throughout the entire cloud or in a considerable volume of the cloud. The intensity of this field may differ significantly from that existing in the atmosphere, both in absolute magnitude and direction.

Still larger electrical charges can develop on individual particles, if they appear as a result of interaction of the particles; high space charges arise if charges of opposite signs occur on particles with significantly different rates of fall, for example, on cloud and precipitation particles, water drops and hailstones, and so on.

Charge accumulation on an individual particle is restricted by charge loss as a result of air conductivity in the space surrounding the particle and by collision with other particles, which have a charge of the opposite sign or are relatively weakly charged. The accumulation of space charges in a cloud and the increase of the electrical fields throughout the entire cloud volume are limited by the conduction currents flowing between regions charged with electricity of opposite signs and also by the currents which arise as a result of air movement (electrical currents associated with turbulent diffusion and convection).

Obviously, the more active the process of the first group (the larger the charges which arise on the individual particles, the larger these particles, the higher the rate of charge separation) the larger the electrical fields which develop in the clouds. The more active the processes of the second group, the smaller the electrical fields which will be generated by the cloud. Quasistationary conditions of the electrical state of the clouds are obviously reached when the rates of arrival and departure of the charges created by the processes of the two groups are equal.

We shall examine the electrical characteristics of clouds of different types.

We must bear in mind that the electrical structures of the clouds presented in Table 2.1 were obtained primarily in the northwestern part of European USSR. However, the data on the cloud particle charges were obtained primarily on the basis of measurements on Mt. Elbrus (in the southern part of European USSR), near Washington (United States), and so on. The electrical characteristics of clouds of all forms depend to a considerable degree on the physical and geographic conditions of the region in which the clouds are formed. Specifically, the magnitudes of the average and maximal field intensity in clouds and the magnitudes of the space charges increase in the direction toward the equator [27]. Therefore, "joining" the general properties of clouds from the data on measurements of their individual characteristics in regions with markedly different physical and geographic conditions, which affect differently the processes of the two groups forming the electrical state of the clouds, yields only a very schematic idea of the properties of a specific cloud in a specific region.

<u>Electricity of stratus and stratocumulus clouds</u>. The electrical structure of stratus clouds is shown in Figure 2.5. In half the cases, the clouds were polarized positively; in 15% of the cases, they were charged negatively. The remaining clouds were charged unipolarly. The characteristic data for these clouds are summarized in Table 2.1. The magnitudes of the average field intensity in the clouds and the space charges increase somewhat toward the south [27]. In the first approximation, we can consider that in all the measurement regions, the magnitudes of the drop charges in these clouds are proportional to the drop radii.

Table 2.1 presents information only on the vertical component of the field. The horizontal components of the field intensity in these clouds are usually considerably smaller than the vertical

TABLE 2.1

ELECTRICAL CHARACTERISTICS OF DIFFERENT FORMS OF CLOUDS

cloud form	characteristic arrangement of principal charges	source	field intensity in cloud, V/m		source	field intensity in zones of cloud nonuniformities, V/m		source
			average	extremal		average	extremal	
stratus and stratocumulus	+ −	[27]	+100	+1400	[27]	—	—	—
	− +	[27]	−160	−1600	[27]	—	—	—
cirrostratus	+ − and − +	[27]	0	−900, +2000	[27]	—	—	—
nimbostratus	+ − − +	[27]	+500 −600	+15 000	[27]	—	—	—
altostratus	+ − and − +	[27]	−200	−650, +1450	[27]	—	—	—
cumulus and cumulus congestus	+ − and − + (75%) (25%)	[49, 50]	500	2000	[49, 50]	1000	10 000	[40]
thunderheads	+ − and − +	[52, 26]	40 000—100 000	300 000	[26, 10, 25, 55]	300 000	probably ~1 000 000	[10, 26, 25, 55]

TABLE 2.1 (CON'T.)

ELECTRICAL CHARACTERISTICS OF DIFFERENT FORMS OF CLOUDS

cloud form	characteristic arrangement of principal charges	field intensity in cloud, V/m		source	field intensity in zones of cloud nonuniformities V/m		source
		average	extremal		average	extremal	
stratus and stratocumulus	—	$+0{,}8\cdot10^{-9}$ $-0{,}8\cdot10^{-9}$	$\sim10^{-8}$ $\sim-10^{-8}$	[27]	$+0{,}7\cdot10^{-11}$ $-0{,}5\cdot10^{-11}$	$\sim+5\cdot10^{-11}$ $\sim-5\cdot10^{-11}$	[27]
	—	$-3\cdot10^{-9}$ $+3\cdot10^{-9}$	$\sim-10^{-8}$ $\sim+10^{-8}$		$-0{,}15\cdot10^{-11}$ $+0{,}8\cdot10^{-11}$	$\sim-10^{-11}$ $\sim+5\cdot10^{-11}$	[27]
cirrostratus	—	$+10^{-9}$ -10^{-9}	—	[27]	$+0{,}2\cdot10^{-11}$ $-0{,}2\cdot10^{-11}$	—	[27]
nimbostratus	—	$+7\cdot10^{-9}$ $-8\cdot10^{-9}$ $-11\cdot10^{-9}$ $+9\cdot10^{-9}$	—	[27]	$0{,}5\cdot10^{-11}$ $-0{,}7\cdot10^{-11}$ -10^{-11} $+0{,}5\cdot10^{-11}$	from 10^{-10} to 10^{-9}	[27]
altostratus	—	$+10^{9}$, -10^{-9}	$+10^{-8}$, $-3\cdot10^{-8}$	[27]	—	—	
cumulus and cumulus congestus	120	—	—		$+5\cdot10^{-12}$, $-5\cdot10^{-12}$	$5\cdot10^{-11}$	[49]
thunderheads	400—600 м	from 20—40 to 100 к (general charge)		[26]	$(0{,}3\div3)\cdot10^{-9}$	$(3\div30)\cdot10^{-9}$	[49, 26]

TABLE 2.1 (CON'T.)

ELECTRICAL CHARACTERISTICS OF DIFFERENT FORMS OF CLOUDS

cloud form	charge density in heterogeneous zones, C/m^3		source	charges, C·10^{-19}					source
				of cloud droplets of radius, microns				of precipitation particles	
	average	extremal		2	5	8	10		
stratus and stratocumulus				32 48 43 61 9 150	82 116 160 165 12 170	— 140 220 — 15 —	— 176 150 — 17 —	—	[42] [43, 44], [46]
cirrostratus				—	—	—			—
nimbostratus	—	—	—	—	340	1350	2050	$10^4 \div 10^6$	[45, 53, 54, 57]
altostratus	—	—	—	—	—	—	—	—	—
cumulus and cumulus congentus	10^{-10}	$3 \cdot 10^{-9}$	[40]	—	—				
thunderheads	$\sim 3 \cdot 10^{-8}$	$\sim 10^{-7}$	—	—	400	550	—	$10^5 \div 10^7$	[56, 57]

TABLE 2.1 (CON'T.)

ELECTRICAL CHARACTERISTICS OF DIFFERENT FORMS OF CLOUDS

cloud form	conductivity (in fractions of the conductivity of the clear atmosphere at the same altitude)		source	average current density in clouds, A/m^2	source	remarks
	ohmic	turbulent and convective				
stratus and stratocumulus	$^1/_3$—$^1/_6$ to $^1/_{25}$	$^1/_{10}$	[43, 47, 48] [27]	$(1\div2)\cdot10^{-12}$	[27]	1. The values of the particle charges, ohmic and turbulent conductivities and currents were not identified for different structures of this form;
cirrostratus	—	—	—	—		2. values given for Ns clouds of mixed structure. Conductivity in Ns is approximate;
nimbostratus	$^1/_3$—$^1/_{10}$	$^1/_6$—$^1/_{10}$	[27]	$(1\div3)\cdot10^{-11}$	[27]	3. effective conductivity made up of ohmic, turbulent, and convective conductivity is presented for thunderheads;
altostratus	—	—	—	—		4. values of principal charges of thunderheads given in Coulombs.
cumulus and cumulus congestus	$\sim^1/_3$—$^1/_{10}$	$^1/_6$—$^1/_{10}$		10^{-10}	[51]	
thunderheads	10—100		[58, 26, 21]	10^{-8}—10^{-7}		

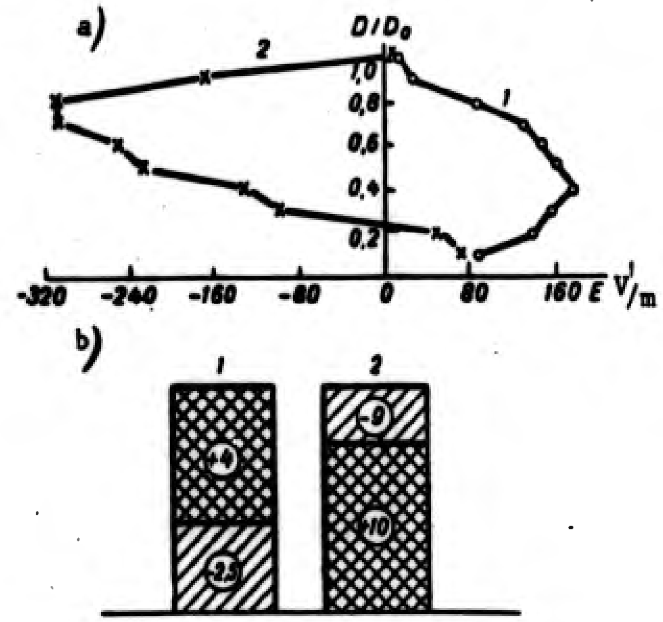

Figure 2.5. Reduced atmospheric electrical field intensity $\underline{E}$ (a) and charge distribution in stratiform clouds (b).

(1) positively polarized clouds (50% of cases; (2) negatively polarized clouds (15% of cases); $\underline{D}_0$ is the cloud thickness, $\underline{D}$ is height above cloud base. Numerals in circles are the electric charge in esu/m^2 in a unit column of the corresponding part of the clouds (from [27]).

components. The electrical fields in these clouds cannot give rise to the appearance of marked induced charges on an airplane.

Electricity of nimbostratus clouds. The electrical structure of nimbostratus clouds of mixed structure is shown schematically in Figure 2.6. The structures of warm clouds and clouds lying entirely in the negative temperature region are approximately similar to the structure shown, although the values of the field intensity and charges of these clouds are somewhat lower (by 1.5 - 2 times) on the average than in the clouds of mixed structure. The characteristic data for these clouds are summarized in Table 2.1. This electrical structure is typical for clouds in the Leningrad region. The cloud droplet charge data were obtained in Tasmania (Australia), the cloud particle charges were measured in European Russia;

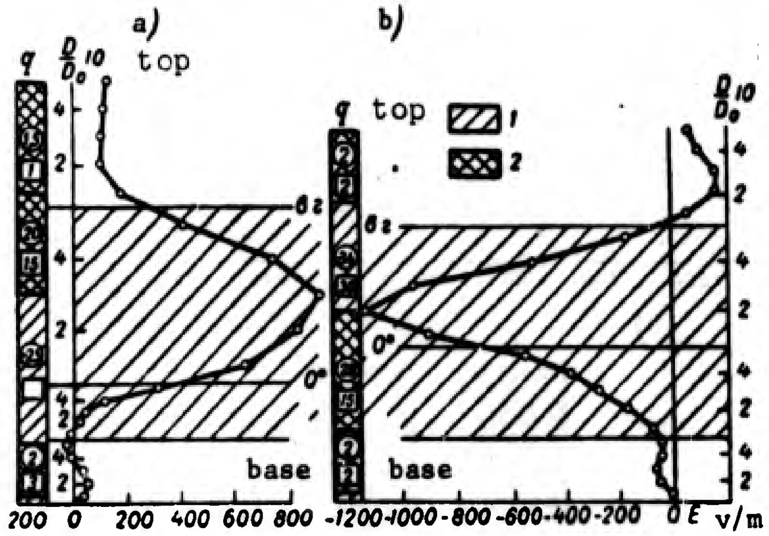

Figure 2.6. Reduced atmospheric electric field intensity E and charge distribution pattern in cumulonimbus clouds with mixed structure.

D_0 is cloud thickness. D is height above cloud base; (a) positively polarized clouds (2/3 of cases); (b) negatively polarized clouds (1/3 of cases); "base" denotes cloud base, "top" denotes cloud top, 0° is the freezing isotherm; (1) regions of negative charge; (2) regions of positive charge; numbers in circles are the electrical charge in esu/m^2 in a unit column of the corresponding part of the cloud, numbers in squares are the space charge density in esu/$m^3 \cdot 10^3$ (from [27]).

including the region around Leningrad. The field intensities, space charges, and precipitation particle charges in these clouds increase on the average as we move toward the south [27]. With increase of the cloud thickness, there is an increase of the average field intensity in the clouds, particularly, the extremal values of the field (Figure 2.7), and the cloud charges increase correspondingly. We should bear in mind that usually the surface measurement data show that the number of positively charged precipitation particles and the number of negatively charged precipitation particles, and also the magnitudes of the charges on oppositely charged particles, are approximately equal and change synchronously in time [53]. In the high altitude measurements, regions are noted in which the drops are charged basically by electricity of the same sign. In each case, such regions develop in clouds yielding heavy precipitation

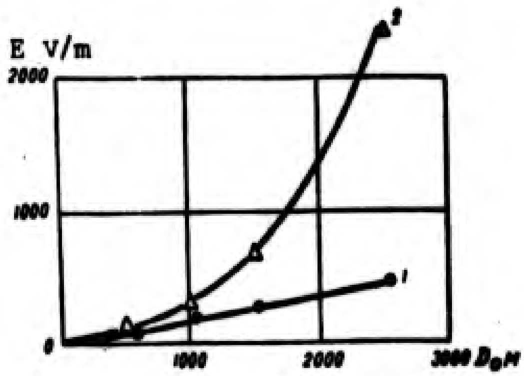

Figure 2.7. Variation of average (1) and maximal (2) value of electric field intensity in cumulonimbus clouds with increase of cloud thickness D.

[57]. The horizontal component of the field intensity is not large and amounts to a small fraction of the vertical component, but at certain points, it may approach the vertical component in magnitude.

The field intensity may reach tens of thousands of V/m in individual clouds or parts of clouds. Usually, there is no marked turbulence in these clouds and there are large drops which give strong radar reflection. Whether this anomalous increase of the field intensity is associated with intensification of the electrification processes or with reduction of the electrical losses in the clouds remains to be clarified.

Electrical structure of cumulus and cumulus congestus clouds. The general scheme of the charge distribution in these clouds is shown in Figure 2.8. In contrast with the structures examined previously, in these clouds there are nonhomogeneous zones with high charge densities and strong electrical fields. The characteristic dimension of these zones is about 120 m; the probability of encountering zones of different sizes may be represented by a log-normal distribution. The sizes of these zones correlate closely with the air current dimensions obtained from accelerograph and thermometer data (Figure 2.9). There is a marked variation of the magnitude of the airplane charge in these same zones.

Both the particle charges [60] and the particle size and concentration spectrum [61] vary quite markedly in the nonhomogeneous zones. Higher space charges are usually associated with zones which are smaller in size. The horizontal components of the field intensity in these zones are very high [59], and approximately equal to the vertical components of the field intensity [49]. In these clouds,

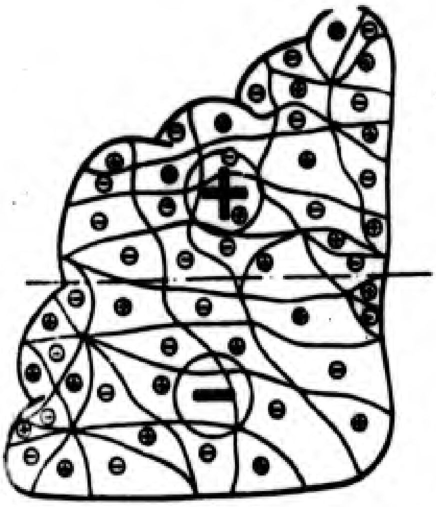

Figure 2.8. Electrical structure of cumulus and cumulus congestus clouds.

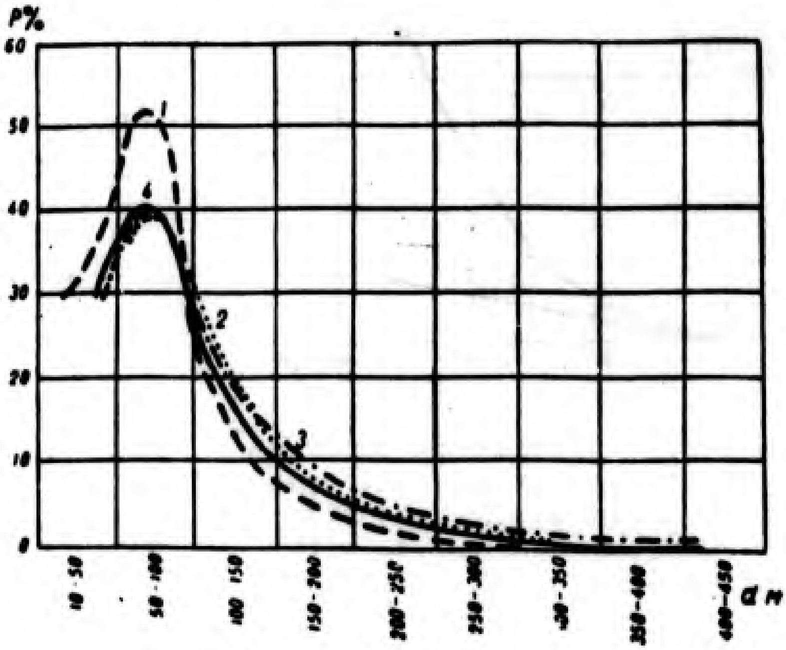

Figure 2.9. Repeatability P of linear dimensions of air currents (1), zones of airplane charge extrema (2), field intensity (3), and temperature (4) [49].

charges of significant density induced on the airplane can occur only in the nonhomogeneous zones. The magnitude of the field intensity in these zones is sufficient for corona currents to develop on the airplane static dischargers. The margnitudes of the induced charges vary quite sharply throughout flight through these clouds. Other conditions being the same, the rate of change of these charges is proportional to the flight speed.

Electrical structure of thunderclouds. The electrical structure of thunderclouds is similar to the structure shown in Figure 2.8. However, there is a region of small positive charge located below the cloud, which is associated with the precipitation region and was first discovered by Simpson [52]. At the same time, we should also note several essential differences between the actual structure of the clouds and that suggested by Simpson. First, the cloud polarity is not constant in time. In the initial stage of cloud development (up to and including the mature stage) a negative-charge field dominates in the upper part of the cloud [62]. Second, some clouds are polarized negatively, even in the mature stage; this usually applies to the shower-type clouds. Third, the presence in the cloud of zones of nonhomogeneous charges, which are a characteristic feature of the active thundercloud; it is in these zones that the lightning discharge develops, which the primary cloud charges can only support. The average electrical characteristics of thunderclouds are shown in Table 2.1.

The average characteristics of the structure depend very strongly on the physical and geographical conditions and the pecularities of the synoptic process, in which the clouds develop (Table 2.2).

Here, we must bear in mind that the charges of individual clouds may differ by an order of magnitude from the average values shown.

TABLE 2.2

ELECTRICAL STRUCTURE OF THUNDERHEADS IN DIFFERENT REGIONS

Latitudes of studies	Average electrical moment of cloud, C · km	Cloud charge C	Distance between principal charges, m	Maximal field intensity created by principal charges, V/m	Reference
60 - 50°N	35	23	1500	400,000	[26]
50°	72	24	3000	140,000	[52]
35°	234	39	6000	45,000	[63]
35°S	200	40	5000	60,000	[64]

The dimensions of the nonhomogeneous zones in thunderclouds are larger than in the cumulus and Cu cong clouds and increase from about

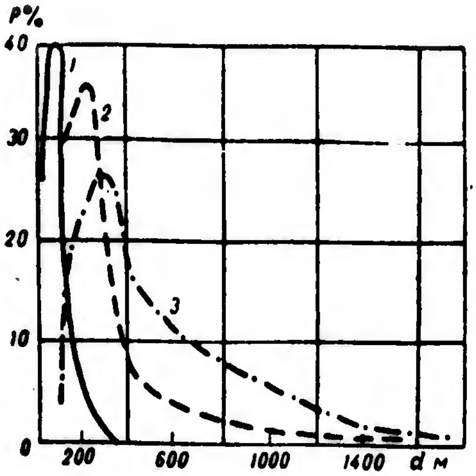

Figure 2.10. Repeatability P of dimensions of charge nonomogeneity zones in cumulus congestus clouds (1), mature thunderheads (2), and decaying thunderheads (3).

400 m in the mature cloud stage to 600 m in the decaying stage. Figure 2.10 shows the zone size distribution [65]. In the cumulonimbus cloud, the electric field intensity in the nonhomogeneous zones is higher than the average field intensity in the cloud, but by a smaller factor than in the Cu cong clouds. The field in the vicinity of the cloud is formed almost entirely under the influence of the primary charges.

Both the primary charge electrical field and the nonhomogeneous zone charge field lead to intense corona discharge from the airplane extremities and induce on the airplane surfaces charges which vary rapidly with displacement of the airplane. The variation of these charges can serve as an additional source of interference. The horizontal and vertical components of the field created by the primary and random cloud charges are approximately equal.

The average current density is very high in thunderclouds: it may reach 10^{-7} A/m^2, and may exceed by several orders of magnitude the current density in clouds of other forms.

The average current above the thundercloud in the latitudes of the Soviet Union is about 0.1 - 0.2 A [67] (which exceed by 1000 times the current density in fair-weather clouds) and reaches 1 A in regions near the Equator [63, 66]. The currents above individual thunderclouds may be an order of magitude higher.

A characteristic property of thunderclouds is the high effective electrical conductivity in their active region. It is still not clear whether this conductivity is associated with the presence of strong ionization or with the action of turbulence and convection. In the first case, the conductivity may decrease the airplane charge markedly; in the second case, it can affect only the currents flowing to the airplane, and may even increase the airplane charge.

We recall that the storm part proper of the cloud — the region in which strong electrification, lightning discharges, strong air currents, high conductivity, and so on develop — occupies only a small part of the overall thundercloud volume [19].

The probability of the appearance of thunderstorm processes is determined to a considerable degree by the magnitude of the losses, i.e., the magnitude of the effective conductivity in the cloud [26]; in clouds in which the losses are small, large charges, high electrical fields, and lightning discharges can occur even if these clouds have relatively small depth and water content and their electrification processes take place very sluggishly.

The lightning repetition frequency in the cloud is also determined by the relationship between the cloud electrification process and the magnitude of the losses in the cloud.

The electrical characteristics of clouds of other forms are presented in Table 2.1; these characteristics are given in greater detail in [27]. The characteristics of altocumulus clouds are also given in [27].

§ 3. Charging of Airplanes in Clouds of Different Forms

Clouds of different forms with different states of aggregation, clouds and precipitation with different particle concentrations and sizes, snowstorms, dust clouds, haze, and the like, which are encountered along the airplane path, charge the airplane differently, even if its flight speed and engine operating conditions remain the same.

The first systematic studies on the connection between airplane charging and meteorological conditions were carried out in the nineteen fifties. The work of Gunn, Hall, and Kinzer [4], and that of Edwards and Brock [73], demonstrated the influence of synoptic conditions on airplane electrification. The basis of the analysis was the fact, established in [4], that airplane electrification increases with the increase of the snowfall intensity. The authors of [4] characterized the probability of snowfalls of different intensity on the basis of the synoptic chart, without devoting any attention to the pecularities of airplane charging in clouds and precipitation of different forms. The connections established in [73] between airplane charging and the synoptic situation were too general a nature.

The results of studies of airplane charging in various clouds were presented in [68], and we shall make use of information from this paper. Data on charging of the Li-2 airplane, obtained as a result of several years of systematic observation in different regions and in different seasons, are presented in [68]. Although the instrumentation lag was less than 0.1 sec., in analyzing the data, the results were averaged over 100-meter layers of the cloud (which corresponds approximately to averaging over a horizontal distance of 4-5 km, during a time of the order of one minute); this averaging, on the one hand, makes it possible to select more characteristic numbers and, on the other hand, excludes from the statistics large deviations from the mean value. The analysis showed that these deviations are small in stratiform clouds, with the exception of the nimbostratus and altostratus clouds; in the altostratus and minbostratus clouds, the extremal values at individual points may exceed the values shown.

The magnitude of the charge acquired by the airplane during flights in clouds of different forms varies. Table 2.3 shows the average and extremal values of these charges in relative units.

TABLE 2.3

CHARGING OF Li-2 AIRPLANE IN CLOUDS OF DIFFERENT FORMS (IN RELATIVE UNITS)

Cloud form	Number of clouds studied	Average airplane charge $\lvert\bar{q}\rvert$	Maximal airplane charge $\lvert\bar{q}\rvert_{max}$	Minimal airplane charge $\lvert\bar{q}\rvert_{min}$
St	100	3	6	0
Sc	334	4	8	2
Ac	172	5	7	2
As	146	10	16	5
Ns	136	13	54	5

We see from Table 2.3 that the average and maximal airplane charges in clouds yielding precipitation are higher than in clouds without precipitation. But, even for airplane flight in clouds of the same form, the airplane is charged differently in different clouds, and the airplane charge changes during flight in the same cloud. Table 2.4 presents information on the distribution of the airplane charge magnitude in clouds, and on clear days. Even on clear days, the charges on the Li-2 airplane are different at different altitudes. In the lower layers of the atmosphere, the average absolute airplane charge magnitude is about $5 \cdot 10^3$ esu; above 2 km it is about $2 \cdot 10^3$ esu. As a rule, the airplane charge magnitude in the clear atmosphere does not exceed in absolute magnitude $20 \cdot 10^3$ esu. The airplane charge magnitudes in clear weather presented in Table 2.4, $(40 - 50) \cdot 10^3$ esu, were obtained during airplane flights in ice crystals with low concentration, in aerosol layers, and similar conditions.

The data of Table 2.4 show that the airplane charge spectrum in precipitating clouds is relatively broad and has no clearly

TABLE 2.4

DISTRIBUTION OF AVERAGE VALUES OF Li-2 AIRPLANE CHARGE IN CLOUDS OF VARIOUS FORMS. LENINGRAD, 1960-65.

cloud form	repeatability	Q, esu·10^{-3}									
		less than −280	−280, −261	−260, −241	−240, −221	−220, −201	−200, −181	−180, −161	−160, −141	−140, −121	−120, −101
clear weather	number of cases										
	percent										
St	number of cases										2
	percent										0,3
Sc	number of cases				2	2	6	6	3	10	11
	percent				0,1	0,1	0,3	0,3	0,2	0,5	0,6
Ac	number of cases							7	2	11	22
	percent							0,6	0,2	0,9	1,9
As	number of cases	25	9	4	16	9	9	11	17	36	81
	percent	1	0,4	0,2	0,7	0,4	0,4	0,5	0,8	1,7	4,0
Ns	number of cases	113	45	30	64	36	117	75	122	230	289
	percent	2,5	1	0,7	1,4	0,8	2,6	1,7	2,7	5,1	6,5

TABLE 2.4 (CON'T.)

DISTRIBUTION OF AVERAGE VALUES OF Li-2 AIRPLANE CHARGE IN CLOUDS OF VARIOUS FORMS. LENINGRAD, 1960-65.

cloud form	repeatability	Q, esu·10^{-3}										
		−100, −81	−80, −61	−60, −41	−40, −21	−20, −0	1–20	21–40	41–60	61–80	81–100	>100
clear weather	number of cases	10	76	208	524	6624	9174	691	174			
	percent	0,1	0,4	1,1	3	37,8	52,4	4,0	1,0			
St	number of cases	5	18	31	85	293	194	17	22			
	percent	0,8	2,7	4,6	12,7	44	29	2,5	3,3			
Sc	number of cases	19	44	95	221	771	475	109	63			
	percent	1,0	2,4	5,2	12,1	42,2	25,9	5,9	3,4			
Ac	number of cases	41	74	86	119	423	325	42	20			
	percent	3,5	6,4	7,3	10,1	36,0	27,7	3,7	1,7			
As	number of cases	205	297	244	221	425	236	94	144			
	percent	9,9	14,2	11,8	10,7	20,3	11,3	4,5	7,0			
Ns	number of cases	521	379	431	383	812	345	155	109	93	54	83
	percent	11,7	8,5	9,6	8,5	18,1	7,7	3,5	2,4	2,1	1,2	1,8

NOTE: Number of cases is the number of airplane charge values, averaged over 100 meters, obtained in reducing the flight data.

defined maximum, in contrast with the stratiform clouds. In comparison with the clear weather spectrum, the airplane charge spectrum in the St, Sc, and Ac clouds is shifted in the direction of negative charges. It should be noted that in clouds of all forms, the airplane can (with differing probability) acquire both negative and positive charges. The probability of negative charging is considerably higher in the coulds being considered here. For a more complete characterization of the charging conditions in clouds, it is convenient to utilize an equation which describes sufficiently and completely the connection between the probability of the presence on the airplane of a charge of a particular sign and the magnitude of the charge itself. The parameters of this equation must depend on the cloud properties. Figure 2.11 shows the connection between the integral probability P of the appearance of a charge greater than a given magnitude and the charge magnitude Q. The form of the curve does not yield a simple representation of the equation which approximates the curve.

Figure 2.12 shows on a semilog scale the curves of the integral probability of the appearance of a charge greater than a given magnitude on the Li-2 airplance in clouds of different forms, obtained from the results of soundings at Leningrad in 1960 - 1965.

The integral probability P is represented well on this scale by the equation

$$\lg P(\%) = \lg 100 - mQ, \quad (2.1a)$$

or

$$\lg P = -m'Q. \quad (2.1b)$$

The higher the probability of large charges, the smaller the coefficient m. The quantity $\gamma = \frac{1}{m}$ characterized the dispersion of the probability curve. The curves of Figure 2.12 are convenient for finding the probability of encountering a charge greater than a given magnitude. By specifying the number of flight hours in clouds

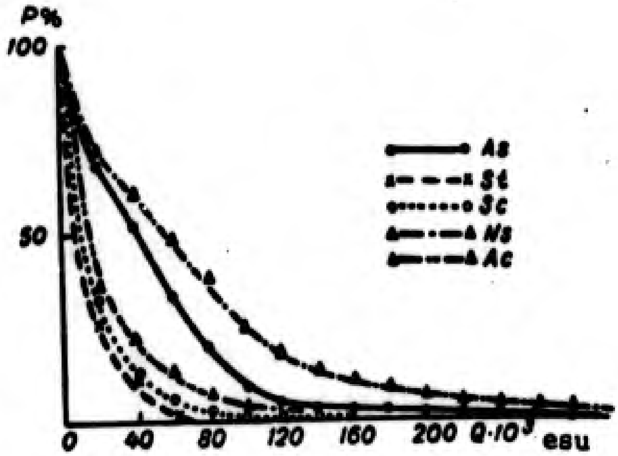

Figure 2.11. Curves of integral probability of finding a charge greater than a given value on the Li-2 airplane (in absolute magnitude) [68].

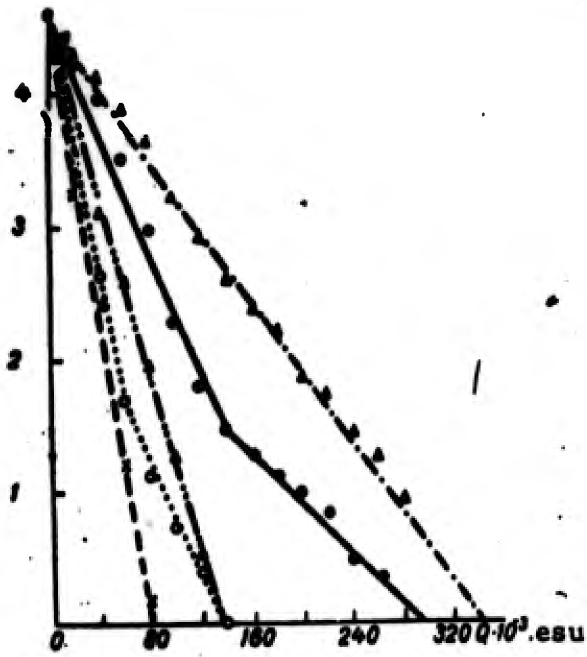

Figure 2.12. Integral probability of a charge greater than a given level on the Li-2 airplane, represented in semi-log coordinates. For notation see Figure 2.11.

of a given form or the distance traveled by the airplane in these clouds, we can with the aid of the curves of Figure 2.12, determine the corresponding flight duration and flight distance for which the airplane charge will exceed the given value.

This linear relationship between the logarithm of the probability of the appearance on the airplane of a charge exceeding a given magnitude and the charge itself permits a very complete characterization of the airplane charging condition in clouds using the quantity γ (or $\underline{m}$), and the magnitude of the average charge acquired. In clouds yielding precipitation, for example, both the average airplane charge and the dispersion are greater than in clouds which do not yield precipitation.

Returning to Figure 2.12, we note that the breaks in the probability curves for the nimbostratus and altostratus clouds for large values of the charges can be related with the appearance of precipitation particles in these clouds and, correspondingly, with the charging conditions characteristic for large particles. An indirect confirmation of this assumption is the fact that the points of the integral probability curves after the breakpoints again fit quite well on a straight line. Moreover, the slope of the curves in the segment after the break is very close to the slope of the curves for nimbostratus clouds, i.e., clouds which yield precipitation for certain. The curves in Figure 2.12 confirm the correctness of the assumptions made above on the reasons for the break in the integral probability curves if about one-third of the altostratus and one-seventh of the stratoculumus clouds carry precipitation particles.

If we calculate the integral probability characteristic for this one-third of the altostratus clouds, it is obviously again represented by a straight line (dashed line in Figure 2.12).

The curves in Figure 2.12 indicate a curious situation: clouds of different forms which are basically characterized using what would seem to be very formal characteristics — external appearance and the altitude at which they are located — have on the average characteristic microstructure features which lead to different probabilities of airplane charging. In those cases, in which clouds whose microstructure may differ significantly (for example, raining and non-raining altostratus clouds) are included in a given cloud form, it appears that it is advisable to construct the integral probability curves separately for clouds having different microstructures.

In many cases, it is convenient to represent the distribution in a form similar to that of the Gaussian distribution, or in the form of a distribution which retains the main Gaussian feasures, but is referred not to the quantities themselves, but to their orders of magnitude — the log-normal distribution. In fact, the airplane charging probability can be approximated satisfactorily by the log-distribution

$$\Phi(Q)=\frac{1}{\lg\beta_g\sqrt{2\pi}}e^{-\frac{(\lg Q-\lg Q_g)^2}{2(\lg\beta_g)^2}}, \qquad (2.2)$$

where Q_g is the geometric mean of the airplane charge; β_g is the standard geometric deviation; $(\lg \beta_g)^2 = \overline{(\lg Q - \lg Q_g)^2}$ — is the mean square deviation of the logarithm of the airplane charge magnitude.

Figure 2.13 shows the integral probability versus charge in probability-logarithmic coordinates. The data in Figure 2.13 can be used to determine in the usual fashion the dispersion β_g of the probability for different clouds, the mean value Q_g of the airplane charge, and the probability of the occurrence of a charge greater than a given magnitude. The values of these quantities are shown in Table. 2.5.

TABLE 2.5

BASIC PARAMETERS CHARACTERIZING INTEGRAL PROBABILITY OF Li-2 AIRPLANE CHARGING IN CLOUDS OF VARIOUS FORMS

Cloud form	$Q_g \cdot 10^{-8}$ esu (geometric mean)	Dispersion $\lg(\beta_g)$	Dispersion $20 \lg(\beta_g)$ dB
Sc	34	0.4	3.4
Cs	47	0.5	4.4
As	55	0.65	5.6
Ns	63	0.82	7.2

We must bear in mind that the data of Table 2.3 are presented for the arithmetic mean values of the airplane charges, and the numbers in Table 2.5 are found from the average values of the logarithm of the airplane charge for the geometric mean values.

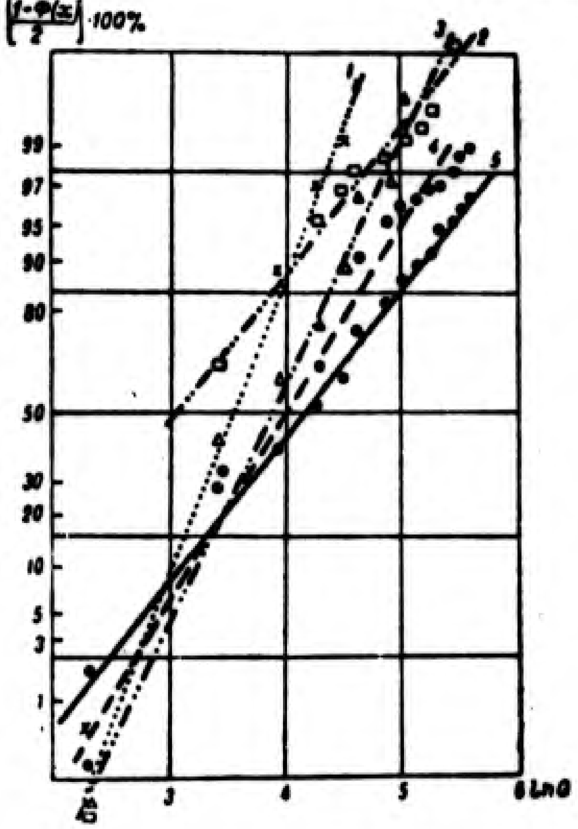

Figure 2.13. Integral probabilities curves of airplane charging above some level (in the integral probability scale), Li-2 airplane, Leningrad, 1960-65. (1) St; (2) Sc; (3) Cs; (4) As; (5) Ns; $\Phi(\underline{x})$ is the probability integral.

The probability that the Li-2 airplane will acquire a charge greater than $2 \cdot 10^5$ esu does not exceed 0.01% in stratus clouds, 0.3% in altostratus clouds, and 9% in nimbostratus clouds.

It is essential to explain the degree to which the charging conditions differ for airplanes of different types of clouds. It is also of interest to compare the charging of airplanes of significantly different types flying at markedly different speeds.

We shall examine the data on charging of the Tu-104B jet airplane in clouds of different forms [69], and compare these data with the data obtained for the Li-2 piston engined airplane.

Figure 2.14 shows the logarithm of the integral charge probability for the Tu-104B airplane as a function of the magnitude of the airplane charge. This relationship is linear, just as it is for the Li-2 airplane. Comparing the curves of Figures 2.14 and 2.12 for the corresponding clouds, we see that the Tu-104B airplane acquires charges which are about ten times greater than those acquired by the Li-2 airplane, i.e., the coefficient $\underline{m}$ in (2.1) is ten times smaller for the Tu-104B, than for the Li-2.

It is somewhat surprising that the ratio of the coefficients $\underline{m}$ for the Li-2 and Tu-104B in clouds of different forms remains nearly constant, while it would appear that the coefficient should be

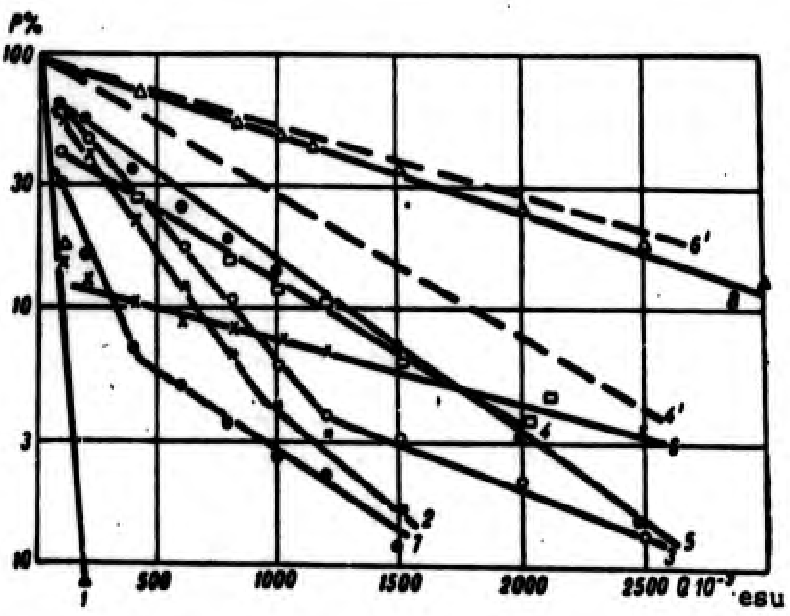

Figure 2.14. Integral probability curves of charge above some level. Tu-104B airplane.

(1) St; (2) Ci developing on anvil of thunderheads; (3) As; (4) non-thunderstorm Cb; (5) Ns; (6) Cu Cong; (7) Ci; (8) upper part of active thunderhead; (4') values of charging probability in non-thunderstorm Cb, without account for charging in gaps between their tops; (6') values of charging probability in Cu Cong, without accout for charging in gaps between their tops.

different in clouds of different forms. The difference between the ratios m in clouds of different forms does not exceed 20 - 30% for these types of airplanes. The potential of the Tu-104B airplane (electrical capacitance equal to 1740 cm), exceeds that of the Li-2 airplane (electrical capacitance equal to 435 cm), by a factor of three, and the field intensity at selected points of the Tu-104B airplane is great by 1.5 times than at the corresponding points of the Li-2 airplane having the same charge. However, we must bear in mind that in clouds of the same type, the charging currents of the Tu-104B airplane must be considerably high than those of the Li-2, since for the same field intensities at the corresponding points of the airplanes the discharging currents of the Tu-104B exceed by several fold the corresponding discharging currents of the Li-2. Still higher ratios of the charge currents of the Tu-104B and Li-2 airplanes are possible in cirrostratus clouds. It should be pointed out that because of the different ceilings of the airplanes, their electrification was compared in Cs clouds lying at different altitudes and having different probabilities of the existence of liquid and ice particles and differing sizes of these particles. The data in Figure 2.14 show a very high probability of high airplane charges in towering cumulus clouds and thunderclouds. During the measurements in the upper part of the towering cumulus and cumulonimbus clouds, the airplane frequently breaks out into gaps between the cloud tops. The observer cannot distinguish these gaps on the recorder tape,and data on clear regions of the atmosphere are unintentionally included. If we exclude those regions where the charge is less than 10^5 esu, then curve 4 should be replaced by curve 4' and curve 6 by 6'. Curve 7 was obtained for cirrostratus clouds which were not associated with thunderstorms, while curve 2 was obtained for the cirrostratus clouds developing from the anvils of thunderclouds. Although the magnitudes of the electrical space charges of the particles in towering cumulus clouds are much lower than in thunderclouds (see Table 2.1), the charge acquired by the airplane in the towering cumulus may be greater than in thunderstorms. We shall return to a discussion of this fact later. Here, we shall simply note that the active part of the thundercloud occupies only a small part of its volume; therefore, the inclusion in the statistics of charging data over the entire flight path in a thunderstorm leads to relatively low values of the airplane charges. If we include in the statistics, only the flight segments in the active parts of the active thundercloud (identified by radar or an instrument measuring the electric field intensity in the clouds), then the values of γ will be higher than in the towering cumulus clouds. On the other hand, curve 8 is plotted from data including information obtained in the very active thundercloud which inflicted tremendous damage on Voronezh on 14/August 1961. Therefore, curve 8 characterizes very active clouds.

The Tu-104B charging relations in different clouds can be presented in log-probability coordinates. As in the case of the Li-2 airplane, this relation approximates the relations obtained quite well.

The basic cloud charge distribution parameters [see (2.2)], corresponding to the log-normal distribution are presented in Table 2.6, the data for which were obtained on the basis of the Tu-104B airplane charge measurements.

The fact that the airplane charging probability is approximated well by a linear connection between the logarithm of the probability and the charge, and by the log-normal distribution, makes it possible to utilize a simple method for comparing the changeability of different airplane types.

TABLE 2.6

BASIC PARAMETERS CHARACTERIZING THE INTEGRAL PROBABILITY OF CHARGING Tu-104B AIRPLANE IN CLOUDS OF VARIOUS FORMS

Cloud form	$Q_g \cdot 10^{-3}$ esu. (geometric mean)	$\lg(\beta_g)$	$20\lg(\beta_g)$ O/B
St add Sc	1	0.63	13
Ci and Cs	60	0.66	13
As	30	0.59	12
Cu cong.	240	2	40
Cb inc.	320	1.06	21

This leads to two very important conclusions:

1. Data on the charging of an airplane of one type (Li-2, for for example) obtained in different clouds can be converted for airplanes of other types, if a small number of parallel measurements

are made of the charges on the reference airplane and the airplane of the other type.

2. On the basis of detailed data on the charging of an airplane of one type (the Li-2, in our case) under different conditions, we can obtain a very complete climatological pattern of the peculiarities of the charging of airplanes of any type in clouds of different forms, existing in different physical and geographical regions, in different synoptic conditions, at different latitudes, and in different seasons. For this purpose, it is necessary to study the laws governing airplane charging, both those associated with the charging characteristics in clouds at various times of the year, in different regions, and so on; and also, those associated directly with the cloud characteristics.

§ 4. Airplane Charging in Clouds at Different Latitudes

At the beginning of the chapter we noted that such electrical characteristics of clouds as the space charges, electric field intensity, and individual particle charge have a tendency to increase as we approach the equator. The increase of these characteristics is related with corresponding changes of the microphysical characteristics of the clouds as we move into the southerly latitudes. Therefore, it is natural to expect changes in the airplane charging conditions in the clouds which develop in different latitudes.

The data in Table 2.7, obtained during the 1958 - 1965 period, illustrate this difference in charging.

We see from Table 2.7 that the magnitude of the average airplane charge in the clouds increases by a factor of two to five in the Tashkent region in comparison with the airplane charge at Leningrad.

TABLE 2.7

AVERAGE ABSOLUTE CHARGE OF Li-2 AIRPLANE (esu · 10^{-3})
IN CLOUDS OF DIFFERENT FORMS [68]

Region of study					
Leningrad (60° C)	15 (100)	20 (334)	25 (172)	50 (146)	65 (136)
Kiev (50° C)	18 (73)	—	35 (48)	90 (76)	80 (73)
Tashkent (40° C)	14 (34)	35 (82)	60 (81)	200 (87)	250 (69)

Along with the tendency toward a higher airplane charge in the clouds in the lower latitudes, we also note come increase of the coefficient γ, characterizing the dispersion.

It should be pointed out that in the regions studied, the clouds developed under the influence of different physical and geographical factors. The coastal location of Leningrad, and the closeness of the desert and moutain regions to Tashkent,affected the values of the airplane charge (Table 2.7). However, the lack of suitable studies to date makes it impossible to identify the effect of the physical and geographical factors in pure form; therefore, we must limit ourselves to the ideas formulated in the heading of this section.

The data of Table 2.7 can be extrapolated to other latitudes which differ markedly in their physical and geographical characteristics to even a lesser degree. For example, in the far North and in the Arctic—regions with extensive ice crystal clouds in which the airplane will be charged very strongly—the airplane charges may again increase. We can expect that there will be characteristic airplane charging peculiarities in the clouds of different latitudes and in the ocean and desert regions, where the cloud microstructure may be quite very specific.

§ 5. Seasonal Characteristics of Airplane Charging in Clouds

It appears that the airplane charging characteristics in different seasons are due to two factors which act in opposite directions. On the one hand, the cloud water content is lower in the winter [70], which leads to reduced airplane charging. On the other hand, the probability of the occurrence of solid particles in the clouds increases in the winter [70], and airplane charging is more intense in ice-crystal clouds (for the same water content), than in water-droplet clouds [5], (see Table 2.10). The magnitude of the Li-2 airplane charge during flight in snow reaches $(500 - 600) \cdot 10^3$ esu [68]. The degree of the influence of each of these two factors is different for different latitudes and for clouds at different levels. Therefore, airplane charging may increase in clouds of certain types as we go from summer to winter, while in clouds of other types, conversely, the charging may decrease.

Table 2.8 shows how the Li-2 airplane charge changes in different seasons in clouds of the same type.

TABLE 2.8

AVERAGE ABSOLUTE CHARGE OF Li-2 AIRPLANE (esu $\cdot 10^{-3}$) IN CLOUDS IN DIFFERENT SEASONS [68]

cloud form	Leningrad		Kiev		Tashkent	
	summer	winter	summer	winter	summer	winter
St	7 (11)	16 (65)	35 (3).	15 (51)	—	15 (35)
Sc	27 (40)	18 (140)	—	---	—	33 (81)
Ac	22 (87)	25 (35)	32 (25)	28 (17)	27 (11)	77 (70)
As	62 (41)	36 (63)	80 (39)	50 (37)	124 (3)	225 (84)
Ns	69 (30)	56 (73)	80 (9)	70 (36)	—	250 (69)

In the Leningrad region, the magnitude of the average absolute charge was higher in the winter than in the summer in all clouds, other than the stratus and altocumulus types. In the Kiev region, the airplane charge was lower in the winter than in the summer in all cloud types. However, the difference between the charge in the winter and in the summer in the altocumulus and nimbostratus clouds was small. In the stratus clouds in the Leningrad region the charge in the winter was half that in the summer, while in the Kiev region the charge in these clouds in the winter was half the summertime value. In the altostratus clouds the average airplane charge decreased by a factor of 1.5 from summer to winter in Leningrad and Kiev, while at Tashkent the charge nearly doubled. If the assumptions stated in the beginning of the section are valid, then in the altostrutus clouds the airplane charge reduction due to the reduction of the water content and the associated change of the microphysical characteristics is greater than the charge increase due to the relative increase in the number of solid particles at Leningrad and Kiev; at Tashkent the effect of the second factor is weaker. It is obvious that identification of the nature of the seasonal characteristics is closely related with the development of studies of cloud microphysics.

§ 6. Correlation Between Airplane Electrical Charge and Cloud Thickness

The variation of the absolute magnitude of the charge as a function of cloud thickness is shown in Table 2.9.

We see from Table 2.9 that at a given station the magnitude of the airplane charge, in general, increases with an increase of the cloud thickness. In individual cases, the magnitude of the airplane charge in the thicker clouds may be greater by an order of magnitude than in thin clouds of the same type. The extremal values of the airplane charge increases with an increase of the cloud thickness more rapidly than the average values [9].

We recall that, on the average, there is an increase of the water content and particle concentration in clouds with an increase of their

TABLE 2.9

AVERAGE ABSOLUTE AIRPLANE CHARGE (esu · 10^{-3}) AS A FUNCTION OF CLOUD THICKNESS. 1958 - 1965

cloud form	station	cloud thickness, m			
		0–200	200–500	500–1000	>1000
St	Leningrad	14 (12)	11 (52)	18 (26)	30 (10)
	Kiev	14 (8)	13 (40)	26 (22)	42 (3)
	Tashkent	2 (1)	8 (24)	29 (7)	40 (2)
Sc	Leningrad	13 (27)	16 (167)	20 (104)	28 (36)
	Tashkent	13 (11)	18 (45)	54 (21)	136 (5)
Ac	Leningrad	17 (23)	17 (81)	28 (42)	37 (26)
	Kiev	30 (9)	30 (27)	50 (12)	—
	Tashkent	42 (24)	49 (35)	66 (18)	183 (4)

cloud form	station	0–500	500–1000	1000–2000	2000–3000	3000–4000	4000–5000	>5000
As	Leningrad	24 (36)	58 (29)	60 (41)	55 (26)	74 (14)	—	—
	Kiev	77 (52)	86 (8)	102 (10)	209 (5)	311 (1)	—	—
	Tashkent	127 (29)	181 (25)	238 (24)	360 (7)	300 (2)	—	—
Ns	Leningrad	19 (3)	28 (11)	50 (23)	57 (28)	74 (24)	68 (27)	87 (20)
	Kiev	15 (2)	40 (16)	46 (22)	90 (10)	95 (8)	167 (9)	140 (6)
	Tashkent	133 (11)	170 (16)	160 (22)	380 (15)	360 (3)	—	462 (2)

NOTE: Number of clouds studied is shown in parentheses.

thickness [70]. Obviously, the tendency for an increase of the airplane charge is connected with this situation. In analyzing the influence of the "climatological" factors, we must always take into account the microphysical characteristics of the clouds. Comparison of the data of Tables 2.9 and 2.7 leads to the conclusion that the thickness of clouds of corresponding type may even decrease as we move toward the south, while charging in clouds of a given type increases regularly with reduction of the latitude. Therefore, the correlation between airplane charge and cloud thickness must be made with account for the physical geographical factors.

§ 7. Cloud Phase State and Airplane Electrical Charge. Connection Between Airplane Electrification and Icing

The role of the cloud phase state in airplane electrification can be illustrated by the data of Table 2.10, from which we see that airplanes charge less strongly in water-droplet clouds than in clouds of mixed structure and in clouds yielding solid precipitation.

TABLE 2.10

DEPENDENCE OF AIRPLANE CHARGE (esu · 10^{-3}) ON CLOUD STATE OF AGGREGATION (WITH RESPECT TO FALLING PRECIPITATION) [68]

cloud form	clouds: water droplet	producing solid precipitation	mixed	water droplet	producing solid precipitation	mixed	water droplet	producing solid precipitation	mixed
	Leningrad			Kiev			Tashkent		
Sc	17 (253)	48 (5)	26 (43)	—	—	—	24 (2)	75 (13)	98 (2)
Ac	20 (106)	38 (7)	28 (41)	—	—	—	—	93 (33)	—
Ns	50 (56)	76 (49)	80 (68)	72 (8)	177 (6)	85 (12)	61 (2)	265 (40)	360 (13)
As	33 (34)	52 (75)	60 (49)	—	—	—	—	377 (62)	—

NOTE: Number of clouds studied is shown in parentheses.

The strongest charging takes place in clouds whose tops are located at temperatures below -10° C. It should be noted that the factor leading to the electrification change may be both the icing-up of the airplane and the appearance of the solid phase, and the rearrangement of the droplet spectrum which is characteristic for the supercooled clouds [70].

In order to find the connection between the airplane charge magnitude and the temperature distribution in the clouds, we plotted the airplane charge as a function of the reduced (relative) height

D/D_0 (Figure 2.15), where we took as the unit intervals (D_0), the segments from the ground up to the base of the clouds, from the base to the 0° C isotherm; from the 0° C isotherm to the -10° C isotherm, from the later altitude to the top of the clouds and from the cloud top to the maximal sounding altitude (6000 m). The charge is shown as a function of height in nimbostratus clouds for three sounding stations. For each station, we calculated the airplane charge magnitude on the basis of averaged data on airplane charging in several clouds studied.

In addition to the previously noted fact that the airplane charge in clouds increases, in general, as we move toward the lower latitudes, the curves of Figure 2.15 show that the highest airplane charge occurs at altitudes where the temperature is below freezing.

We note that the airplane charge is very small in the rain below the cloud and increases markedly upon entry into the cloud. In combination with the fact that the radar reflectivity is nearly constant from the ground up to the freezing isotherm (i.e., the rain particle spectrum changes very little with altitude), this situation indicates clearly that airplane charging in nimbostratus clouds (just as in non-precipitating clouds) is basically connected with the action of the cloud particles. This explains the similarity of the charging of airplanes of different types in clouds of different form, since the balloelectric effect — electrification of particles during their breakup — shows up only for large drops, depends significantly on the airplane speed, and therefore does not play an essential role in the clouds.

In order to define more accurately the temperature region in which the charging is most intense, we isolated the temperature region 0, -10° C (Figure 2.15). We see from the curves of Figure 2.15 that at Tashkent the region of maximal charging was located between the isotherms 0, -10° C, while in Leningrad and Kiev, it was located at a higher altitude (up to the -15° C isotherm). As a rule, airplane

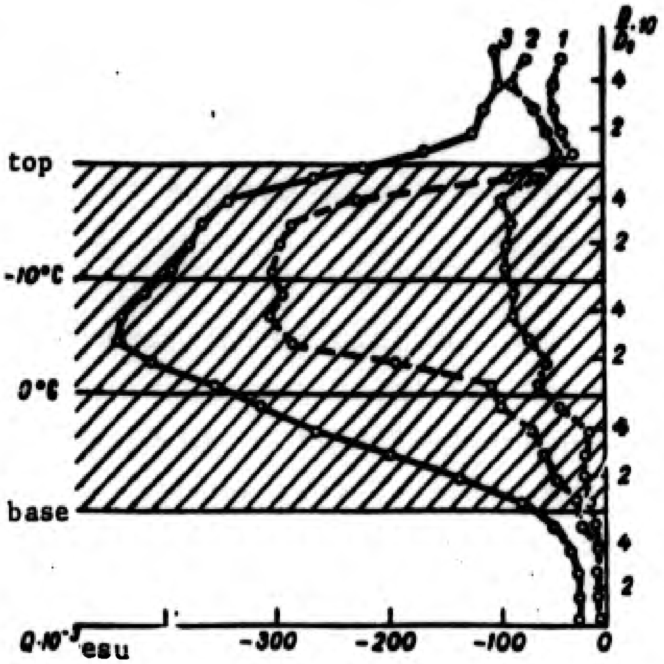

Figure 2.15. Airplane charge in Ns clouds in temperature range 0, -10° C. $\underline{D}/\underline{D}_0$ is relative height in the corresponding layer; "base" and "top" are cloud base and top; (1) Leningrad (18 clouds, 1960 - 1962); (2) Kiev (7 clouds, 1960 - 1963); (3) Tashkent (10 clouds, 1960 - 1962).

charging above the clouds is associated with airplane flight through bands in which ice crystals are falling from clouds at still higher altitudes.

Airplane charging measurements in nimbostratus clouds, made together with measurements of the atmospheric field intensity, make it possible to identify the role of cloud space charges in airplane electrification.

We have noted previously (see Figure 2.6 and Table 2.1) that the nimbostratus clouds are polarized: their upper and lower parts have space charges of opposite signs. At the same time, the airplane charge does not change sign in these clouds (see Figure 2.15). Consequently, the cloud space charge does not have any marked effect on the airplane charge. This becomes still clearer from a comparison of the charges of the cloud and the airplane in the cloud. Figure 2.16 shows the distribution of the field intensity and space charges in a "typified" Ns cloud [27], and also the values of the airplane charge. It is obvious that the airplane was charged negatively all the time, regardless of the sign of the cloud charges.

Returning to the reasons for airplane charging in a cloud, we note that the charging increase above the freezing isotherm may be ascribed to one of four factors: (1) change of the droplet spectrum; (2) appearance of ice particles at these altitudes; (3) the strong electrifying action of wet snow at these altitudes; (4) the onset at

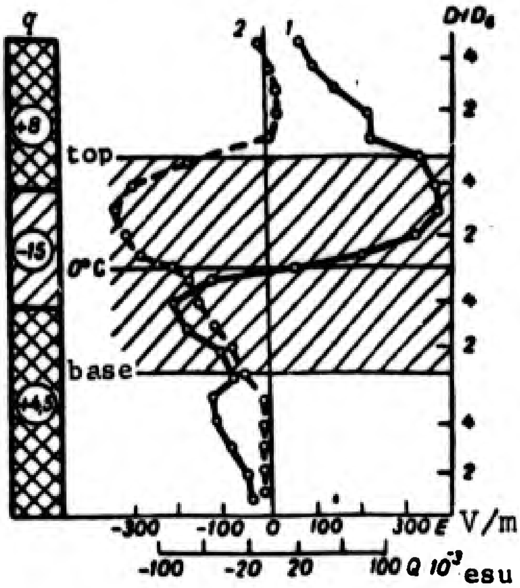

Figure 2.16. Effect of space electric charges in Ns clouds on airplane charge.

(q) altitude distribution of space charges in cloud; (1) electric field intensity versus height D/D_0; (2) airplane charge Q (Leningrad, 1958 - 1959, 30 cases).

these altitudes of electrification on the iced-up airplane, whose surface properties are changed as a result of the appearance of the ice layer.

The analysis of the contribution of all these factors to airplane electrification can be made on the basis of very general considerations. We shall return again to the evaluation of the role of the particle spectrum change in Chapter 4. It will be shown at the end of this chapter that the appearance of ice particles usually alters the sign of the airplane electric charge and makes it positive. Since the airplane was electrified negatively in the clouds studied, we can assume that the presence of ice crystals in the region of the 0, -10° C isotherms could lead only to a reduction of the airplane charge. Intensification of airplane electrification at temperatures of -7, -9° C was also noted previously in [6]. The amount of charge transferred per unit mass of the colliding particles in the temperature range -5, -10° C can increase by a factor of ten in comparison with electrification at a freezing temperature and can decrease from the maximum to a few tenths of the peak value at temperatures below -10, -15° C [6] (see Figure 2.25).

In order to find the degree of influence on the airplane charge on the third and fourth factors, whose effect must increase simultaneously in the temperature range from 0° C to -10, -15° C, we can compare airplane charging in clouds in which airplane icing is noted and in clouds in which there is no icing. Figure 2.17 presents

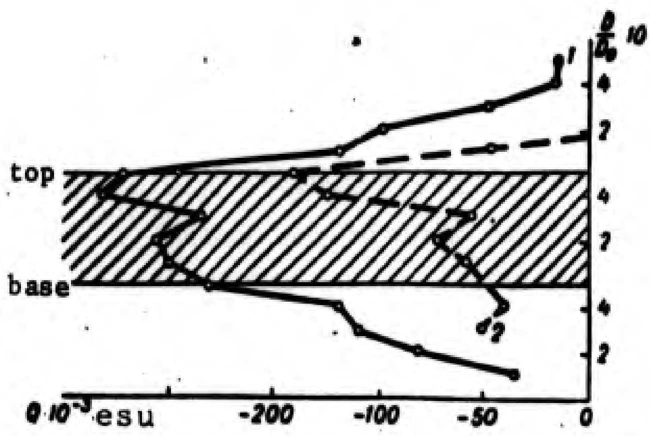

Figure 2.17. Airplane charging with and without ice formulation in Ns clouds.

"top" and "base" denote top and base of clouds; (1) airplane iced up (70 clouds); (2) no ice formation (40 clouds). Leningrad, 1958 - 1962.

curves which show that in Ns clouds in which icing is noted, the airplane charge is higher. A similar effect is also noted in Cs clouds and in Ac clouds. High airplane charging is observed in As clouds without airplane icing (Table 2.11). A change of airplane charging during icing was also noted in [6].

The different sign of the correlation between icing and charging in clouds of different types may be associated with the difference in their microstructure.

TABLE 2.11

RATIO (n) OF AVERAGE CHARGES OF ICED AND CLEAN AIRPLANE

Cloud form	St	Sc	Ac	As	Ns
n	1.1	1.5	1.2	0.7	2

The increase of the charge during airplane icing takes place under conditions in which a considerable part (0.7 - 0.8) [70, 71] of the drops colliding with the airplane "stick" to the airplane surface and cannot have any effect on airplane electrification. It may be that the increase of the droplet fraction adhering to the airplane leads to a reduction of charging during ice formation in the As clouds. Further studies are necessary to obtain the answer to this question.

Thus, the airplane charging characteristics above the freezing isotherm may be ascribed, first, to the intensification of the electrifying capability of the particles at these altitudes and, second, to the changes of the charging conditions during icing of the airplane.

Still unclear is the question of the degree to which the airplane charging increase, which occurs in the cloud zone where there is wet snow, leads to the appearance of icing, as a result of the action of the electrical forces which facilitate spreading of the droplets during impact on the surface of the charge airplane and promote freezing of the droplets [18, 24]. The resolution of this question requires additional experimentation. We should point out, it is true, the indirect circumstantial evidence that the most intense natural electrification of the cloud and precipitation particles takes place in the 0, -10° C isotherm range. However, according to the data of Pruppacher [18], the probability of supercooled particle freezing increases markedly in strong electric fields. During flights in clouds of many types, the field intensity at the leading edges of the wings and other extremities may increase under the influence of the airplane charge to values of the order of 10^6 V/m, which are sufficient to increase the freezing probability. To this, we must add that the probability of charged particle freezing also increases in strong fields.

The increased airplane charging in the region lying between the 0, -15° C isotherms may have a marked influence on the probability of lightning striking the airplane. According to NACA data, the airplane lightning strike zone in clouds is concentrated primarily in the cloud region bounded by the 0, -10° C isotherms (Figure 2.18). We recall that according to Simpson [52], the region of separation of the basic charges and, consequently, the region of highest electric field intensities in the cloud, coincides with this region. But lightning discharges even those which arise in the region of the strongest fields, pass through the entire thundercloud, and the probability that an airplane entering a thundercloud will encounter lightning discharges depends very little on the flight level in the cloud.

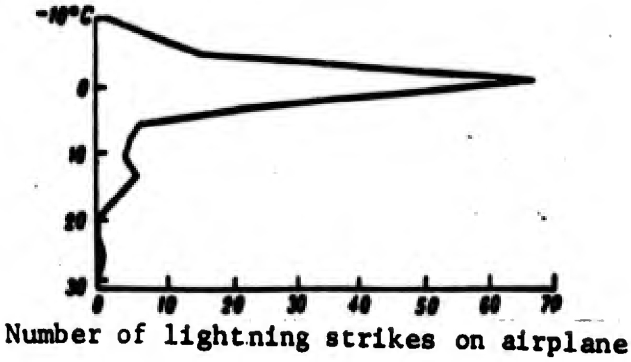

Figure 2.18. Probability of airplane lightning strikes in thunderheads (NACA data).

Consequently, the increase noted in Figure 2.18 of the lightning strike probability is associated, as noted previously for active thunderclouds, on the one hand with the influence of the charged airplane on the lightning generation probability, and on the other hand with the effect of the airplane on the trajectory of lightning strokes which have already developed. In low-activity thunderclouds, we can expect that the airplane charge will have an effect on the lightning generation probability.

§ 8. Nonuniform Zones in Clouds and Their Effect on Airplane Charge Variation

The microphysical characteristics of clouds are variable not only vertically, but also horizontally. The convective clouds — towering cumulus and cumulonimbus — are particularly nonuniform in the horizontal direction. These nonuniformities have an effect on the electrical structure of the convective clouds (see Figure 2.8). The airplane charge also experiences significant variations in these nonuniform zones, at times dropping to zero and returning to the extremal values over a distance of a few hundred or even a few tens of meters. The charge rate of change on a modern high-speed passenger airplane may exceed 2,000,000 esu/sec, even on an airplane flying at a speed of 300 km/hr. This rate exceeds 500,000 esu/sec [6]. These charge variations modulate, in particular, the corona currents from the static dischargers and create additional interference.

The largest nonuniformities are encountered in towering cumulus clouds. The repeatability of the dimension of the airplane charge extrema zones is shown in Figure 2.9 from the data of measurements made in 140 clouds. In order to be certain that the airplane charge relaxation time has no marked effect on the measured dimensions of the charge nonuniformity zones, we should examine the distribution shown in Figure 2.9 of the dimension of the vertical air currents in the clouds studied, the electrical field extrema zones, and the temperature pulsations (studies made by Vul'fson [72]). The similarity of all the curves indicates that the noted airplane charge variations are determined by the variation of the cloud properties — the variation of the droplet spectrum [61], and water content in the individual air currents, which penetrate thunderclouds.

The small influence of the relaxation time is also confirmed by direct estimates. If an airplane is flying in a homogeneous cloud, its charge becomes steady relatively rapidly. The electrical capacitance of the modern airplane C = 500 - 2000 cm; the resistance of the exhaust gas jet "connected" between the airplane and the atmosphere $R_{esu} = 10^9$ cm (see Chapter 3). Thus, the airplane charge relaxation time, equal to $\frac{1}{4\pi\lambda_{ef}} = CR_{ef}$ [see (3.19a)], amounts to about one second.

If the airplane charge reaches a magnitude such that the corona dischargers operate, then the "leakage resistance" connecting the airplane electrically with the atmosphere is still less (see Chapter 3) and may decrease to a value of $10^8 - 10^7$ Ohms. In other words, the relaxation time in this case will not exceed 0.1 sec or even 0.01 sec. Since the dimensions of the cloud mesononuniformities usually exceed 50 - 100 m, while the speeds of the airplanes used did not exceed 250 m/sec, we can assume that the measured zone dimensions were determined by variation of the cloud microphysical characteristics.

Nonuniformity zones of somewhat larger dimensions are observed in thunderclouds (see Figure 2.10) [65]. While in the towering cumulus clouds the most probable dimension of the electrical charge extremum zone was 50 - 100 m, in mature thunderclouds the most

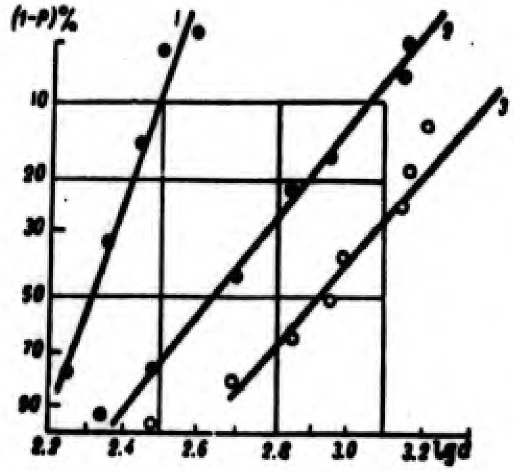

Figure 2.19. Integral probability $\underline{P}$ of the occurrence of mesononhomogeneities of given dimension $\underline{d}$ versus lg $\underline{d}$.

(1) Cu cong; (2) mature thunderheads; (3) decaying thunderheads.

probable dimension of the extremum zone increases to 200 - 400 m, and in the decaying thunderclouds this dimension reaches 400 - 600 m. The data for the mature stage were obtained in very active thunderclouds, in particular, in the thundercloud mentioned previously occurring on 14/ August 1961, which is described in all the modern books on aviation meteorology as one of the most active thunderclouds observed over the territory of the USSR.

The relations shown in Figure 2.10 can be approximated quite well by the log-normal distribution [65]. Figure 2.19 shows the integral probability of the appearance of a zone of length greater than a given value as a function of the logarithm of the zone length. We see from the curves of Figure 2.19 that the dependence is nearly linear. Knowing the probability of the occurrence of an airplane charge greater than a given value and the probability of the existence of a zone of given size, we can find the probability that the airplane will acquire a charge of a given magnitude in the course of a given time interval.

In clouds of other type, the dimensions of the airplane charge nonuniformity zones are considerably larger than those considered in the present section.

§ 9. Airplane Charging and Cloud Microstructure

So far we have considered the influence of the meteorological factors which affect airplane charging indirectly. This analysis was necessary in view of the fact that meteorology in general, and climatology in particular, have available relatively large observational archives and operational data characterizing cloud types, percent of cloud skycoverage, cloud thickness, and the like. Thus, in order to find, say, the length of time an airplane will have a charge greater than a given value (during flight in an overcast) we use the climatological data on the clouds, supplemented by the information presented in the present volume on the airplane charging characterisitics under the particular conditions. Unfortunately, complete meteorological data are not available on the factors which affect directly the airplane charge — the cloud microphysical characteristics. However, to identify the physical processes leading to airplane charging, it is necessary to investigate the effect of cloud microphysical characteristics on the charge acquired by the airplane.

Airplane charging studies in snowfall and rain, carried out in in the 1940's, showed that charging is more intense in snowstorms [6]. If we take the magnitude of the charge acquired by the airplane in moderate rain as unity, then in a light snowstorm this value is 3.5; in a moderate snowstorm the value is 4, and in a heavy snowstorm it is 8 [6]. The magnitude of the airplane charge may also change markedly as a function of the shape of the snow crystals. It is noted in [6] that the most intense charging occurs during encounter with snow pellets and snow crystals in the form of hexagonal plates. A marked influence of the snowflake form on electrification intensity was also noted by Schaefer [74] (see Table 2.13); however, he was not able to establish any clear quantitative connections between snowflake shape and electrification intensity. An important result of Schaefer's study [74] was the proof that the charge carried by the snowflakes prior to collision with the body is much less than the charge given up by the snowflakes after collision and separation (Table 2.12). The measurements were made on models in a special tunnel in which the snowflake velocity reached 100 km/hour.

TABLE 2.12

CONNECTION BETWEEN AVERAGE CHARGE q_1 CARRIED BY ONE GRAM OF SNOW CRYSTALS AND THE CHARGE q_2 ACQUIRED BY A BODY FOR FRICTION AND FRAGMENTATION OF ONE GRAM OF SNOW [74]

sequential number of snowfall studied	tempera-ture, °C	water content, g/m^3	amount of snow impacting per second, g/sec	q_1	q_2/q_1
1	−7,2	0,094	0,019	0,66	91
2	−7	0,188	0,038	0,25	120
3	−7,8	0,176	0,0358	0,11	137
4	−1,1	0,141	0,0286	0,46	18,2

We see from Table 2.12 that the charge given up to the body is 20 - 140 times greater than the charge of the snowflakes when in free flight. Schaefer notes that for the higher collision velocities which are characteristic for the airplane the electrification was still more intense, i.e., the ratios shown in the last column of Table 2.12 would be still larger. Later MacCready and Proudfit [75] showed that even the sign of the airplane charge may differ from the sign of the precipitation particle charge, both solid and liquid.

To understand the mechanism of charge transfer by the cloud particles to the airplane, it is very useful to examine the connection between the airplane charge and the cloud water content under simpler conditions — in pure water clouds. Two basic processes of cloud water separation from the airplane are possible: 1) the water droplets can rebound from the airplane after striking it, transferring the corresponding charge to the airplane; 2) upon striking the airplane the water droplets may wet the airplane surface, and the airstream will then tear off the water film which is formed.

In the first case, the connection between the airplane charge and the water content may be very indefinite, since the charging rate will be determined by the form of the droplet spectrum. Obviously, on the average there is a dependence between the characteristics of the cloud particle spectrum and the cloud water content

[70]. However, there may not be any such dependence in individual specific clouds, or particularly at different points of the same cloud.

In the second case, the airplane charging is determined basically by the cloud water content and depends very little on the droplet spectrum. The droplet spectral composition will affect the amount of water impinging on the airplane only as a result of the different conditions for capture by the airplane of droplets of different diameters. As a resultof this, the amount of water striking the airplane will constitute only some fraction of the total amount of water which would strike the airplane if the capture coefficients of all the droplets were equal to one. Usually, the large drops, whose capture coefficients are relatively large, make the largest contribution to the water content. Therefore, the connection between the airplane charge and the water content should show up clearly in this case. The influence of the spectral composition may not be so characteristic, since the "captured" water content is defined basically by the large-drop part of the spectrum. It is obvious that both of these processes exist at the same time, but whichever is clearly dominant will serve as the connection between the airplane charge and the cloud water content.

By means of frequent measurements of the water content during Li-2 flights in Cs and Ns clouds and synchronizing the times when the water content samples were taken with the corresponding segments on the airplane charge recording tape, we obtained the relation represented by the points in Figure 2.20 [68]. It follows from the point pattern that although a general tendency toward an increase of airplane charging with increase of the water content is observed, this connection shows up very weakly in the individual measurements.

If we examine the airplane charging characteristics in small-droplet clouds, cloud with droplets of intermediate size, and in large-droplet clouds (the identification is based on microphotography

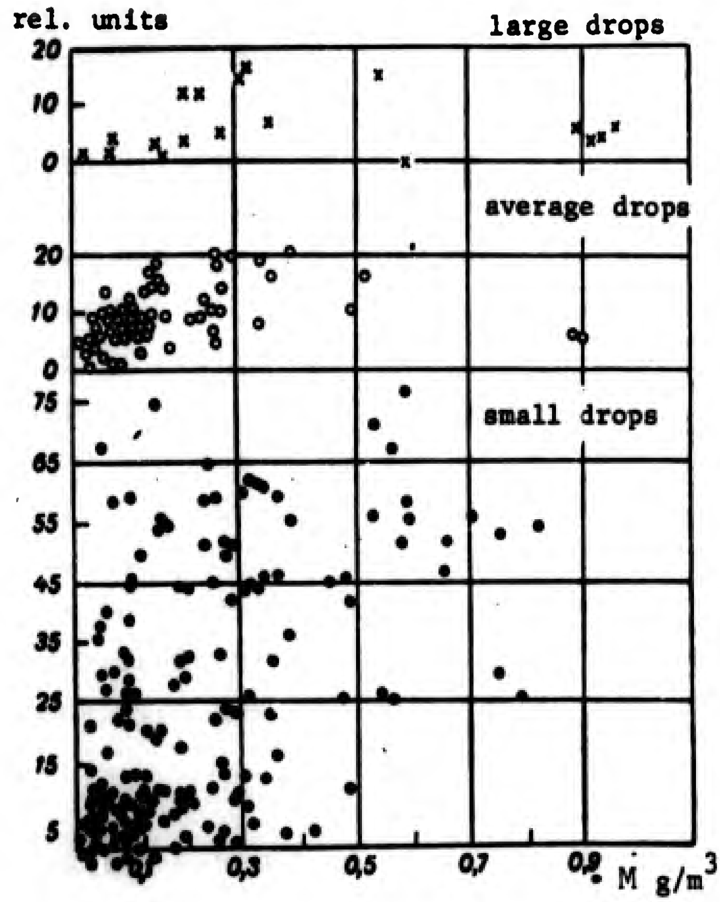

Figure 2.20. Correlation of instantaneous values of cloud water content M and airplane charge Q [68].

data), we find that for the same water content the most intense charging is noted in the small-droplet clouds, charging is less intense in clouds with droplets of intermediate dimensions, and still less intense in clouds with large droplets. At the same time, the tendency for growth of the airplane charge with increase of the cloud water content shows up more clearly for clouds with smaller droplets.

Specifically, the data of Figure 2.20 show that the electrification associated with the balloeffect is small, otherwise the electrification would increase with increasing droplet size and with increase of the water content of the large droplet clouds. The very weak correlation between airplane charge and cloud water content, obtained from the results of individual measurements, and also the stronger electrification for the same water content in the small-droplet clouds, make it possible to conclude that airplane charging in finely dispersed clouds is created primarily by particles impacting on its surface and rebounding from the surface at the same point. The possibility of elastic rebound of small droplets during impact was confirmed by the experiments of Keily and Millen [76], which show that for subsonic speeds, water droplets of diameter from 2 to 60 microns impinging on a metallic obstacle experience elastic collision. If the spectrum in the clouds is subject to small variations, then the connection between airplane charge and cloud water content becomes clearer. This is illustrated by the curves of Figure 2.21a, which shows the results of measurements of cloud water content and airplane charge during flight in the same cloud, and also Figure 2.21b, which shows the correlation between airplane charge and cloud water content in this flight [68].

The idea of charging by elastic impacts may seem surprising to the individual flying in an airplane in clouds. Actually, streams of water seem to pour over the windshield when flying in warm clouds with high water content; actually, these same thin streams flow over the airplane surfaces during flights at speeds up to 200 - 300 km/hr. It would appear that the electrification mechanism associated with separation of water with an "indifferent" spectrum should act on the airplane. In reality, the answer to the question of whether or not the airplane surface is wetted by the water does not resolve the question of what water separation mechanism electrifies the airplane. Actually, as we shall see in detail in Chapter 4, the charge q_i acquired by individual particles during separation is proportional to the particle volume and therefore, to the particle radius r_i.

$$q_i = \alpha r_i, \tag{2.3}$$

where α is the coupling factor between the charge acquired by the particle and its radius; α depends on the properties of the colliding surfaces and the particle separation velocity.

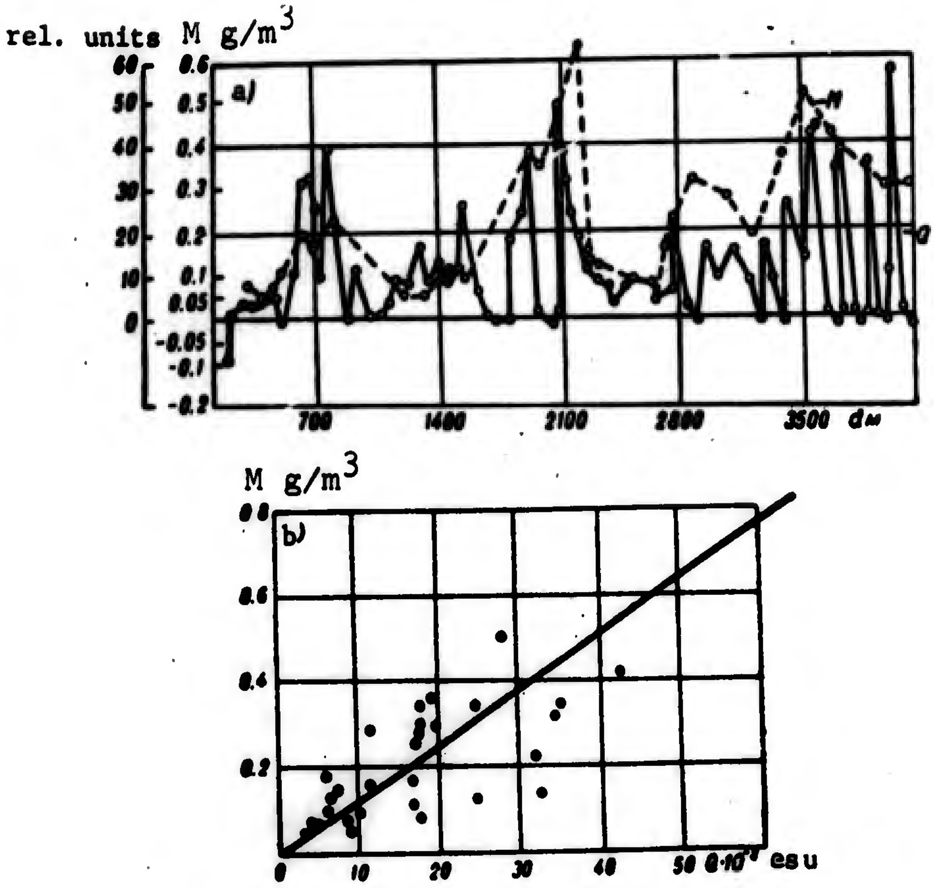

Figure 2.21. Airplane charge Q and water content M in a given cloud [68].

(a) distribution of Q along flight path over distance d; (b) correlation between Q and M in a given cloud. Flight on 17/December 1964, LI-2 airplane.

The charge per unit volume created by the water mass striking the airplane will be

$$q=\sum_i q_i n_i=\frac{3}{4\pi}\frac{\varepsilon}{\delta}\sum_i \frac{r_i}{r_i^3}\approx\frac{3}{4\pi}\frac{\varepsilon}{\delta}\frac{1}{\overline{r^2}},$$

where n_i is the concentration of particles with radius r_i, δ is the water density, $\overline{r^2}$ is the average value of the square of the effective radius. Then the ratio of the charges q_I and q_{II} transferred to the airplane by water masses which are identical in weight, but differently dispersed, will be

$$\frac{q_I}{q_{II}}=\frac{\varepsilon_I}{\varepsilon_{II}}\frac{\overline{r^2_{II}}}{\overline{r^2_I}}. \qquad (2.4)$$

i.e., the charge ratio is inversely proportional to the average values of the effective radii squared. If cloud droplets with average radius about 10 - 20 microns impinge on the airplane and relatively large drops of radius 100 - 200 microns (which are observed on the windshields) separate, the charge acquired by the impinging particles during elastic impact is greater than the charge acquired by the drops leaving (for the same mass of water) by about factor of 10^2, i.e., even if only a few percent of the entire cloud water mass experiences elastic collisions, the airplane charging will be determined by the elastic collisions in this case as well.

Jumping ahead, we note that the quantity α has a tendency to be larger in those cases in which the collision velocity is higher, i.e., droplets of a certain radius rebounding from the airplane surface can acquire higher charges than droplets of the same radius separating from the airplane surface after forming a water film (see Chapter 4).

It appears that one of the factors leading to higher charging of the airplane in ice-crystal type clouds (cirrus, cirrostratus) than in the purely water clouds (although the water content is usually considerably lower in the former than in the latter) is the fact that in the ice-crystal clouds, the entire mass of the crystals striking the airplane creates strong electrification, while in the water clouds only that portion of the droplets which experience elastic collisions creates a charge. Another factor in the strong electrification during impact of ice crystals may be their disintegration. For example, Schaefer [74] notes that a snowflake in the form of a six-point star impacting with a velocity of 100 km/hr on a metal surface inclined at a 45° angle to the stream breaks up into about 500 parts, while the hexagonal platelets and columnar crystals break up into about 30 pieces during collision under the same conditions. It is obvious that in accordance with (2.4), the charge transferred during contact of equal colliding particle masses increases for the solid particles. The third factor in the difference in the charging in clouds of the two types are the differences in the properties of the particles forming the clouds — the differences in the coefficients α.

During icing of the airplane, when in the small-droplet clouds a considerable portion of the colliding particles is captured by the airplane, we would expect a reduction of the electrification. Therefore, the fact noted previously (see Figure 2.17, Table 2.11) that the airplane charge increases in icing conditions is even more unexpected. If we consider that the airplane integral particle capture coefficient can reach values of 0.7 - 0.8 [70, 71], then we would assume that ice formation must be associated with an increase of the number of individual particle electrification events; it appears that this effect is associated with an increase of α.

It should be noted that very specific particle separation conditions can arise on insulated surfaces of the airplane. Our measurements showed that the airplane "glasses" are charged very shortly during flight in clouds to potentials of the order of hundreds of kilovolts, with respect to the airplane structure (the charges creating these potentials sometimes lead to the appearance on the windshields of sparks 20 - 30 cm long, phenomena which are very familiar to pilots). The field intensity at the windshield surface reaches tnes of kV/cm, even in the case of moderate electrification of the airplane as a whole. Under these conditions the adhesive forces between the droplets and the windshield, associated with the action of the electrical forces, may become higher than the droplet cohesive forces, and the droplets will begin to spread out over the windshield. The field intensity $\underline{E}_g$ at the surface of the glass is close to the critical value at which breakdown of the air begins; $\underline{E}_g \approx 30$ kV/cm ≈ 100 esu. Marked deformation of the droplets begins at this field intensity [77, 78]. The effect of the body's electric field will be different, depending on whether the droplet impinges on a dielectric or conducting surface. In the first case, the electric field will interact with the charge induced on the droplet and tend to hold the droplet at the surface of the body. In the second case the droplet, after becoming a "part of the surface",will be repelled from the latter by the electrical forces.

It is more difficult to analyze the connection between airplane electrification and the cloud particle spectrum than it is to analyze the connection with the water content, since there are no methods available which permit continuous recording of the cloud particle spectrum. Therefore, for the time being, we must limit ourselves to finding the connection between the airplane charge and the average characteristics of the clouds.

An increase of the average water content of clouds is associated with an increase of the number of particles in the clouds, including the small particles. There must be a corresponding increase of the probability of charge growth of an airplane of a given type with increase of the water content. Figure 2.22 shows the dispersion of the airplane charging probability [defined in the scale $\lg \underline{P} = \underline{f}(\underline{Q})$] in clouds of different types as a function of cloud water content [68]. The data on cloud water content were taken from [70]. We see from Figure 2.22 that there is a linear relationship between these quantities.

The correlation observed in Figure 2.23 indicates the possibility of finding a connection between the dispersion of the airplane charging probability curve and cloud radar reflectivity. An attempt has been made [79] to compare the data on the average reflectivity $\underline{Z}$ of clouds of different types, measured in the Leningrad region, with the magnitude of the average charge of an airplane in these clouds in order to study the connection between cloud reflectivity and airplane charge. The reflectivity data were obtained with the aid of a weather radar. This comparison did not show good correlation between these two quantities. An attempt has been made to compare the statistical characteristic — the dispersion of the curves of the corresponding integral airplane charging probabilities

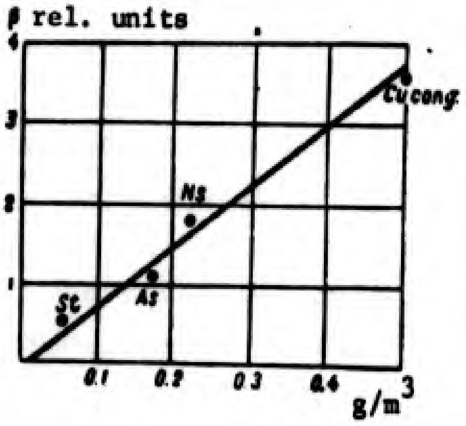

Figure 2.22. Correlation between dispersion β of airplane charging probability in various clouds and their average water content M [68].

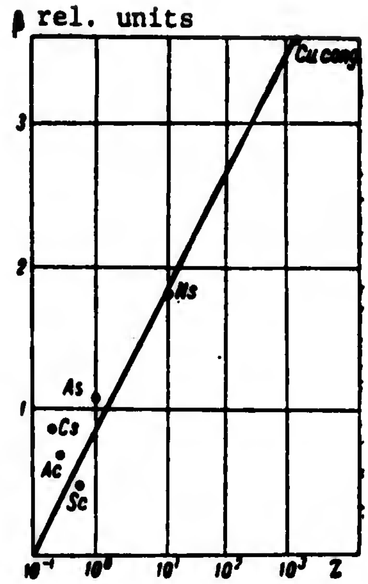

Figure 2.23 Correlation between dispersion β of airplane charging probability in different clouds and their average reflectivity Z [68].

— with the radar reflectivity of the clouds [68]. Figure 2.23 shows the results obtained. Data on charging in clouds of all types (except towering cumulus) are presented for the Li-2 airplane; the data for the towering cumulus clouds were obtained on a Tu-104B airplane and then converted to the Li-2. The plot of Figure 2.23 shows that there is a quite definite linear dependence between the logarithm of the reflectivity of the water-drop clouds and the dispersion of the integral charge probability curve. The deviation of the charge in the cirrostratus clouds from this relationship is explained by the presence in these clouds of ice crystals, which cause, on the one hand, a reduction of the reflectivity from particles of the same dimensions as the water particles and, on the other hand, an increase of the airplane electrification. Similar deviations from the linear relationship can be observed in the other high-altitude clouds.

We note that there is a marked increase of the probability of an airplane being charged positively during flight in ice-crystal clouds in comparison with the probability of positive charging in the purely warm clouds. The differential probability of charging of the Li-2 airplane in clouds of various types is shown in Figure 2.24. We see that in the higher altitude clouds (in comparing, for example, St and Sc with Ac or Ns with As), the probability of positive airplane charging increases. The probability of positive charging in Cs is relatively high, while the probability in Ci is very high. We recall that the Li-2 sounding airplane could not climb above 6000 m, and Cs and even Ci consisting of water droplets are rarely found at altitudes of 6000 m and below. Thus, the phase composition of the clouds can affect both the magnitude and sign of the charge.

§ 10. Studies of the Effect of Surface Characteristics and Flight Conditions on Airplane Charge Magnitude

In the preceding sections, we did not examine the question of how the airplane properties and flight conditions affect the magnitude of the charge acquired by the airplane. In the following chapter, we shall examine in detail the questions of the balance of the currents flowing to the airplane, but for the moment we shall restrict ourselves to a clarification of how and under what conditions the airplane surface properties affect the magnitude of the charge acquired by the airplane.

For several reasons the study of the effect of the airplane surface properties on the magnitude of the airplane charge is more conveniently made using models — test bodies — located either on the airplane [4, 69] or on the ground. In the latter case, the model is mounted either on a rapidly rotating rod [6], or in a wind tunnel through which the airstream is drawn at the required velocity [74].

The significant effect of coating properties on the results of measurements in snowfall was demonstrated by Schaefer [74] in a

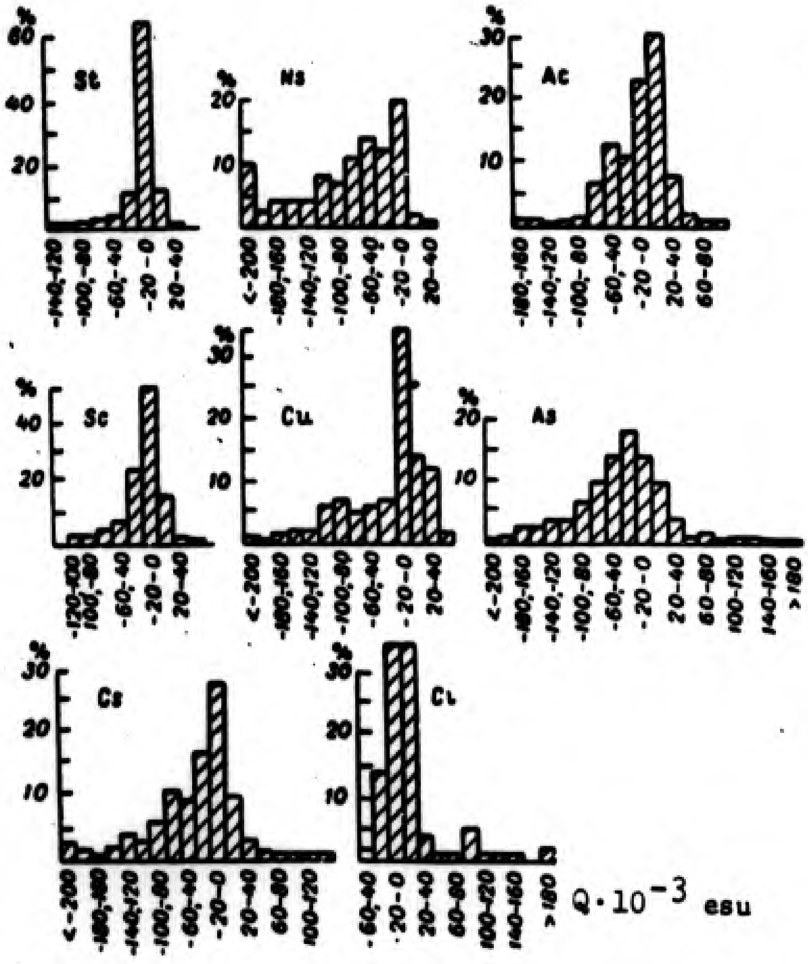

Figure 2.24. Differential probability of Li-2 airplane charging in clouds of different form. Leningrad, 1958.

study of surface charging in snow traveling at a speed of about 100 km/hr. The data of Table 2.13, taken from [74], show that the magnitude and sign of the charge transferred by the snow can be changed by changing the coating on duraluminum.

Thus, variation of the snowflake form and the coating properties has a significant effect on the charge transferred by the snow to the body. (We recall that the charge transferred to the surface is much greater than the self-charge carried by the snowflakes.) Snowflakes of a given form can charge a body weakly in the case of one coating and strongly in the case of a different coating.

It appears that the fact that crystals of different shape appear with different probability at different temperatures may have some effect on the results of Schafer's experiment. A study of the effect of surface properties and temperature on the magnitude of the charge transferred to a surface by snow was carried out by Gunn et al. [6]. The measurements were made on electrodes mounted on long rods which rotated with a given speed in a snowfall. The results of the investigations of [6] are shown in Figure 2.25. We see from the figure that the temperature has a marked effect on the magnitude of the charge transferred by the snow; the effect of surface properties on the magnitude and sign of the charge acquired by the surface is also significant. The charge transferred can change by a factor of ten, depending on the surface material (see Chapter 2, § 7). At the same time, it was found in [6] that clean aluminum is charged negatively, while Schaefer (see Table 2.13) notes that pure duraluminum is regularly charged positively.

TABLE 2.13

EFFECT OF SNOWFLAKE FORM AND COATING MATERIAL ON THE CHARGE (esu/g) TRANSFERRED BY SNOW TO THE SURFACE [74]

Snow form	snowfall intensity, g/m^3	dural: uncoated	dural: coated with ethylcellulose layer 0.01 cm thick	dural: coated with nitrocellulose layer 0.01 cm thick	dural: coated with a layer of nitrocellulose-ethylcellulose 0.10 cm thick
Stellate snowfall	0,24	+12,7	+27,8	−24,3	−9,2, +17,4
Hexagonal bars, ice needles	0,16	+51	+22,3	−32,5	—
Stellate snowflakes with soft rime	0,094	+60	+84,4	−139,5	−24,5
Hexagonal plates and columns, asymmetric crystals	0,19	+48	+10,5	−148,5	−51
Hexagonal bars	0,18	+15	8	−70	−11
Hexagonal bars with rime	0,14	+8	−14	−34	−16
Stellate snowflakes with rime, needles, splinters.	0,52	+7	−8,5	−14,0	−9,8

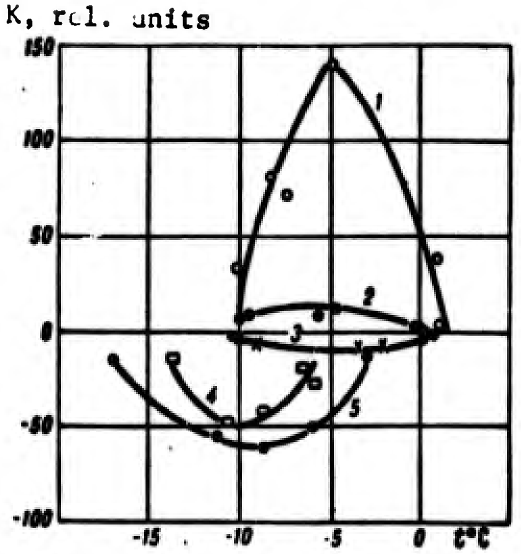

Figure 2.25. Temperature dependence of charge transmitted to the surface by unit mass of snow impacting on the surface (in relative units) of temperature t° C [6].

(1) dural coated with thin TiO_3 film; (2) colloidal silicon dissolved in nitrocellulose; (3) clean aluminum; (4) aluminum airplane lacquer; (5) paint.

The magnitudes of the charge transferred per unit particle mass in [6] and [74] differ considerably.

The inconsistency between the results obtained in [6] and [74] is also associated with the difference between the conditions under which the experiments were conducted (different materials, and also different snow forms, mixed in different proportions and at different temperatures), and in particular, with the effect of the velocity and form of the bodies.

The effect of body shape shows up in the fact that the snow particles apparently transfer during impact on the surface of a smaller charge for a larger deflection of the angle from the normal [6]; therefore, bodies of different shape can acquire charges which differ in magnitude.

The velocity effect is different at different snow temperatures. If we consider that the dependence of the charge Q transmitted to the surface per unit time t on the body velocity w can be expressed by the relation

$$\frac{dQ}{dt} = \varkappa w^{\eta}, \tag{2.5a}$$

where κ and η are coefficients which depend on both the properties and dimensions of the body and on the properties and amount of the snow, then under uniform conditions for a given body, the temperature dependence of n is given by the curve shown in Figure 2.26 [6]. With a temperature change from -5 to -7° C, the exponent n can change by more than a factor of two, i.e., the charge transfer rate may change by several orders of magnitude. Thus, body charging conditions can be compared only if the bodies are exposed to absolutely the same conditions and travel with the same velocities. Attempts to compare the charging of test bodies with airplane charging may be effective if the test body charging measurements are made on bodies mounted on the airplane whose charge is being studied or if we compare the two distributions — the probability of the appearance of charges of different magnitudes on the airplane with the test body charging probability.

Nevertheless, Gunn et al [6] assume that the charging current in snow is proportional on the average to the third power of the body velocity

$$\frac{dQ}{dt} = \varkappa w^3; \tag{2.5b}$$

It is obvious that the velocity dependence of the airplane charge is determined not only by the charging current, but also by the discharging current. Since the discharge current is associated with the engine operating regime, the velocity dependence of the airplane charge when approximated by an equation of the Form (2.5) is expressed with $n < 3$.

In accordance with this discussion, or order to study the effect of the material on the charge acquired by the body, we must compare the charging of different surfaces under the same conditions.

Such a study was made using the Tu-104B flying laboratory [69] and the Li-2 flying laboratory. Test bodies were mounted on the airplanes — spheres of the same diameter (or streamlined bodies having the same projected frontal area), installed in tubes which

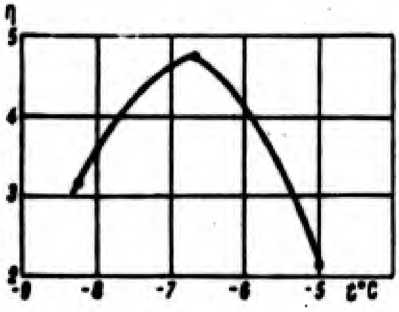

Figure 2.26. Temperature dependence of exponent η in (2.5a). Measurements in snow; aluminum test body.

shielded the spheres from the external field and from the airplane charge field. The test bodies were located as close as possible to one another (Figure 2.27) and also at symmetrical points on the right and left sides of the fuselage [69].

The distance between the instrument pickups varied from 30 cm for bodies located side-by-side to about 400 cm for the symetrically located bodies. Since the minimal dimension of the nonuniformity zones in clouds is about 100 meters, we can consider that the sensors were essentially exposed to the same conditions.

The test body charging measurements of the Li-2 airplane were carried out in the Leningrad region at altitudes from 1600 to 5100 meters in clouds of different types (Sc, Cu, Cu cong., As), and with different state of aggregation of the water in the clouds (water droplets, ice-crystals, and also mixtures of the two). The airplane speed was 180 - 200 km/hr. During each test comparisons were made of the charging of the standard test body — a nickel-coated sphere — with the charging of test bodies with chromium coating and test bodies made from brass and textolite. Thus, we measured and compared charging of the following pairs of materials: nickel-chromium (Ni - Cr), nickel-brass (Ni - Br), nickel-textolite (Ni - T); the measurements were made simultaneously for each pair.

Upon entry into the cloud the test bodies were charged up to some potential which then remained unchanged. The charging followed a nearly exponental law (see Figure 2.31). Thus, from the curve of test body potential variation with time, we can determine both the charging current (in the beginning of the process), the relaxation time τ, and the equilibrium charge. The strongest charging took

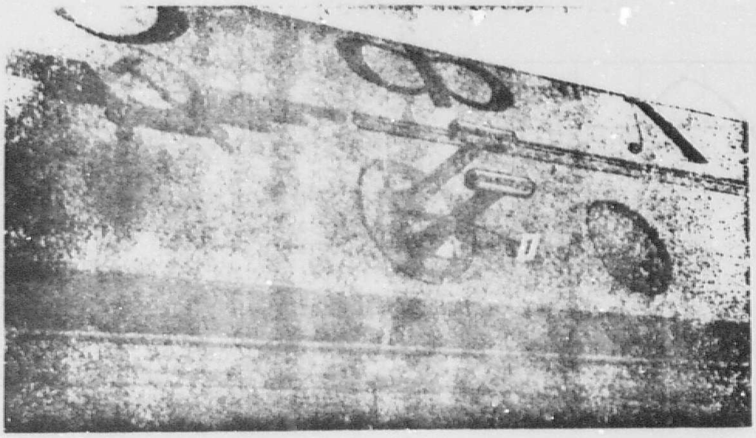

Figure 2.27. Test bodies in screens 1 on Tu-104B airplane.

place in the mixed As clouds, in which the nickel sphere potential reached -100 V, while the textolite sphere reached +530 V. In Sc clouds, the sphere potentials did not exceed a few tens of volts. The average current density flowing to the spheres in the Sc clouds varied from 10^{-11} to 10^{-10} A/cm^2; in the As clouds the currents were an order of magnitude higher. With a capacitance of about 300 cm connected with the test body, the relaxation time was about 100 sec. The limiting ratios of the charges of the test body pairs were significantly different: they varied from 0.1 to 7, i.e., by two orders of magnitude. The current density varied from $2 \cdot 10^{-12}$ to $7 \cdot 10^{-10}$ A/cm^2.

Let us examine the cases in which we can reliably assume that the charging took place either in streams of pure water particles or in streams of pure ice particles. Table 2.14 presents the values of the charge ratios for the different bodies, their signs, and the body material. The table omits the measurements with the textolite sphere, which was often charged with a charge of sign opposite the sign of the charge on the nickel sphere.

TABLE 2.14

TEST BODY CHARGING MEASURED ON AN AIRPLANE

flight condition number	material: first sphere	material: second sphere	in water drops: sign of first sphere charge Q_1	in water drops: sign of second sphere charge Q_2	$\frac{Q_1}{Q_2}$	flight condition number	material: first sphere	material: second sphere	in ice particles: sign of first sphere Q_1	in ice particles: sign of second sphere charge Q_2	$\frac{Q_1}{Q_2}$
	7/V 1964						11/V 1964				
1	н.	х.	+	+	3,5	30	н.	л.	—	—	0,5
2	н.	х.	+	+	3,8	31	н.	х.	—	—	0,15
4	н.	х.	+	+	3,8	32	н.	х.	—	—	0,3
8	н.	л.	+	+	1,4						
10	н.	л.	+	+	2,9	23	н.	х.	—	—	0,12
11	н.	л.	+	+	4	23a	н.	х.	—	—	0,38
12	н.	л.	+	+	4						
13	н.	л.	+	+	3,5						
16	н.	л.	+	+	4,5						
17	н.	л.	+	+	3,8						
18	н.	л.	+	+	2,3						
	н.	х.	+	+	2,1						
	11/V 1964										
7	н.	х.	+	+	2,1						
5	н.	л.	+	+	1,3						
9	н.	л.	+	+	1,3						

We see from the data of Table 2.14 that the metal spheres were charged positively in water clouds and negatively in ice clouds. While the nickel sphere was charged more strongly than the brass and chromium spheres in the water-drop clouds, in the ice-crystal clouds the nickel sphere was charged less strongly.

The four test bodies were mounted simultaneously for the measurements on the Tu-104B airplane. The limiting potentials acquired by the bodies differed markedly (Table 2.15).

We see from the data of Table 2.15 that, depending on the material, the value of the potential to which the body is charged may change by several fold; moreover, it may change by several tens of times even for the metals, and we also see that the charge sign may even change, depending on the material selected.

TABLE 2.15

LIMITING POTENTIALS (V) OF TEST BODIES DURING FLIGHTS IN Cs CLOUDS

	2/VIII 1965		3/VIII 1965
Flight condition number	3	4	1
Weather conditions	top of Cs	in Cs, above Cb	upper part of Cs
Altitude, m	10,300	9,100	10,200
Sphere coated with:			
Palladium	290	333	20
Chromium	475	88	-25
Gold	770	415	170
Nickel	1,450	370	465

The positive charging of the test bodies in the Cs clouds at altitudes of 9000 - 10,000 m may be associated both when the presence of supercooled droplets at these altitudes and with melting of part of the ice-crystals at the point of contact with the body as a result of the impact kinetic energy. The impact kinetic energy at a speed of 200 m/sec is sufficient to melt about 5% of the ice-crystal mass at a temperature of -60° C. This "gable" effect at high airplane speeds (the Tu-104B flight speed was 200 - 250 m/sec) can lead to positive charging of the test bodies.

An idea of the importance of the effect of body surface properties on their electrification can be obtained with the aid of Figure 2.28, which shows the correlation of the potentials of palladium (circles), chrome-plated (dots), and gold-plated (crosses) spheres with the potential $\underline{V}_H$ of the nickel-plated sphere. The measurements were made in cirrostratus clouds (Figure 2.28a) and in the upper part of thunderclouds and Ac clouds (Figure 2.28b). In the

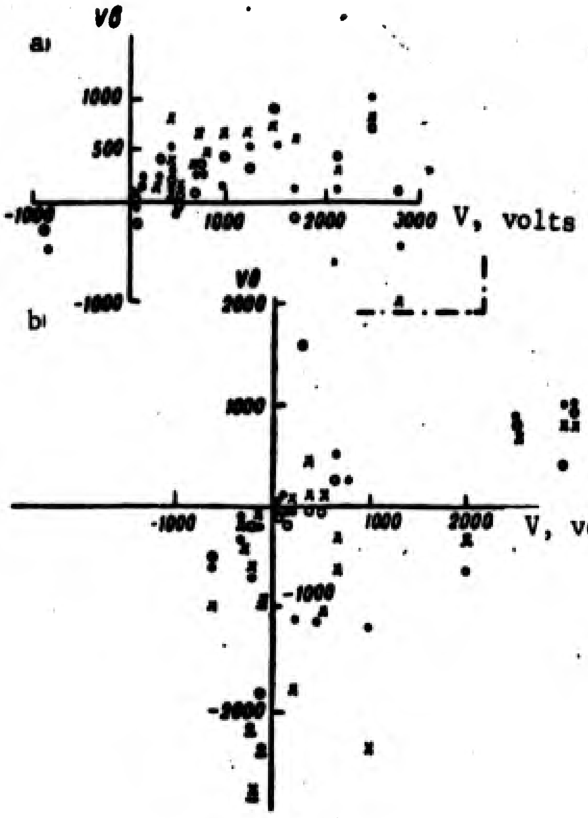

Figure 2.28. Correlation between limiting potential $\underline{V}$ of bodies with different coatings.

(a) Cs clouds; (b) thunderheads; circles are for palladium, points for chromium, and crosses for gold.

latter figure the underlined points apply to the Ac clouds. Three points are of particular interest: 1) all the test bodies were charged in the Cs clouds with essentially a charge of the same sign, with the nickel-plated sphere being charged in these clouds somewhat less strongly than the other sphere (Figure 2.28a); 2) in the tops of the thunderclouds there were several cases of charging of the sphere by electricity of opposite sign: if in the positive charge region the nickel-plated sphere was usually charged more strongly than the other spheres, in the negative charge region all the spheres were charged more strongly than the nickel-plated sphere (Figure 2.28b); 3) the potential of the spheres in these clouds can reach about 3 kV; in the Cs clouds the charge averages about 1000 V (nickel-plated sphere) and 300 - 500 V (other spheres). In the thunderclouds in the positive charge region the corresponding values are 1500 and 400 - 500 V, and in the negative charge region the values are 200 - 400 and about 1000 V. Thus, we see that the spheres which charge more strongly than the other bodies in the positive potential region were charged less strongly than the others in the negative potential region. With an increase of the probability of the occurrence of nonuniformities in the clouds, there is an increase of the probability of unlike charging of the different bodies.

These results may have been affected by surface contamination, which leads to very large changes of the potential acquired by the body and the current flowing to the body. At the same time, it is difficult to avoid contamination; accidental contact with the test bodies after they have been cleaned, precipitation of dust, contact with insects during flight — all this leads to contamination of the test body surface. For example, it was noted in [6], that coating the surface with oil led to a change of the charge sign.

In order to evaluate the effect of surface contamination, we made measurements in which the two test bodies had the same nickel coating. By comparing the difference of the potentials of these control bodies with the difference of the potentials of the bodies coated with nickel and with the other materials, we can determine the confidence with which we can ascribe the charging difference obtained to the effect of the coating materials themselves.

Figures 2.29a, b show the variation of the test body potentials during flight in pure water clouds — stratus (a) and stratocumulus (b). We see from these figures that the potentials of all the bodies change essentially synchronously in time, with the potentials of both bodies with the nickel-plated coating being very similar. The average values of the potentials of the nickel-plated bodies were $\underline{V}_{H_1}$ = 56.9 V and $\underline{V}_{H_2}$ = 56.8 V, that of the dural body was $\underline{V}_D$ = 42 V, and that of the gold-plated body was $\underline{V}_G$ = 28 V. As a measure of the dispersion of the individual values, we can take the quantities $\frac{V_{H_1}-V_{H_2}}{V_{H_1}}$, $\frac{V_{H_1}-V_{D}}{V_{H_1}}$, $\frac{V_{H_1}-V_{G}}{V_{H_1}}$.

The probability of these values is shown in Figure 2.29c (the abscissa is the corresponding value of the above ratios). We see from the curves that the dispersion of the relative values of the difference of the potentials of the nickel-plated bodies is very small, i.e., in this case contamination has very little effect on the measurement results. The dispersion of the relative values of

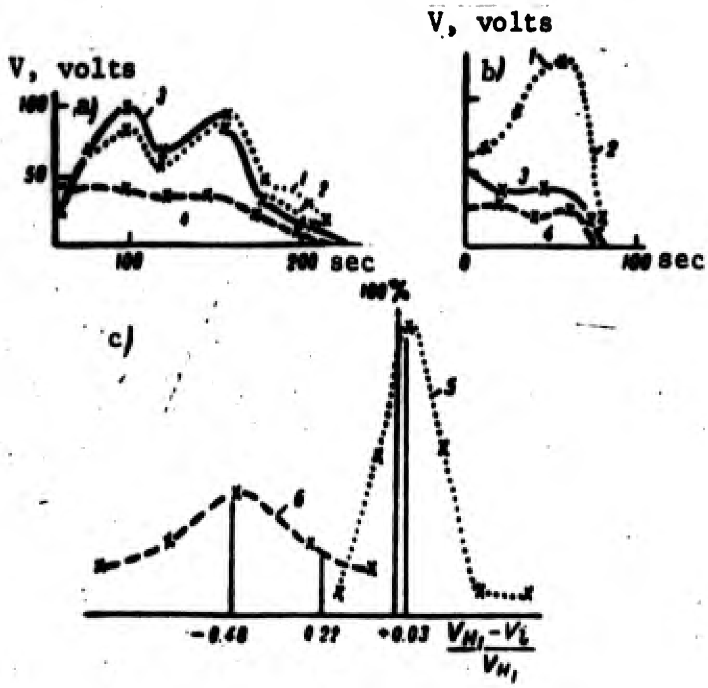

Figure 2.29. Variation of equilibrium potentials V of test bodies during Tu-104B flight in St (a) and Cs (b) clouds at an altitude of 600 - 1000 m and the probability (c) of the values

$$\frac{V_{H_1}-V_{H_2}}{V_{H_1}}\ (5)\ \text{and}\ \frac{V_{H_1}-V_G}{V_{H_1}}\ (6).$$

(1, 2) nickel-plated spheres; (3) dural-coated sphere; (4) gold-plated sphere; V_{H_1}, V_{H_2}, and V_G are respectively the potentials of the nickel-plated and gold-plated spheres.

the difference of the potentials of the gold and nickel-plated bodies, for example, is considerably greater than for the identical bodies. But, at the same time the peaks of the two curves are shifted by a distance which exceeds markedly the dispersion of the curves. Therefore, we can consider that the measurements make it possible to identify in general the influence of the surface properties. The larger values of the dispersion for bodies made from different materials may also be associated with the difference in the composition of the particles in different parts of the clouds.

The complex nature of the charging dependence in snow, noted in [6] and [74], makes it necessary to evaluate the comparability of the measurements in the ice-crystal clouds.

Figure 2.30a shows the variation of the potentials of the same bodies during flight in a Cs cloud. The potentials of the nickel-plated bodies (1 and 2) are again similar. The dural sphere is charged more strongly than the nickel-plated spheres. The abrupt variations of the dural sphere potential between 400 and 500 seconds are associated with synchronous nature of the variations of the absolute values of the potentials of all the bodies. The average values of the potentials are $V_{H_1} = -212$ V, $V_{H_2} = -220$ V, $V_D > |-480 \text{ V}|$, $V_G = +290$ V; Figure 2.30b shows the probability $\frac{V_{H_1} - V_{H_2}}{V_{H_1}}$, $\frac{V_{H_1} - V_D}{V_{H_1}}$ and $\frac{V_{H_1} - V_G}{V_{H_1}}$. We again see that in the ice-crystal clouds the dispersion of the values of the relative deviations of the potentials of bodies made from the same materials is less than for bodies made from different materials, and that the instantaneous values of the potential differencesof the different bodies are basically associated with the effect of their materials.

Comparison of test body charging in pure water and pure ice-crystal clouds (see Figures 2.29 and 2.30) shows that for high flight speeds in the water and ice clouds there is also a tendency toward charging with charges of opposite signs.

Similar charging characteristics were also observed during other flights. We note that the gold-plated sphere was not charged positively in all the Cs clouds. For example, on 22/June 1966, during flight in Cs at an altitude of 8100 m, the average values were $V_{H_1} = -131$ V, $V_{H_1} = -130$ V, $V_D = -162$ V and $V_G = -158$ V.

Very interesting data on test body charging were obtained during flights in clouds in which the body charge sign changed, for example, in the Ns clouds. In this case, we could assume that the surface properties changed very little upon transition from the region of charging by electricity of one sign to the region of charging by electricity of the opposite sign. While the nickel-plated sphere 1 was on the average charged less strongly at positive

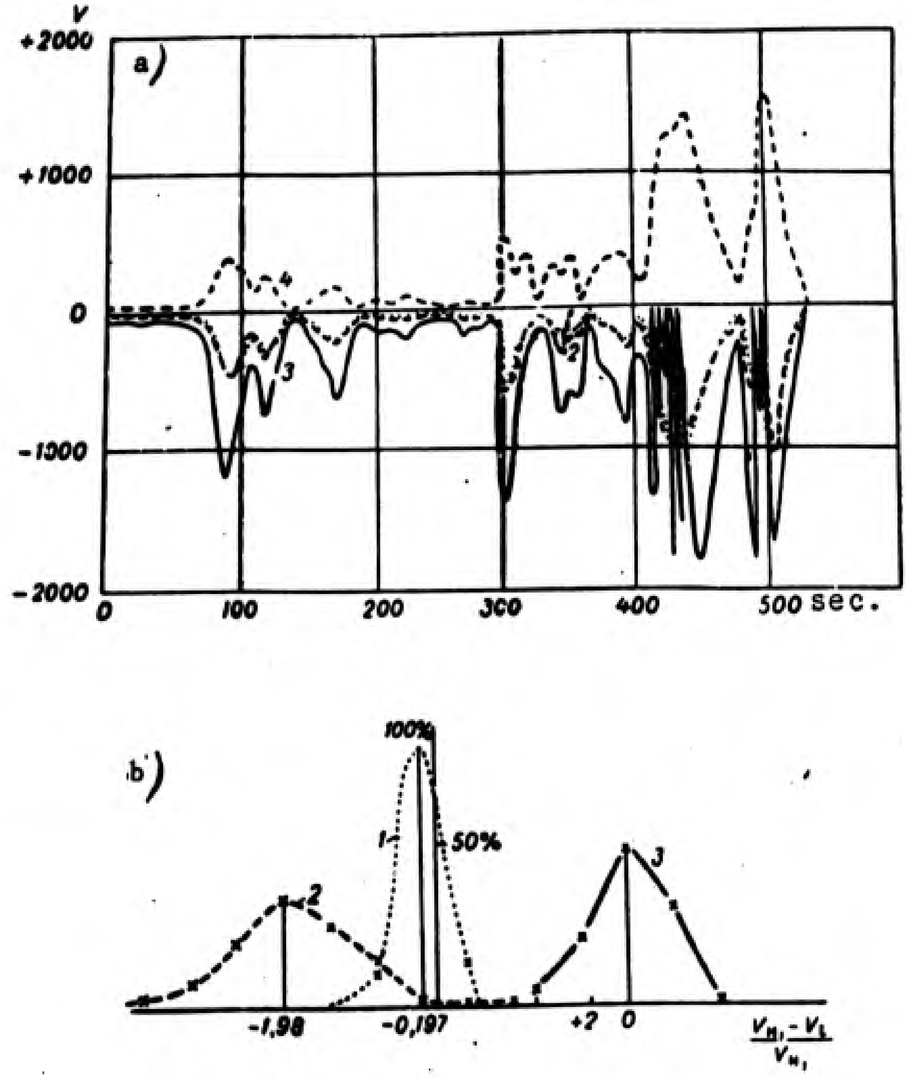

Figure 2.30. Variation of test body potentials during Tu-104B flight in Cs clouds at an altitude of 8000 m (a) and the probability of the values $\frac{V_{н_1} - V_i}{V_{н_1}}$ (b).

(a) 1, 2 are nickel-plated spheres, 3 is the dural sphere; 4 is the gold sphere; (b) 1) $\frac{V_{н_1} - V_{н_2}}{V_{н_1}}$ 2) $\frac{V_{н_1} - V_G}{V_{н_1}}$., 3) $\frac{V_{н_1} - V_D}{V_{н_1}}$.

potentials than the nickel-plated sphere 2, negative potentials $|V_{ш_1}| > |V_{ш_2}|$. The gold-plated sphere at positive potentials was charged on the average less strongly than the nickel-plated spheres, while at negative potentials (particularly, high negative potentials) $|\dot{V}_G| > \left|\frac{V_{ш_1} + V_{ш_2}}{2}\right|$. It was frequently noted that variations of the individual body charging level take place with a shift in time which exceedsconsiderably the circuit relaxation time. Finally, the relationship of the average potentials in the different segments of the recording does not reamin constant either in magnitude or in sign (Table 2.16).

TABLE 2.16

TEST BODY CHARGING DURING FLIGHT IN Ns CLOUDS (Tu-104B AIRPLANE)

time interval, sec.	$V_{ш_1}$	$V'_{ш_2}$	$\bar{V}_G$	$\bar{V}_D$
0–130	+75	+98	−5	+70
130–170	−560	−550	−1250	−280
330–465	−330	−300	−110	−460

In composing the table, we selected segments of the potential recording in which the body charges do not change sign. We shall return to an explanation of the electrification of the test bodies in Chapter 4. For the time being, we simply note that this electrification may be associated with the different concentration ratio of the particles which charge the test bodies positively and negatively.

The data presented above on test body charging indicate clearly the existence of an effect of body properties on the magnitude and, what is particularly significant, on the sign of the charge acquired in both water-droplet and ice-crystal clouds.

The form of the curve of test body potential variation with time is shown in Figure 2.31. We have noted previously that the

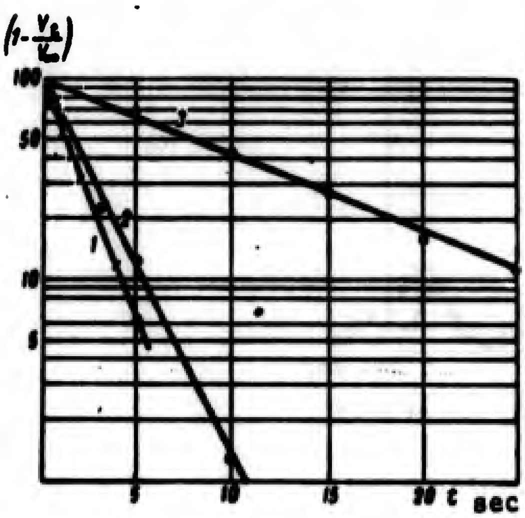

Figure 2.31. Time variation of test body potential.
(1) St cloud (τ = 1.8 sec, τ_{true} = 0.02 sec); (2) Ns cloud (τ_{true} = 2.3 sec, τ_{true} = 0.023 sec); (3) Cs cloud (τ = 11.5 sec, τ_{true} = 0.11 sec).

nature of the curves is represented satisfactorily by an exponential relation. The figure shows typical values of the body charge relaxation time τ. In the different clouds τ varies from a few seconds to several tens of seconds. For the different test bodies in the same time intervals, the values of the relaxation time are the same. We must bear in mind that these values of τ also depend on the metering circuit capacitance. If we exclude the influence of the metering circuit, then the true value of the relaxation time of the test bodies will be about 100 times shorter than the measured times.

The test body charging studies make it possible to identify the surface properties on airplane charging. With proper selection of the test body material, quite good correlation between its charge and the airplane charge may be obtained. Figure 2.32a shows how the airplane charge Q and the dural test body potential vary with time during flight in Cs clouds. The shape of the curves is similar in general. Figure 2.32b shows the relationship between the two values at arbitrarily selected times, and Figure 2.32c shows the correlation at times when the airplane charge and the body charge begin to increase. On the average, the ratio of the airplane charge to the body charge is $1.2 \cdot 10^5 - 2.2 \cdot 10^5$. The authors of [6] came to a similar conclusion by comparing the current flowing to the entire airplane and to a special dural electrode mounted below the airplane wing. According to the data of [6], the current ratio was constant on the average and the error in the determination of the

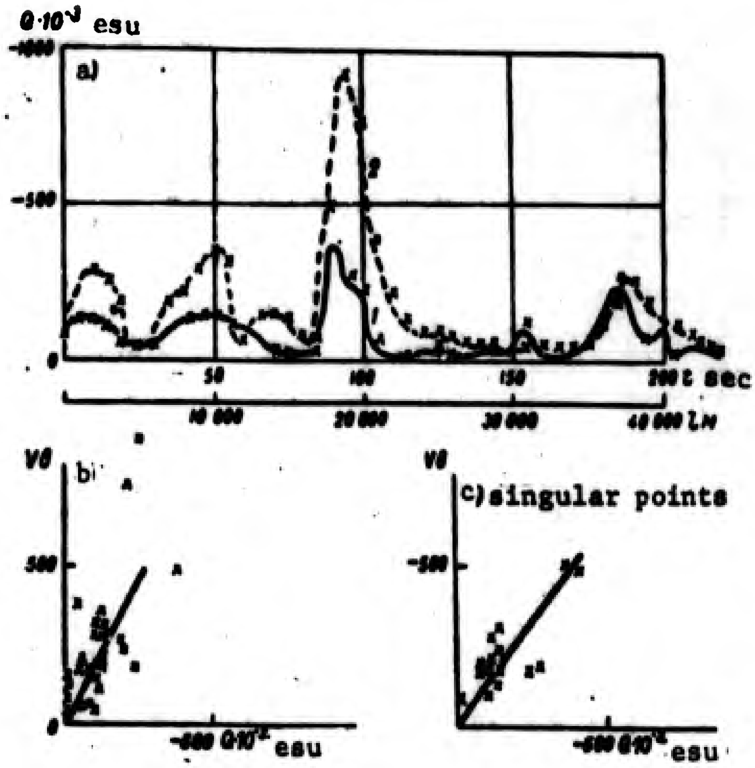

Figure 2.32. Comparison of Tu-104B airplane and dural test sphere charging (t is time, l is distance).

(1) airplane charge, Q; (2) test body potential, (volts); (a) flight in Cs clouds at an altitude of 9000 m; (b) correlation of the values of Q and V; (c) correlation of the values of Q and V taken at the moment of charge growth.

current flowing to the airplane from the electrode charging current did not exceed 10% on the average. However, the charge ratio may vary considerably at individual moments of time (Figure 2.32b). It is true that the variation is reduced considerably if we select times when the airplane charge is increasing (Figure 2.32c), i.e., the differences increase as a result of the marked difference of the discharge conditions of the test body and the airplane.

In the present chapter, we have examined the magnitudes of the charges which arise on airplanes in clouds and precipitation. We have shown the peculiarities of airplane charging in clouds of different types and have established that the airplane acquires a charge of some particular magnitude as a result of interaction between the airplane and the cloud. We shall now consider how the airplane charge is established, i.e., how the airplane current balance is established.

FOOTNOTES

Footnote (1), page 51 For altitudes above 3 - 4 km.

CHAPTER 3

ELECTRICAL CURRENTS FLOWING TO AN AIRPLANE DURING FLIGHT IN CLOUDS AND PRECIPITATION

§ 1. Methods for Determining Current Balance and Measurement Equipment

The electrical charge acquired by an airplane during flight in clouds and precipitation depends both on the properties of the medium in which the airplane is flying (dimensions and number of the cloud and precipitation particles, their phase state and shape, the electrical charges on the particles, and the magnitude of the atmospheric electric field intensity), the airplane characteristics (its structure, particularly the skin material, engine type, and parameters of the static dischargers), and the flight regime (engine power, altitude, and speed). All these atmosphere and airplane characteristics lead in one degree or another to the appearance of currents flowing between the airplane and the atmosphere.

The electrical charge acquired by the airplane depends on both the currents which charge the airplane and those which discharge it. The components of these currents may depend either on certain individual factors among those listed or on some small number of these factors. The effectiveness of existing or prospective devices used to discharge the airplane varies as a function of the airplane charging conditions and can be avaluated only by comparing the individual components of the currents which charge or discharge the airplane. Therefore, it has been necessary, both in order to answer the question of the role of the individual factors in the development of the airplane charge and also to resolve applied problems, to attempt, along with the measurement of the airplane electrical charge, to get an idea of the complete balance of the currents flowing to the airplane and those flowing from the airplane.

The rate of change of the airplane charge Q as a function of time t during flight in clouds, precipitation, dust, and other aerosol accumulations can be represented by the equation

$$\frac{dQ}{dt}=I_{I_1}+I_{I_2}+I_{I_3}-I_{II_1}-I_{II_2}-I_{II_3}-I_{II_4}. \qquad (3.1)$$

Here I_{I_1} is the charge current owing to interaction of the cloud and precipitation particles with the airplane; I_{I_2} is the charge current owing to impingement on the airplane of particles which have already been charged in the atmosphere; I_{I_3} is the charge current owing to interaction of the unburned fuel particles with the airplane. The current $I_{I_1}=\sum_j I_{I_{1j}}$, and the current $I_{I_2}=\sum_j I_{I_{2j}}$ (the currents I_{I_j} are the corresponding charge currents flowing to the airplane surface areas j). I_{II_1} is the current which discharges the airplane as a result of the electrical conductivity of the atmosphere, I_{II_2} is the discharge current owing to the conductivity of the exhaust gases and separation of the charged exhaust gas jet from the airplane. If the airplane has j engines, then $I_{II_2}=\sum_j I_{II_{2j}}$, where $I_{II_{2j}}$ is the current of the j^th engine. I_{II_3} is the discharge current owing to corona discharge of m individual segments of the airplane surface. $I_{II_3}=\sum_m I_{II_{3m}}$, where $I_{II_{3m}}$ is the corona or spark discharge current from the surface of the m^th segment. I_{II_4} is the current carried away by particles separating from the charged airplane (collector effect proportional to the airplane charge). $I_{II_4}=\sum_j I_{II_{4j}}$, where $I_{II_{4j}}$ is the current owing to the particles separating from the j^th segment.

Under steady state conditions $\frac{dQ}{dt}=0$,

$$(I_{I_1}+I_{I_2}+I_{I_3})-(I_{II_1}+I_{II_2}+I_{II_3}+I_{II_4})=0. \qquad (3.2)$$

Flying laboratory airplanes are equipped with special instrumentation [4, 6, 7, 69] to measure the magnitude of the airplane charge and its variations in time, and also to measure the currents mentioned above which flow between individual segments of the airplane surface and the atmosphere.

The major virtue of the studies [4, 6, 7] by Gunn et al. was that in these investigations they studied for the first time the total balance of charge influx and efflux on an airplane. They measured the charge currents and showed that the airplane charge is lost as a result of the corona discharge current I_{II_3}, conductivity of the hot exhaust gases I_{II_2}, collector effect I_{II_4}, and atmospheric conductivity I_{II_1}. The ingenious measurement technique, based on the use aboard the airplane of an artificial charger, made it possible to make measurements of the several balance components during flights in a clear sky.

The resulting current balance made it possible for the first time to make quantitative estimates of the effectiveness of the static dischargers. Gunn et al. also introduced the idea of self-charges and induced charges on the airplane. The majority of the modern studies on airplane electrification (see, for example, the survey paper [23]) are based on these ideas and actual measurement results. Unfortunately, at the present time the current balance data presented by Gunn et al, are not adequate.

First, there are no data on the charge current under different meteorological conditions. This applies particularly to the high-altitude clouds and thunderclouds, which were hardly studied at all by Gunn et al. Second, the current balance depends significantly on the characteristics of the airplane. The new types of engines, their higher powers, the marked change of the shape of the modern airplanes, the appearance of jet airplanes, and the high flight speeds — all these factors make it necessary to re-examine the question of the current balance and most of all the questions on the magnitudes of the charge currents and the discharge currents which occur as a result of corona discharge and conductivity of the hot exhaust gases.

Charging studies of the Tu-104B airplane, for example, have shown that in many cases its charge exceeds considerably the permissible limit.

Let us examine the equipment of the modern Tu-104B flying laboratory [69]. The results of measurements made using this airplane have yielded much valuable data on the current components flowing to the airplane and on the airplane charge.

Plates insulated from the structure — "current receivers"— were installed on the leading edges of the Tu-104B airplane wings, and other plates — "current removers" — were installed on the trailing edges (Figure 3.1) to measure the charge currents I_{1_1} and I_{1_2}. The current flowing to these plates was measured by special devices.

If this current is essentially the current I_{1_2}, then the charge current of an airplane of given design in a given flight regime under given meteorological conditions is a given quantity which is not subject to any sort of regulation. Under these conditions, the airplane charging level can be reduced only by increasing the discharge currents, i.e., by improving the static dischargers, for example.

If the electric charge transferred in clouds and precipitation to an airplane arises basically as a result of the current I_{1_1}, then the airplane charging level can be reduced by selection of the airplane coating at the points where the particles separate.

Measurements made on the Tu-104B airplane with the aid of the special current receivers (Figure 3.2) and current removers (Figure 3.3) together with the test bodies made it possible to clarify the question of which process forms the basis for the airplane charge, and whether the magnitude of the charge current of a given airplane in a given flight regime under given meteorological conditions can be influenced.

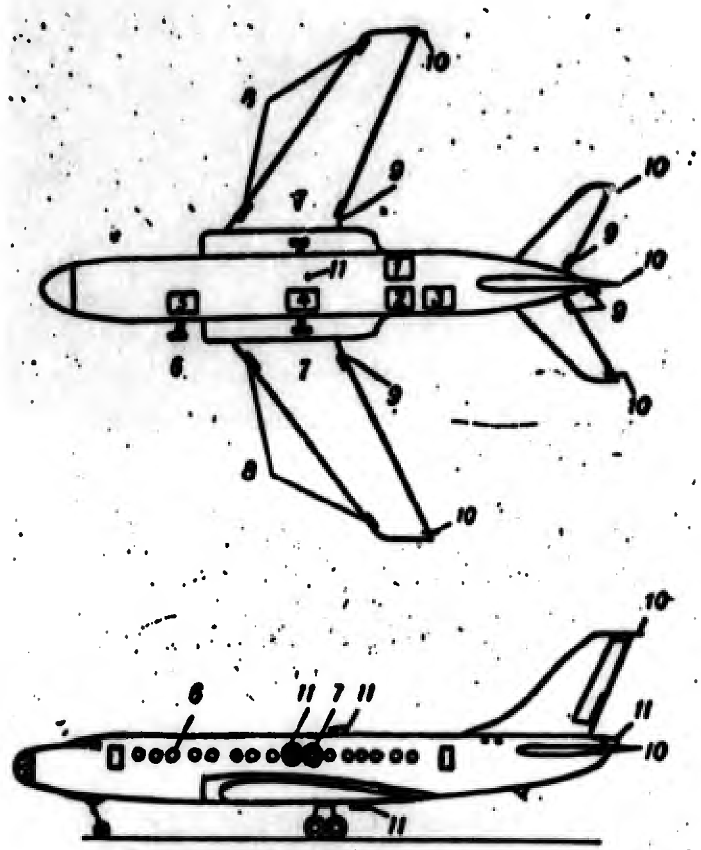

Figure 3.1. Instrumentation locations on Tu-104B flying laboratory.

1) and 11) are instrumentation consoles and pickups for the instruments measuring the field intensity; 2), 8), 9) and 10) are an instrumentation console, current receivers, current removers, and static dischargers; 3) is the apparatus for charging the airplane; 4) and 7) are the instrumentation consoles and test bodies of the equipment for measuring the charge of the test bodies; 5) and 6) are the instrumentation console and pickup of the instrument for measuring the dimensions of the precipitation particles.

Figure 3.2. Location of current receiver 8 on wing of Tu-104B airplane.

Figure 3.3. Location of current remcver 9 on stabilizer of Tu-104B airplane.

Actually, the currents flowing to geometrically identical, symmetrically positioned segments of the airplane surface which are made from different materials must be equal if the airplane electrification is the result of the current I_{I_2}, and must be different if the current I_{I_1} acts. The test bodies mentioned above (Figures 3.1 and 2.27) were also used to study the influence of skin materials and surface shape on the charging current. The current I_{I_3} was determined from the variation of the rate of charge decay of the positively and negatively charged airplane, with the measurement being made using electrostatic fluxmeters.

The conduction current I_{II_1} can be determined if we know the atmospheric conductivity and the airplane electric charge.

The discharge current I_{II_2}, which arises as a result of exhaust gas conductivity, can be measured under given engine operating conditions from the rate of airplane charge decay when the charging sources cease operation. For these measurements, the airplane was equipped with an installation which made it possible to eject crystalline carbon dioxide overboard under pressure through a system of metal nozzles. The airplane was charged during this emission.

Measurements were also made of the corona discharge currents I_{II_3} flowing through the standard dischargers. Finally, measurements on "dischargers" consisting of the current removers and test bodies made it possible to evaluate the magnitude of the current I_{II_4}.

Measurements made with the aid of four specially installed electrostatic fluxmeters made it possible to determine the magnitude of the airplane electric charge and its time variation, and also the values of the atmospheric electric field intensity components in the vertical direction, along the wings, and along the fuselage. We have noted previously that in many cases the atmospheric electric field may have a marked influence on the currents flowing through the static dischargers.

An instrument was installed aboard the airplane to measure the dimensions and concentration of the precipitation particles [80,81] to obtain a quantitative evaluation of the precipitation intensity.

In all flights, measurements were made of the temperature, vertical currents, wind velocity at altitude, navigational position fixes were taken, and the flight turbulence parameters were recorded. Along with the measurements of the airplane electric charge level, the radio operator made an evaluation of the audio radio interference intensity on an arbitrary scale at different radio frequency bands — from longwave to ultrashort.

The results of the measurements of all the instruments were recorded on automatic recorders. The recordings on the various recorders were synchronized with the aid of common electric clocks and special synchronizing marks.

The equipment used in the studies is described in more detail in [69]. We shall not discuss here the equipment used by Gunn et al. in [4], particularly since the measurements in [69] were made on the basis of account for the problems and advantages of the technique [6].

We shall examine the results of studies of the individual components of the balance of the currents to the airplane [Equation(3.1)].

§ 2. Airplane Charging Currents

Airplane charging currents in clouds and precipitation. The electrical currents which charge the airplane depend to a considerable degree on the weather conditions. According to the data of Gunn et al. al. [6], who made several hundred flights in snowstorms and winter clouds, the total charge current on the B-17 airplane was about 100 μA during flight in light snow, increased to 150 μA during flight in moderate snow, and rose to 400 μA during flight in heavy snow. Measurements on test bodies located on the ground showed that the charge transferred to a surface in snowstorms can vary in the limits of $\pm 10{,}000\ \mathrm{esu \cdot m^2/g} = \pm 3 \cdot 10^{-6}\ \mathrm{C \cdot m^2/g}$.

Measurements of the current balance and its components made on the Tu-104B airplane during flights of about 200 hours total duration made it possible to define the charging characteristics in cirrus clouds, clouds at the intermediate and lower levels, and also in towering cumulus, rain clouds and thunderclouds [9, 69].

As mentioned above, the airplane charging current was measured with the aid of current receivers installed on the leading edges of the wings. In the general case, the current flowing to the current receivers $I'_{\text{I}}=I_{\text{I}_1}+I_{\text{I}_2}-I_{\text{II}_4}$, where I_{I_1} and I_{I_2} are the input currents [see (3.1)] and I_{II_4} is the current carried away by the particles separating from the airplane surface. It will be seen from the later analysis that the airplane charge is determined basically by the particles separating from the airplane. Therefore, each particle which brings a charge to the airplane at the same time takes away as a result of the collector effect a charge which is proportional to the airplane charge. The current

$$I_{\text{II}_{4j}}=\alpha_j p_j QS\sum_i n_i r_i^2, \tag{3.3}$$

where p_j is a coefficient relating the field intensity in the j^{th} zone of the area S with the airplane charge Q; α_j is a coefficient characterizing the connection between the charge transferred by a droplet to the j^{th} point of the surface with the field intensity E_j; n_i is the concentration of particles with radius r_i (see Chapter 4). Only at the initial moment of charging, when the airplane charge is small, or in the case of very effective dischargers which do not permit the airplane charge to increase to values at which the collector effect is noticeable, can we measure the quantity $I_{\text{I}_1}+I_{\text{I}_2}$ in Place of I'_i. At the end of this chapter we shall discuss the question of the degree to which the density of the current flowing to the current receiver plates corresponds to the densities of the current flowing to the entire airplane.

Figure 3.4 shows the integral probabilities of the magnitudes of the densities of the current flowing to the current receivers, measured respectively in Ns, Cs, thunderclouds, and in precipitation

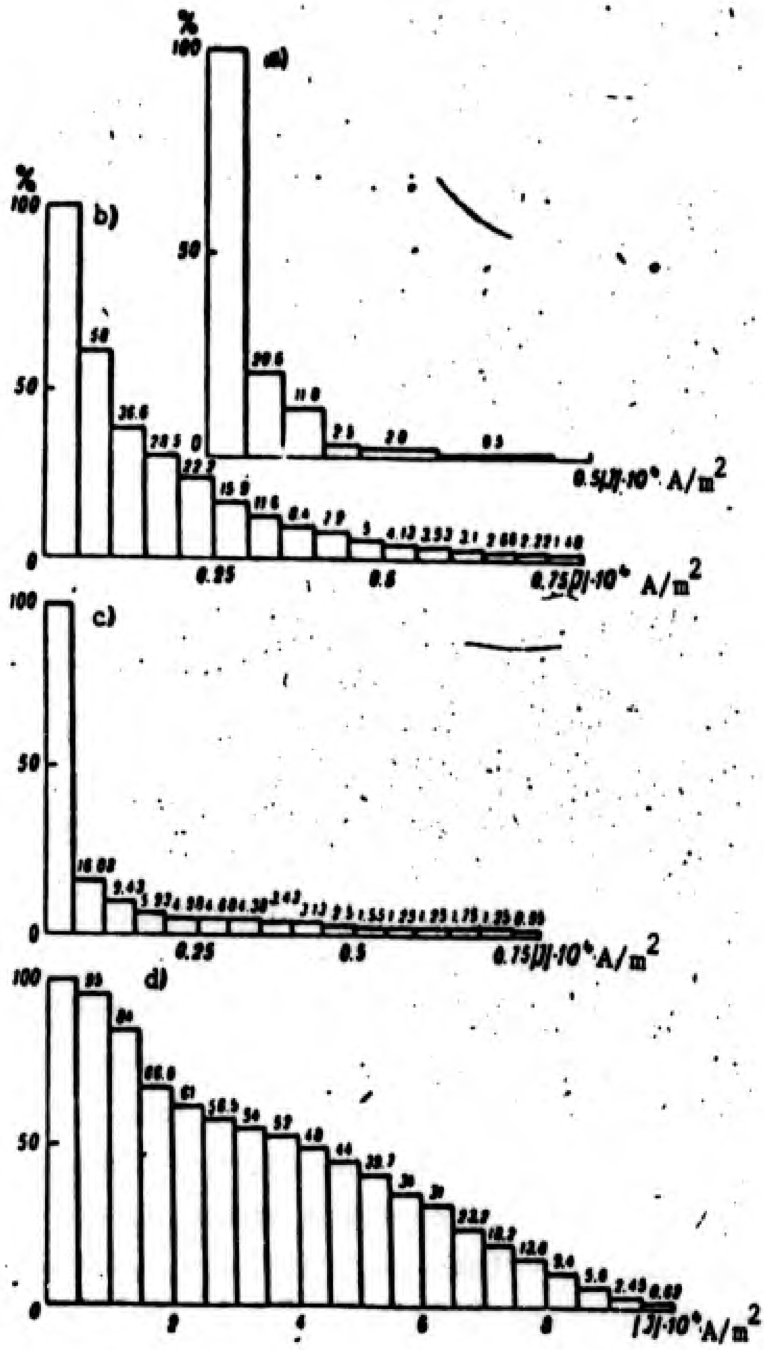

Figure 3.4. Integral probability of density of currents flowing to the current receivers greater than a given value.

a) in Ns clouds; b) in Cs clouds; c) in precipitaion from Cb clouds; d) in thunderheads at an altitude of 7 km.

from shower clouds. Dural plates were installed on the airplane for all the cloud flights except those in thunderclouds; chrome-plated plates were used for the thundercloud flights. The material change could have led to a situation in which the density of the current flowing to these plates would have been less than the density of the current flowing to the dural airplane skin by about 10-20%. The current density distributions in the Ns clouds and below the rainshower clouds are quite similar. In both cases, about one fifth of the values are larger than $5 \cdot 10^{-6}$ A/m^2. However, in the rain-producing clouds small regions (probability of occurrence about 1%) are encountered in which the current density reaches $\sim 10^{-4}$ A/m^2, while in the Ns clouds the current density does not exceed (probability 0.5%) $\sim 0.5 \cdot 10^{-4}$ A/m^2. The current density is markedly higher in the Cs clouds: about one fifth of the values obtained are above $2 \cdot 10^{-5}$ A/m^2. The currents in the thunderclouds are an order of magnitude higher still. The current densities reach 10^{-3} A/m^2 (probability about 1.5%); one fifth of all the current density values are higher than $7.5 \cdot 10^{-4}$ A/m^2. The integral probability of current density values greater than a given value is approximated satisfactorily by the equation (Figure 3.5)

$$\lg(P\%) = \lg 100 - aJ_1, \quad (3.4a)$$

or

$$\lg P = -a'J_1. \quad (3.4b)$$

(compare with (2.1), which characterizes the integral probability of the occurrence of airplane charge).

The curve for the Ns clouds has the highest slope, while the curve for the thunderclouds has the lowest slope. The current probability distribution can also be described by the log-normal distribution and is also represented by a straight line in the probability-logarithmic coordinates.

Let us examine the possible relationship between the current densities J_{1_1} and J_{1_2} in the current flowing to the plates.

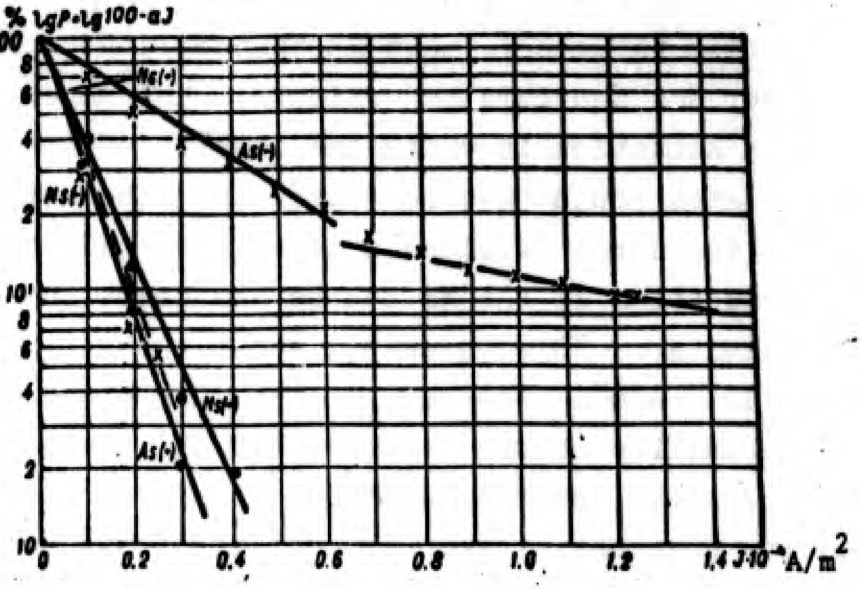

Figure 3.5. Integral probability of currents greater than a given value in semilog scale.

As we have mentioned previously, Schaefer [74] showed that the snowflake charge acquired after collision with the surface is two orders of magnitude larger than their natural charge for collision velocities of the order of 100 km/sec. Gunn et al. [6] showed that the snow charge transferred during collision is proportional to the third power of the velocity. Thus, for the Tu-104B velocities ranging from 600 to 900 km/hr the charge transferred by the snowflakes must be greater than the natural charge by four or five orders of magnitude, i.e., $\frac{I_{1_1}}{I_{1_2}} \approx 10^4 - 10^5$, and the current I_{1_2} can be neglected. Using the data on the magnitude of the space charges in clouds of different types, presented in Chapter 2, Section 2, we can estimate that the magnitudes of the currents I_{1_2} flowing to the airplane are much smaller than the currents I_{1_1} in all types of clouds and precipitation (Table 3.1).

Table 3.1 presents the values of the median measured current densities $(J'_{1_1})_{med} \approx I_{1_1}$ and the maximal values of the current densities $(J_{1_2})_{max}$ in the various clouds. We see that the ratio $\frac{(J_{1_1})_{med}}{(J_{1_2})_{max}}$ for the

TABLE 3.1. CHARGE CURRENTS J_{1_1} AND J_{1_2} FLOWING TO Tu-104B AIRPLANE (FLIGHT SPEED 800 km/hr)

Cloud form	St and Sc	Ns	As	Cs	Cu and Cu cong.	Cb
Current density to airplane due to space charges J_{1_1} (A/m^2)	10^{-8}	$2\cdot10^{-7}$	10^{-7}	$2\cdot10^{-9}$	10^{-8}	$5\cdot10^{-7}$
Current density to airplane due to charge exchange bet wen the cloud particles and the airplane skin $J_{1_2}=(J_1'-J_{1_1})$ ...	10^{-5}	10^{-3}	10^{-3}	10^{-5}	10^{-5}	$5\cdot10^{-4}$
Ratio of current densities $\frac{(J_{1_2})_{med}}{(J_{1_1})_{max}}$	10^3	$5\cdot10^3$	10^4	$5\cdot10^3$	10^3	10^3

different clouds varies from 10^3 to 10^4; the ratio $\frac{(J_{1_2})_{med}}{(J_{1_1})_{med}}$ is several times larger yet. As we have mentioned above (Chapter 2, Section 2) the space charges in precipitation are much smaller than those in clouds, while the airplane charge in precipitation is smaller than in the clouds; therefore, the ratio $\frac{I_{1_2}}{I_{1_1}}$ is somewhat larger in precipitation than in clouds.

If we assume that $I_{1_1}\sim w$ (w is the airplane velocity) and $I_{1_2}\sim w^3$, then the ratio of the current densities, presented in Table 3.1, varies as the square of the airplane velocity. For example, this ratio will be an order of magnitude smaller for the slower Li-2 airplane.

Comparison of the currents flowing to symmetrically located current receivers made from different materials showed that the current densities to the plates can differ by several fold, i.e. the charge current is determined by interaction of the airplane and the cloud particles. Thus, for all modern airplanes $I_{I_1} \gg I_{I_2}$ and the charging current in clouds and precipitation, flowing to the airplane components in accordance with (3.1), is $I'_I = I_{I_1} - I_{II_4}$, where I_{II_4} is the discharge current which occurs as a result of the collector effect.

The relative fraction of the currents I_{I_1} and I_{II_4} in the currents I'_I is determined by the relationship between the current I_{II} and the other discharge currents I_{II_4} [see (3.1)]. If $I_{II_4} \gg (I_{II_1}+I_{II_2}+I_{II_3})$, then under equilibrium conditions the current $I_{I_1} \approx I_{II_4}$; in the limit $I'_I = 0$ for any values of I_I. If $I_{II_4} \ll (I_{II_1}+I_{II_2}+I_{II_3})$, then $I_{I_1} \approx I'_I$. The value of I_{II_4} depends on the number of particles impinging on the airplane surface, their dimensions, the airplane structure and velocity. The relationship between I_{II_4} and $(I_{II_1}+I_{II_2}+I_{II_3})$ is determined by the airplane characteristics. To simplify the estimates, we can compare the density of the currents flowing to the charged airplane and to an uncharged body. Comparing the current density to the test bodies at the moment when the charge on these bodies is still small (i.w., when all the current to the bodies is essentially the current I_{I_1}) with the current density to the current receivers, we find that in most cases these current densities are approximately equal and, consequently, $I_{I_1} \approx I'_I$. This equality is valid to within 1% for the selected plate installation locations. The discharge current I_{II_4} increases at the points where the field intensity resulting from the charge is higher; therefore, on certain segments of the airplane surface $I_{II_4} = I'_I - I_{I_1}$ may amount to a larger fraction of I'_I.

The question arises of whether the current flowing to the frontal surfaces of the airplane where the current receiver plates are located actually represents the entire current, i.e., how representatively the current receivers are located. We shall return to the quantitative estimates of this representativity at the end of the chapter. Here, we simply note that the charge transferred by the particles decreases with reduction of the angle between the particle velocity vector and the surface on which the particle impinges [6], i.e., particles striking the frontal parts of the airplane transfer relatively little charge to the airplane. We have also made measurements of the currents

TABLE 3.2. RATIO OF CURRENT I_{I_f} FLOWING TO THE FORWARD PARTS OF THE WING MODEL SURFACE TO THE CURRENT $I_{I_{rem}}$ FLOWING TO THE REMAINING PARTS OF THE WING MODEL (Il-18 AIRPLANE)

cloud or precipitation form	$I_{I_f}/I_{I_{rem}}$	mean square deviation of measured quantity
Ns	29,5	9,5
Cs	17	6,5
Ci	34	10,5
heavy rain from Cb clouds	23,5	9,5

flowing to wing models (1/20th scale) in which the forward portion (up to the middle section) was insulated from the remainder of the model. During flights on the Il-18 flying laboratory in clouds of different types it was found that the current flowing to the front portions of the models exceeds the current flowing to the remainder of the models by 20-30 times (Table 3.2).

It is important to note that the current ratio $I_{I_f}/I_{I_{rem}}$ remains nearly the same in both media with large drops and media with very small particles, i.e., in both cases, the charge current flows primarily to the frontal parts of the wings. Finally, the current flowing through the current removers was at least 10^2—10^3 times less than the current flowing to the plates of the current receivers. Thus, the current which charges the airplane in clouds flows primarily to its frontal portions, and the current receivers were located quite representatively.

We note that currents of the density indicated in this section will flow to the electrodes of the meteorological instrumentation which will lead to the errors mentioned in Chapter 1.

Airplane charging currents owing to unburned fuel particles. The unburned fuel particles flowing through the exhaust system can acquire a charge of a given sign, leaving a charge of the opposite sign on the airplane. This process is similar to the process which leads to airplane charging in clouds. The only difference is that there is no fuel particle collector current, since they separate from the metal at points where there is no electric field [$p_1 = 0$, see (3.3)].

The airplane charging current I_{I_3} owing to the unburned fuel particles can be measured in three ways. Gunn et al. [6] used a device for artificial charging of the airplane to maintain it at zero charge in the clear atmosphere. For this case, (3.2) can be written in the form

$$I_{I_3} - I_{II_3} = 0, \text{ or } I_{I_3} = I_{II_3},$$

where I_{II_3} is the discharge current created by the artificial charger and measured by an instrument in the charger.

We can also determine the current I_{I_3} by measuring the time decay of both the positive and negative charge of the precharged airplane during flight in the clear atmosphere at moments when the airplane charge is sufficiently small so that there is no corona discharge. Such a decrease is observed, for example, during exit from clouds. It follows from (3.1) that $\frac{dQ_+}{dt} = \pm I_{I_3} - I_{II_1} - I_{II_2}$ for a charge of one sign and $\frac{dQ_-}{dt} = \mp I_{I_3} - I_{II_1} - I_{II_2}$ for a charge of the opposite sign, hence

$$I_{I_3} = \frac{\frac{dQ_+}{dt} - \frac{dQ_-}{dt}}{2}.$$

Finally, by measuring the values of I_{II_1} and I_{II_2} during flight in the clear atmosphere, we can determine I_{I_3}. If the resistance of the exhaust gas jet through which the airplane charge I_{II_1} and I_{II_2} leaks off into the atmosphere equals R_{ef} and the airplane potential is V, then at the moment when $\frac{dQ}{dt} = \frac{dV}{dt} = 0$, and there is no corona discharge current we can determine I_{I_3}:

$$I_{I_3} = -\frac{V}{R_{эф}};$$

The techniques for finding $\underline{R}_{ef}$ are described in the following sections.

The value of the current I_{I_3} is quite different for different engines and flight regimes. For the Tu-104B this current does not exceed 0.5×10^{-10} A, while for the IL-118 airplane in flight near the ground the current I_{I_3} may be of the order of 10^{-8} A or even more.

Deterioration of the fuel burnup ratio (for example, in the case of improper engine operation) leads to a marked increase of the current I_{I_3}.

§ 3. Airplane Discharge Current Owing to Atmospheric Conductivity

The airplane discharging current I_{II_1}, [see (3.1)] owing to atmospheric conductivity λ_a is (see Chapter 1)

$$I_{II_1} = 4\pi \frac{\lambda_a}{\varepsilon_0} Q. \qquad (3.5)$$

For low airplane speeds and high charges, the current may be less than that calculated using (3.5) if a space charge which cannot be carried away by the air stream occurs around the airplane. For most airplanes, even at their highest charges, the effect of the space charge on the conduction current can be neglected in view of the high airplane velocity (see Chapter 1). The relation (3.5) can be used up to airplane speed at which ionization of the air begins as a result of air molecule impact on the airplane surface. This critical velocity exceeds 1-2 km/hr. For the calculations of the leakage currents I_{II_1} it is convenient to use the formula

$$I_{II_1} = \frac{V}{R_a} = \frac{Q}{R_a C}. \qquad (3.6)$$

where $\underline{V}$ is the airplane potential, $\underline{C}$ is its capacitance, and $\underline{R}_a$ is the effective resistance through which the charge leaks off into the atmosphere.

The average values of the conductivity at various altitudes, taken from [41], and the conduction currents discharging the Tu-104B

TABLE 3.3. APPROXIMATE VALUES OF CONDUCTANCE λ_a AT VARIOUS ALTITUDES, RELAXATION TIME τ_{λ_a} OF THE AIRPLANE CHARGE Q, EFFECTIVE LEAKAGE RESISTANCE R_a TO THE ATMOSPHERE, AND CURRENT I_{n_1} (Tu-104B airplane)

altitude, km	air conductance, sec^{-1}	τ_{λ_a} sec	R_a ohm$\cdot 10^{-11}$	current I_{n_1} μA for charge Q in esu		
				10^5	10^7	10^9
3	$5\cdot 10^{-4}$	730	4,3	$2\cdot 10^{-3}$	$2\cdot 10^{-1}$	$2\cdot 10^{1}$
6	11,5	320	1,9	4,6	4,6	4,6
9	21	175	1	8,4	8,4	8,4
12	36,5	100	0,6	14,5	14,5	14,5
15	62,5	59	0,35	25	25	25
30	3 660	1	0,006	$14,5\cdot 10^{-1}$	$14,5\cdot 10$	$14,5\cdot 10^{3}$
50	340 000	0,01	0,00006	$14\cdot 10^{1}$	$14\cdot 10^{3}$	$14\cdot 10^{5}$

airplane at these values of the charges, are shown in Table 3.3.

We recall that Shvarts has shown in [67] that at altitudes above 3-4 km the devations of λ_a in the clear atmosphere from the indicated values usually do not exceed $\pm 20\%$. In clouds (of nonthunderstorm origin) the conductivity values are lower than the indicated values. In thunderclouds, the conductivity can be higher by two orders of magnitude than the values indicated in the table (see Table 2.1). Therefore, although the conduction current discharging an airplane in the troposphere usually should not exceed 10μA, in thunderclouds this value may reach 10^3μA if the effective electrical conductivity in the thunderclouds is essentially ohmic. The conduction current can reach high values at high altitudes in the stratosphere, and particularly so in the ionosphere.

§4. Airplane Discharge Current Owing to the Conductivity of the Exhaust Gas Jet

In (3.1) the current I_{n_2} which discharges the airplane as a result of the conductivity of the exhaust gases may be written in the form

$$I_{II_0} = \frac{V}{R_c} = \frac{Q}{R_c C}, \tag{3.7}$$

where V is the airplane potential, C is the airplane capacitance, and R_c is the resistance of the exhaust gas jet. We recall that the airplane loses its charge because of the fact that the exhaust gas jet as a result of its high conductivity takes a potential close to that of the airplane, and the jet charge is carried away by the turbulent flow around the airplane. Therefore, in reality R_c is some effective resistance and not the purely ohmic resistance; in particular, R_c depends on the airplane velocity if it is sufficiently high (see Chapter 5).

The effective jet resistance is determined from the rate of change of the charge of the artificially charged airplane in clear air. The measurements on the Tu-104B airplane were made during flight in clear air, when the atmospheric electric field was small. During the experiment, the airplane charge could leak off only as a result of air conductivity and conductivity of the exhaust gas jet. Since during the charging of the airplane, its potential did not reach values for which the static discharges begin to operate, there were no corona discharge currents.

In this case, the variation of the airplane charge Q after termination of the charging operation is described well by the equation $Q=Q_0e^{-\frac{t}{\tau}}$, in which Q_0 is the airplane charge at some arbitrary initial time; t is time; τ is the charge relaxation time, $\tau = R_{ef}C$, where R_{ef} is the effective resistance of the exhaust gas jet and the conducting atmosphere $\left(\frac{1}{R_{ef}}=\frac{1}{R_c}+\frac{1}{R_{ex}}\right)$, C is the capacitance of the airplane as an isolated body; for the Tu-104B $C = 1670$ cm.

Since $\frac{Q}{Q_0}=\frac{E}{E_0}$, where E_0 and E are the field intensities at an arbitrary point of the airplane at the moments when its charge equals Q_0 and Q, respectively, the charge decay equation can be written in the form

$$E=E_0e^{-\frac{t}{\tau}}.$$

The airplane charge was measured using electrostatic fluxmeters. From the charge (or field intensity) decay curve after termination of CO_2 emission (or upon exit from a cloud) we can calculate τ and, knowing the airplane capacitance C, we can calculate R_{ef}, and then, knowing R_a , we can determine R_c.

Figure 3.6a shows the form of the recording of the field intensity at the surface of the airplane in the case of artificial charging during the time of carbon dioxide emission and after terminating this emission. Figure 3.6b shows the right-hand portion of ~~the same curve~~ plotted on a semilog scale. The linearity of the relation $\ln E = f(t)$ confirms that the idea of the linear relationship between the current leaking off through the exhaust gas jet and the airplane potential, which was used as the basis for the introduction of the effective resistance R_{ef}, is quite well-justified.

Table 3.4 shows the relaxation time and the corresponding jet resistance R_c for various flight conditions (altitude, flight speed, and engine rpm).

Table 3.5 shows the values of the current flowing from the airplane through the hot exhaust gas jet for various values of the airplane charge.

The dependence of the relaxation time and jet resistance on turbine rpm (engine power) and flight altitude in the altitude range 1000-10,000 is linear, as is easily seen from the curves in Figure 3.7.

As a result of the electrical conductivity of the air, the charged body discharges with $\tau_a = 100-400$ sec, which corresponds for the Tu-104B to $R_a \approx 10^{11}$ ohms (see Table 3.3). In comparing this value with the data of Table 3.4, we see that the values of R_c are much smaller. Therefore, the air conduction currents I_{u_1} can be neglected in comparison with the currents I_{u_2}, flowing through the engine exhaust gas jets (compare also Tables 3.3 and 3.5). It is interesting to compare these values with the data obtained on piston-engine airplanes.

TABLE 3.4. AIRPLANE CHARGE RELAXATION TIME τ AND EXHAUST GAS JET RESISTANCE $\underline{R}_c$ AS A FUNCTION OF FLIGHT REGIME

date	regime number	flight altitude, m	flight speed, km/hr	engine rpm	τ sec	R_c Ohms
15/VII	1	10 000	720	3600	0,7	$4\cdot10^8$
	2	9 600	670	3900	0,6	
	3	1 000	400	3700	3,0	$1,7\cdot10^9$
	9	1 000	400	3600	2,6	
16/VII	1	6 000	700	4400	1,25	
	2	6 000	700	4400	1,3	
	3	8 100	700	4000	0,9	
	4	8 100	700	4000	0,9	$5,4\cdot10^8$
	5	8 100	700	4000	0,9	
	6	8 100	650	3500	1,3	
	7	8 100	650	3500	1,5	
	8	8 100	650	3500	1,4	
	9	8 100	650	3500	1,3	
11/VIII	1	10 000	750	4200	0,9	
		10 000	750	4200	0,7	$4,8\cdot10^8$
		10 000	750	4200	0,8	
	2	10 000	750	4500	0,6	
		10 000	750	4500	0,6	$3,6\cdot10^8$
	3	10 000	750	3500	1,2	
		10 000	750	3500	1,2	$7,2\cdot10^8$
		10 000	750	3500	1,1	
		10 000	750	3500	1,3	

TABLE 3.5. CURRENT I_{II_2}, FLOWING FROM AIRPLANE THROUGH ENGINE EXHAUST GAS JET

flight altitude, m	engine rpm	current I_{II_2} μA for charge Q in esu		
		10^3	10^5	10^7
10 000	3600	$4\cdot10^{-1}$	$4\cdot10^1$	$4\cdot10^3$
1 000	3600	10^{-1}	10^1	10^3

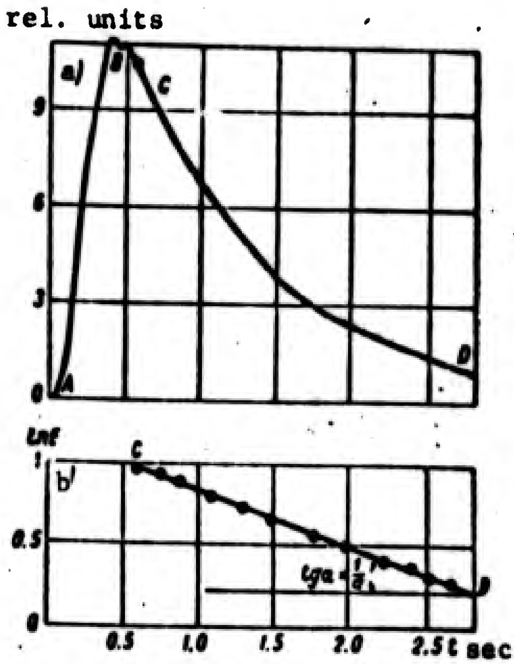

Figure 3.6. Variation of field intensity E at the airplane surface as a function of time τ for artificial charging (a) and the segment CD in semilog scale (b).

Carbon dioxide release started at point A and terminated at point B; the segment CD is used to calculate the effective resistance R_{ef} and the jet resistance R_c.

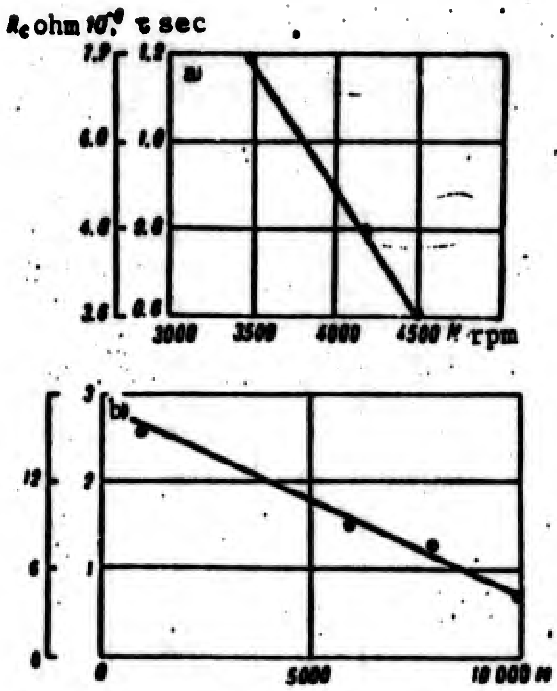

Figure 3.7. Airplane charge relaxation time τ and R_c versus engine rpm (H=10 000 m) (a) and altitude (N = 3800 rpm) (b).

The value measured using the same technique for the Li-2 airplane was τ = 4.5-5 sec. Since the Li-2 airplane capacitance C = 435 cm [11], the exhaust jet resistance for the Li-2 is $1.2 \cdot 10^{10}$ ohms, i.e., about 50 times higher than for the Tu-104. For the B-25 bomber the measured values were τ = 2.8 sec, and R_c of all engines was $6.2 \cdot 10^{9}$ ohms at an altitude of about 1000 m [6].

It is interesting to note that in [6] the maximal measured currents on an airplane flying at a speed of about 300 km/hr were estimated to be several hundred (up to 300-400) μA, and the airplane potential at this time was several hundred kilovolts. Engines of the type installed on the Tu-104 would compensate for such a current with an airplane charge of about 10^6 esu (potential $2 \cdot 10^5$ V), i.e., the exhaust jet on the Tu-104 has a resistance equal to the effective resistance of the static dischargers on the airplane on which Gunn's studies were made. Potentials exceeding one million volts were recorded on the Tu-104 airplane. In this case, the discharge current through the exhaust jet alone reached 4000 μA. Thus, the charge current exceeded this value considerably. We see from this example how the charging currents and the discharge conditions for airplanes of different types traveling at different speeds differ.

§ 5. Airplane Discharge Currents Flowing Through Static Dischargers

The primary device for discharging the airplane at high charges are the so-called "static dischargers". The discharger current is a function of the electrostatic field intensity at the point where they are located. The latter depends on the magnitude of the airplane charge and the atmospheric electric field intensity.

Measurements were made in flight of the currents through standard dischargers located at the extremities of the wings, stabilizers, and tip of the fin. No measurement was made of the currents flowing through the dischargers located on the trailing edge of the flaps, since they were in a very weak electrostatic field.

Let us examine the basic equation relating the current $I_{\text{П}_з}$, flowing from the dischargers with the electric charge magnitude Q. In calculations of the corona discharger current it is often assumed that [6]

$$I_{\text{П}_з} = A_к(E_i^2 - E_{i\,кр}^2) = A_к[(p_iQ)^2 - (p_iQ_{кр})^2] = A_кp_i^2(Q^2 - Q_{кр}^2). \tag{3.8}$$

where A_k is a constant determined by the properties of the discharger point, the airplane and the air; E_1 is the field intensity at the discharger point location; $E_{1\ cr}$ is the field intensity at which discharge from the point starts.

Formula (3.8), originally obtained empirically, can also be derived theoretically. For example, Gunn and Parker [5] examined the corona current near a charged sphere located in a steady air stream. Assuming that there are numerous points located on the sphere to permit corona discharge to begin at low field intensities and at the same time causing very little distortion of the field near the sphere, Gunn derived a formula of the Form (3.8). However, it was shown later by Hendrick and Chapman [84] that the corona current depends significantly on the ambient flow velocity — the rate of removal of the space charge which forms at the point during corona discharge. It was shown experimentally in [84] that in the pressure variation range from 0.25 to 0.95 atm, and over a wide range of variation of the potential applied to the point, the current flowing from the point is proportional to the ambient velocity in the velocity range from a few tens of meters per second to 290 m/sec.

Flight velocity does actually have a significant effect on the magnitude of the airplane corona current. Data are presented in [5] (Figure 3.8) on the corona current of the static dischargers of an airplane located in a hangar (2) and of the same airplane in flight at a speed of about 300 km/hr (1). We see from Figure 3.8 that the airplane corona currents in flight may exceed by several fold the analogous currents of the airplane located in a hangar.

The effect of the velocity of the air stream past a charged point on the current flowing from the point can be accounted for if we supplement the aforementioned scheme of Gunn [5] by the concept of the air stream which is expelled from the corona discharging sphere. The basic equation relating the corona discharge current with the field intensity on a sphere of radius a and air stream velocity w can be derived as follows.

The current I_{II_2} flowing through the spherical surface of radius R is given by the relation

$$I_{II_2}=4\pi R^2\rho(KE+w), \tag{3.9}$$

where ρ is the space charge density, K is the ion mobility, E is the field intensity, and w is the flow velocity at the distance R. The connection between the space charge density and the field intensity is given by the Poisson relation

$$\frac{1}{R^2}\frac{\partial}{\partial R}\left(R^2\frac{\partial V}{\partial R}\right)=-4\pi\rho, \tag{3.10}$$

where V is the potential at a point located at the distance R.

Substituting (3.10) into (3.9) and using $\frac{\partial V}{\partial R}=-E$, we can obatin the basic equation

$$I_{II_2}=\left(2RE+R^2\frac{\partial E}{\partial R}\right)(KE+w)+G, \tag{3.11}$$

where G is the constant of integration. Assuming that at the surface of the sphere $w=w_a$, and $E=E_a=\frac{Q}{a^2}$ (Q is the sphere charge) and that corona discharge begins when $E_a=E_{a\,cr}$, we can determine the constant of integration G.

In the case in which the stream velocity is small in comparison with the ion velocity in the field ($w_a \ll KE_a$), the solution of (3.11) is obtained in the form suggested by Gunn

$$I_{\text{п}_a}=\frac{3}{2}Ka(E_a^2-E_{a\,\mathrm{cr}}^2). \qquad (3.12)$$

However, if the stream velocity is high in comparison with the ion velocity in the field, i.e., $w_a \gg KE_{a\,\mathrm{cr}}$, then the solution of (3.11) has the form

$$I_{\text{п}_a}=2aw_aE_a-\frac{D}{R^2}aw_a,$$

where D is the constant of integration, and w_a is the stream velocity as it leaves the sphere. We can find the constant of integration from the condition that the corona discharge current be zero for $E_a \lesssim E_{a\,\mathrm{cr}}$,

$$I_{\text{п}_a}=2aw_a(E_a-E_{a\,\text{кр}}). \qquad (3.13)$$

This relation is similar to the formula presented in [84].

The solution of (3.11) has a form similar to the empirical formula given in [85]

$$I_{\text{п}_a}=A_k'(w_a+KE_a)(E_a-E_{a\,\text{кр}}). \qquad (3.14)$$

where A_k' is a constant.

For flow velocities of hundred of meters per second the solution (3.14) can be written in the form (3.13), i.e., the dependence of the current on the field intensity is actually found to be linear and proportional to the stream velocity. The corona discharge point is subjected to somewhat different conditions than the sphere examined above: on the airplane the current is created by the space charge carried by the stream from the hemisphere, but the general form of the solution (3.14) remains valid in this case as well.

We note that (3.12), in spite of the fact that it was derived for the sphere case, also describes quantitatively the corona discharge point current on an airplane in stationary air satisfactorily [5].

Equation (3.13) describes with good approximation the current flowing through the discharger on an airplane in flight.

We shall assume that the basic relation describing the volt-ampere or the coulomb-ampere characteristic — the connection between the static discharger current and the airplane potential or charge — is [see (3.13)]

$$I_{\text{пз}m}=A_{k_m}(Q-Q_{m\,\text{кр}})w=AC_c(V-V_{m\,\text{кр}})w, \qquad (3.15)$$

where C_{apn} is the electrical capacitance of the airplane in flight; Q and V are the airplane charge and potential respectively; and $Q_{m\ cr}$ and $V_{m\ cr}$ are the airplane charge and potential at which corona discharge begins at a given point m of the discharger. In the general case, the discharger volt-ampere (or coulomb-ampere) characteristic depends on the external field. In spite of the fact that at present-day airplane flight speeds the characteristic $I_{\text{пз}}=\Phi(Q)$ must be linear, to date the currents are calculated in practice using the characteristic $I_{\text{пз}}=\Theta(Q^2)$, obtained during measurements in stationary air. Hundreds of measurements which we have made, during which the curves $I_{\text{пз}}=f(E)=\Phi(Q)$, were recorded, have shown that this relation is very nearly linear [69]. Figure 3.9 shows the coulomb-ampere characteristic of a static discharger installed on the right wing. In selecting the data for plotting this curve we excluded the iime intervals during which strong atmospheric fields were noted. We see from the curve in Figure 3.9 that the coulomb-ampere characteristic of the static discharger is very linear within the experimental accuracy. At this altitude corona discharge begins at $Q_{cr} = 10^5$ esu (or $V_{m\ cr} \approx 20$ kV). The slope of the curve in the experimental conditions was about 0.5 A/C $\approx 1.5\times10^{-4}\,\mu$A/esu.

The coulomb-ampere characteristic of the static dischargers depends very little on the type of clouds in which the flights are made. Only in those cases in which the airplane flew in heavy precipitation or in strong external fields, and also in the case of very high airplane charges, were deviations of the coulomb-ampere characteristic from the linear relation noted. The effect of precipitation

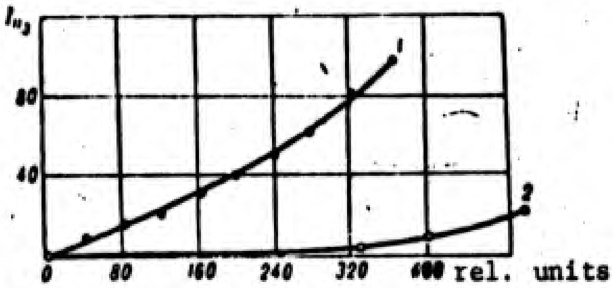

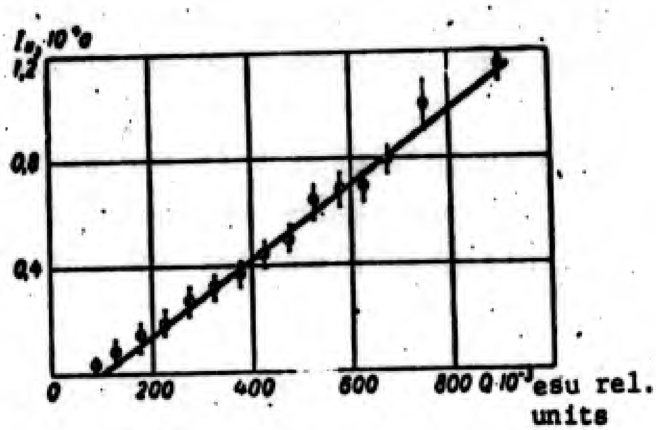

Figure 3.8. Coulomb-ampere characteristic of airplane static dischargers in flight (1), and on a parked airplane (2) [5].

Figure 3.9. Coulomb-ampere characteristic of static discharger installed on right wing of Tu-104B airplane. Recorded in Cs clouds at altitude 7000 m and speed range 730-800 km/hr in six flight regimes. Curve plotted from 179 points.

apparently reduced to wetting of the plastic cone in which the discharger points were enclosed. As a result of this wetting, the cone became electrically conductive, which led to an increase of the effective radius of curvature of the discharger point and, therefore, to decrease of the magnitude of A_k and increase of the value of Q_{cr}. The collector effects resulting from the water flowing from the discharger may play some role in the reduction of the field intensity at the discharger.

As we have mentioned previously, the existence of an external field whose intensity combines with the intensity of the field from the self-charge also leads to deviations from the relation described above. This deviation may be taken into account if we convert the coulomb-ampere characteristic into a characteristic of the form

$$I_{\text{н}_0} = B\left[p_m Q \pm \sqrt{(k_{\text{в}} E_{\text{в}})^2 + (k_{\phi} E_{\phi})^2 + (k_{\text{к}} E_{\text{к}})^2} - E_{m\,\text{кр}}\right] w, \tag{3.16}$$

where $E_{\text{в}}$, E_f and $E_{\text{к}}$ are the components (vertical and directed along the wings and fuselage) of the field intensity vector in the Cartesian coordinate system; $\underline{E}_{m\ cr}$ is the field intensity at which corona discharge begins at the given point; and the coefficients p_m, $k_\text{в}$, k_f and $k_\text{к}$ relate the magnitude of the field intensity at the corona discharge point with the value of the airplane charge and the corresponding components of the external field.

Thus, the coulomb-ampere characteristics depend on the meteorological conditions to the degree that the latter define $A_{\text{k}m}$, $E_\text{в}$, E_f, $E_\text{к}$ and $\underline{E}_{m\ w}$.

At high current densities the space charge which arises at the dischargers and other points and extremities of the airplane may affect the coulomb-ampere characteristic.

On the flying-laboratory airplane, initiation of corona discharge on the sharp parts of the airplane was noted from the appearance of a current on the current removers mounted on the trailing edges of the wings and stabilizer. The airplane structural design made it impossible to install these current removers at the tips of center sections of the wings; it was necessary to locate the current removers at points close to the fuselage, in regions where the airplane charge field is relatively weak. Therefore, it is possible that corona discharge occurred at the tips of the wings and stabilizer somewhat before the currents in the current removers. We shall return to this question in the next section. For the moment, we note that the currents in the current removers appear with an airplane charge of $5 \cdot 10^5$ esu.

Figure 3.10 shows the values of the total current $I_{\text{п}_\text{к}}$ flowing through the current removers (referred to the entire length of the wings and stabilizer) and the currents $I_{\text{п}_\text{з}}$ flowing through the static dischargers. The measurements were made in relatively strong and irregular atmospheric electricity fields, which led to relatively large scatter of the points. However, the general pattern is clear. The slope of the static discharger coulomb-ampere characteristic begins to decrease with increase of the corona current on the wings and stabilizer. For airplane charges not exceeding $\sim 10^6$ esu the current flowing from the trailing edges of the wings and stabilizer remains less than the currents flowing through the static dischargers, although the former begins to increase quite steeply. For an airplane charge of $8 \cdot 10^6$ esu the current flowing through the trailing edges of the airplane wings, stabilizer, rudder and elevator exceeds markedly the current flowing through the dischargers. Since the calculation was based on the minimal estimate, the total corona discharge current flowing through the trailing edges of the airplane surfaces may exceed considerably the calculated values.

Thus, at high airplane charges the corona dischargers cease to be an effective means for protecting against static electrification.

The use of equations of the form (3.8) in practice for calculating the characteristics of static dischargers leads not only to too low a calculated value of the airplane charge in comparison with its actual value, but also to the occurrence of a discharge at several points of the airplane which are not protected by static dischargers.

If we restrict ourselves to the region of charges less than $(1-2)\times 10^6$ esu, then the coulomb-ampere characteristics of the dischargers located at the indicated extremities of the airplane are in general similar (Figure 3.11); the only exception is the discharger located on the elevator tip fairing (i_1). The characteristic of this discharger is flatter. The region of values in which the currents of the remaining four dischargers lie is shown by the dashed lines.

Thus, we can speak of the integral coulomb-ampere characteristic of all five dischargers

$$I_{\text{пз}} = \sum_{m=1}^{m=5} I_{\text{пз}_m} \approx 4.5 A_s (Q - Q_{\text{кр}}) w, \qquad (3.17)$$

and also of the integral effective leakage resistance of these dischargers.

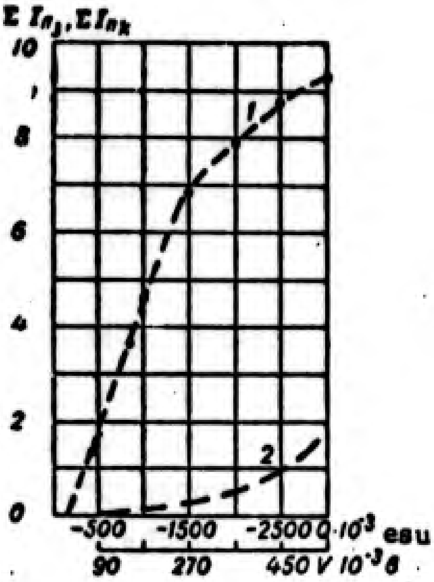

Figure 3.10. Currents of all static dischargers $I_{\text{п}_3}$ (1) and current removers $I_{\text{п}_2}$ (2) for strong charging. Flight in thunderhead anvil at an altitude 8000 m.

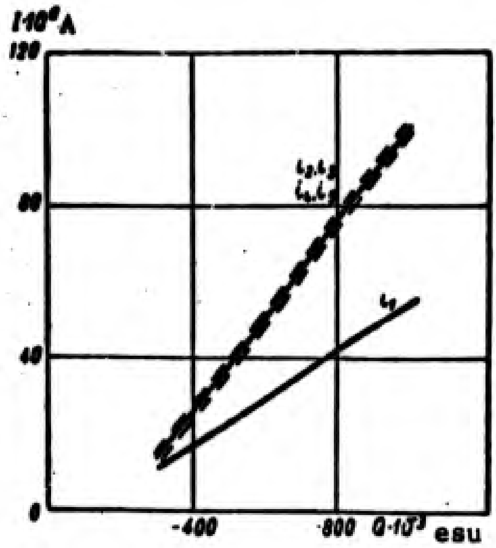

Figure 3.11. Coulomb-ampere characteristics of static dischargers installed on Tu-104B rudder fairing (i_1), on left and right stabilizers (i_2 and i_3), and on left and right wing surfaces (i_4 and i_5).

The discharger coulomb-ampere characteristic depends on the flight altitude. Both A_k and Q_{cr} depend on the air pressure. The pressure dependence of the corona current was studied by Tamm [86], who obtained the connection between the current $I_{\text{п}_3}$ and the variation of the pressure P

$$I_{\text{п}_3} = I_{\text{п}_{3_0}} \left(\frac{P_0}{P}\right)^{1.6}, \tag{3.18}$$

where P_0 and $I_{\text{п}_{3_0}}$ are the standard pressure and the corresponding current. However, this dependence (just as the similar dependences obtained later [31]) did not take into account the influence of the ambient air flow on the corona current.

On the basis of data from measurements made in a series of flights, we attempted to find the pressure (flight altitude) dependence of the static discharger current. Figure 3.12 shows this relation. Curve 1 a

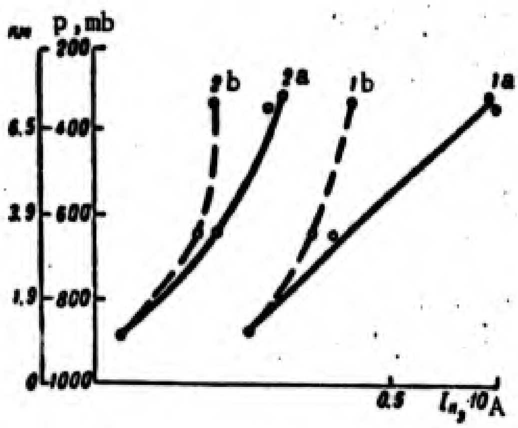

Figure 3.12. Discharger current $I_{п}$ (in relative units) versus flight altitude (pressure for, Q=const.

shows the measurement results for Q = $5 \cdot 10^5$ esu. Since the airplane speed changes with change of flight altitude, an attempt was made to reduce all the measured current values to a constant speed [in accordance with (3.13)]. The result of this conversion for a speed of 450 km/hr is shown by curve 1b. Curves 2a and 2b represent the same dependences for the charge Q = $3 \cdot 10^5$ esu. The differences between curves 1 and 2 are associated, in particular, with the difference between the magnitude of the airplane charge and the corona discharge threshold. Without any pretense of being universal, the curves of Figure 3.12 show that although the static discharger corona currents increase with reduction of the pressure, this increase is slower than was predicted. Since the Tu-104B airplane speed increases markedly with altitude in this altitude range, the discharger current still increases markedly with an increase of the flight altitude. There is a corresponding reduction of the overall resistance of the dischargers with altitude.

The operation of the dischargers located on the Tu-104B can be evaluated with the aid of the data of Table 3.6. We note that these data are very approximate, since they were obtained only for the airplane cruising flight speed at a given altitude,and the pressure dependence of the discharger current is accounted for only approximately.

The discharger corona discharge current $I_{п_3}$ begins to exceed the current $I_{п_2}$ flowing through the exhaust jet only for a charge Q of the Tu-104B airplane greater than $\sim 10^6$ esu (see Table 3.5).

Propeller driven aircraft differ from jet propelled airplanes in the presence of the propellers. On the one hand, a current of

TABLE 3.6. TOTAL CURRENT $I_{п.з}$ FLOWING THROUGH DISCHARGERS AND EFFECTIVE RESISTANCE R_p OF DISCHARGERS ON Tu-104B AIRPLANE

flight altitude, m	current (μA) during airplane charging, esu				Resistance $R_p \cdot 10^{-8}$ Ohm, for airplane charge, esu			
	10^4	10^5	10^6	10^7	10^4	10^5	10^6	10^7
1000	0	0	260	2600	∞	∞	7,5	7,0
4000	0	0	530	5300	∞	∞	3,7	3,3
8000	0	0	750	7500	∞	∞	2,5	2,25

significant density flows to the propeller, which travels with a linear velocity exceeding by several fold the airplane velocity, during flight in clouds. On the other hand, the location and construction of the propeller lead to the appearance on the propeller of corona discharge currents if the airplane acquires a charge. The action of these two factors is seen from the curve of Figure 3.13, taken from [6]; this figure shows the connection between the current flowing through the propeller and the charge of the four-engined B-17 airplane. For low values of the charge the current flowing through the propellers charges the airplane; for high values of the charge this current discharges the airplane. According to the data of [6], the charge current flowing to all four propellers can reach 20-25% of the total airplane charge current.

Effective electrostatic protection on an airplane must not permit its charge to increase to values at which corona discharge begins at any points of the airplane other than the static dischargers. If the airplane's electrostatic protection is not adequate, corona discharge currents occur at the trailing edges of the wings, stabilizer, stub antennas, and wire antennas. The occurrence of these discharges leads to marked increase of the radio interference, which at times leads to communication loss at the shortwave or even UHF frequencies.

Closely spaced groups of dischargers are installed on many airplanes to increase the effectiveness of the dischargers. The ineffectiveness of this measure in increasing the slope of the coulomb-ampere characteristic of the dischargers is clear from general considerations, since this technique leads to a reduction of the field intensity at the corona discharge points. Actually, Jhawar and Chalmers [87] showed that if the discharge points are arranged at the corners of a hexagon at the center of which a seventh point is located, then for distances between the points of less than half the length of the point the current through all seven points is equal to (or even somewhat less than) the current through a single isolated point. When the points are separated from one another by a distance equal to one and a half times their length, the current through the seven points is equal to three times the current through a single isolated point. As the points are brought closer together, there is not only a reduction of the slope of the coulomb-ampere characteristics but also a marked increase of the corona discharge threshold [87]. To evaluate the role of these effects, comparative measurements were made on the airplane of the coulomb-ampere characteristics of single dischargers and double and quadruple dischargers. The results of this comparison are shown in Figure 3.14.

In some flights single and double dischargers ($\underline{i}_3$ and $\underline{i}_2$ are the currents of the single and double dischargers on the stabilizer) were installed at symmetric points of the airplane, while in other flights single (Figure 3.15a) and quadruple (Figure 3.15b) dischargers were installed ($\underline{i}_5$ and $\underline{i}_4$ are the currents of the single and quadruple dischargers on the wings). We see from the curves of Figure 3.14 that an increase of the number of closely positioned dischargers leads to some deterioration of their coulomb-ampere characteristics.

Another way to increase the total discharger current which is frequently used in practice is to install additional dischargers along the edges of the wings, stabilizer, and so on. It follows from general considerations that these additional dischargers are located at points where the intensity is much less than at the tips of the wings and stabilizer (see Chapter 2, Section 1), and therefore, their discharge

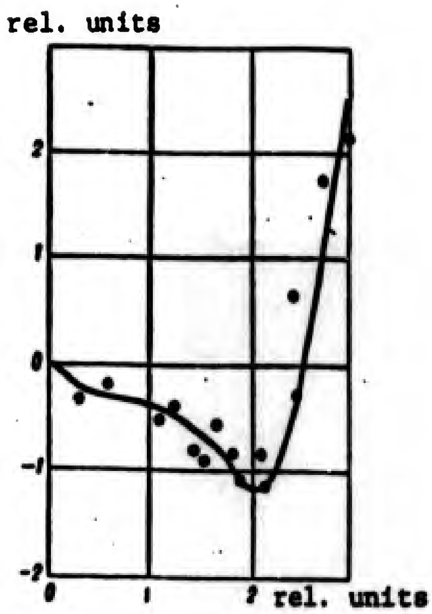

Figure 3.13. Current flowing to airplane propeller for various airplane charges [6].

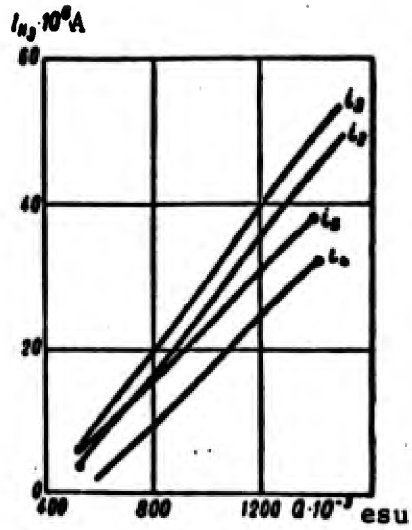

Figure 3.14. Comparative coulomb-ampere characteristics of dischargers (single, paired, and quadruple).

i_3 is the current on the single discharger on the right stabilizer; i_2 is the current on the dual discharger on the left stabilizer; i_5 is the current on the single discharger on the right wing; i_4 is the current on the quadruple discharger on the left wing.

action will not be very effective. This is confirmed by the data shown in Figure 3.11. The discharger located on the rudder tip fairing (current i_1) is mounted 200-250 mm below the very topmost point of the airplane tail because of structural considerations. The current flowing through this discharger (identical to that of all the other dischargers) is less by about a factor of two than that flowing through the other dischargers. At the same time, the field intensity due to the airplane charge at the tip of the rudder fairing is even somewhat greater than that at the wingtips, for example. Since the field intensity decreases very rapidly with the distance from the tips of the wings, stabilizer, and so on, the slope of the coulomb-ampere

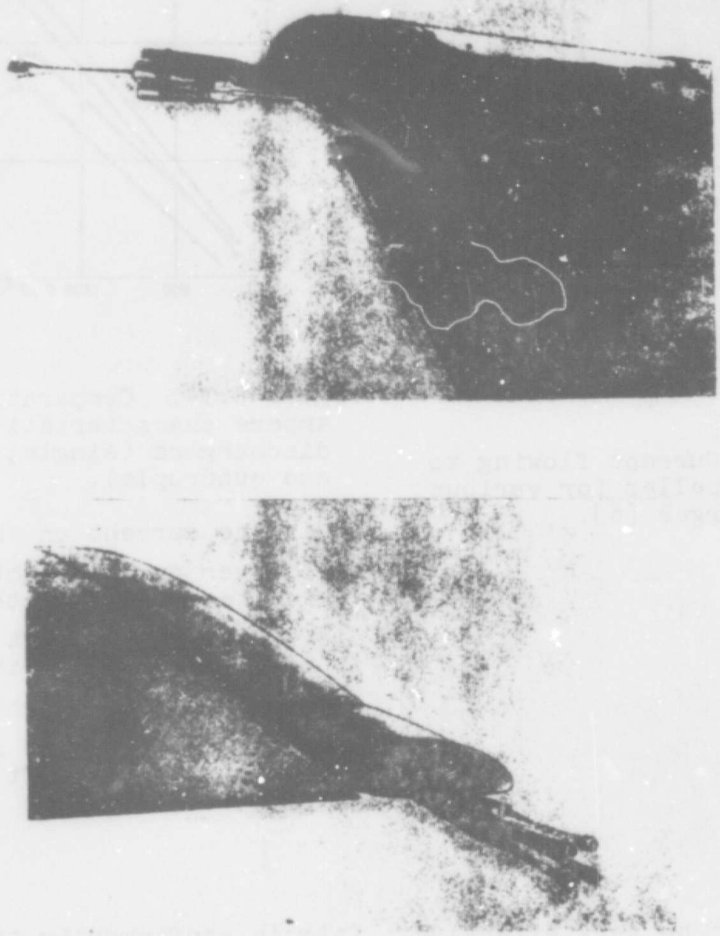

Figure 3.15. Wingtip dischargers. Upper—single;

Upper— Single; lower — quadruple

characteristics of the dischargers will also decrease with shift of the latter toward the fuselage, i.e., the increase of the number of dischargers does not have any marked effect on the magnitude of the airplane charge. At the same time, for high airplane charges the dischargers installed at the central parts of the wings and tailplane may become fixed discharge points, which makes it possible to reduce the level of the radio interference.

The effectiveness of the discharger action and its coulomb-ampere characteristic, therefore, depend both on the characteristics of the discharger itself and the discharger location. The relative advantages of dischargers of different forms and their locations are readily seen in a corresponding comparison of the discharger currents.

Figure 3.16 shows the connection between the current flowing through an experimental discharger (I_{exp}) and the current through a standard discharger (I_{st}). The two dischargers were located at symmetric points of the airplane so that the effect of location on the currents flowing through them was eliminated. If $d = 0$ and $\alpha=45°$, the characteristics of the two dischargers are identical. The larger the value of d, the lower the potentials (or airplane charge) at which the new discharger begins to operate. If the angle $\alpha>45°$, the slope of the volt-ampere characteristic of the experimental discharger is steeper than that of the standard discharger. The larger the angle α, the greater the advantage of the experimental discharger in comparison with the standard version. If the coulomb-ampere characteristic of one of the dischargers is known, then from a relation similar to that shown in Figure 3.16 it is easy to calculate the coulomb-ampere characteristic of the other discharger.

By comparing similarly the currents flowing through identical dischargers located at different points of the airplane (Figure 3.17), we can identify the relative advantages of the discharger location points. Figure 3.17 shows a comparison of the currents flowing through dischargers of the same type located at selected (see Figure 3.11) points of the airplane. The curves of Figure 3.17 were plotted from the results of all the flights in Cs clouds and show that the currents flowing through dischargers installed on the wings (i_4 and i_5) and on the stabilizers (i_2 and i_3) are equal, i.e., the locations of these dischargers are equivalent. The slope of the i_1 current line for the discharger mounted above the rudder is less than 45°; consequently, the location of this discharger is less favorable than the location of the other dischargers. The slope of the line $I_m = f(I_n)$ shows how many times more effective one location is than another.

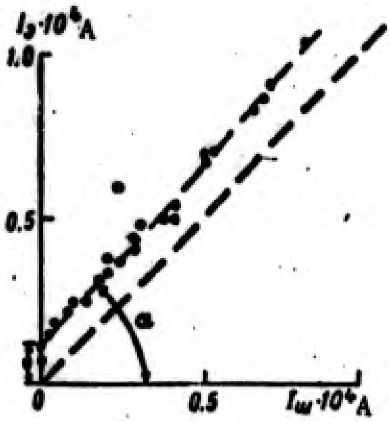

Figure 3.16 Comparative characteristics of dischargers of two types located at symmetric points of the airplane.

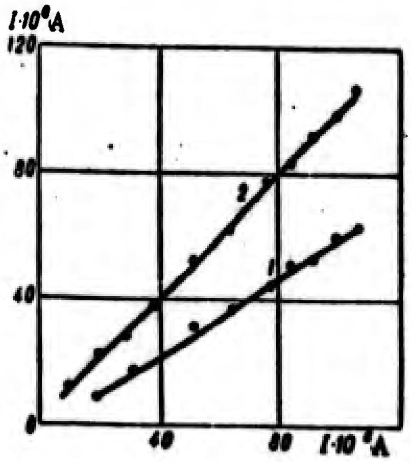

Figure 3.17. Comparative characteristics of discharger location points (all dischargers single).

1) current of discharger located above rudder (i_1) and current of discharger on wing surface (i_5);
2) current of discharger on one wing surface (i_4), current of discharger on one stabilizer (i_2), and current of discharger on the other stabilizer (i_3).

Plotting the relations in the $I_m = f(I_n)$ coordinates is also convenient, in that it does not require reducing the measurement results to a fixed altitude and speed. Therefore, this comparison technique is very convenient for relative measurements. In addition to the simplicity of the construction, this technique for comparing discharger currents is also convenient in that as soon as the coulomb-ampere characteristic of one of the dischargers is known for a given type of airplane at a given installation position, the characteristics of other forms of dischargers and their locations can be determined without measuring the airplane charge.

§ 6. Balance of Currents Flowing to Airplane and Effectiveness of Dischargers

Study of the balance of the currents flowing to the airplane makes it possible to determine the accuracy of the measurements of the individual components of the current flowing to the airplane and the effectiveness of the dischargers.

The solution of (3.1) with account for what has been said concerning the effect of airplane charge on the individual current components [Equations (3.3), (3.6), (3.7)] has the form

$$Q=\frac{I_{1_1}+I_{1_2}+I_{1_3}}{\alpha\bar{p}S\sum_i n_i r_i^2+\frac{1}{R_s C_e}+\frac{1}{R_c C_e}+m\bar{A}_k\gamma}\left(1-e^{-\frac{t}{\tau_{1,2}}}\right), \tag{3.19a}$$

where $\bar{A}_k$ is the average value of A_k for the dischargers; S is the area from which the particles rebound; $\bar{p}$ is the average value of the coefficient p.

For charges $Q \gg Q_{cr}$ we denote

$$\tau_2=\frac{1}{\alpha\bar{p}S\sum_i n_i r_i^2+\frac{1}{R_s C_e}+\frac{1}{R_c C_e}+m\bar{A}_k\gamma}. \tag{3.19b}$$

where τ_2 represents the charge relaxation time of the airplane from which the corona currents flow, and for charges $Q < Q_{cr}$

$$\tau_1=\frac{1}{\alpha\bar{p}S\sum_i n_i r_i^2+\frac{1}{R_s C_e}+\frac{1}{R_c C_e}}, \tag{3.19c}$$

where τ_1 is the charge relaxation time of the airplane prior to the moment when the corona discharge current begins.

Then (3.19) takes the form

$$Q=(I_{1_1}+I_{1_2}+I_{1_3})\tau_{1,2}\left(1-e^{-\frac{t}{\tau_{1,2}}}\right). \tag{3.20a}$$

and under steady-state conditions, when the charge and discharge currents are equal, the steady-state charge Q_∞

$$Q_\infty=(I_{1_1}+I_{1_2}+I_{1_3})\tau_{1,2}. \qquad (3.20b)$$

Equations (3.19) and (3.20) show that in a uniform cloud the airplane charge Q tends to reach the steady-state value Q_∞. The time for reaching the steady-state value is determined by the relaxation time $\tau_{1,2}$. The increase in time follows the curve $\left(1-e^{-\frac{t}{\tau}}\right)$. At the initial moments of time, when $Q \ll Q_\infty$, the increase of $Q(t)$ is determined by the magnitudes of the charge currents $I_{1_1}+I_{\text{II}_2}+I_{1_3}$. During this period the discharge current has no effect on dQ/dt. The discharge currents have an increasing effect on the values of dQ/dt as the charge increases. The contribution of the collector effect to the values of 1 of modern airplanes is usually small, and therefore the collector current I_{II_4} has no effect on airplane charging.

The equivalent electrical circuit of the charged airplane is shown in Figure 3.18 in accordance with (3.1) and (3.19) or (3.20). We note that the internal resistance of the generator which charges the airplane is very high, and therefore it operates as a current generator in which the energy comes from the motion of the airplane. In fact, the energy of the particles which charge the airplane in clouds is equal to $\frac{mw^2}{2}$, where m is the particle mass. The airplane potential V_{cr} affects the particle separation conditions if $qV_{cr} > \frac{mw^2}{2}$, where q is the charge of the separating particles. For possible values of the airplane potential $V \ll V_{cr}$. For example, if $m = 10^{-6}$ g, $q = 10^{-6}$ esu, and $w = 5 \cdot 10^4$ cm/sec, then $V_{cr} = 10^9$ V. Therefore, the current charging the airplane is practically independent of the airplane potential.

For scattering bodies (3.19c), (3.20), and (3.21) take the form

$$Q=(I_{1_1}+I_{1_2})\tau\left(1-e^{-\frac{t}{\tau}}\right), \qquad (3.21a)$$

$$Q_\infty=(I_{1_1}+I_{1_2})\tau, \qquad (3.21b)$$

$$\tau=\frac{1}{e\bar{\rho}S\sum_i n_i r_i^2+\frac{1}{R_0 C_0}}. \qquad (3.21c)$$

i.e., by measuring $Q(t)$ and Q_{∞} we can, as noted above, determine the current J_{II_4}, which appears as a result of the collector effect. Usually

$$\alpha \bar{p}_j \sum_i n_i r_i^2 \gg \frac{1}{R_c C_c}.$$

Synchronous measurements of the components of the currents flowing to the airplane and the magnitude of the airplane self-charge make it possible to write the balance of these currents. In accordance with (3.1) and what has been said previously concerning the relationship of the currents flowing to the airplane, the balance equation can be written in the form

$$\frac{\Delta Q}{\Delta t} = (J_{I_1} - J_{II_4}) S_{эф} - \frac{Q}{C_c R_c} - \sum_m I_{II3_m} - L J_{II_4}. \qquad (3.22)$$

where $J_{I_1} - J_{II_4} = J_I$ is the density of the current flowing to the forward plates (J_{I_1} is the charging current density, J_{II_4} is the collector current density); S_{ef} is the effective area from which droplets separate from the airplane; C_c is the airplane capacitance; J_{II_4} is the linear density of the current flowing through the rear plates; L is the length of the trailing edges of the wings, rudder, and stabilizer (L = 50 m for the Tu-104B).

We can determine the area S_{ef} from (3.22), since all the other terms appearing in the formula are known. Considerable errors may occur in the calculation in cases in which a corona discharge occurs on the airplane at unprotected points, i.e., when the current flowing through the rear plates reaches noticeable values.

Examples of the current balance under various meteorological conditions are shown in Table 3.7.

The measurement of the current balance makes it possible to estimate the degree to which the density of the charging current flowing to the forward plates corresponds to the density of the charge current flowing to the other portions of the airplane surface.

TABLE 3.7. BALANCE OF ELECTRIC CURRENTS FLOWING TO Tu-104B AIRPLANE 1965

	regime number				
	2	2	2	10	5
	7/VIII	7/VIII	7/VIII	2/VIII	11/VIII
weather conditions	at top of Cs	Cs	Cs	Ac, As, rain	below Cb in rain
flight altitude, m	10 400	10 400	10 400	5000	1200
current density flowing to forward plates, A/m^2	$-6\cdot10^{-5}$	$-3,3\cdot10^{-5}$	$1\cdot10^{-5}$	$1,5\cdot10^{-5}$	$3,2\cdot10^{-5}$
total current through dischargers, A	$300\cdot10^{-6}$	$380\cdot10^{-6}$	$75\cdot10^{-6}$	$250\cdot10^{-6}$	$250\cdot10^{-6}$
per-unit-length current density through aft plates (dischargers) xL, A	$2\cdot10^{-6}$	$0,5\cdot10^{-6}$	—	$2\cdot10^{-6}$	$4\cdot10^{-6}$
current through exhaust gas jet, A	$180\cdot10^{-6}$	$200\cdot10^{-6}$	$55\cdot10^{-6}$	$300\cdot10^{-6}$	$100\cdot10^{-6}$
jet resistance, Ohms	$4,8\cdot10^{8}$	$4,8\cdot10^{8}$	$4,8\cdot10^{8}$	$6\cdot10^{8}$	$1,7\cdot10^{9}$
change of airplane charge $\frac{\Delta Q}{\Delta t}$ A . .	$5\cdot10^{-6}$	$5\cdot10^{-6}$	$1\cdot10^{-6}$	$7\cdot10^{-6}$	10^{-9}
airplane charge in esu	$-0,5\cdot10^{6}$	$-0,6\cdot10^{6}$	$-0,15\cdot10^{6}$	10^{6}	$0,95\cdot10^{6}$
in Coulombs	$-0,15\cdot10^{-3}$	$-0,2\cdot10^{-3}$	$-0,05\cdot10^{-3}$	$3,3\cdot10^{-4}$	$0,3\cdot10^{-3}$
calculated particle separation area, S_{eff}, m^2	8,5	17,5	13	35	11,3

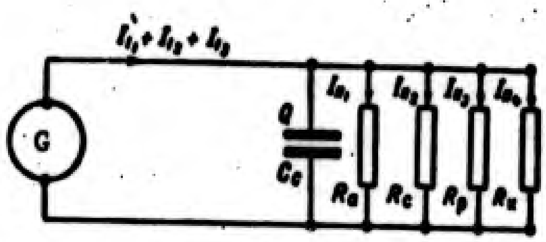

Figure 3.18. Equivalent electrical scheme for airplane charging in flight.

G is the generator; I_{I_1}, I_{I_2} and I_{I_3} are the charging currents; I_{II_1} is the conduction current; I_{II_2} is the current through the exhaust gas jet; I_{II_3} is the current through the dischargers and the surface segments having a corona discharge; I_{II_4} is the current arising as a result of the collector effect of the particles; R_a, R_c, R_p, R_K are the corresponding resistances; C_c is the airplane capacitance; Q is the airplane charge.

The data of Table 3.7 show that the calculated particle separation area varies in the range from 10 to 35 m^2. The airplane surface area is 750 m^2 and the projected frontal area is $S_M = 42$ m^2. Thus, even in rain, the particle separation area is less than the projected frontal area.

We see from (3.22) that if the measured current density J_I is greater than the average density, J_{av}, then the calculated area S_{ef} will be less than the actual area S_{act}; however, if $J_I < J_{av}$, then $S_{ef} > S_{act}$. In finely dispersed clouds the relation $S_{act} \leq S_M$ must be satisfied. Since, in reality, $S_{ef} < S_M$, this means that the density of the current flowing to the forward plates must be greater than J_{av}. If the charge is transferred to the airplane as a result of its interaction with large particles, then we would expect that $J_{meas} < J_{act}$, i.e., $S_{ef} > S_{act}$. However, the measurement results show that in this case as well $S_{ef} < S_M$, i.e., the charge current is basically created by particles striking the frontal surface of the airplane.

If the density of the current flowing to the forward plates is not close to the average density of the current charging the airplane, then the quantity S_{ef} must change markedly with variations of the dimensions of the particles in which flight is taking place. For example, rain droplets must impact on a cross section close to the projected frontal section, or even on the entire airplane platfrom area; small particles must impact basically on the regions in the

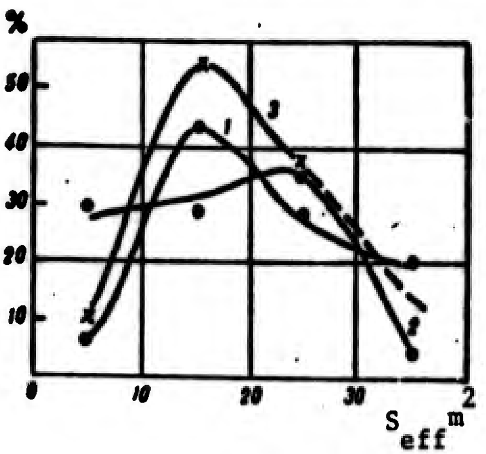

Figure 3.19. Probability of the value of the effective area on which the particles charging the Tu-104B airplane impact.

1) in Cs (plotted from 62 measurements in different clouds); 2) in Ns (plotted from 47 measurements in different clouds); 3) in heavy precipitation (11 cases).

central part of the wings, where the plates were located. Figure 3.19 shows the values of the area S_{ef} calculated from the equation of the current balance measured in clouds and precipitation. These values make it possible to conclude that the area S_{ef} remains approximately constant (~20 м²) during measurements in quite different meteorological conditions: in finely dispersed Cs clouds (1), in Ns clouds containing small and large drops (2), in large-drop precipitation from a Cn cloud (3). In other words, the conclusion drawn previously that the current flowing to the forward plates is quite representative and that the airplane is charged basically by particles whose angles of incidence to the airplane surface are close to 90° is confirmed. If we take S_{ef}=15 м², then the error in the determination of the total current flowing to the airplane from the data on the current flowing to the plates will not exceed ±50% and on the average this error amounts to about ±20%.

Measurements on the IL-18 turboprop airplane also showed that in this case as well the current flowing to the front parts of the airplane is the primary current charging the airplane during flight in clouds and precipitation.

At the beginning of this chapter, we noted that the effectiveness of special dischargers installed on an airplane can be evaluated by comparing the current flowing through these dischargers with the currents flowing to the airplane and comparing these values with the airplane's "natural" dischargers (discharge owing to conductivity of the exhaust gases, collector effect, corona discharging at individual points of the airplane surface). Having available information on the individual components of the current flowing to the airplane and the connection between these components and the airplane charge, it is natural to try to find the discharger effectiveness criterion.

According to (3.19), there is a connection between the airplane charge (potential) and its overall effective conductivity to the atmosphere Λ ($4\pi\Lambda = \frac{\varepsilon}{\tau}$) where ε is the dielectric constant of air), which can be represented graphically by the curves in Figure 3.20. Each curve is plotted for a given charge current I_1, where $I'_1 < I''_1 < I'''_1$. Returning to (3.1) and (3.19), and also to Figure 3.18, we can write

$$4\pi\Lambda = \frac{1}{CR_p} + \frac{1}{CR_c} + \frac{1}{CR_a} + \frac{1}{CR_K}.$$

For example, if on the basis of the operating conditions of the radio equipment or atmospheric electricity instrumentation the charge of an airplane of a given type must not exceed Q_{cr} (or the potential V_{cr}), then the requirements on the effective conductivity vary depending on the charging current. For I'_1 Λ must be not less than Λ', for I''_1 and I'''_1 it must be no less than Λ'' and Λ''', respectively. After determining for the given flight weather conditions the charge current I_1 and the required value of Λ with the aid of the equation above and knowing $\frac{1}{R_a}$, $\frac{1}{R_K}$ and $1/R_c$, we can find how many dischargers need to be installed on the airplane at the selected points and what the discharger coulomb-ampere characteristics should be in this case. If for the given arrangement of the dischargers and given discharger characteristics the overall effective conductivity is not sufficient, it is necessary to install additional dischargers after selecting the proper points on the airplane. A nomogram similar to that shown in Figure 3.20 is basic for calculating the protective action of the dischargers on the airplane. It is obvious that the relative effectiveness of the protective dischargers is determined by the degree to which the effective conductivity which they create is greater than the effective conductivity appearing in the exhaust gas jet and as a result of the collector effect. We recall that the values of R_c, R_K, R_p, and R_a depend on the airplane type, flight altitude and speed, therefore, a series of such nomograms must be available.

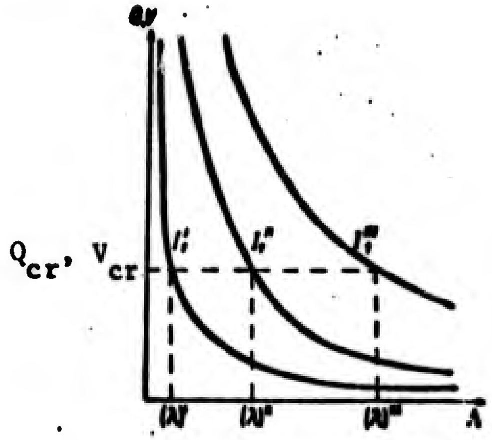

Figure 3.20. Connection between airplane charge Q and overall effective conductivity Λ for different charge currents $I_з$.

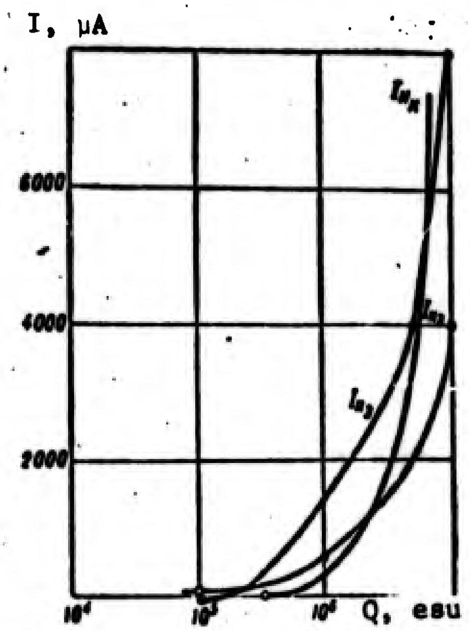

Figure 3.21. Discharge currents through dischargers ($I_{п_3}$), exhaust gas jet ($I_{п_2}$), and aft edges of wings, stabilizer, and rudder ($I_{п_к}$) for different charges of the Tu-104B airplane.

It is very convenient to evaluate the effectiveness of the dischargers and the exhaust gas jet in fractions of R_K for the given weather conditions. It is obvious that the dischargers are ineffective if $\frac{1}{R_р}<\frac{1}{R_к}$; they are also ineffective for $\frac{1}{R_р}<\frac{1}{R_к}+\frac{1}{R_e}$. Finally, the dischargers become ineffective if even a very small corona discharge current develops, flowing from points of the airplane which are not protected by dischargers [8, 120, 121].

The effectiveness of the dischargers installed on the Tu-104B airplane can be illustrated graphically as in Figure 3.21, which shows the dependence of the currents flowing through the exhaust gas jet $I_{п_2}$, through the dischargers $I_{п_3}$, and through the trailing edges of the wings, stabilizer, and rudder $I_{п_к}$ as a function of the airplane charge. Up to a charge of $Q=3\cdot10^5$ esu the current $I_{п_2}$ dominates the other currents. On the segment of the curve for the charge $3\times10^5-3\cdot10^6$ esu and $I_{п_3}\approx2I_{п_2}$ the dischargers and the exhaust gas jet provide leakage for the incoming current. Finally, on the segment of the curve for $Q>3-5\cdot10^6$ esu the current $I_{п_{3_к}}$ increases markedly, and by the time the charge increases to

$Q > 8 \cdot 10^{5}$ esu this current becomes dominant and — together with the currents from the other segments of the airplane which are not protected by dischargers—creates the primary static radio interference. It is obvious that the current flowing through the dischargers must be increased to 7-8 mA with an airplane charge of 10^6 esu (recommended limiting airplane charge on the basis of radio static) in order to improve the static protection of the airplane, i.e., for $\underline{V} = 2 \cdot 10^5$ V. This requires the development of more effective dischargers and study of methods for locating the dischargers.

CHAPTER 4

PHYSICAL PROCESSES LEADING TO AIRPLANE CHARGING

In the preceding chapter we examined the components of the currents flowing to the airplane but did not study the factors which lead to the appearance of the currents which charge the airplane. We shall now examine how these currents are created.

§ 1. Basic Physical Mechanisms Leading to Electrification of Airplanes

At the present time there are at least four theories explaining how airplanes are charged in clouds.

1. Airplane charging as a result of capture of electrically charged cloud and precipitation particles. If the average space charge of a cloud droplet is q $1/m^3$, the airplane speed is w m/sec, and the effective capture cross section of the droplets by the airplane is S_{ef} m^2, then the time t rate of change of the airplane charge Q should not exceed

$$\frac{dQ}{dt}=I_1=qwS_{\text{эф}}=S_{\text{м}}\sum_i n_i q_i \gamma_i. \qquad (4.1)$$

where n_i is the concentration of the droplets carrying the charge q_i; S_M is the body projected frontal area; γ_i is an aerodynamic coefficient indicating what fraction of S_M captures droplets having the charge $q_i = f(r_i)$, where r_i it the particle radius.

The actual charge change can be only less than this value, since along with the charging as a result of the process in question the airplane will lose charge as a result of the conductivity of the exhaust gases, corona discharge, and so on. Hucke [3] noted that the current flowing away through the points of the dischargers with which he equipped an airplane was much greater than the current which in accordance with his estimates of the magnitude of q could flow to the airplane in accordance with (4.1). This led Hucke to assert that the mechanism in question cannot explain the observed electrification of the airplane. However, the information on the magnitudes of the space charges in clouds available to Hucke amounted to a speculative estimate. In 1939 the information not only on the magnitudes of the charges of droplets in clouds, but even on the droplet sizes was inadequate. It may be for this reason, or perhaps because of its simplicity, that this theory is still in existence, and relatively recently Krasnogorskaya [91] suggested that the charge of an airplane on which she was conducting studies was determined by the precipitation charge. Krasnogorskaya based her assertion on the similarity of the curves of the curves of precipitation charge variation and airplane charge variation. At present we have available data which make it possible to compare the airplane charge rate of change with data on space charges in clouds and precipitation (see Chapter 2, Section 2 and Table 2.1). The data of Table 3.1 show that the density of the current flowing to the Tu-104B airplane in various clouds and precipitation exceeds by 10^3-10^4 times the density calculated using (4.1). Even on airplanes flying with a speed of only about 200 km/hr the actual current density is much greater than that calculated using (4.1). For example, for the Li-2 airplane the rate of charge change in nonraining stratiform water clouds is usually more than $10^{-6}-10^{-5}$ C/sec, while the charge flowing to the airplane (see Table 2.1), calculated for $S_{ef} = 10$ m^2 and $W = 60$ m/sec using (4.1), cannot exceed $1.5 \cdot 10^{-8}$ C/sec, i.e., the calculated current is 2-3 orders of magnitude less than the observed current. In Ns clouds, heavy precipitation, and so on, the observed rate of charge change exceeds by 10^2-10^3 times the maximal possible value calculated using (4.1) (see Table 2.1). Measurements also show that in many cases the sign of the current created by the space charge is opposite the sign of the current flowing to the airplane (for example, see Figure 2.16).

On the other hand, if the measured current flowing to the airplane had been created by impact of space charges in accordance with (4.1), then in the clouds there must have existed space charges amounting to hundreds and thousands of esu/m^3; space charges of such density would have created breakdown field intensities in a cloud extending over hundreds of meters and would have caused lightning discharges in clouds of all types. The absence of strong fields in stratus, cirrostratus, and similar clouds shows that the primary current flows to the airplane as a result of a mechanism which differs from that described by (4.1).

It might be assumed that the current flowing to the airplane is created not by the entire space charge, but only by some part of the space charge, say by the part associated with large drops, i.e., as a result of the difference in the coefficients γ_i of (4.1) particles of different dimensions are captured differently. Then, if a charge of one sign is found on the large drops while in the air and on the small drops the charge has the opposite sign, and if even with a relatively small overall space charge its components are large, then a significant current can flow to the airplane. However, if we examine data on the currents flowing to the test bodies, we are forced to discard this assumption as well.

In actuality, as noted previously, the currents flowing to test bodies having the same sections S_{ef} [see (4.1)] and exposed to the same conditions not only differ by many factors, they may even differ in sign. These differences in the currents apply to flights in stratiform and stratocumulus clouds, in nimbostratus and altostratus clouds, in cirrus and thunderstorm clouds, and in heavy precipitation. Consequently, in all these cases, the charging is determined by some mechanism other than that considered in this section. The data of MacCready and Proudfit [75] lead to this same conclusion.

In the experiments of [75] the measured charges of heavy precipitation particles were compared with the airplane charge. It was noted that not only was the airplane charge not proportional to the current magnitude or precipitation charge, but these quantities frequently had opposite signs. We can with good basis suggest that the results obtained by Krasnogorskaya [91] are associated with the fact that both the charges of the drops flowing through the metering instrument and the airplane charge arose as a result of the action of the same electrification mechanism during the corresponding contact of the drops on part of the metering instrument and the airplane. We have previously [93] indicated the probability of such charging of the drops in the instrument used in [91], which makes it impossible to measure the self-charges of precipitation drops. It is also obvious that attempts [94] to measure the space charge of clouds from data on the current flowing to the airplane are not promising.

Thus, the mechanism involving cloud and precipitation space charge flowing to the airplane cannot create more than 0.01 - 0.0001 of the current actually flowing to the airplane surface, and consequently this mechanism cannot play any significant role in airplane charging.

2. Airplane charging owing to the balloelectric effect. Upon impact on the airplane or the air cushion on the frontal parts of the airplane, the droplets or snowflakes break up and this leads to balloelectric electrification, in which the large fragments of the particles are charged by electricity of one sign while the small fragments are charged by electricity of the opposite sign [41a, 96]. During breakup of distilled water drops (or drops in clouds and precipitation) the small particles are charged basically negatively, while the large fragments are charged positively [41]. If the particles contacting the airplane are primarily the large particles which give up their electrical charge to the airplane, while the small fragments of the fractured particles are carried away by the stream without allowing them to settle on the airplane and transfer their charges to the airplane, then the airplane acquires some charge Q. The time rate of change of this charge t cannot exceed the value

$$\frac{dQ}{dt} = w \sum_i q_i n_i S_i. \tag{4.2}$$

where n_i is the concentration of particles of given size and composition in the cloud; w is the airplane speed; S_i is the effective airplane section receiving impacts of particles of the sort i (for example, of radius r_i); q_i is the charge given up by a single particle of the i^{th} sort.

It is difficult to evaluate precisely the role of the balloelectric effect on the basis of the known laboratory studies. The balloeffect depends strongly on the structure of the ice particles and chemical composition of the drops, and also on the velocity of the particle collision with the surface; at the same time the quantitative connection between the charging with these listed parameters has not received adequate study. We can assume that the balloeffect is not realized in finely dispersed water clouds containing drops of diameter less than 30-50 microns [76], and in clouds with large drops the maximal value of the electrification does not exceed $5 \cdot 10^{-10}$ C/g (according to Chapman [95], who studied electrification by breakup of drops in a stream with velocity 10 m/sec). For S = 10 m^2, w = 60 m/sec, and cloud water content not exceeding 2 g/m^3, we find that the maximal charging rate in clouds resulting from this effect cannot exceed $+5 \cdot 10^{-7}$ C/sec.

We have noted previously that even in stratus and cumulostratus clouds the observed rate of charge change reaches $10^{-6}-10^{-5}$ C/sec; in cirrostratus and nimbostratus clouds this quantity is at least an order of magnitude larger. Therefore, it would appear that the airplane electrification in water clouds must result from effects which are not associated with disintegration of the particles. However, the intensity of the balloeffect increases with speed, and electrification has not been investigated thoroughly at impact speeds greater than 50 m/sec. Therefore, on the basis of the available laboratory studies, we cannot definitely exclude the balloeffect as a possible source of airplane electrification. Gunn et al. came to this same conclusion [4, 6].

Still less reliable are the existing estimates of the intensity of the electrification resulting from the balloeffect in snow and in ice crystals. The estimates here are particularly arbitrary since the dependence of the effect on the velocity and structure of the particles is not known. We can expect that the balloeffect of large solid particles is greater than for liquid particles. We recall (see Chapter 2) that a snowflake in the form of a six-pointed star, impacting with a velocity of 100 km/hr on a surface, breaks up into about 500 parts, while hexagonal platelets and column break up into about 30 smaller bits when impacting under the same conditions [74].

Experiments with charging test bodies mounted on an airplane have made it possible to evaluate uniquely the role of the balloeffect in airplane electrification in the velocity range from 160 to 900 km/hr.

Actually, we see from (4.2) that two bodies having similar form and the same effective cross section areas $S_{ef\ i}$, exposed to identical streams of particles with the concentration n_i and traveling with the velocity w, must be charged identically (or the currents to them must be equal) if the electrification takes place as a result of the balloeffect. The quantity q_i depends on the properties of the disintegrating particles, and on the body material to the degree to which the latter affects the disintegration of the particles. The differences in the properties of the test bodies used (well-polished metal spheres) cannot affect the differences in the balloeffect observed [96].

However, it was shown in Chapters 2 and 3 that the magnitudes of the currents flowing to the test bodies in given time intervals differ by a factor of ten, or even differ in sign. Similar differences are also observed in measurements of the currents flowing to the leading-edge plates (current receivers) made from different materials. The differences in the currents cannot be explained by the fluctuations of the number of particles incident on the test bodies. Thus, for example, during 10 seconds with an airplane speed of 200 m/sec and particle concentration $n_i = 100\ 1/м^3$ the probability of deviation of the number of particles striking an area of 10 cm^2 from the average value by more than 2% amounts to less than 1% when using the Stirling formula for the calculation, i.e., the currents flowing to the different bodies can differeby 2% in less than 1% of the number of cases. Larger differences of the currents flowing to two identical bodies are impossible in practice.

Therefore, we must assume that the differences in the currents are caused not by the balloelectric effect but rather by some other mechanism, and the intensity of the action of this mechanism is at least ten times greater than the intensity of the balloeffect action. Significant differences in the currents charging test bodies have also been observed in both finely divided and coarsely divided water-drop clouds and in precipitation, in ice-crystal clouds, in snow, and so on, i.e., in all these cases, the contribution of the ballo-effect could not exceed a few percent of the total current flowing to the test bodies.

3. Airplane charging as a result of triboelectric effects associated with the relationship between the dielectric permeabilities of the contacting bodies. Several authors [3, 6, 83] have suggested that the airplane charging process is associated with the relationship of the dielectric constants of the colliding bodies in accordance with the Coehn rule [97]: "Two substances with different dielectric permeability which are in contact with one another become charged; the substance with the higher dielectric constant is charged positively while the other is charged negatively". It is difficult to make a quantitative estimate of this process, which is now believed to be the most probable process [83]. We can write an equation characterizing the airplane charge current

$$\frac{dQ}{dt} = w \sum_j \alpha_j n_j S_j, \qquad (4.3)$$

where α_j is a constant of proportionality connecting the charge transferred to the airplane by particles of the j^{th} form with concentration n_j with the given properties of the particles and the airplane: $q_j = \alpha_j n_j$.

Because of the absence of good information on the coefficient α_j, it is not possible in this case to evaluate the relationship between the observed charging intensity and that calculated using (4.3), as was done previously for the estimate of the effectiveness of the charging mechanisms. It is irrational to use for the estimate of α_j the data obtained by Gunn [6] or Schaefer [74] on the connection between dQ/dt and n_j as a result of ground-level measurements, since their experiments are a copy of the airplane measurements except that they were conducted at the surface of the Earth. Even if the charging is due to a mechanism which differs from that being described, if we use the data of the ground-level measurements to evaluate the charging intensity using (4.3), we obtain electrification values which are close to those observed, but we do not find an answer to the question of the nature of electrification.

According to the data of [6], during flights in clouds with solid particles, the airplane was charged negatively. The authors of [6] explained this effect in accordance with the Coehn rule: the metal, having a dielectric constant close to zero, is charged negatively, while the ice particles with a higher dielectric constant are charged positively. To confirm the validity of this mechanism, the series of experiments mentioned in Chapter 2 was conducted which showed the dependence of the airplane electrification intensity and the maximal charge acquired by the airplane on the properties of the airplane coating, for example, by selecting a corresponding coating the sign of the airplane charge can be changed. The charging intensity was reduced quite effectively by coating the airplane with a colloidal silicon solution. Schaefer [74], studying the dependence of electrification on the type of coating in a ground-level setup in snow storms, showed that the condition of the coating has a significant influence on the magnitude and sign of the charge (see Table 2.13).

In spite of some deviations from the regular pattern, the table still shows that while clean aluminum was always charged positively, the surface coated with nitrocellulose was charged negatively, i.e., the influence of the surface condition on its electrification is very large. Although the effect of the surface properties on its electrification shows up clearly, there are some questions on whether the electrification follows the Coehn rule.

We have noted previously that while in Gunn's experiments an airplane with clean dural skin was charged negatively in snow and in ice crystals, in Schaefer's experiments under the same condition a clean aluminum surface was charged positively. Studies of the charging of the IL-14 airplane with clean dural skin, made in [98], showed that the airplane charge signs were different in water clouds and ice-crystal clouds. But according to the Coehn rule, any metal should be charged negatively with respect to any dielectric. Therefore, the question arises: is airplane electrification by friction really explained by the relationship between the dielectric permeabilites?

We have mentioned previously that collision of the airplane with an ice crystal may be accompanied by partial melting of the ice crystal at the point of contact. In this case, the surface will be charged with the charge whose sign is characteristic for water. It is possible that this is the reason why Schaefer noted positive charging of the dural surface in snowstorms. The influence of the surface properties can best be studied by measuring the charging of several test bodies under the same conditions.

The experiments described in Chapter 2 with test bodies coated by such metals as gold, palladium, and nickel (see Tables 2.14 and 2.15) showed that under the same conditions, the bodies were charged differently, and sometimes even acquired charges of different signs. In these experiments the probability of crystal melting was the same for the different bodies, while the probability of the occurrence of oxide films was reduced by the use of noncorroding materials.

Thus, the theory under discussion cannot explain the observed effect even qualitatively. Therefore, there is no point in making quantitative evaluations of airplane electrification in accordance with this theory.

4. <u>Airplane charging owing to contact potential difference between airplane surface material and cloud and precipitation particles</u>. It has been shown [99] that if a conducting body is placed in a particle stream, the body can be charged to a limiting potential as a result of the contact potential difference V_K between the material of the particles and the body

$$V = V_K \frac{R}{\delta}, \tag{4.4}$$

where R is the linear dimension of the body (for example, for a sphere R is its radius), and δ is the distance at which the exchange of charges between the particles which have separated from the body and the body itself terminates. For the atmosphere up to an altitude of 10-20 km $\delta = 10^{-6} - 10^{-7}$ см. We see from (4.4) that a body of dimension 1 m with a contact potential difference between the particles and the body of the order of 1 V can be charged to a potential of $10^8 - 10^9$ V. In actuality, the steady-state value of the airplane potential will be less than this because of the discharge currents.

The application of this charging scheme to airplane electrification theory runs into certain problems. If two bodies with electronic conductivity come into contact with one another, a contact potential difference is established between them, equal to the difference of the electron work functions of the contacting bodies. In the general case in which the charge exchange takes place both as a result of electron transfer and as a result of migration of ions of different sorts, in order to estimate the steady-state potential difference we must know the chemical potentials of each of the bodies for the corresponding charge carriers. The equilibrium potential will be reached with equality of the chemical potentials of the contacting bodies.

Upon contact with the airplane surface, water and ice will exchange charges both as a result of electron transfer and as a result of ion migration. Therefore, in the following we shall use the term "contact potential difference" in referring, not to the difference of the potentials between two metallic bodies as is usually done, but rather referring to the difference of the potentials of any two bodies which arises when they come into contact.

If the contact potential difference between the airplane skin and water is of one sign while that between the skin and ice is of the other sign, then in water clouds the airplane will be charged with electricity of one sign, while in ice clouds it will be charged by electricity of the opposite sign. If the skin material has some chemical potential as a result of its treatment, we can expect that a particular material can be charged either positively or negatively in snow. The influence of surface treatment is illustrated by the fact that tabulated data [100] on the electron work function of aluminum differ by nearly 1 eV.

Let us examine the effectiveness of the subject process. If we follow Schaefer [74] and assume that each cubic meter of air contains about 11,500 ice crystals of total mass 0.175 g (average weight of each crystal is $15 \cdot 10^{-6}$ g), the airplane velocity is 200 km/hr, and its effective particle collision cross section is on the order of 10 m^2, then the airplane collides with $\sim 10^7$ particles per second and $\sim 2 \cdot 10^6$ particles rebound from the airplane. If we assume that the contact area S_K of each particle amounts to 1% of its surface area, then in accordance with [99, 101] the charge per particle is $q_K = \frac{\varepsilon S_K}{4\pi\delta} \times V_K = 10^{-2}$ esu and the current created by all these particles, which flows to the airplane, will be about 1 mA. These particles will yield a charge of about 10^4 esu per gram of substance, i.e., during electrification, currents which are larger than those observed can arise as a result of the action of this mechanism (see Chapter 3).

Thus, the very powerful subject mechanism can explain the airplane electrification phenomenon. The electrification mechanism based on the contact potential difference will be examined in greater detail in the next section.

It should be noted that nearly any cloud particle electrification mechanism can lead to airplane electrification as well. Specifically, airplane electrification may result from particle disintegration in the airplane's electrical field (Muchnik's study [102] for clouds), electrification upon rapid freezing of supercooled droplets, when they are strongly charged as they "explode" (Kachurin's study [103] for clouds), electrification effects during phase transformations (studies of Workman and Reynolds [104]), and so on. However, all these mechanisms, which superficially appear to be different, can be reduced to the subject mechanism, which arises as a result of the contact potential difference.

The electrification conditions depend to a considerable degree on the impact velocity. The balloeffect role can increase markedly at very high velocities. It appears that electrification conditions may change at body velocities greater than the speed of sound. Electrification conditions may change significantly if the contact time is less than the time for sound wave transmission through the particle. Finally, electrification conditions may change if the energy transferred to the atoms and molecules of the colliding bodies exceeds their binding energy, ionization potential, and the like.

§ 2. Airplane Electrification Under the Influence of the Contact Potential Difference Between the Airplane Surface Material and the Cloud and Precipitation Particles

Charging of a body in a monodisperse particle stream owing to the contact potential difference. We have mentioned previously that the electrification of bodies in clouds and precipitation can be explained by the charging of the body and the aerosol particles in the atmosphere which arises during separation of the particles from the body as a result of the contact potential difference between the body and the particles. If a very small flat particle contacts a large body and if the contact potential difference between them is V_K, then charges q which are equal in magnitude but opposite in sign [99] will remain on the body and the particle. Let us assume that the body is charged negatively

$$q_{\kappa}=V_{\kappa}C_{12}=\frac{\varepsilon S}{4\pi d}V_{\kappa}, \qquad (4.5)$$

where $V_K = \varphi_1 - \varphi_2 - V_1 - V_2$, ($\varphi_1$ and φ_2 are the work functions of the body and particle current carriers, V_1 and V_2 are respectively the potential drop within the body and the particle at the point of contatct; V_1 and V_2 are determined by the field penetration depth into the bodies and depend on the magnitude of the current carrier concentration in the corresponding bodies [105]; for the metals $V_K = \varphi_1 - \varphi_2$); C_{12} is the capacitance between the particle and the body; d is the width of the average gap between the body and the particle at the instant of its separation, when charge exchange between the particle and the body can be considered to have terminated. The quantity d (and, therefore, the quantity C_{12}) depends on the separation velocity, the adhesion forces between the particle and the body, their elastic constants, resistivity, and dimensions, on the dielectric constant and resistance of the surrounding medium, viscosity of the air, and hydrodynamic flow conditions, but for poorly conducting media and body velocities from 1 m/sec to several km/sec we can consider that the value of d does not exceed $10^{-4}-10^{-7}$ cm [96, 106].

If another particle, similar to the first, now contacts the body and then separates from it, as a result of the contact potential difference between the particle and the body a charge less than $-q_K$ will be transferred to the body. The magnitude of the charge transferred to the body is reduced, since the particle acts as a sort of discharger and carries away the charge q_K' which is less than q_K by the amount q_m, proportional to the surface charge density at the point where the particle separates, i.e., $q_K' = q_K - q_m$, and

$$q_m = m q_K \frac{S}{S_T}, \qquad (4.6)$$

where S_T is the body surface area, m is a coefficient which in the general case accounts for the factor by which the average surface charge density at the point of separation differs from the average surface charge density on the body.

Thus, after separation of the second particle the charge $-(2q_K - q_m)$ remains on the body. If the body is contacted successively by other particles which then separate from the body, the body will become charged. It is obvious that in the absence of other charge sources the charging of the body will cease when the difference $q_k - q_m = 0$. The magnitude of the potential to which the body is charged is easily calculated for bodies of very simple shapes (for example, the thin disk, sphere, ellipsoid).

For a sphere of radius R with m = 1 (i.e., considering that the surface charge density on the particle is equal to its average density on the sphere), (4.6) may be written as

$$q_m = VC_T \frac{S}{S_T} = V \frac{S}{4\pi R}, \tag{4.7}$$

where C_T is the sphere capacitance and V is the potential acquired by the sphere during charging.

It follows from (4.5) and (4.7) that the potential to which a body may be charged by means of the subject process can reach the values [see (4.4)]

$$V = V_k \frac{R}{d}. \tag{4.8}$$

Thus, if there is some contact potential difference between the body and the particles, then in the absence of other charge sources the body in the particle stream can be charged to very large potentials. For example, a sphere of radius 1 m can be charged to a potential $\sim 10^8 - 10^9$ V and can acquire the charge $\sim 10^7 - 10^8$ esu if V_K = 1 V; a sphere of radius 1 cm can be charged to a potential of $10^6 - 10^7$ V. Incidentally, an isolated body can experience a similar charging process if, as a result of melting, droplets of matter which have transitioned into the liquid phase separate from the body.

Equation (4.8) can also be derived from the more general condition that the charging of the body in the process described above terminates at the moment when the levels of the chemical potentials of the charged body and the particle become equal [99].

The subject charging mechanism makes it possible to explain one of the triboelectric processes and, as follows from the preceding discussion, the high values of the potentials acquired by the airplane, and also the influence of the body properties on the magnitude and sign of the charge acquired by the body. However, for this purpose we must examine a more realistic picture of the phenomenon, rather than the highly stylized version above. Specifically, we must examine in more detail the charge exchange between the particles and the body, account for the influence of the discharge currents, and compare the calculated values with the observed values.

Assume a metal sphere of radius R enters a uniform monodisperse stream of particles of radius r with concentration n, traveling along parallel trajectories with the velocity w, and rebounding elastically from the sphere after collision with it. As indicated in Chapter 3, such a collision mechanism defining the body charging actually takes place. Assume also that the contact potential difference at the interface between the particle and the body equals V_K. We also assume that the effective conductivity of the medium in which the body is located is equal to λ_{ef} (as noted in Chapter 3, all the basic airplane discharge currents are related linearly with the airplane charge and, consequently, by replacing the value of the conductivity components by λ_{ef} we can approach the actual conditions). The sphere charging equation analogous to (3.1) can be written in the form

$$\frac{dQ}{dt}=I_1-\sum_i I_{1i}. \qquad (4.9)$$

In accordance with (4.5) the charge current is

$$I_1=k_1 nwSC_{12}V_\kappa\left(1-e^{-\frac{\Delta t}{\tau_\kappa}}\right), \qquad (4.10)$$

where S is the sphere cross section area; C_{12} is the mutual capacitance of the sphere and the particle at the moment of particle separation; Δt is the contact time; τ_K is the (droplet) particle charge relaxation time; and k_1 is a coefficient indicating what fraction of the particle flux nwS impacts the sphere surface, i.e., k_1 depends on the flow velocity and the radius of the body (or in the general case, the body geometry), viscosity of the air, and particle size and mass [70, 107, 108], and accounts for the fact that particles impacting at different angles on the sphere surface may acquire different charges.

The value of the capacitance C_{12} can be calculated in the solution of the problem of the interaction of two spheres, one of which is grounded while the other has unit charge, with account for the action of the charge images of suitable orders [for example, (34)].

Denoting $Ch\alpha=\frac{D^2-R^2-r^2}{2Rr}$ in accordance with [34], we can obtain the relation

$$C_{12}=-\frac{\varepsilon rR}{D}\sin h\,\alpha\sum_{n=1}^{\infty}\operatorname{cosec} h\,(n\alpha). \tag{4.11}$$

The rate of decrease of this series depends significantly on the distance between the two bodies and diminshes rapidly as the bodies appraoch, i.e., as $\frac{r+R}{D}\to 1$. The value of the capacitance at the moment when the electrical contact between the bodies is broken and further charge interchange between them becomes impossible appears in (4.10). We have indicated above that this breaking of the contact occurs for $D-(R+r)>10^{-6}-10^{-7}$ cm.

We must bear in mind that for $R\gg r$, $r\gg D-(R+r)$ the total capacitance between the spheres is

$$C_{\pi}=\frac{C_{11}C_{22}-C_{12}^2}{C_{11}+C_{22}-2C_{12}}\approx C_{12}.$$

For an estimate of the value of the capacitance C_{12} under the indicated conditions we can use the Russel formula [109]

$$-C_{12}=\frac{\varepsilon Rr}{R+r}\left[C+\frac{1}{2}\ln\frac{2Rr}{(R+r)\Delta}\right]. \tag{4.12}$$

where $C=0{,}577$ is the Euler number, and $\Delta=D-(R+r)$. Since $R\gg r$, (4.12) can be written as

$$-C_{12}=\varepsilon r\left(0{,}58+\frac{1}{2}\ln\frac{2r}{\Delta}\right). \tag{4.13}$$

For particles of radius from 10^{-4} to 10^{-2} cm and $\Delta=10^{-6}-10^{-7}$ cm (4.13) can be simplified

$$C_{12}=Ar. \tag{4.14}$$

The values of the coefficient A for the indicated extreme particle dimensions and separation distances lie in the range 3-8. We can take A = 5 with adequate accuracy. Further refinement is illusory, both because the droplet is not spherical at the time of separation from the body and because several of the cofactors appearing in (4.10) are evaluated with lesser precision.

The magnitude of the charge transferred to the drop depends on the contact time, conductivity, and dielectric constant of the drop. In any case, the time for collision of a drop with the surface is no less than $\Delta t=\frac{2r}{w}$ [81]. The resistivity of the water in clouds is $\sim 10^4$ Ohm/cm; consequently (see [4.10]) $\tau_K \approx 10^{-6}$ sec.

For airplane speeds from 50 to 250 m/sec the drop charge relaxation time τ_K is comparable with the contact time Δt; therefore, we can expect that the cofactor $\left(1-e^{-\frac{\Delta t}{\tau_K}}\right)$ in (4.10) may be less than one and its magnitude changes with drop velocity. However, the experiments of Keily and Millen [76], conducted with drops of diameter from 2 to 60 microns, charged during impact on a metal plate, showed that no dependence of the charge acquired by the drop on its velocity is observed up to speeds close to the speed of sound. Therefore, we can assume that the actual collision time is longer than the predicted time, and hereafter we assume that $\left(1-e^{-\frac{\Delta t}{\tau_K}}\right)\approx 1$.

Using the computation scheme suggested by Fuks [107], we can predict that spheres of radius 1.5 cm traveling with a velocity of $\simeq 2\cdot 10^4$ cm/sec capture practically all drops of radius greater than 10 microns (for drops of radius 10 microns the capture coefficient $\psi_{10}\approx 1$, for drops of radius 5 microns $\psi_5\approx 0{,}9$, for drops of radius

2 microns $\psi_2 \approx 0.5$). The coefficient $k_1 = \psi k_q$, where the coefficient k_q, characterizing the dependence of the acquired charge on the particle incidence angle, is subject to further investigation.

The resulting relations reflect the charging conditions only in the first approximation. The drop impacting on the airplane has a shape which is not spherical. Actually, the drop kinetic energy $\Phi_к = \frac{mw^2}{2}$ (m is the drop mass) may be comparable with or even exceed its free energy $\Phi_c = 4\pi r^2 \Theta$, where θ is the surface energy per unit surface. It is obvious that for $\Phi_к > \Phi_c$ the drop must be deformed markedly; in this case, the capacitance C_{12} may change markedly.

The degree of deformation is defined by the ratio $\Phi_к/\Phi_c$, and therefore the charge which is carried away may depend on the velocity to a degree higher than first (but no higher than third, on the basis of obvious considerations). Even very small drops of diameter about one micron with velocity greater than 50 m/sec may have $\Phi_к > \Phi_c$; for large drops this inequality becomes still stronger. On the other hand, we must consider that the small drops impact on the airplane surface with a velocity which is less and sometimes much less than the airplane motion velocity because of friction in the air which is retarded at the front surface of the airplane. Therefore, the actual ratios $\Phi_к/\Phi_c$ may be less than the values calculated directly from the data on the airplane speed. We must also remember that the mutual capacitance of the drop and the airplane is determined at the moment of drop separation, when its deformation as a result of impact is reduced.

The detailed analysis of all these factors require information on the process of drop collision with the airplane — a process which has received quite inadequate study; this is why we have restricted ourselves to an approximate examination of the charging process. Study of the discrepancies between theoretical and actual electrification, particularly study of the influence of velocity on this discrepancy, may be useful not only for study of electrification but also for study of the process of particle collision with a surface.

The discharge currents $I_{\text{п}}$ in (4.9) can be represented in the form of the current $I_{\text{п}_4}$, which appears as a result of the collector effect, and the effective conductivity currents $I_{\text{п}_1}$.

$$I_{\text{п}_4}=k_2 n w S p Q e^{-\frac{\Delta t}{\tau_\text{к}}}, \tag{4.15}$$

where Q is the body charge; p is a coefficient which shows how the charge of a spherical particle colliding with a charged sphere is related with the sphere charge; k_2 is a coefficient showing what fraction of the particle flux nwS strikes the sphere surface $(k_2=\psi)$.

If two conducting spheres of radii r and R come into contact, if their potentials V are the same, and $R\gg r$, then the charge on the large sphere under steady state conditions will be [34]

$$Q=\varepsilon Q_c\left[1-\frac{\pi^2 r^2}{6(R+r)^2}\right]. \tag{4.16}$$

where Q_c is the charge on the large sphere prior to contact with the small sphere (assuming that the small sphere was not charged initially).

The charge on the small sphere will be

$$q=pQ=\frac{\varepsilon\pi^2 r^2}{6(R+r)^2}Q_c\left(1-e^{-\frac{\Delta t}{\tau_\text{к}}}\right). \tag{4.17}$$

or approximately

$$q=pQ=\frac{1.5}{R^2}r^2Q=\frac{1.5}{R}r^2V. \tag{4.18}$$

If we assume that the discharge current reduces to the current $I_{\text{п}_4}$, then by equating (4.10) and (4.15) we can find that the equilibrium conditions in the considered case are reached with the sphere potential V

$$V=\frac{k_1}{k_2}\frac{AR}{1.5r}V_\text{к}. \tag{4.19a}$$

Setting $k_1/k_2\approx 1$ and $A/1.5\approx 3$, we obtain the relation

$$V \approx 3\frac{R}{r}V_{\kappa}. \tag{4.19b}$$

Comparing (4.19) and (4.8), we see that their difference reduces to replacement of the distance d between the colliding bodies by the radius r of the small body. If the limiting potential of a sphere of radius 1 m during contact with flat particles was equal to 10^8 V ($V_K = 1$ V) then during contact with drops with r = 10 microns the potential will be equal to $3 \cdot 10^5$ V.

The conduction current I_{Π_1} equals

$$I_{\Pi_1} = 4\pi\frac{\lambda_{\text{э}}}{\varepsilon}Q, \tag{4.20}$$

where λ_{ef} is the effective conductivity, equal to the sum of the atmospheric conductivity and the conductivity created by the additional ionization near the body, and ε is the dielectric constant. If corona discharge has not started near the body, we can substitute into (4.9) the values of the quantities appearing therein from (4.10), (4.13), (4.15), (4.18) and (4.20) and obtain the basic equation for calculating the charge acquired by the body in a monodisperse particle stream

$$\frac{dQ}{dt} = k_1 nwSArV_{\kappa} - \left(k_2 nwS\frac{1.5r^2}{R^2} + 4\pi\frac{\lambda_{\text{э}}}{\varepsilon}\right)Q. \tag{4.21}$$

If we assume that at the moment t = 0 the charge Q = 0, then the solution (4.21) has the form

$$Q = \frac{k_1 nwSArV_{\kappa}}{1.5k_2 nwS\frac{r^2}{R^2} + 4\pi\frac{\lambda_{\text{э}}}{\varepsilon}}\left[1 - e^{-\left(1.5k_2 nwS\frac{r^2}{R^2} + 4\pi\frac{\lambda_{\text{э}}}{\varepsilon}\right)t}\right], \tag{4.22a}$$

or

$$Q = k_1 nwSAV_{\kappa}r\tau\left(1 - e^{-\frac{t}{\tau}}\right), \tag{4.22b}$$

where

$$\tau = \frac{1}{1{,}5\pi k_3 n w r^2 + 4\pi \frac{\lambda_\phi}{\varepsilon}}. \qquad (4.23)$$

It is obvious that in this case the limiting sphere potential $V_\infty = \frac{Q_\infty}{R}$ is less than that obtained using (4.19) because of the discharge currents associated with the conductivity λ_{ef}.

Formulas (4.22) make it possible to evaluate the influence of the stream water content and the degree of dispersion of the drops on the magnitude of the equilibrium charge. If the collector conductivity [11] $\lambda_\phi = \frac{\varepsilon}{4\pi}(1{,}5\pi k_3 n w r^2)$ created by the separating drops is much larger than the effective conductivity, then the equilibrium charge $Q \sim 1/r$, i.e., changes in the water content will affect the magnitude of the equilibrium charge only to the degree to which r depends on these changes. The electrification must increase with reduction of the drop size. When the effective conductivity λ_{ef} is much larger than the collector conductivity λ_{co} the equilibrium charge $Q \sim nr$. Then, if the drop size does not change with increase of the water content the equilibrium charge must increase linearly with the increase of the water content; however, if the drop radius changes with a constant water content, the equilibrium charge increases as $Q \sim 1/r^2$.

Since in real clouds the drop spectrum usually changes with variation of the water content, and since the relative role of the effective conductivity also does not remain constant, the weak dependence of the charge of the airplane and the test bodies on the water content at individual points of the cloud becomes understandable. The dependence of the airplane or probe charge on drop size can be studied only for measurement distances over which the relationship between the collector and effective conductivities is relatively constant.

Let us evaluate the relaxation time associated with the collector effect of the particles. Let $n = 10^2$ 1/cm^3, $w = 10^4$ cm/sec, and $r = 10^{-3}$ cm be numbers characteristic for the cloud and the airplane;

then $\tau = 0.2$ sec, i.e., during a time amounting to a few tenths of a second a sphere in the cloud would be charged as a result of the action of the subject mechanism to the equilibrium potential. It follows from comparison of the resulting time τ with the relaxation time due to atmospheric conductivity that the influence of leakage due to conductivity can be neglected up to very high altitudes. Then λ_{ef} is important only in those cases in which a high ionization level develops near the body.

So long as the relaxation time τ is defined by the collector effect it will vary as $1/\underline{nr}^2$, i.e., it will diminsh with increase of the concentration and radius of the particles. If at the same time the water content remains constant, then $\tau \sim r$.

If the field intensity at the sphere reaches the breakdown values, or if a corona discharge point is located on the sphere, then upon reaching the corona discharge threshold the current flowing from the sphere, as indicated above, will be (see [3.15])

$$I_{II_s} = A_k (Q - Q_{\kappa p}) w.$$

Substituting this value of the current into (4.22) and making the corresponding calculations, we can obtain the equation for the sphere charge after initiation of the corona current

$$Q = (k_1 \pi w S A r V_\kappa + A_k w Q_{\kappa p}) \tau' \left(1 - e^{-\frac{t}{\tau'}}\right) + Q_{\kappa p} e^{-\frac{t}{\tau'}}, \tag{4.24}$$

where

$$\tau' = \frac{1}{1{,}5\pi k_2 n w r^2 + 4\pi \frac{\lambda_0}{\varepsilon} + A_k w}. \tag{4.25}$$

Equations (4.22) and (4.24), which are suitable for calculating the sphere charge in a monodisperse stream both in the absence of corona discharge and when corona discharge is present, can also be used to estimate the charging of airplanes in clouds and to estimate the currents flowing to the airplanes. However, we must bear in mind that the magnitude of the charge which is lost as a result of the collector effect during drop separation is proportional to the field intensity at the point where the drop separates [see (4.17) and (4.18)]. For drops whose radius is small in comparison with the radius of curvature of the airplane at the point of separation, (4.18) can be written in the form

$$q = Br^2E_m = 1{,}5r^2p_mQ, \tag{4.26}$$

where E_m is the airplane field intensity at the point of drop separation; B is a coefficient relating the charge of the separating drop with its radius and the airplane field intensity; p_m is a coefficient relating the airplane field intensity at a given point with its charge. If the drops separate at airplane locations where the field is intensified, the collector effect may increase markedly and the equilibrium charge Q will decrease correspondingly.

In this case (4.22) and (4.23) will have the form

$$Q = nw\sum_i (k_{1i}S_i)ArV_{\kappa}\tau_c\left(1 - e^{-\frac{t}{\tau_c}}\right), \tag{4.27a}$$

$$\tau_c = \frac{1}{1{,}5nw\sum_i (k_{2i}S_ip_{mi})r^2 + 4\pi\frac{\lambda_0}{\varepsilon}}, \tag{4.27b}$$

where the indices i relate to segments of the airplane surface which differ both with regard to ambient flow conditions and the field intensification conditions, and S_i are the areas of the corresponding sections. In (4.21) and (4.27) no account is taken for the fact that the magnitude of V_K is not the same for the different segments of the airplane, nor is there any consideration for the fact that individual segments of the airplane surface may be fabricated from a dielectric material.

<u>Charging of a body in polydisperse particle streams as a result of the contact potential difference</u>. In polydisperse streams the Equations (4.22) and (4.23) for spheres take the form

$$Q = wS\sum_j (k_{1j}n_jA_jV_{\kappa}r_j)\tau\left(1 - e^{-\frac{t}{\tau}}\right). \tag{4.28a}$$

$$\tau = \frac{1}{1.5\pi w \sum (k_{2j} n_j r_j^2) + 4\pi \frac{\lambda_0}{\varepsilon}}, \qquad (4.28b)$$

where the index j characterizes the value of the corresponding elements for particles of the sort j.

For the same stream water content, a shift of the distribution toward larger drops must lead to a reduction of the sphere charge and an increase of the relaxation time. The Formulas (4.24) and (4.25) for the corona-discharging sphere are transformed similarly.

Equations (4.27) for bodies of more complex form — airplanes, for example — take the form

$$Q = w \sum_i \left[S_i \sum_j (k_{1j} n_j A_j V_\kappa r_j)_i \right] \tau_c \left(1 - e^{-\frac{t}{\tau_c}}\right), \qquad (4.29a)$$

$$\tau_c = \frac{1}{1.5w \sum_i S_i \sum_j (k_{2j} n_j p_j r_j^2)_i + 4\pi \frac{\lambda_0}{\varepsilon}}. \qquad (4.29b)$$

The indices j show the value of the corresponding elements for particles of sort j; the indices i are the values of the corresponding elements for the i^{th} segments of the surface. For particles of nonspherical form the values of the coefficient A [see (4.14)] may differ markedly from the value presented previously. The coefficient 1.5 in (4.29) was obtained for spherical particles; in the general case, the coefficient p [see (4.18)] depends on the particle shape and particle location at the moment of separation. Therefore, in the case of nonspherical particles the coefficient p must be calculated for each particle form and placed under the summation sign.

The equation for a corona-discharging airplane can be obtained from comparison of (4.29a) and (4.29b) with (4.24) and (4.25). Equations (4.29) make it possible to compare the charging conditions for airplanes of different types in the same cloud. The airplane charging currents will be the higher, the higher the airplane speed and the larger its dimensions. In ice-crystal clouds, in which the solid particle breaks up into a multitude of fragments as it strikes the airplane and the number of fragments depends on the collision velocity, we can expect a stronger influence of the velocity than in the finely dispersed water-drop clouds. A similar remark can be made concerning the charging conditions in clouds having large drops. The steady-state airplane charge increases with increase of the charge current and decreases with an increase of the effective conductivity, which for airplanes is determined primarily by the conductivity of the exhaust gases and the current of the corona dischargers.

It should be noted that this is the theory for a whole class of electrostatic generators. However, we shall not examine here the application of this theory to generators of various types.

§ 3. Theory of Test Body Charging in Particle Streams as a Result of the Contact Potential Difference and Application of this Theory to the Methods for Studying Cloud Physics

The theory developed in the preceding sections can be compared relatively easily with the results of measurements in clouds, made with the aid of test bodies. The simple form of these bodies, the absence of corona discharge current and high ionization level near the bodies, and their shielding from external fields and the airplane charge field make it possible to exclude several factors which complicate the study of charging of the airplane as a whole.

In analyzing the results of measurements using test bodies, it is necessary to take into account three factors which may lead to differences between sphere charging in a stream and the theoretical model charging. First, the drops impact on the body support as well as on the scattering body itself. Let us assume that the test body radius is 1.5 cm, the support radius is 0.3 cm and the support length in the stream is 1.5 cm. Then in accordance with (4.21) and (4.27) the equilibrium charge of the sphere and support as a result of the collector effect will be less than the equilibrium charge of the sphere by 40%. Second, the field intensity at the sphere located in a cylindrical shield is somewhat higher than the intensity near an isolated sphere. Consequently, the collector effect for the same charge will be greater than was estimated previously for the sphere.

The increase of the surface charge density can be evaluated from comparison of the charge density σ_K on a sphere which is the inner plate of a spherical capacitor with the charge density σ_{sph} on an isolated sphere at the same potential. On the sphere in the capacitor the surface charge density (see, for example, [34])

$$\sigma_K = \frac{\varepsilon R_1 R_2}{4\pi (R_2 - R_1)} \frac{1}{R_1^2} (V_1 - V_2), \tag{4.30}$$

where R_1 and R_2 are the radii of the inner and outer spheres, and V_1 and V_2 are their potentials. Thus,

$$\sigma_K = \frac{R_2}{R_2 - R_1} \sigma_{sph}.$$

If the diameter of the outer sphere were equal to the diameter (6 cm, say) of the shield used, then

$$\sigma_K = 2\sigma_{sph}.$$

In reality, the value of σ_T of the test body must be

$$2\sigma_{sph} > \sigma_T > \sigma_{sph}.$$

To refine the bounds of the value of σ_T we can find the degree of point charge shielding by a cylinder [110]. For the shield used, nearly 100% of the charge lines of force are closed in the interior of the shield [111]. If the outer plate of our spherical capacitor has a radius equal to half the length of the shielding cylinder, then for such a capacitor $\sigma_K'' = 1{,}2\sigma_{sph}$. Thus,

$$2\sigma_{sph} > \sigma_T > 1{,}2\sigma_{sph}.$$

The maximal field force will be observed at the points of the test body lying closest to the cylindrical shield; the minimal force will be observed at points located along the line of flight. In this case the coefficient k_2 [see (4.15)] must be represented in the form $k_2' = k_\sigma k_2$, where k_σ accounts for the nonuniformity of the charge density distribution over the sphere. Taking on the average $\sigma_T = 1{,}5\sigma_{sph}$ (refinement of this estimate is not likely to have any marked effect on the actual precision of the test sphere charging calculation), we can estimate the maximal error introduced by this approximation as ±33%.

As a result of the high charge density, the coefficient p increases [see (4.18)]; consequently, both of these factors — the effect of the support and the shield — lead to an increase of the discharge current and a reduction of the equilibrium charge. The equilibrium charge of the test body will be equal to about 0.4-0.5 times the charge of an isolated sphere under the same conditions.

A third factor which may affect the measurement results is the influence of the shield on the ambient flow past the sphere. This influence shows up primarily in some variation of the particle flux as a result of turbulence of the air stream, and if the sphere diameter is relatively small in comparison with the shield diameter, this factor should not alter significantly the values of k_1 and k_2.

Thus, the working formulas for evaluating the charging of test bodies in a monodisperse stream can be written in the form [see (4.22), (4.23), (4.17), (4.10), (4.14)]

$$Q = \frac{k_1 nwSArV_\kappa}{3k_2 nwS\frac{r^2}{R^2}}\left(1 - e^{-3k_2 nwS\frac{r^2}{R^2}t\frac{C_T}{C_T+C_c}}\right), \tag{4.31a}$$

or

$$Q \approx \frac{1{,}5k_1 R^2 V_\kappa}{k_2 r}\left[1 - e^{-\frac{t}{\tau}\left(\frac{C_T}{C_T+C_c}\right)}\right], \tag{4.31b}$$

where $\tau = 1/3\pi k_2 nwS\frac{r^2}{R^2}$; C_T is the capacitance of the test body; C_c is the capacitance of the entire system of leads connected with the body. These estimates of collector conductivity and atamospheric conductivity show that the latter can be neglected. Consequently, the effective (measured) relaxation time τ_{ef} will be

$$\tau_{эф} = \tau\left(\frac{C_т + C_c}{C_т}\right) = \frac{C_т + C_c}{3\pi k_2 n w r^2 C_т}. \qquad (4.32)$$

For measurements in a polydisperse stream we can use the formulas

$$Q = \frac{1.5\bar{k}_1 R^2 \bar{V}_к \bar{r}}{\bar{k}_2 \bar{r}^2}\left[1 - e^{-\frac{t}{\tau_{эф}}}\right] \qquad (4.33a)$$

and

$$\tau_{эф} = \frac{C_c + C_т}{3\pi \bar{k}_2 \bar{n} w \bar{r}^2 C_т}, \qquad (4.33b)$$

where $\bar{r}$ and $\bar{r}^2$ are respectively the average values of the radius and radius squared of the drops in the cloud, and $\bar{k}_1$, $\bar{k}_2$, $\bar{V}_к$ and $\bar{n}$ are the average values of the corresponding quantities.

The magnitudes of the equilibrium charges of test bodies on which corona discharge have not yet started depend on a very small number of parameters; specifically, they are independent of the particle concentration, the charge transfer time Δt, and τ_K (at least, obviously, as long as the air conductivity remains much less than the apparent conductivity resulting from the collector effect). This situation increases the accuracy of the comparison of the theoretical and measurement results.

It should also be remembered that although in many cases k_1 and k_2 differ from unity, the values of k_1 and k_2 must be close to one another.

The ratio of the equilibrium charges $Q_{т_1}$ and $Q_{т_2}$ of two test bodies will be

$$\frac{Q_{т_1}}{Q_{т_2}} = \frac{V_{к_1}}{V_{к_2}}. \qquad (4.34)$$

where $V_{к_1}$ and $V_{к_2}$ are the contact potential differences between the particles and the first and second bodies, respectively.

When using these formulas to calculate charging in real clouds, we must bear in mind that the charging depends not on the particle size spectrum in the cloud but rather on the spectrum of the particles which depart after collision. In finely dispersed clouds the spectrum of the particles which strike and charge the body will be even narrower than the spectrum of the particles in the clouds themselves, considering the particles of small dimensions which either partially or entirely miss the body as they flow around it. Therefore, the values of the average radius and average radius squared of the particles charging the body will be larger than in the cloud.

In coarsely dispersed clouds the particles will break up after striking the body and a great many small particles which are formed from a relatively small number of large particles striking the body will then separate from the body. We have mentioned previously that according to Schaefer [74] snowflakes which impact with a velocity of 100 km/hr on a surface break up into hundreds of parts. The number of particles formed depends, in particular, on the collision velocity (impact kinetic energy) and the angle between the particle velocity vector and the surface on which the particle impacts.

Large drops of radius larger than $(50-100)\cdot 10^{-4}$ cm are particularly strongly fractured after impact. As a result, the values of the average radius and average radius squared of the particles which charge the body in coarsely dispersed clouds will be less than the values in the cloud itself as a result of this factor. It is obvious that the presence in coarsely dispersed clouds of very small particles which do not impact on the test body also leads to a shift of the average radius of the particles charging the body into the direction of larger values in comparison with the drop radius in the cloud itself.

Thus, in coarsely dispersed clouds, depending on the spectrum of the particles in the cloud and on the conditions of particle flow past the body and particle breakup as they strike the body, the average radius and average radius squared of the particles charging the body may be either larger or smaller than the values of the particles in the clouds themselves. As the cloud particle spectrum is broadened in the direction of larger dimensions, there is an increase of the probability of a reduction of the values of $\bar{r}$ and $\bar{r}^2$ of the particles charging the body in comparison with their values in the cloud. An increase of the velocity of the particle collision with the body, or more precisely an increase of the impact kinetic energy, leads to an analogous effect. To the degree to which both of these effects influence the ratio $\bar{r}/\bar{r}^2$, the electrification must become dependent on body velocity in clouds of different types.

We shall use these formulas to evaluate the test body charging characteristics. Upon contact of the bodies with particles the bodies are charged positively if the particles have an overall work function of the electrons and ions greater than the body, and they are charged negatively if the overall work function of the electrons and negative ions of the particles is less than that of the body [see (4.31)]. The electron work function of water is 6.09-6.13 eV [100]. The work function of the metals from which the test bodies were fabricated lies in the range of 4-5 eV [100].

Thus, in accordance with the theory in question, if charging is associated only with the transfer of electrons the bodies would have been charged positively in water. Incidentally, in accordance with this scheme an airplane with a dural skin should acquire a positive charge in water-droplet clouds. We have no data on the work function of ice.

In [112] Arabadzhi describes a measurement of the contact potential difference of water and ice. He made the measurements using a radioactive thorium collector mounted at a distance of 0.5 cm from the surface of the water. The change of the potential between the collector and the water prior to and after freezing served as a measure of the contact potential difference between the water and ice. A value of the contact potential difference equal to 0.15 V is presented in [112].

Unfortunately, the experimental technique leads to some questions.

First, with the thorium work function of about 3 eV [100] and the water work function of about 6 eV, the measured deviations resulting from the effect being studied amount to only about one twentieth of the electrometer scale; second, no steps were taken to avoid the occurrence of a layer of water (ice) on the surface of the collector, which could completely distort the measurement results.

In [113] Dinger and Gunn present a value of the water-ice contact potential difference of about 6 V. It appears that this value is too high. A rough estimate of the change of the work function of ice in comparison with that of water on the basis of data on the heat of melting shows that the work function of ice should be less than that of water by at least 1 eV.

In pure ice clouds the test bodies and the airplane were charged negatively. According to (4.31) this means that the work function of ice must be less than that of the metals of the test bodies and the airplane skin material. If electrification is accomplished as a result of the contact potential difference, and if the work functions of the two materials in question lie between the values of the work functions of water and ice, then in accordance with (4.34), while material No. 1 is charged more strongly in water than material No. 2, in an ice-crystal stream material No. 2 will be charged more strongly than material No. 1. Table 2.14 and the data of Chapter 2, Section 10 show that such an effect is actually observed.

Let us estimate using (4.31) the values of the equilibrium charges acquired by bodies in water-droplet clouds. We assume the contact potential difference between the water and the test body material to be 1 V. Then for stratus and cumulostratus clouds, for which $r=3-13$ microns [70], $\sqrt{\overline{r^2}}$ does not differ from $\bar{r}$ by more than 10%, the limiting charges of the test bodies used in the measurements should lie in the range of 8-30 esu, and their potentials should lie in the range 1600-6000 V. If we take into account the influence of the shield and the support, then these potentials should be equal to 800-3000 V. The values of the test body potentials measured on the Tu-104B airplane vary from a few tens of volts to several hundred volts, i.e., the electrification mechanism in question can undoubtedly provide the observed charging even if the contact potential difference equals 0.01-0.1 V. In the mixed Ns clouds drops of radius 2-3 microns are observed most frequently and the spectrum has a sharp narrow peak [70], i.e., $\bar{r} \approx \sqrt{\overline{r^2}}$. According to (4.33) the limiting charge in these clouds should reach 30-50 esu, corresponding to a potential of up to 6000-10,000 V or (after appropriate corrections) to 3000-5000 V. The observed potentials varied from a few hundred volts to (about) a thousand volts.

The lack of complete data on the microstructure of the Cs clouds makes it difficult to estimate the charging of bodies in these clouds. We note that in spite of their very low water content (about 0.03 g/m^3 or even 0.003 g/m^3) [70], the potentials of test bodies in these clouds reached several thousand volts. If we assume, following Kampe and Weickman [114], that the crystals have a columnar form and their dimensions are $200 \cdot 10^{-4} \times 20 \cdot 10^{-4} \times 20 \cdot 10^{-4}$ cм, and if in accordance with Schaefer's data [74] we assume that the crystals fragment on impact into 30 pieces [(1)], then the equilibrium charge acquired by the test body, according to (4.33), will be (for $\underline{V}_K = 1$ V) about 15 esu, and the corresponding potential will be about 3 kV. After introducing appropriate corrections for the influence of the shield and support, the equilibrium potential is 1500 V, i.e. close to the observed values.

We can estimate the magnitudes of the charging currents flowing to the test bodies (4.10) for given conditions in the clouds. If the particle concentration in the stratus, Cs, and Ns clouds is $\underline{n} = 200$ 1/cm^3, then in the stratus and Cs clouds the charging currents flowing to the test bodies should be $2 \cdot 10^{-8} - 2 \cdot 10^{-7}$ A (current density $3 \cdot 10^{-9} - 3 \cdot 10^{-8}$ A/cm^2) and in the mixed Ns clouds about $8 \cdot 10^{-8}$ A (current density $3 \cdot 10^{-9}$ A/cm^2), i.e., the calculated currents are somewhat higher than those actually observed.

Footnote (1) appears on page 211

The corresponding values of the effective relaxation time (from [(4.32)] are from 10 to 1 sec for the stratus and Sc clouds and about 10 sec for the Ns clouds, which are somewhat lower than the observed values.

The values of the characteristics actually observed are shown in Table 4.1. We see from the table that the mechanism in question is sufficiently strong to create the observed values of the equilibrium potential, the currents charging the test bodies, and consequently their observed charging time. The calculated values of the potentials and currents presented in Table 4.1 exceed somewhat the observed values, although they are similar in order of magnitude. The differences are apparently associated with the approximate nature of the estimates of the basic parameters.

Thus, the contact potential difference was taken as 1 V, and the calculation of the capture coefficients of the particles by the body were based on the concept of potential flow past the body. In reality, the highly turbulent flow around the test bodies must lead to some reduction of $\underline{\bar{r}}$ and $\overline{\frac{r}{r^2}}$ in comparison with the theoretical values, i.e., to a corresponding reduction of the current and the equilibrium potential and some increase of the relaxation time. At individual points of the surface of the test bodies the drops may rebound,not from the metal but rather from the water film, which corresponds to a reduction of the contact potential difference between the separating drops and the body. Finally, the assumed values of the drop sizes and concentration may differ from the true values.

The most complete quantitative evaluation of the charging theory could be obtained by substituting the experimental data into (4.34), since in the case of comparative measurements it is possible to exclude from consideration the very indefinite cloud microstructure parameters. It follows from (4.34) that the ratio of the equilibrium potentials of two test bodies is proportional to their contact potential differences with respect to the cloud particles.

TABLE 4.1. COMPARISON OF TEST BODY CHARGING CHARACTERISTICS MEASURED ON THE TU-104B AIRPLANE AND THE CALCULATED VALUES (ASSUMING THAT V_K = 1 V)

cloud form	dimensions of leaving particles (radius in microns)	particle concentration, in 1 cm^3	equilibrium potential		charge current density, A/cm^2		relaxation time, sec	
			calculated	measured	calculated	measured	calculated	measured
St, Sc	3÷13	200	1000–3000	10–500	$3 \cdot 10^{-9}$ $3 \cdot 10^{-8}$	10^{-10}–10^{-9}	10÷1	15÷1
Ns (supercooled)	3	200	3000–5000	100–1000	$3 \cdot 10^{-9}$	10^{-10}–$3 \cdot 10^{-9}$	10	15÷2
Cs	6	—	1500	up to 3000				

Such estimates are hindered by the fact that the work function depends to a considerable degree on the condition of the surface, in particular the presence on the surface of very thin (down to monatomic) films of oxides, water, and the like. Even in physical laboratories, where the experimental conditions permit careful cleaning of the specimens and the experiments themselves are conducted in a vacuum, a very large scatter of the values of the electron work function is obtained as a result of the measurements.

Figure 4.1 shows histograms of the measured values of the work function for nickel, copper, chromium, palladium, and gold, plotted from the data of a survey made by Fomenko [100] of studies on work function measurements. The figure also shows the values of the work function recommended in [100]. We note that for the different metals the scatter of the measured values of the work function amounts to from 0.8 to 1.2 eV. Consequently, the contact potential difference measured between different specimens may vary by 2 V, with a mean deviation of 1 V, as a result of accidental contamination and surface treatment. We would expect that the scatter would be no less for the ion work function. For measurements in the atmosphere, and

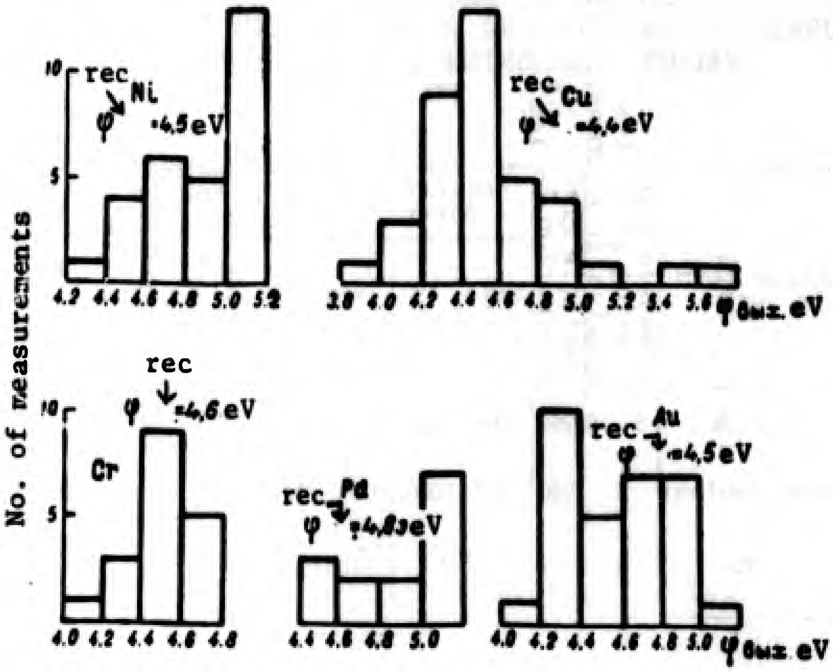

Figure 4.1. Values of electron work function for different materials, measured under laboratory conditions.

particularly in clouds, we would expect that the work function of the test bodies may vary even more than shown in the histograms of Figure 4.1.

Consequently, the tabulated data on the work functions of the metals cannot usually be used in estimating the contact potential differences for the calculation using (4.34). At the same time, since the work function of water is clearly larger than that of the metals and most of their oxides, while the work function of ice is apparently lower than that of most of the materials used, the general charging pattern in water and ice crystals has certain characteristic features. These characteristics are shown in Table 4.2.

In comparing the data of Tables 2.14 and 4.2 we see that if the work functions of brass, nickel, and chromium are larger than the work function of ice, then the relations presented in Table 4.2 are

TABLE 4.2. RELATIONSHIP BETWEEN THE EFFECT OF WORK FUNCTION OF MEDIUM AND TEST BODY MATERIALS ON CHARGING OF LATTER

relationship between work functions of test bodies and medium	in water drops			in ice particles		
	sign of first body charge Q_1	sign of second body charge Q_2	Q_1/Q_2	sign of first body charge Q_1	sign of second body charge Q_2	Q_1/Q_2
$\varphi_i<\varphi_1<\varphi_2<\varphi_w$	+	+	>1	−	−	<1
$\varphi_1<\varphi_i<\varphi_2<\varphi_w$	+	+	>1	+	−	−
$\varphi_1<\varphi_2<\varphi_i<\varphi_в$	+	+	>1	+	+	>1
$\varphi_i<\varphi_w<\varphi_1<\varphi_2$	−	−	<1	−	−	<1
$\varphi_i<\varphi_1<\varphi_w<\varphi_w$	+	−	−	−	−	<1

NOTE: φ_1 is the effective work function of the material of the first body; φ_2 is the effective work function of the material of the second body; φ_w is the effective work function of water; φ_i is the effective work function of ice.

confirmed in the measurements. The distribution of the test body potentials in water clouds (see Figure 2.29) and in pure ice clouds (see Figure 2.30) is explained similarly.

If a cloud contains both ice and water particles, (4.34) now cannot be used to determine the ratios of the body potentials. For the simplest case of monodisperse distributions of particles of both sorts we have in accordance with (4.28)

$$Q_{\text{равн}} \approx \frac{k_1 R^3 (A_1 n_1 r_1 V_{\kappa_1} + A_2 n_2 r_2 V_{\kappa_2})}{5k_2 (n_1 r_1^2 + n_2 r_2^2)} \tag{4.35}$$

and

$$\frac{Q_1}{Q_2} = \frac{A_1 n_1 r_1 V'_{\kappa_1} + A_2 n_2 r_2 V'_{\kappa_2}}{A_1 n_1 r_1 V''_{\kappa_1} + A_2 n_2 r_2 V''_{\kappa_2}}, \tag{4.36}$$

where V'_{κ_1} and V'_{κ_2} are the contact potential differences of one of the bodies with water and ice, and V''_{κ_1} and V''_{κ_2} are the same quantities

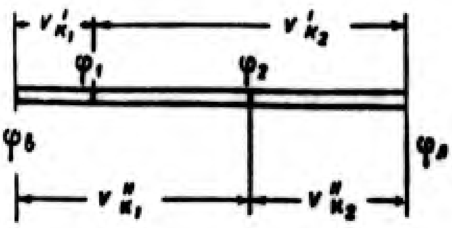

Figure 4.2. Diagram for calculating charging in a mixed cloud.

for the other body (Figure 4.2). It is not impossible that the wetted particles may have a work function which differs from the work function of water and ice; then in (4.35) and (4.36) the corresponding new terms appear. We would also expect that the work function is different for ice particles of different shape. Finally, impurities and surface-active materials may also affect the work function of water and ice.

In all these cases we must add to (4.35) and (4.36) new terms in accordance with (4.28). But even in the simplest case, described by (4.36), the sign and magnitude of the ratio of the charges of the bodies are determined not only by the magnitude of the contact potential difference, but also by the aerosol particle concentration and dimensions. For example, during flights in Ns clouds above the freezing isotherm, regions are noted in which test body charging of first one and then the other sign dominates. Here, if in a certain part of the cloud certain bodies are charged positively and others negatively. Transition into the region in which the first bodies begin to be charged negatively leads to positive charging of the other bodies.

Apparently, the relationship between the number of water and ice particles is different in these regions. The value of the equilibrium potentials of bodies, measured in Ns clouds, suggests that the work function of water (φ_w), the corresponding materials, and ice (φ_i) are arranged in the following sequence: $\varphi_w > \varphi_G > \varphi_D > \varphi_{H_1} > \varphi_{H_2} > \varphi_i$.

The application of (4.35) and (4.36) to polydisperse clouds leads to the necessity for the use of appropriately averaged values in the calculations.

The measurement of test body charging in clouds may be of assistance in studying cloud microstructure.

Cloud development depends significantly on the magnitude and scales of the nonhomogeneities of their microphysical structure [49, 115]. At the present time, adequately effective and simple methods for studying these nonhomogeneities with the aid of modern high-speed pressurized airplanes do not exist. The theory discussed above can be used to study certain peculiarities of the particle dimension spectrum.

Let us return to (4.31). If in place of the measurements of the potential on the test body we measure the current i_T flowing to the body, then for a body potential $V_T \ll V_{T_\infty}$, where V_{T_∞} is the limiting potential acquired by an isolated body in a monodisperse cloud,

$$i_T = Ak_1 nwSrV_K, \tag{4.37a}$$

and in a polydisperse cloud

$$i_T = Ak_1 nwS\bar{r}V_K, \tag{4.37b}$$

i.e., the variations of the current flowing to the body will reflect the variation of the average particle radius, their concentration, and the contact potential difference between the particles and the test body.

For the measurement of both the values of the concentration and the average radius of the cloud particles, we can measure simultaneously the limiting potentials of bodies similar to those on which the currents are measured.

In a monodisperse cloud [see (4.31)]

$$V_{T\infty} = \frac{1.5k_1R^2}{k_2(C_T + C_c)} \frac{V_K}{r} = M\frac{V_K}{r}. \tag{4.38a}$$

where

$$M = 1{,}5\frac{k_1}{k_2}\frac{R^2}{C_т + C_c}.$$

In the polydisperse cloud

$$V_{т\infty} = 1{,}5\frac{k_1}{k_2}\frac{R^2}{C_т + C_c}\frac{\overline{r^2}}{\overline{r}}V_к = M\frac{\overline{r^2}}{\overline{r}}V_к. \quad (4.38b)$$

In a finely dispersed cloud we can take $\frac{\overline{r^2}}{\overline{r}} \approx \overline{r}$. Then it follows from (4.37) and (4.38) that by measuring the current flowing to the test bodies and their potential we can determine the variations of the particle concentration and average radius at different parts of the cloud if we assume that V_K remains constant.

Simultaneous measurements of the potentials of several test bodies or of the currents flowing to the bodies make it possible to evaluate the homogeneity of the chemical composition of the water at various points of the clouds.

In warm clouds the ratio of the potentials of two identical test bodies made from different materials, as follows from (4.34), depends on the work function of water

$$\frac{V_{т_1}}{V_{т_2}} = \frac{\varphi_{т_1} - \varphi_в}{\varphi_{т_2} - \varphi_в}. \quad (4.39)$$

We recall that the diffusion potential of water depends on the concentration and composition of the impurities in the water. The dependence of the ion work function difference Φ_D of two solutions on the concentration and properties of the solutes is given by the Formula (4.40), taken from [116]

$$\varphi_д = 2\frac{K_1}{K_1 + K_2}\frac{RT}{zF}\ln\frac{n_1}{n_2}, \quad (4.40)$$

where n_1 and n_2 are the solute concentrations in the two solutions, R is a constant, K_1 and K_2 are the cation and anion mobilities, T is absolute temperature, z is the ion charge number, F is the solute atomic weight.

We see from (4.36) that measurements of the charging of identical test bodies made from different, specially selected materials make it possible to determine the changes of the relationship between the number of water and ice particles in various parts of a cloud.

§ 4. Comparison of Theoretical and Experimental Data on Airplane Charging in Clouds

Formulas (4.29) can be used to find the value of the airplane equilibrium charge and charge relaxation time. The combined resistance of the static dischargers and exhaust gas jet of the TU-104B airplane (if the airplane charge is much higher than that at which the dischargers operate) is $R \approx 2 \cdot 10^8$ см, and the jet resistance is $R \approx 5 \cdot 10^8$ Ohms. The resistance created by the collector effect of the drops is about 10^{10} Ohms. The capacitance of the TU-104B airplane is about 1700 cm.

Table 4.3 shows the approximate values of the calculated and measured airplane electrical characteristics during flights in clouds.

The average measured values of the charges in Table 4.3 are taken to be those values lying in the 10-90% probability interval. The data of this table show that the electrification mechanism in question explains the airplane quantitative electrification characteristics.

The formulas presented above can be used to calculate the limiting charge which the airplane would acquire in clouds if we exclude the exhaust gas jet and corona discharge effects. In stratus and Ns clouds this charge would reach $4 \cdot 10^7 - 1{,}2 \cdot 10^8$ esu, and the corresponding potential would reach $0{,}8 \cdot 10^7 - 2{,}5 \cdot 10^7$ V. In this case, the relaxation time would be 10 sec.

We see from (4.21) and (4.24) that two bodies of different size, traveling with the same velocity in the same cloud, will have different equilibrium charges. The ratio of these charges is proportional to the square of the body dimension ratio and inversely

TABLE 4.3. COMPARISON OF CALCULATED AND MEASURED CHARACTERISTICS OF TU-104B AIRPLANE DURING FLIGHT IN CLOUDS ($\underline{V}_K$ = 1 V)

cloud form	radius of particles charging the airplane, microns	particle concentration, 1/cm^3	equilibrium potential, V		charge current density, A/cm^2	
			calculated	measured	calculated	measured
St, Sc	3÷13	200	$3\cdot10^5 \div 10^6$	$5\cdot10^5 \div 1,5\cdot10^6$	$5\cdot10^{-9} \div 2\cdot10^{-8}$	$10^{-10} \div 10^{-9}$
Ns supercooled	3	200	$3\cdot10^6$	$2\cdot10^6 \div 3\cdot10^6$	$>5\cdot10^{-9}$	$10^{-10} \div 3\cdot10^{-9}$
Cs	6	—	$>5\cdot10^6$	$10^6 \div 1,5\cdot10^6$		

proportional to the ratio of the conductivities of these bodies to the atmosphere. Figure 2.32 shows how the dural test body potential and airplane charge vary with time. The general similarity of the nature of the charging of the two bodies is obvious. Figure 2.32 also shows how the ratios of the charges of the two bodies are related at individual moments of time. Cases of correlation of body charging at the times of charge growth are particularly clear.

The magnitude of the average ratio of the airplane charge to the sphere charge can be found from the data of Figure 2.32. This ratio equals $1,2\cdot10^5$—$2,2\cdot10^5$. On the basis of the data presented above and taking as the characteristic airplane dimension the radius of a sphere with the same capacitance as the airplane, we can calculate that the ratio of the airplane and test body charges in accordance with the theory must be 10^5—10^6. In accordance with the data presented above the sphere, leakage resistance owing to the collector effect is assumed to vary from 10^{10} to 10^{11} Ohms.

For high airplane charges (above $5\cdot10^5$ esu) the measured ratio of the airplane charge to the sphere charge decreases by about a factor of three in comparison with that measured in the same clouds at lower airplane charges. The ratio of these quantities calculated in accordance with the proposed theory must decrease by the same factor, since with increase of the airplane charge the effective resistance of the corona dischargers and exhaust gas jet decreases by a factor of two or three.

In examining the charging of the airplane as a whole, we must also mention another charging source of nonatmospheric origin. If total burnup of the fuel does not take place in the combustion chambers during airplane engine operation, then the unburned fuel particles (in the form of small drops or solid particles), as they come into contact with the inner surface of the exhaust pipes and separate from this surface will, as noted in Chapter 3 (the current I_{1_3}), transfer to the airplane a charge similar to the action of the cloud particles

The difference is that the collector action of the fuel particles will be very slight, since the field intensity from the airplane charge at the point of particle separation will be infinitesimally small. In this case, the current created by the fuel particles, calculated using the formulas presented above, enters in (4.29) into the sum of the currents charging the airplane.

In fact, if the engines are not properly adjusted and the air flow into the combustion chambers is not adequate, an increase of the airplane charge, sometimes very marked, is observed. Usually, the periods of strong airplane charging coincide with the appearance of a smoke trail behind the plane. On the TU-104B airplane, where the required relationship between the amount of fuel burned and the amount of air supplied is established automatically, we observe only a brief change of the charging during an abrupt change of the turbine shaft rpm. During such a change of turbine speed there is incomplete combustion of the fuel for a very short time period, which leads to brief charging. In designs in which incomplete fuel burnup is inherent in the engine operation, the charging in the clear atmosphere may be quite comparable in magnitude with that which occurs in clouds and precipitation.

When operating in media in which the conductivity is low because of a small number of particles and in which corona discharge is not possible (for example, in interplanetary space), the condition which limits the maximal potential of the body being charged by the particles separating from the internal parts of the body is the previously mentioned retardation of the particles by the body field. If particles of mass m carry the charge q and are ejected with the velocity w, then the limiting potential to which the particles charge the body is $V=\frac{mw^2}{2q}$. The magnitude of the potential V can reach billions of volts.

FOOTNOTE

Footnote (1) page 199

The degree of fractionation depends on the impact energy. In [74] a study was made of fractionation for a crystal velocity of about 100 km/hr, while for TU-104B flights the velocity is 800 km/hr, i.e., there is an impact energy ratio of about 60; therefore we take the obviously somewhat high dimensions of the particles after fractionation.

CHAPTER 5

METHODS FOR REDUCING AIRPLANE CHARGE AND THE ASSOCIATED INTERFERENCE

Methods for reducing the airplane charge can be divided into two basic groups:

1) those which reduce the airplane charging current, i.e., prevent the appearance of a charge;
2) those which increase the airplane discharge current, i.e., remove the charge which develops.

§ 1. Methods Which Reduce the Airplane Charging Current

As indicated in the preceding chapter, reduction of the airplane charging currents while maintaining constant effective conductivity leads to reduction of the airplane charge. Along with the reduction of the charging currents, there is obviously a reduction of the interference currents.

For a given airplane type flying at a given speed under given conditions, the charging current can be reduced by minimizing the potential difference which develops between the airplane skin material and the cloud and precipitation particles. It was noted previously that changing the coating composition can lead to either positive or negative charging of the surface (see Table 2.13) [74].

It was shown in [5] that colloidal silicon coatings applied to the airplane reduce markedly the magnitude of the charging (see Figure 2.25). However, we must remember that the coating which is optimal for flight in water clouds may be ineffective in ice-crystal clouds and vice versa.

The strong dependence of the contact potential difference on the surface properties makes this method difficult to realize in practice. Sometimes a simple touch of the hand on the surface is sufficient to alter the charging current. Dirt and spray which adhere to the surface during airplane takeoff can alter the airplane surface properties and its electrification conditions.

Application of suitable coatings to the frontal surfaces of the airplane is sufficient to reduce effectively the charge current. The surface properties can be stabilized either by wetting the surface in flight with a suitable, continuously renewed solution, or by introducing a system of opening and closing shutters which are charged with electricity of obviously different signs. The charging current can be reduced by varying the relationship of the areas of the shutters upon contact with which the airplane acquires a positive or negative charge. The control of the shutters can be automated with the aid of signals coming from an on-board charge meter. The shutter area variation technique makes it possible to reduce the electrification in flights in both warm and ice-crystal clouds.

Even if special devices are not used, a careful selection must be made of the coating material and the technique used for its treatment in order to reduce the overall electrification of the airplane. This is particularly important in selecting the materials for the nonconducting portions of the airplane surface (antenna fairings, struts, and the like).

When using nonrecoverable flight vehicles, radiosondes, for example, the proper selection of the surface material may provide a marked reduction of their electrification.

§ 2. Methods Which Remove the Airplane Charge

Whatever device is used to remove the airplane charge (corona dischargers, flame dischargers, spray dischargers, ion dischargers, and so on) its action reduces to transfer of the charge from the airplane to the atmosphere. In this process even with the most advanced discharger the airplane charge propagates into a region somewhat larger than the airplane, which includes both the airplane itself and the very small atamospheric volume to which the charge is transfered. If the airplane were not moving the charge density on its surface, with the exception of the region adjacent to the charged volume of the atmosphere, would remain approximately the same as it was without the action of the discharger.

We have mentioned previously that the airplane motion alters fundamentally the charge removal conditions. We shall examine in more detail the general laws governing the loss of electrical charge by the airplane.

Assume the charge current I_{I} flows to a body traveling with the velocity w relative to the stream (Figure 5.1). The current I_{II} from the body flows through the highly conductive region St. Without examining the specific conditions under which the region St appears, we shall characterize it by the area S_{II} of its outer boundary, the coefficient p relating the average charge density σ_{II} on the outer surface of St with the body charge, and the resistance R_{II} connected between the outer surface of the region and the body.

If the region St arose as a result of ionization of the air by a corona discharge or by the hot exhaust gases, then the resistance R_{II} depends on the degree of ionization, the gas composition, and so on, while the dimensions of the region depend on the conditions of its creation and the body velocity. If the current I_{II} arose as a

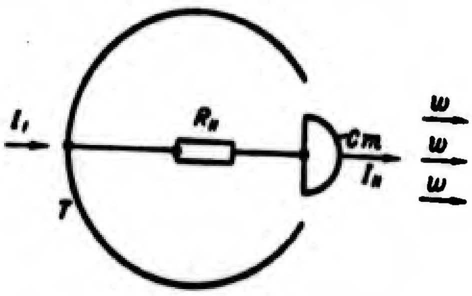

Figure 5.1. Diagram illustrating calculation of effectiveness of discharging devices.

result of separation of conducting particles from the charged body (collector effect), then the region St coincides with the surface of the body at the points of particle separation. The magnitude of the resistance is determined by the number and size of the separating particles, their separation velocity, the particle conductivity, and the shape of the body — the quantities which characterize the effective (apparent) resistance of liquid collectors [11].

The equation describing the variation of the body charge may be written in the form [see (3.1)]

$$\frac{dQ}{dt} = I_{I} - I_{II}. \tag{5.1}$$

If the particle charge removal velocity $\underline{w}$ equals the velocity of the body, the magnitude of current I_{II} is given by the expression

$$I_{II} = \alpha w \int_{S_{II}} \sigma dS = \alpha w q, \tag{5.2}$$

where $\underline{q}$ is the charge of the region St, and α is a coefficient showing the effectiveness of the removal of the charged particles from the body. In the general case α depends on the density of the air and the flow conditions around the region St, and also on the ionization intensity and the recombination conditions in this region.

The potential V_{II} at the outer boundary of the conductive region will differ from the body potential $\underline{V}$ by the magnitude of the voltage drop across the resistance of the region St

$$V_{II} = V_{I} - I_{II} R_{II}. \tag{5.3}$$

Substituting into (5.3) $V=\frac{Q}{C}$ and $V_{II}=\frac{q}{C_{II}}$ (C is the body capacitance, and C_{II} is the capacitance of the region St) and comparing (5.2) and (5.3) after substitution, we obtain

$$I_{II}=\frac{\alpha w\frac{C_{II}}{C}}{1+\alpha wR_{II}C_{II}}Q. \tag{5.4}$$

Hence, it follows, in particular, that if R_{II} is very small, i.e., $1\gg\alpha wR_{II}C_{II}$ (highly effective discharger), then

$$I_{II R_{II}\to 0}=\alpha w\frac{C_{II}}{C}Q, \tag{5.5a}$$

while if $1\ll\alpha wR_{II}C_{II}$ (ineffective discharger), then

$$I_{II}=\frac{Q}{R_{II}C}. \tag{5.5b}$$

We note that αw characterizes a quantity which is the inverse of the time T required for removal of the charge by the air stream, while the quantity $R_{II}C_{II}=\tau_{II}$ is the risetime of the charge of the region St resulting from the current I_{II}'. This implies that $\alpha wR_{II}C_{II}\ll 1$ provided $\tau_{II}\ll T$, i.e., the charge inflow time through the resistance R_{II} is much less than the time required for charge removal by the air stream. When $\tau_{II}\gg T$, i.e., the charge inflow time through the resistance R_{II} is much longer than the time required for the charge removal by the stream, the current is determined by the resistance R_{II}.

Substituting into (5.1) the value of the current I_{II} and assuming that the charge $Q = 0$ at the time $t = 0$, we obtain

$$Q=I_1\tau\left(1-e^{-\frac{t}{\tau}}\right), \tag{5.6a}$$

$$\tau=\frac{C(1+\alpha wR_{II}C_{II})}{\alpha wC_{II}}, \tag{5.6b}$$

or

$$\tau=CR_{II}\left(\frac{T}{\tau_{II}}+1\right). \tag{5.6c}$$

For $R_{\text{п}} \to 0$ (5.6b) can be written in the form

$$\tau_1 = \frac{C}{aw C_{\text{п}}}, \tag{5.7a}$$

and for $aw R_{\text{п}} C_{\text{п}} \gg 1$

$$\tau_2 = R_{\text{п}} C. \tag{5.7b}$$

We can conclude from (5.5a), (5.6), and (5.7a) that for a very effective discharger ($\tau_1 \ll T$) its current is proportional to the airplane velocity and to the ratio of the capacitances of the region St (Figure 5.1) and the entire airplane, while the airplane charge is the smaller, the higher the flight speed and the quantity $\frac{C_{\text{п}}}{C}$. For large resistances $R_{\text{п}}$ and capacitances $C_{\text{п}}$ ($\tau_{\text{п}} \gg T$) the current $I_{\text{п}}$ is larger, the lower the resistance $R_{\text{п}}$, while the charge Q is smaller, the smaller $R_{\text{п}}$. In other words, for very small discharger currents, when the space charge created by these currents can be completely dissipated, the magnitude of the charge is determined by the magnitude of the discharger resistance $R_{\text{п}}$; for very high currents the leakage resistance and the magnitude of the charge are determined by the removal of the space charge, in our case by the motion of the airplane.

Thus, for effective discharging it is desirable to reduce the resistance $R_{\text{п}}$, increase the discharger surface area, locate the dischargers at points with good ambient flow, and in the case of passive dischargers they should be located at points with maximal surface charge density.

Let us examine in more detail the individual forms of dischargers. All forms of dischargers can be divided into two basic classes:

1) passive, in which the currents flowing from the dischargers depend on the airplane charge;

2) active, in which the currents flowing from the dischargers depend on the voltage of an auxiliary source.

Regardless of the specific physical mechanism on which the action of a particular discharger is based, all passive dischargers should be located at points where the maximal surface charge density is observed, where the ambient flow velocity $\underline{w}$ is high, and where the value of the coefficient α is maximal. In particular, the pointed extremities of the fuselage, tailplane tips, and wingtips meet these conditions. The dischargers located on the trailing edges of the tailplane and wings are more effective than those located at the leading edges, since the value of the coefficient α is smaller for the latter because of settling of part of the ions on the airplane surface.

The active dischargers, rarely used to date, create a discharge current which is independent of the airplane charge. Their location is selected in accordance with the conditions for best ambient flow and maximal possible values of the coefficient α. All the devices with active dischargers have an airplane charge meter of one form or another. The discharger receives a signal from the meter and generates a current of the proper polarity and magnitude. The use of active dischargers makes it possible to maintain the airplane at any required level.

When necessary, all the active dischargers can operate as devices to charge the airplane.

The choice of the particular discharger type is determined by the flight vehicle design, its velocity, the conditions under which it is to be operated, the acceptable radio interference level, and so on. We would expect that increase of the airplane velocity and size, the characteristic changes taking place in airplane construction, and the ever increasing role of the radio and electronic equipment will lead to more extensive use of the active dischargers.

Depending on the mechanism on which the operation of the dischargers is based, the latter can be divided into two basic types:

1) dischargers which alter the conductivity $R_{\text{п}}$ of the medium at the point where they are located;

2) dischargers which eject from the airplane charged particles which have a charge of sign opposite that of the airplane charge.

The first type includes: 1) corona dischargers (the passive version of this discharger is most often used at the present time), 2) flame dischargers (these dischargers utilize the effect of increased ionization of the air with increase of the temperature in accordance with the Saha formula. The engine exhaust gas jets are usually used as these dischargers), 3) radioactive dischargers (devices of this type are not used on manned airplanes because of the high radioactivity level necessary for sufficiently efficient operation).

The second type includes: 1) dischargers which emit an ion stream of suitable sign or (in certain special cases) an electron stream, 2) dischargers which emit a stream of charged particles.

Let us examine the operation of the dischargers which alter the conductivity of the medium. These dischargers create a region of high ionization near the airplane. Part of the airplane charge leaks off into this region. The ionized region is carried away from the airplane by the ambient airstream. We see from (5.4) and (5.5) that the discharger operates more effectively the smaller $R_{\text{п}}$, i.e., the higher the ionization created by the discharger, the larger the ionized region, and the more effectively this region is carried away. These considerations hold for all the dischargers which alter the conductivity of the medium.

Without discussing the methods for calculating the magnitude and parameters of the ionized region when using particular types of dischargers, since this is the subject of the specialized literature, we shall mention briefly certain characteristic features of these dischargers.

In Chapter 3 we examined the operation of the passive corona dischargers and the effect on their operation of the flight conditions and their placement. For today's airplane and antenna designs, the magnitude of the airplane potential at which discharge begins is about 100 kV [8, 121]. Usually, the discharge begins at this voltage at the tips of the wing or tail fairing. After installation of corona dischargers, this potential decreases to a typical value of about 10 kV. Therefore, the average coulomb-ampere characteristic of all the dischargers installed on the airplane must provide a condition in which the airplane potential for the largest charge currents will not exceed, say, 80-90 kV if discharge from the airplane surface points which are not protected by dischargers is undesirable.

We note that the effectiveness of the dischargers can be increased by using them in the active version. Figure 5.2 shows one such version. The additional voltage V from an internal source makes it possible to improve considerably the volt-ampere characteristic of the discharger. The discharger current increases even for small airplane charges. Figure 5.2 shows the distribution of the field lines of force in the absence of airplane self-charge. The appearance of the air stream leads to a situation in which part of the ions from the discharger cannot return to the airplane, and the latter begins to charge.

In the resulting electric generator, the energy is supplied at the expense of the kinetic energy of the airstream which carries the ions away. If the value of $\underline{V}$ is not regulated, this can lead to charging of the airplane to potentials which may exceed the value of $\underline{V}$ considerably. Therefore, it is necessary, as noted previously, that the value of $\underline{V}$ be regulated on the basis of information on the airplane charge. The scheme shown in Figure 5.2 can thus be used for artificial charging of the airplane. In the general airplane charging case, this scheme operates in the mixed passive-active version.

As the flight altitude is increased (ambient air pressure decreases) the corona dischargers become more effective, the value

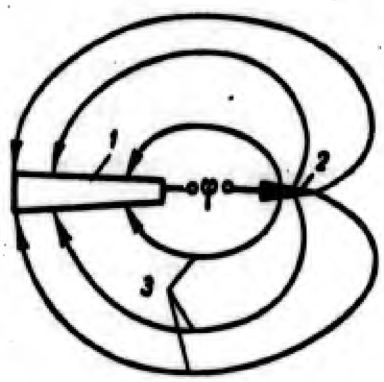

Figure 5.2. Schematic of action of active corona discharger.

1) wing trailing edge;
2) discharger; 3) distribution of lines of force of electric field created by supplementary voltage source.

$R_{\text{п}}$ decreases, and at the same time the effectiveness α of charged particle removal by the air stream decreases. On reaching a minimum of the discharge voltage on the Paschen curve [31], further increase of the flight altitude leads to a marked increase of the value of $R_{\text{п}}$, i.e., the effectiveness of dischargers of this type decreases; at altitudes above 50-70 km they become ineffective.

We have noted previously that the exhaust gas jets may be considered flame dischargers. Since they have large surface areas, they can provide large discharge currents even with relatively weak ionization. The degree of gas ionization in the flame dischargers can be estimated using the Saha formula [117, 118]

$$\frac{\beta^2}{1-\beta^2}=\left(\frac{2g_i}{g_a}\right)\left(\frac{2\pi m}{h^2}\right)^{3/2}\left(\frac{kT}{p}\right)^{3/2}e^{-\frac{\omega_i}{kT}}, \qquad (5.8)$$

where β is the degree of ionization, i.e., the ratio of the number of ionized atoms to the total number of atoms; p is the pressure, equal to the sum of the partial pressures of the neutral atoms, ions, and electrons; ω_i is the atom ionization energy; g_a and g_i are the statistical weights of the neutral atoms and ions; m is the electron mass; k and h are respectively the Boltzmann and Planck constants. The degree of ionization in these dischargers increases markedly with increase of the flame temperature. Therefore, the increase of the gas temperature in the modern aircraft engines and the use of turbojet engines leads to an increase of the effectiveness of the discharge action of the exhaust gases.

With increase of the flight altitude, i.e., with reduction of the air density, there is a reduction of the intensity of the removal of the charged particles (the coefficient α in [5.4]). Therefore, other conditions being the same, the effectiveness of the discharge through the exhaust gas jet decreases with increasing altitude.

The flame-type static dischargers have not been used directly because of the undesirability of having an open flame aboard airplanes, low effectiveness at low fuel flowrates, and design complexities.

When radioactive dischargers are used, the ionization density decreases with altitude, and therefore, the discharger resistance $R_{\text{п}}$ increases. The coefficient α [see (5.4)] also decreases with altitude because of reduction of the air density. Thus, the operation of these dischargers deteriorates with increasing altitude. At very high altitudes the flight vehicle may begin to be charged as a result of release of charged particles by radioactive decay. As a result of this charging the sounding body may be charged to a potential equal in magnitude to the charged particle ejection energy.

Let us examine the operation of dischargers based on the emission of charged particles.

Very high discharge currents $I_{\text{п}}$ per unit mass of material ejected per unit time can be achieved by emitting ions or electrons. The magnitude of the current will depend on the particle ejection velocity. In this case, the current $I_{\text{п}}$ [see (5.1) and (5.2)] can be written in the form

$$I_{\text{п}} = \alpha w_e n e, \tag{5.9}$$

where e is the ion charge; n is the number of ions ejected per unit time; w_e is the velocity with which the ions leave the body. Under dense atmospheric conditions, it is difficult to eject ions with a velocity differing from the flight vehicle velocity w, since, as a result of collision with atmospheric particles, the ions lose very rapidly the velocity imparted to them by the accelerating device.

Therefore, the value of α in (5.9) is close to the value of α in (5.2).

At the same time, under the action of the airplane's electric charge, the slow ions will tend to return to the airplane, which results in a reduction of the effective charging current. If the ion mass is m, then airplane charging terminates when its potential V reaches the value defined by the inequality

$$eV < \frac{mw^2}{2}. \tag{5.10}$$

and for lower potentials the current is defined by the equality

$$I_{11} = \alpha \sqrt{w^2 - \frac{2eV}{m}}\, ne, \tag{5.11}$$

where w is the stream velocity.

If we neglect the viscosity of the air, then all the ions will return to the airplane for an airplane speed $w \approx 100$ m/sec and for airplane potentials which exceed a fraction of a volt. An effective discharging action of the ion-type emitters can be achieved only at very high flight altitudes when using an active discharging device with particle ejection velocity on the order of several kilometers or even several hundreds of kilometers per second. Thus, in contrast with the dischargers which increase the conductivity of the ambient medium, the characteristics of the dischargers of this type improve with increase of the flight altitude.

Improvement of the effectiveness of the operation of these dischargers in the atmosphere is achieved by increasing the mass m and charge q of the ejected particles and simultaneous reduction of the ratio $\frac{q}{m}$ [see (5.10)] and (5.11)]. With increase of $\frac{q}{m}$ we can achieve an effective discharge at particle ejection velocities less than the airplane velocity (accompanied, of course, by an increase of the material consumption per unit electric charge removed). In this case, the airplane motion can be utilized for separation from the charged particles, which reduces significantly the requirements on the power of the device used to eject the particles into the atmosphere. On the other hand, when ejecting charged particles in place of ions, it is also possible to get along with a relatively small weight of the ejected material.

It was noted in [119] that a specific charge per unit ejected mass Q = 80 C/kg was achieved when ejecting liquid metal droplets of average diameter from 0.5 to 0.75 microns. For a discharge current equal to, say, 10 mA, one kilogram of ejected material would suffice (even under these severe conditions) for two hours of continuous operation. In this case, the influence of the airplane potential on the discharge current would become noticeable only for $V>10^5-10^6$ V.

Let us examine the criterion for the optimal choice of the magnitude of the charge and mass of the particles and the amount of material ejected per unit time for dischargers emitting charged particles. The active discharger version is most optimal in this case. We have mentioned previously that a device of this type was first used by Waddel et al. [7]. They used the device primarily for artificial charging of the airplane. The device described in [7] consisted of a system of nozzles through which highly dispersed water was ejected from the airplane. As the water droplets left the nozzles they were exposed to an electric field created by an electrode located upstream of the nozzles (a potential from a high-voltage source was applied to the electrode); therefore the droplets carried away an electric charge as they separated from the airplane. The maximal current generated by the installation described in [7] did not exceed 300 μA.

Let it be required that the discharge current I_{II} be generated by ejecting n particles per second with the velocity w, each of which carries the charge q; let the airplane potential V be sufficiently small (5.11), and therefore it has no marked effect on the particle motion: $V \ll \frac{mw^2}{2q}$.

Then (5.11) can be written as

$$I_{\text{II}} = anqw. \qquad (5.12)$$

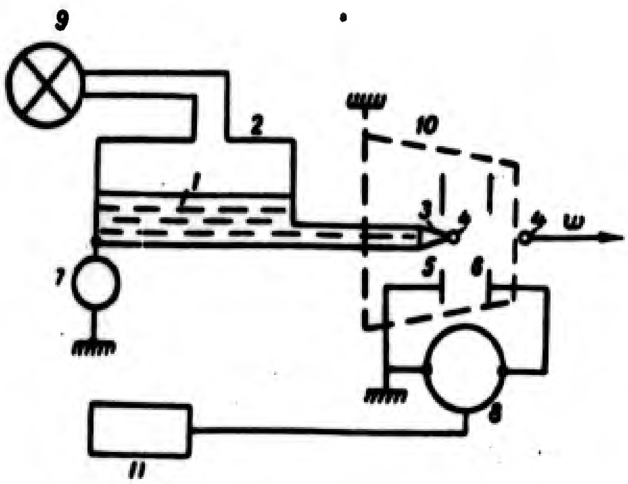

Figure 5.3. Schematic of active discharger emitting charged liquid particles.

If the device is properly designed, the value of w can be made equal to the airplane velocity if the particles are ejected into the undisturbed stream, and if their inertial travel is sufficiently small.

The schematic in Figure 5.3 illustrates the operation of the device. The electrifying, conducting liquid flows from the tank 2 under the pressure created by the compressor 9; the droplets 4 are ejected from the nozzles 3 into the space between the electrodes 5 and 6, between which there is applied the potential Θ from the supply source 8. The sign of the potential is determined by the airplane charge meter 11. The current $I_{\text{п}}$, discharging the entire system (the airplane, say) from which the droplets separate, can be measured by the galvanometer 7. As the separating particles 4 leave the nozzles they strike the screen 10 into which air flows with the velocity w.

If the charging liquid droplets have the radius r and density ρ, the entire mass of material ejected per second is M, and the charge q transferred to the droplet constitutes some part K of the maximal charge (the maximal charge is determined by the condition that the potential on the surface of the droplet equal that E_{cr} for which electrical discharge begins), then the current $I_{\text{п}}$ is obviously

$$I_{\text{п}}=\alpha KE_{\text{кр}}wn=\frac{\alpha KE_{\text{кр}}Mw}{4\rho r}. \tag{5.13}$$

In order to ensure the absence of contact between neighboring droplets, i.e., to be certain that there is some space between successive droplets, it is necessary to use several nozzles operating in parallel.

Let us evaluate the droplet charging conditions in the scheme of Figure 5.3. The droplets 4 are ejected from the nozzle 3 into the space between the planar electrodes 5 and 6, located at the distance d from one another. If the potential difference Θ is applied to the electrode plates from the source 8, then the field intensity $E=\frac{\Theta}{d}$ arises between the electrodes. Assume the nozzle projects the distance h from the plate 5. Then the induced charge q on the droplet of radius r at the moment of its separation from the nozzle will be

$$q\approx Ehr=\frac{\Theta}{d}hr. \tag{5.14}$$

On the other hand, the field intensity E at the droplet cannot exceed some fraction K of E, at which discharge begins

$$KE_{\text{кр}}=\frac{q}{r^2}. \tag{5.15}$$

The required characteristics of the charging device can be evaluated from (5.14) and (5.15).

The external part 10 of the device should be located so that the droplets which separate from the nozzles cannot again contact the airplane.

It is obvious that α will decrease as the airplane climbs [see (5.4) and (5.9)]. At high altitudes, where the air friction is low, a high particle velocity can be provided by the device which ejects the particles.

§ 3. High-Frequency Radiations Arising on an Airplane During Corona Discharge and Measures for Suppressing Their Influence

The methods used to eliminate the effect of airplane charge on particular on-board instruments or on the airplane operating characteristics depend on the nature of the problem. Some cases of this charge influence were investigated in Chapter 1. In the present section we shall examine only the particular, but quite important case of the effect of the alternating component of the discharge current on the operation of the on-board high-frequency equipment.

So far, we have examined only the connection between the intensity of the static field at various points of the airplane and its charge. Let us see how the high-frequency field at various points of the airplane surface is connected with the alternating component of the corona discharge current.

Connection between inerference signal on antenna and noise source. The connection between the radio noise characteristics at any point and the interference signal arising on the antenna can be characterized with the aid of the so-called coupling theorem [120], which states that

$$I_2(\omega) = \frac{1}{V_1(\omega)} \int_{T_2} \mathbf{E}_1(X, \omega) \cdot \mathbf{j}_2(X, \omega)\, dS. \tag{5.16}$$

The coupling theorem can be interpreted as follows: if we know the space and time distribution of the density of the current $\mathbf{j}_2$ created by the radio interference occurring in the region T_2 (Figure 5.4), and if we can determine the field intensity $\mathbf{E}_1$ in the region T_2 when the potential V_1 is applied to the antenna output, then we can calculate the short-circuit current $I_2(\omega)$ induced at the antenna output terminals (X is the coordinate of the corresponding point; ω is the corresponding interference frequency).

The coupling theorem thus states that the noise current generated by a discharge occurring at some point in the receiving antenna is

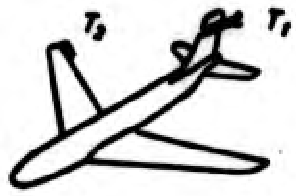

Figure 5.4. Diagram illustrating calculation using coupling theorem.

Version 1: Voltage applied to antenna terminals in region T_1 forms a field at all points of space and, in particular, in the region T_2.

Version 2: Radio noise develops in the region T_2 and the current density j_2 flows. When discharge occurs in T_2, the current I_2 flows through the shorted antenna input in T_1. T_1 is the region in which the antenna is located, T_2 is the region where the noise develops [121].

proportional to the potential of the high-frequency field which would exist at the point of discharge with operation of the same antenna in the transmit mode.

For evaluation of the effect of noise on radio reception, it is convenient to introduce the so-called coupling function [120].

Let us examine a point located near the origin of a corona discharge. The magnitude of the field intensity $E_1(\xi, \omega)$ at the selected point will change as a function of the frequency and position along, say, the wing surface just as does the field intensity at the discharge point. Therefore, the field intensity at the discharge point can be connected with the field intensity at the reference point by the relation

$$\mathbf{E}_1(X, \omega) = \mathbf{E}_1(\xi, \omega)\frac{E_1(X)}{E_1(\xi)}. \qquad (5.17)$$

We note that the cofactor $\frac{E_1(X)}{E_1(\xi)}$ is determined by the boundary conditions introduced by the airplane surface structure in the discharge region and is independent of the antenna characteristics.

Substituting (5.17) into (5.16), we obtain

$$I_2(\omega) = \frac{\mathbf{E}_1(\xi, \omega)}{V_1(\omega)}\frac{1}{E_1(\xi)}\int_{T_1}\mathbf{E}_1(X)\cdot\mathbf{j}_2(X, \omega)dX. \qquad (5.18)$$

Introducing the notations

$$\psi(\xi, \omega)=\frac{E_1(\xi, \omega)}{V_1(\omega)}$$

and

$$D(\omega)=\frac{1}{E_1(\xi)}\int_{V_0} \mathbf{E}_1(X)\cdot \mathbf{j}_2(X_1, \omega)\,dx,$$

we can write (5.18) in the form

$$I_2(\omega)=\psi(\xi, \omega)\cdot D(\omega), \tag{5.19}$$

where $\underline{D}(\omega)$ is the noise current spectrum for the value of the coupling function $\psi(\xi, \omega)=1$. This spectrum accounts for the effect of the "fine structure" of the trailing edge of the wing but does not depend on the antenna characteristics. The cofactor $\psi(\xi, \omega)$ — the coupling factor — describes the nature of the spectrum changes with changes of the coupling between the antenna and the region near the source.

The noise can be reduced in several ways in addition to reducing the airplane charge current and the airplane charge.

1. Reduce the noise caused by the discharge source.
2. Reduce the coupling between the discharge source and the receiver.
3. Process the received signal suitably to eliminate the noise components.
4. Select a reception frequency lying in the region of low power generated by the discharge.

Equation (5.16) shows that there are several ways to realize points 1 and 2. These include:

a) overall reduction of the discharge current alternating component $\underline{j}_2$; b) minimizing the ratio E_1/V_1 (reducing the coupling); c) making the vectors $\mathbf{j}_2$ and $\mathbf{E}_1$ orthogonal (reducing the coupling).

We recall that in addition to the corona discharge, another source of noise associated with the airplane charge can be the charge distribution over the airplane surface. This form of interference is usually not reduced by the dischargers and may increase when the dischargers are activated.

Connection between radio interference from the corona discharge on an airplane and the airplane characteristics and flight conditions. A characteristic feature of any discharge from an airplane is the presence of noise components with amplitude φ_n proportional to the average direct current $I_\text{П}$ flowing from the discharger. For each type of discharger the ratio $\frac{\varphi_n}{I_\text{П}}$ remains nearly constant in the real range of values of $I_\text{П}$, and this noise has the nature of "white" noise. In the case of the typical uncontrolled discharge occurring from points having relatively large radius of curvature, and in the absence of a resistance limiting the discharge current, the ratio $\frac{\varphi_n}{I_\text{П}}$ will be larger, particularly in the region of currents lying near the corona discharge threshold.

Not only is the interference amplitude large in this region, the noise spectrum includes several modulations which create additional interference which exceeds by several fold that resulting from the white noise. When the airplane charge exceeds slightly the value at which corona discharge begins at a given point, the magnitude of the peaks of these modulations not infrequently reaches values which make radio reception or operation of the radio equipment impossible. Although the ratio $\frac{\varphi_n}{I_\text{П}}$ at a given point decreases with further increase of the charge, discharges usually develop at other points and again create strong interference.

The typical uncontrolled discharge may create a ratio $\frac{\varphi_n}{I_\text{П}}$ which is thousands of times larger than that which occurs near the corona discharge threshold,or in the case of higher currents when using a modern discharger. A corona current of the order of a microampere flowing from an unprotected point may increase the noise on the order of 60 dB in comparison with a current of 100 microamperes flowing from a special discharger.

The amplitude-frequency characteristic of the noise depends to a considerable degree on the flight altitude. With increase of the flight altitude, the noise level increases for the same discharge current. The noise amplitude increases with flight altitude faster than the noise spectrum broadens in the high-frequency region. Figure 5.5 [120] shows how the noise current spectral density changes with increase of the altitude. The noise level will increase with further increase of the altitude until the altitude region is reached at which the pressure corresponds to the minimum of the Paschen curve. Further increase of airplane altitude will then lead to a reduction of the corona discharge noise current amplitude.

Measures to reduce interference.

1. Noise can be reduced by eliminating the possibility of the occurrence of corona discharge directly from the antenna. In addition to reducing the airplane charge, for this purpose we must take all possible steps to, first of all, increase the corona threshold of the antennas and, second, reduce the corona threshold of the dischargers. Increase of the antenna corona threshold is achieved by increasing the antenna radius and eliminating any sort of sharp extremities at the edges of the antennas. Increase of the antenna radius leads to an increase of its aerodynamic resistance. Therefore, antennas are covered with an insulator, polyethylene for example, to prevent corona discharge. Naturally, when the antenna is enclosed by an insulator, the individual points of the covering become nonequipotential and may be charged to significant potentials relative to one another.

This circumstance leads to the occurrence of discharges along the antenna. However, the power of such charges is very low because of the negligible capacitances of the antenna segments, and they do not create any significant radio interference. We must bear in mind that breakdown of the protective covering at any point can lead to the occurrence at this point of a corona discharge which will create interference of the same magnitude as that on an unprotected antenna [8].

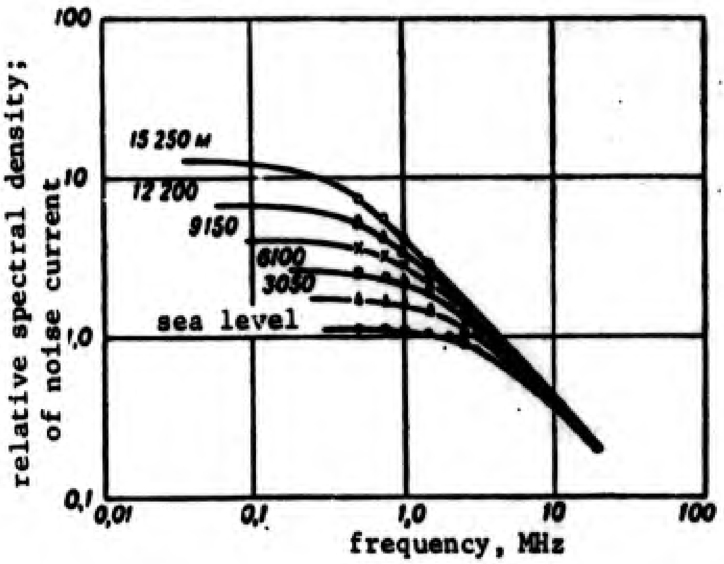

Figure 5.5. Normalized noise current spectrum for discharge current 100 μA from wing trailing edge of Boeing 367-80 [120].

2. To reduce the coupling between the corona discharge point and the antenna, it is desirable that the discharge be shifted to a point as far as possible from the antenna. For example, [8] presents results of measurements of the noise induced at a frequency of 900 KHz on a fuselage-mounted communication antenna when the corona discharge rod is located at the wingtip, at the tip of the vertical fin, and on the antenna strut; the noise voltage for these cases was 20, 200, and 500 mV. However, for higher frequencies,the coupling factor [see (5.19)] may not change monotonically with distance. Figure 5.6 [120] shows how the coupling factor $\varkappa(l)$ changes for frequencies of 4 and 14 MHz. Thus, measurements of the interference level from the different dischargers should be made for each type of antenna. As shown in [120], these measurements can be made with the aid of suitable ground test stands if the characteristic magnitudes of the currents charging the airplane and the corresponding electrical charges are known.

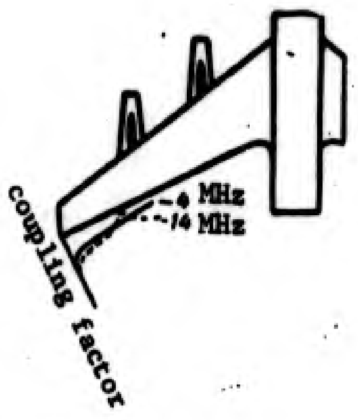

Figure 5.6. Variation of coupling factor with lower antenna near wing trailing edge on the KS-135 airplane [120].

It is possible to estimate, although very approximately, how the airplane dimensions affect the low-frequency interference level [120]. If two completely similar airplanes which differ only in dimensions [the linear dimensions of airplane No. 1 exceed those of airplane No. 2 by a factor of n (n > 1)] are flying under identical conditions, the currents charging them will be proportional to their projected frontal areas as long as the interference frequency does not exceed the quasi-static limit; the equivalent noise field intensities at corresponding points of the two airplanes are related as

$$\frac{E_2}{E_1} = n^{3/2}.$$

We have noted previously that this relation does not hold for the high frequencies. Thus, the static interference is stronger on smaller airplanes.

3. Simple corona-type dischargers are often used to reduce the noise in the region in which corona discharge occurs, although dischargers which emit charged particles, flame and radioactive dischargers make it possible to remove the airplane charge without the occurrence of any noticeable radio interference. In many cases, the use of corona dischargers also makes it possible to reduce markedly the interference level.

By selection of the discharger construction it is possible to obtain a minimal intensity of the high-frequency (HF) interference field at the point where the discharger is located, while the static field will be sufficiently large and will provide adequate steepness of the discharger coulomb-ampere curve [122].

Let us examine [121], for example, the field in a small region near the wing trailing edge (Figure 5.7a). The geometry of the HF coupling field [see (5.16)] or the static field is determined by the shape of the conductor with the charges creating the field. The technique for creating a region with small values of the HF coupling field is clear from Figure 5.7b, which shows the cross section of the aerodynamic surface. The trailing edge proper is electrically isolated from the remaining surface.

On the surface of the isolated trailing edge there appear two points at which the intensity of the HF coupling field equals zero, and a region with a weak HF coupling field develops around this edge. If the corona discharge were to take place from a point with zero HF coupling field, there would be no noise in the receiving system. However, for the occurrence of a corona discharge at a point with zero HF coupling field the DC potential of the isolated part must be maintained close to the potential of the entire airplane.

The combination of the requirement that the trailing edge be isolated with regard to HF and the requirement that it be connected with the airplane structure with regard to direct current can be achieved by connecting the trailing edge with the airplane through a very high ohmic resistance. If the magnitude of this resistance is large in comparison with the HF capacitive reactance between the isolated trailing edge and the remainder of the surface, then the HF field remains approximately as shown in Figure 5.7b, while the DC field in the immediate vicinity of the trailing edge will have a structure similar to that shown in Figure 5.7c. Since the direct current through the discharger is usually small and the airplane potential is high, the voltage drop across the resistance can be neglected.

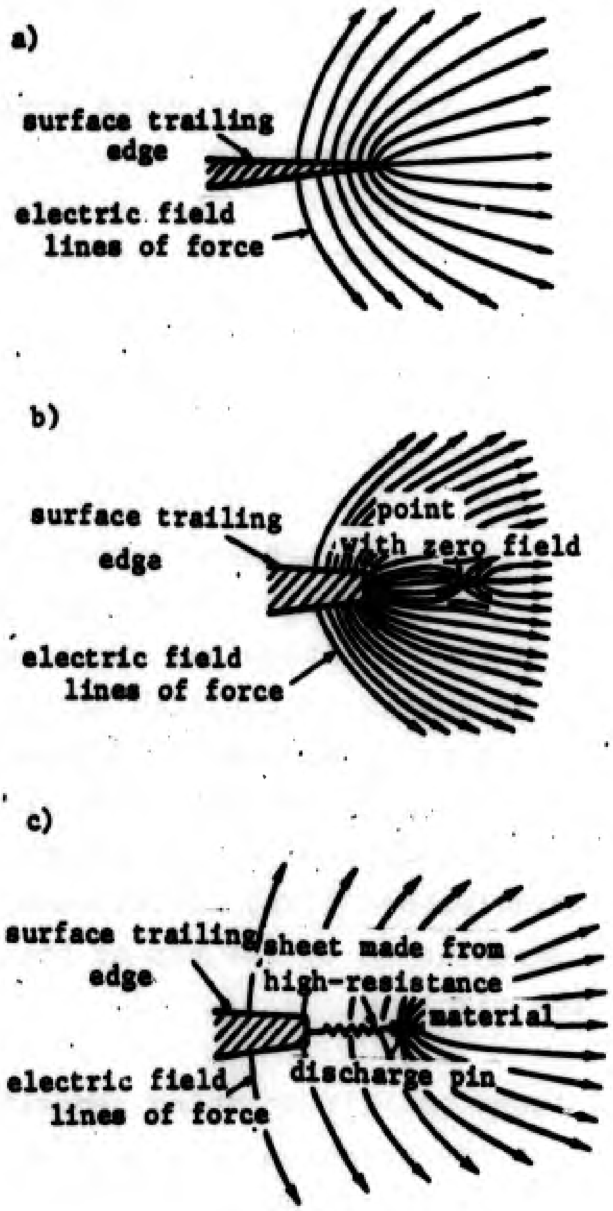

Figure 5.7. Geometry of electric DC and HF field at trailing edge of aerodynamic surface (a); geometry of HF coupling field near insulated trailing edge of aerodynamic surface (b); geometry of static field in the vicinity of flush decoupled discharger (c).

We see from comparison of Figures 5.7b and 5.7c that the region with the high DC field at the trailing edge coincides with the region of minimal intensity of the HF coupling field. Since the DC discharge takes place in the direction of the lines of force of the DC field, the discharge current flows at approximately right angles to the lines of force of the HF coupling field. Thus, interference from the discharge will be reduced both as a result of the orthogonality of the coupling field and the current and as a result of the reduction of the coupling field.

The interference reduction,when inserting the decoupling resistance,is connected with the fact that its insertion alters the nature of the discharge. In the absence of the resistance, a large fraction of the airplane charge can create a discharge current pulse, whose steepness and amplitude may be very large. The insertion of the decoupling resistance limits the amplitude and duration of the current pulse to the magnitude of the charge accumulated at the tip of the discharger. Therefore, in place of the powerful current pulses which are present without the decoupling resistance, when the latter is inserted there will be a large number of weak current pulses. In the first approximation the interference level is decreased by a factor of $\underline{C}_p/\underline{C}$, where $\underline{C}_p$ is the capacitance of the tip of the discharger and $\underline{C}$ is the capacitance of the airplane.

The decoupling resistance and its shunting capacitance act as a sort of filter to smooth out the pulsations created by the generator — the airplane discharging into the atmosphere. In combination with an increase of the taper of the trailing edges (which leads to a reduction of the amplitude of the current pulses [31]) the use of the decoupling resistance has made it possible to reduce the noise level by 35 dB [121].

It is obvious that an isolated discharger of the type shown in Figure 5.7 must of necessity be located at the wing trailing edge.

These arguments apply equally well to the rod-type dischargers discussed in Chapter 3. The dischargers of this type are termed decoupled passive dischargers. Application of an additional direct voltage in series with the resistance makes this discharger active (compare with Figure 5.2).

We recall that for a given discharge current the noise generated by sharp points having smaller radii is less than the noise generated by points having larger radii. The amplitude of the impulsive current in a corona discharge is proportional to the radius of the tip of the discharging point [31]. For example, laboratory tests have shown [121] that the noise generated by points with tip radii less than 0.013 mm is less by 6-11 dB than the noise level created by a total current of the same magnitude during discharges directly from the trailing edge of a typical aerodynamic surface.

In reality, just as in the considered case of the smoothing action of the decoupling resistance, for a given magnitude of the average current the mean square value of the noise current generated by a signal consisting of small pulses with high repetition frequency is less than the mean square value of the noise current from a signal which is a sequence of large pulses with low repetition frequency.

Thus, the use of decoupled dischargers having sufficiently small radii of the points can markedly (up to 60 dB [121]) reduce the noise level created by the corona discharge.

Let us examine various versions of the corona dischargers [121].

a) Wire dischargers. The first dischargers which appeared as soon as it became known that the primary source of static interference is the discharge from the receiving antenna itself were the dischargers fabricated from wire of small radius. Such devices, when located at points where the self-charge field is high, will provide for charge drain-off in the case of low airplane charges and will prevent corona discharge from the antenna. However, significant interference can occur when discharges develop from the trailing edges of the wings and tail. Needles or wires can be installed on the trailing edge of the aerodynamic surfaces to prevent these discharges. Data of laboratory measurements (Figure 5.8b) show that discharges from a bundle of needles mounted on the trailing edge reduce the noise level by 7 dB in comparison with the level created by the discharge from the same trailing edge without the needles.

When carefully selected needles with point radius no more than 0.013 mm were installed at the same place, the noise level was reduced by 11 dB. The same noise reduction was noted when using wire of diameter 0.025 mm (Figure 5.8c). Extension of the wire discharger in order to reduce the threshold corona potential causes at the same time an increase of the magnitude of the HF coupling field, which may even lead to an increase of the noise.

b) High-resistance rods and plates. Discharges from plates, rods, and braids made from insulating materials and coated with high-resistance films should create weak noise levels. We can assume that such high-resistance conductors are in themselves satisfactory dischargers. For a plate attached to the trailing edge of the airplane surface the noise component of the discharge current j_1 will be directed along the lines of force of the HF coupling field E_1.

Thus, it follows from (5.16) that the noise which occurs when using a high-resistance plate is reduced as a result of the fact that the plate is conductive for the radio frequencies, and the discharge takes place at some distance from the trailing edge of the surface in the region where the coupling field intensity E_1 is low (when the antenna is transmitting). In addition, the decoupling resistance of the plate reduces the noise component. The degree of reduction of the noise level can be estimated by taking into consideration the fact that the field intensity in the plane of the conductive plate follows the law

$$E(X)=\frac{A}{\sqrt{X}},$$

where X is the distance from the trailing edge of the surface in the direction toward the rear of the airplane; A is a constant characterizing the amplitude of the applied potential. Then, if E_1 is the HF coupling field intensity at the trailing edge of the surface, and

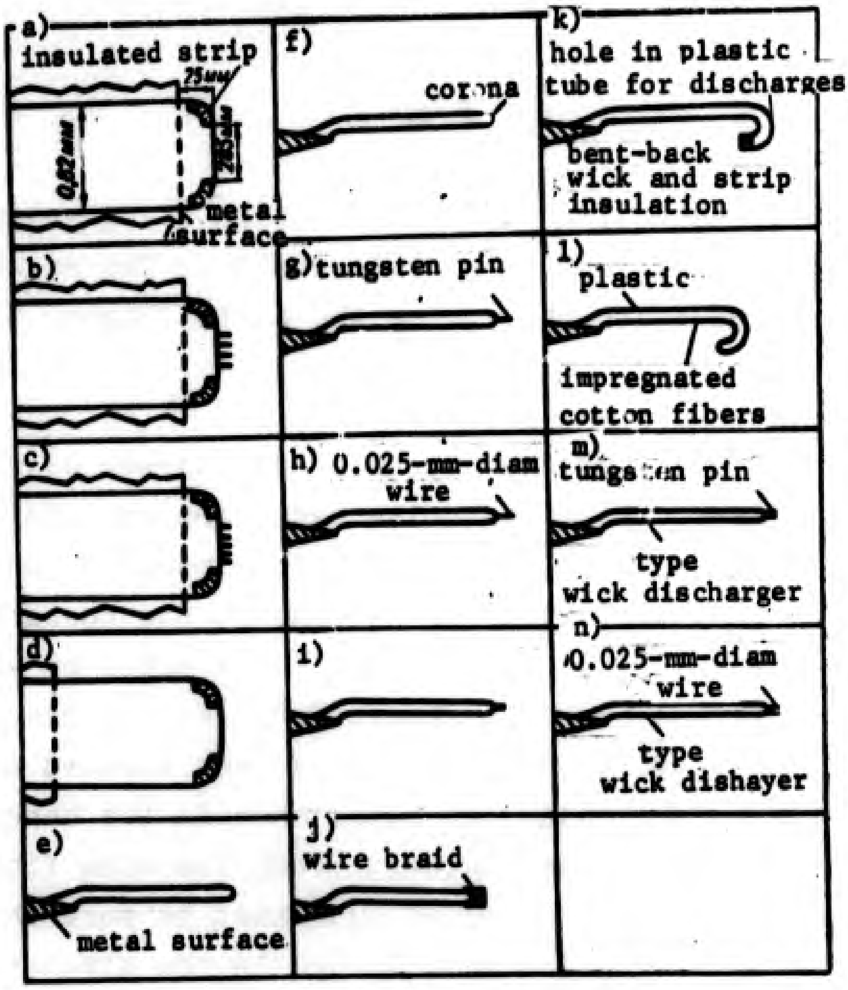

Figure 5.8. Results of noise level measurements for given value of direct current flowing through discharger.

Noise values are referred to the noise level for the same current flowing directly from the wing trailing edge [121]; a) flat aluminum edge 0.28 mm thick, relative noise level 0 dB; b) edge with needles, relative noise level -7 dB; c) edge with 0.025 mm diameter wire, relative noise level about -11 dB; d) plexiglass 0.125 mm thick, resistivity 0.3 MOhm/cm^2, rectangular edge, relative noise level -25 dB; e) decoupled discharger, relative noise level -51 dB; f) high-resisance rod, relative noise level from -29 to -30.5 dB; g) high-resisance rod with tungsten pin at end, relative noise level -27 dB; h) high-resistance rod with 0.025 mm diameter wire at end, relative noise level -27 dB; i) type AN/ASA/3 wick discharger, relative noise level -63 dB; j) high-resistance rod with wire braid at end relative noise level -22 dB; k) wick discharger doubled back, relative noise level from -12 to -21 dB; l) cotton rope discharger, relative noise level from -40 to -54 dB; m) type AN/ASA/3 wick discharger ending in tungsten poins, relative noise level -14 dB; n) type AN/ASA/3 wick discharger terminating with 0.025 mm diameter wire, relative noise level -25 dB.

AN/ASA/3

E_2 is the same at the trailing edge of the high-resistance plate,

$$\frac{E_2}{E_1}=\sqrt{\frac{X_1}{X_2}}.$$

To calculate the coupling field attenuation using this formula we must determine the value of X_1 experimentally. The measured value of the noise level reduction when using the plate (Figure 5.8d) was about -25 dB.

The points at the end of the decoupled discharger play a major role in reducing noise. While the noise reduction was -51 dB when using the points (Figure 5.8e), with the points removed the noise increased by 20 dB (Figure 5.8f). If we compare the operation of the wick discharger (Figure 5.8i), which reduces the noise by -63 dB, with the same wick modified as shown in Figure 5.8k (end of discharger wick and about 12.5 mm of the plastic tubing bent forward and wrapped with insulating tape; small diameter holes made in the bend of the plastic tubing to make possible discharge from the wick fibers in the tubing), in the latter case, the noise increased by more than 40 dB, i.e., when using only decoupling resistances in the dischargers the noise reduction is relatively small.

c) High-resistance rods with metallic discharging points. The wick dischargers (Figure 5.8i) work effectively only in the course of a limited time period. Their characteristics deteriorate rapidly in flight as the conductive coating of the individual fibers disintegrates or the conductive impregnant drys out. To reduce the effect of wick deterioration it was suggested that metallic discharging points be used at the end in place of the dielectric fibers coated with a conductive layer.

We see from comparison of Figures 5.8m and 5.8n with Figure 5.8i that the use of metallic discharging points leads to about a 35-40 dB deterioration of the wick characteristic. It follows from comparison of the data for Figures 5.8e with 5.8g and 5.8h that the installation of a discharging point at the end of the discharger rod leads to a reduction of the discharger effectiveness.

d) General remarks on the operation of corona dischargers. It follows from comparison of Figure 5.8i with Figures 5.8k, 5.8m and 5.8n that the main factor in noise reduction by the wick discharger is the small radius of the fibers, the high resistance and low capacitance of the individual fibers at the end of the discharger, which limit the amplitudes of the pulses. This conclusion is confirmed by comparison of the data of Figures 5.8l and 5.8k. The plastic tubing was removed from the wick discharger (Figure 5.8l) and it was bent back as shown in Figure 5.8k. In so doing, part of the conducting fibers protruded.

Initially, while these fibers were undamaged, the noise level in the scheme of Figure 5.8l was 30 dB lower than in the scheme of Figure 5.8k. Only after deterioration of these fibers did the characteristics of the discharger of Figure 5.8l become similar to those of the discharger of Figure 5.8k.

Thus, the wick dischargers reduce noise most effectively. Unfortunately, they do not stand up well in service. It appears that an acceptable solution would be the creation of wick dischargers having the required bulk strength.

4. The noise resulting from corona discharge can be suppressed by the use of special reception schemes.

Noise reduction is accomplished by choice of suitable antenna systems, selecting their location, and the receiver circuitry.

a) Effect of antenna characteristics on noise level at the receiver input. The noise field for a dipole antenna depends very little on its location along the fuselage, while the noise field of a loop antenna increases as the loop is moved from the nose toward the center section. Consequently, the signal/noise ratio will increase as the loop antenna is moved toward the airplane nose [121].

In selecting the antenna type we start from the fact that for a given value of the noise current the equivalent noise field of the dipole antenna is inversely proportional to the frequency. Therefore, although a given noise current may not affect the reception quality at high frequencies, it may lead to failure of the communications and navigation equipment operating at the lower frequencies. The noise field of the loop antenna is independent of the frequency. Therefore, shielded loop antennas are used more often than dipole antennas for reception of the low radio frequencies under static interference conditions. If the distribution of the magnitude of the noise current of the corona-type discharger along the fuselage has, for example, a triangular form, then the ratio of the equivalent noise field intensities E_{di} of the dipole and E_p of the loop antennas is given by the relation

$$\frac{E_{д}}{E_{р}}=\frac{\omega}{c_{св}}z,$$

where z is the antenna distance from the nose of the fuselage; ω is the reception frequency; and c_{lt} is the speed of light. The advantage of the loop antenna over the dipole increases with reduction of the frequency and as both antennas are moved toward the nose of the airplane [121].

A reduction of the interference in the case of the loop antenna can also be achieved by locating the loop so that the effect of the HF coupling field at the point where the discharger is located is reduced. As the plane of the loop is rotated through 90° from the direction in which the noise is maximal, the noise level decreases by about 25 dB.

To reduce the effect of static interference on the dipole antennas, they can be located so that the interference signals induced on two antennas connected to the receiver input will be subtracted while the useful signals will be combined. On two dipole antennas located, for example, on the fuselage centerline, one above and the other below the fuselage, the noise currents are equal in phase and approximately equal in magnitude. However, signals with vertical polarization will induce in the antennas currents which are equal in magnitude but shifted 180° in phase. By applying the signals from the antennas to a symmetric input transformer, we can compensate for the effect of the interference currents. In practice, this method has made it possible to obtain noise attenuation up to 25 dB [121].

It is obvious that a similar connection scheme is possible for noise suppression when using loop antennas.

b) Reduction of the effect of static interference with the aid of receiving devices. The effect of static interference on the operation of the receiver can be reduced by selection of the reception frequencies. Reception in the UHF band and particularly in the shorter waveband is free of interference in most cases (see Figure 5.5).

Another circuitry solution is the use in the receivers of a blocking device which is automatically activated on the appearance of strong interference pulses [121].

REFERENCES

1. Morgan, H.K. Rain Static. Proc. I.R.E., Vol. 24, 1936, pp. 959-963.

2. Gunn, R. Electric Field Intensity Inside a Natural Cloud. J. Appl Phys., Vol. 19, 1948, pp. 481-484.

3. Hucke, H.M. Precipitation-Static Interference on Aircraft and at Ground Stations. Proc. I.R.E., Vol. 27, 1939, pp. 301-316.

4. Gunn, R., W. Hall, and G. Kinzer. The Precipitation-Static Interference. Problems and Methods for its Investigation. Proc. I.R.E., Vol. 34, 1946, pp. 156-161.

5. Gunn, R. and J. Parker. The High-Voltage Characteristics of Aircraft in Flight. Proc. I.R.E., Vol. 34, 1946, pp. 241-247.

6. Stimmel, R., E. Rogers, F. Waterfall and R. Gunn. Electrification of Aircraft Flying in Precipitation Areas. Proc. I.R.E., Vol. 34, 1946, pp. 167-177.

7. Waddel, R., R. Drutowski and W. Blatt. Aircraft Instrumentation for Precipitation-Static Research. Proc. I.R.E., Vol. 34, 1946, pp. 161-166.

8. Kinzer, G.D. and J.W. McGee. Investigations of Methods for Reducing Precipitation-Static Radio Interference. Proc. I.R.E., Vol. 34, 1946, pp. 234-240.

9. Imyanitov, I.M. Metody issledovaniya elektrichestva atmosfery. Avtoreferat dissertatsii (Methods for Studying Atmospheric Electricity. Author's Summary of Dissertation). Main Geophysical Observatory (GGO), Leningrad, 1967.

10. Fitzgerald, D.R. Probable Aircraft "Triggering" of Lightning in Certain Thunderstorms. Monthly Weather Review, Vol. 95, No. 12, 1967, pp. 835-842.

11. Imyanitov, I.M. Pribory i metody dlya izucheniya elektrichestva atmosfery (Instruments and Methods for Studying Atmospheric Electricity). GTTI, Moscow, 1957.

12. Tikhodeyev, N.N. K teorii fizicheskogo modelirovaniya v elektronike (On the Theory of Physical Modeling in Electronics). Moscow, 1959.

13. Zachek, S.I. Issledovaniye polyarnoy elektroprovodnosti vozdukha v svobodnoy atmosfere s samoletov. Avtoreferat dissertatsii (Study of Polar Electrical Conductivity of Air in the Free Atmosphere Using Airplanes. Author's Summary of Dissertation) GGO, Leningrad, 1968.

14. Coroniti, S.C. et al. Effect of Aircraft Charge on Airborne Conductivity Measurements. J. Geophys. Res., Vol. 57, 1952, pp. 197-205.

15. Zachek, E.I. Theory of the Differential Dynamic Electrometer. Trudy GGO, No. 157, 1964, pp. 87-93.

15a. Zachek, S.I. On the Question of the Measurement of the Electrical Conductivity of Air in the Free Atmosphere From an Airplane. Trudy GGO, No. 157, 1964, pp. 94-120.

16. Moore, C.B., B. Vonnegut and F.J. Mallahan. Airborne Filters for the Measurements of Atmospheric Space Charge. J. Geophys. Res., Vol. 66, No. 10, 1961, pp. 3219-3226.

17. Krasnogorskaya, N.V. and A.A. Seredkin. On the Space Charge of the Lower Atmospheric Layers. Izvestiya AN SSSR, Ser. Geofiz, No. 4, 1964, pp. 587-595.

18. Pruppacher, H.R. The Effect of an External Electric Field on the Supercooling of Water Drops. J. Geophys. Res., Vol. 68, 1963, pp. 4463-4474.

19. Byers, H. and R. Braham. The Thunderstorm. Washington, D.C., U.S. Weather Bureau, 1949, pp. 47-50.

20a. Sal'man, Ye.M. and K.S. Zhupakhin. Some Results of Radar Studies of the Vertical Structure of Squalls and Thunderstorms. Trudy GGO, No. 159, 1964, pp. 59-64.

20b. Ignatova, R.V., V.A. Petrushevskiy and Ye.M. Sal'man. Radar Characteristics of Clouds. Trudy GGO, No. 173, 1965, pp. 26-33.

21. Aiya, S.V.C. Some Characteristics of Tropical Thunderstorms. Nature (Engl), Vol. 208, No. 5011, 1965, pp. 641-644.

22. Schonland, B.F.I. The Flight of Thunderbolts. Oxford, 1964.

23. Ferrary, G.A. Electrical Charges and Discharges on Aircraft in Flight. L'elettrotecnica, Vol. 47, No. 7, 1960, pp. 499-511

24. Loeb, L.B.A. Tentative Explanation of the Electric Field Effect on the Freezing of Supercooled Water Drops. J. Geophys. Res., Vol. 68, 1963, pp. 4475-4476.

25. Cobb, W.E. and F.J.A. Holitza. A Note on Lightning Strikes to Aircraft. Monthly Weather Review, Vol. 96, No. 11, 1968, pp. 807-808.

26. Imyanitov, I.M., B.F. Yevteyev and I.I. Kamaldina. Grozovoye oblako. Doklad na IV Mezhdunarodnoy konferentsii po elektrichestvu atmosfery (The Thundercloud, Report to 4th International Conference on Atmospheric Electricity). Tokyo, 1968

27. Imyanitov, I.M. and Ye.V. Chubarina. Elektrichestvo svobodnoy atmosfery (Electricity of the Free Atmosphere). Gidrometeoizdat, Leningrad, 1965.

28. Newman, M.M. Triggered Lightning Discharges and Application to V.L.F. Propagation Studies. a) Lightn. and Transients Res. Inst. Minneapolis, Minn., 1964, 23 pp. b) U.S. Govt Res. and Developm. Repts, Vol. 40, No. 15, 1965, pp. 12-13.

29. Creedon, J. The Last 1000 Feet. Aerospace Safety. Vol. 22, No. 3, 1966, pp. 6-7.

30. Trichel, G.W. The Mechanism of the Negative-Point-to-Plane Corona Near Onset. Phys. Rev., Vol. 54, 1938, pp. 1078-1084.

31. Loeb, L.B. Basic Processes of Gaseous Electronics. Translated from English. GTTI, Moscow-Leningrad, 1950.

32. Stuetzer, O.M. Apparent Viscosity of a Charged Fluid. The Physics of Fluids., Vol. 4, No. 10, 1961, pp. 1226-1231.

33. Imyanitov, I.M. Author Patent No. 440042-IV dated December 16, 1950.

34. Smythe, W.R. Static and Dynamic Electricity. Translated from English, 1954.

35. Findeisen, W. Orientation Regarding Electric Potential Differences and Potential Drops on Aircraft Passing Through Clouds. Reich A, Berlin, No. 25, 1944.

36. Wigand, A. Electric Investigations of Aircraft Ascent in Air.
a) Physik. Zschr., Vol. 25, No. 24, 1924, pp. 684-685.
b) Fortschr. d. Chemie Physik u. Physik Chemie, ser. B, Vol. 18, No. 5, 1924, pp. 1-52.

37. Vonnegut, B. and C.B. Moore. Apparatus Using Radioactive Probes for Measuring the Vertical Component of Atmospheric Potential Gradient from an Airplane. Bull. Amer. Meteorol. Soc., Vol. 42, No. 11, 1961, pp. 773-777.

38. Imyanitov, I.M. and V.P. Kolokolov. Study of the Distribution of the Induced and Autogeneous Electric Charge on the Surface of an Airplane. Trudy GGO, No. 58, 1956, pp. 8-16.

39. Clark, J.F. The Fair-Weather Atmospheric Electric Potential and Its Gradient. Recent Advances in Atmospheric Electricity. Ed. I.G. Smith, Pergamon Press, 1958, pp. 61-73.

40. Tverskoy, P.N. Atmosfernoye elektrichestvo (Atmospheric Electricity). Gidrometeoizdat, Leningrad, 1949.

41. Israël, H. Atmosphärische Elektrizität (Atmospheric Electricity). Leipzig, 1957, I.

41a. Israel, H. Atmosphärische Elektrizität (Atmospheric Electricity). Leipzig, 1961, II.

42. Katsyka, A.P. et al. Electric Charges of Cloud and Fog Droplets. Izvestiya AN SSSR, Ser. Geofiz, No. 1, 1961, pp. 162-165.

43. Allee, P.A. and B.B. Phillips. Measurements of Cloud Droplet Charge, Electric Field, and Polar Conductivities in Supercooled Clouds. J. Met., Vol. 16, No. 4, 1959, pp. 405-510.

44. Phillips, B.B. and G.D. Kinzer. Measurements of the Size and Electrification of Droplets in Cumuliform Clouds. J. Met., Vol. 15, No. 4, 1958, pp. 369-374.

45. Twomey, S. The Electrification of Individual Cloud Droplets. Tellus, Vol. 8, No. 4, 1956, pp. 445-452.

46. Krasnogorskaya, N.V. Electricity of Warm Clouds. DAN SSSR, Vol. 181, No. 5, 1968, pp. 1111-1114.

47. Krasnogorskaya, N.V. Variation of Electrical Conductivity of Air Under Various Weather Conditions. Izvestiya AN SSSR, Ser. Geofiz., No. 4, 1958, pp. 527-535.

48. Zachek, S.I. Instrument for Measuring Electrical Conductivity of Air in the Free Atmosphere. Meteorol i Gidrol., No. 9, 1965, pp. 51-55.

49. Imyanitov, I.M. Electrical Structure of Cu Cong. and Its Connection With Air Movement in Clouds. In: Issledovaniye oblakov, osadkov i grozovogo elektrichestva (Study of Clouds, Precipitation, and Thunderstorm Electricity). IZd. AN SSSR, Moscow, 1961, pp. 225-238.

50. Imyanitov, I.M. Electric Fields in the Free Atmosphere. Trudy GGO, No. 35, 1952, pp. 3-11.

51. Imyanitov, I.M. and K.S. Shifrin. Present Status of the Study of Atmospheric Electricity. Uspekhi Fiz. Nauk, Vol. 76, No. 4, 1962, pp. 593-642.

52. Simpson, G.C. and G.D. Robinson. The Distribution of Electricity in Thunderclouds. II. Proc. Roy. Soc. A, Vol. 177, 1940, pp. 281-329.

53. Fedorov, E.K. Electric Charges of Precipitation Particles. DAN SSSR, Vol. 78, No. 6, 1951, pp. 1131-1134.

54. Anikiyev, I.S. Electric Charges of Raindrops and Snowflakes. Meteorol. i Gidrol, No. 4, 1951, pp. 37-39.

55. Gunn, R. Electric Field Intensity Inside a Natural Cloud. J. Appl Phys., Vol. 19, 1948, pp. 481-484.

56. Gunn, R. and C. Devin. Raindrop Charge and Electric Field in Active Thunderstorm. J. Met., Vol. 10, 1953, pp. 279-284.

57. Imyanitov, I.M. and V.V. Mikhaylovskaya. Experience in Studying the Charges of Precipitation Particles in the Free Atmosphere. Trudy GGO, No. 97, 1960, pp. 16-33.

58. Imyanitov, I.M. On the Problem of Electrification and Conductivity of Thunderclouds. DAN SSSR, Vol. 109, No. 1, 1956, pp. 77-83.

59. Fitzgerald, D.R. and H.R. Byers. Aircraft Observations of Convective Cloud Electrification. Recent Advances in Atmospheric Electricity. Pergamon Press, 1958, pp. 245-268.

60. Petrov, G.D. On the Distribution of Droplet Charges in Cumulus Clouds. Izv. AN SSSR, Ser. Geofiz, No. 7, 1961, pp. 1085-1087.

61. Vul'fson, N.I., A.G. Laktionov and B.I. Tulupov. Some Peculiarities of the Structure of Cumulus Clouds. Izvestiya AN SSSR, Fiz. Atm. i Okeana, Vol. 4, No. 8, 1968, pp. 844-849.

62. Kamaldina, I.I. On the Measurement of the Electric Structure of Cb Clouds During Their Development. Trudy GGO, No. 225, 1968, pp. 85-91.

63. Gish, O.H. and G.C. Wait. Thunderstorms and Earth's General Electrification. J. Geophys, Res., Vol. 55, 1950, pp. 473-484.

64. Malan, D.I. Discharges in the Air and the Low Positive Charge of Thunderclouds. Ann. Geophys, Vol. 8, 1952, pp. 385-401.

65. Imyanitov, I.M. and T.V. Lobodin. On Zones of Heterogeneity in Thunderclouds. Trudy GGO, No. 157, 1964, pp. 3-8.

66. Stergis, C.G., G.C. Rein and T. Kangas. Electric Field Measurements Above Thunderstorms. J. Atmosph. Terr. Phys., Vol. 11 (2), 1957, pp. 83-90.

67. Imyanitov, I.M. et al. Electric Currents Above Thunderclouds. Trudy GGO, No. 204, 1967, pp. 3-17.

68. Imyanitov, I.M. and Ye.V. Chubarina. Charging of the Li-2 Airplane in Stratiform Clouds. Trudy GGO, No. 225, 1968, pp. 117-127.

69. Imyanitov, I.M. et al. Study of Aircraft Static Electrification. Trudy GGO, No. 225, 1968, pp. 106-116.

70. Fizika oblakov (Cloud Physics). Edited by A.Kh. Khrgian. Gidrometeoizdat, Leningrad, 1961.

71. Trunov, O.K. Obledeneniye samoletov i sredstva bor'by s nim (Aircraft Icing and Means for Combatting It). Mashinostroyeniye, Moscow, 1965.

72. Vul'fson, N.I. Convective Movement in Cumulus Clouds. DAN SSR, Vol. 97, No. 1, 1954, pp. 77-80.

73. Edwards, R.C. and G.W. Brock. Meteorological Aspects of Precipitation Static. J. Met., Vol. 2, No. 4, 1945, pp. 205-213.

74. Schaefer, V.J. Properties of Particles of Snow and the Electrical Effects They Produce in Storms. Transact. Amer. Geophys. Union, Vol. 28, No. 4, 1947, pp. 587-614.

75. MacCready, P.B., (Jr.) and A. Proudfit. Observations of Hydrometeor Charge Evolution in Thunderstorms. Quar. J. Roy. Meteorol. Soc., Vol. 91, No. 387, 1965, pp. 44-53.

76. Keily, D.P. and S.G. Millen. An Airborne Cloud-Drop-Size Distribution Meter. J. Met., Vol. 17, No. 3, 1960, pp. 349-356.

77. Macky, W.A. Some Investigations on the Deformation and Breaking of Water Drops in Strong Electric Fields. Proc. Roy. Soc. A, Vol. 133, 1931, pp. 565-587.

78. Chow Shin-Ji and Chin Jen-chung. A Theoretical Analysis of the Critical Electric Field Strength for the Breaking-up of a Charged Drop. Scientia sinica, Vol. 15, No. 3, 1966, pp. 394-402.

79. Gashina, S.B. et al. Correlation Between Radar Characteristics of Clouds and Their Turbulent and Electric State. Trudy GGO, No. 173, 1965, pp. 58-62.

80. Imyanitov, I.M. and G.T. Kryukova. Technique for Measuring the Size and Number of Cloud Precipitation Particles From Data of a Given Interval of Their Spectral Distribution, and Also the Water Content of Clouds and Precipitation. Author's Certificate No. 115699, Bulletin of Inventions, No. 10, 90, 1958.

81. Imyanitov, I.M., V.V. Mikhaylovskaya and B.F. Yevteyev. Instruments for Measuring Water Droplet Size For Use on Aircraft and Radiosondes. Trudy VNMS, Vol. 9, Gidrometeoizdat, Vol. 9, Leningrad, 1963, pp. 269-277.

82. Gunn, R. Precipitation Electricity. B. Compendium of Meteorology, Boston, Mass, 1951, pp. 128-135.

83. Bennet, W.H. Snow Static on Aircraft. Electrical Engineering, Vol. 67, No. 10, 1948, pp. 947-953.

84. Hendrick, R.W. and S. Chapman. Corona Discharge Current Measurements From an Isolated Point in Wind. Bull. Amer. Meteorol. Soc., Vol. 36, No. 10, 1955, p. 544.

85. Kirkman, I.R. and I.A. Chalmers. Point Discharge From an Isolated Point. J. Atmos. Phys., Vol. 10, 1957, pp. 258-265.

86. Tamm, F. Influence of Air Pressure and Humidity on the Discharge of Static Electricity From Points. Ann. Phys., Lpz., Vol. 6, 1901, pp. 259-279.

87. Jhawar, D.S. and J.A. Chalmers. Point Discharge From Multiple Point. J. Atmos. Terr. Phys., Vol. 27, No. 3, 1965, pp. 367-371.

88. Vonnegut, B., C.B. Moore and V.J. Mallahan. Adjustable Potential-Gradient Measuring Apparatus for Airplane Use. J. Geophys. Res., Vol. 66, No. 8, 1961, pp. 2393-2397.

89. Gunn, R. The Electrical Charge on Precipitation at Various Altitudes and Its Relation to Thunderstorms. Phys. Rev., Vol. 71, 1947, pp. 181-186

90. Gunn, R. Free Electrical Charge on Precipitation Inside an Active Thunderstorm. J. Geophys. Res., Vol. 55, 1950, pp. 171-178.

91. Krasnogorskaya, N.V. Results of Measurement of Precipitation Particle Charges in the Free Atmosphere. Izv. AN SSSR, Ser. Geofiz, No. 7, 1956, pp. 844-852.

92. Frenkel', Ya.I. Teoriya yavleniy atmosfernogo elektrichestva (Theory of Atmospheric Electricity Phenomena). GTTI, Leningrad-Moscow, 1949.

93. Imyanitov, I.M. and V.V. Mikhaylovskaya. Airborne Instrument for Measuring Precipitation Particle Charges. Pribory i Tekhn. Eksperim, Vol. 2, 1958, pp. 86-91.

94. Krasnogorskaya, N.V. Study of Cloud and Precipitation Electricity. Author's Summary of Dissertation. GGO, Leningrad, 1968.

95. Chapman, S. Thundercloud Electrification in Relation to Rain and Snow Particles. Thunderstorm Electricity, Chicago, Press, 1953, pp. 207-230.

96. Loeb, L.B. Static Electrification. Translated from English. Gosenergoizdat, Moscow-Leningrad, 1963.

97. Coehn, A. A Law of Motion for Electricity. Annual. d. Phys. u. Chem., Vol. 64, No. 1, Leipzig, 1898, pp. 217-232.

98. Imyanitov, I.M., M.M. Kulik, and A.P. Chuvayev. Experience in Studying Thunderstorm Zones in the Southern Regions of the European Territory of the USSR and in Transcaucasia. Trudy GGO, No. 67, 1957, pp. 3-32.

99. Imyanitov, I.M. On the Problem of the Electrostatic Charging Mechanism. DAN SSSR, Vol. 121, No. 1, 1958, pp. 93-96.

100. Fomenko, V.S. Emissionnyye svoystva elementov i khimicheskikh soyedineniy (Emission Properties of the Elements and Chemical Compounds). Naukova dumka, Kiyev, 1964.

101. Imyanitov, I.M. and A.T. Starovoytov. Some Questions of Electrostatic Charging Theory. ZhTF, Vol. 32, No.6, 1962, pp. 759-765.

102. Muchnik, V.M. Ionization During Droplet Breakup in an Electric Field. ZhETF, Vol. 26, No. 1, 1954, pp. 109-114.

103. Kachurin, L.G. and V.I. Bekryayev. Study of the Crystallizing Water Electrification Process. DAN SSSR, No. 1, 1960, pp. 57-60.

104. Workman, E.J. and S.E. Reynolds. Electrical Phenomena Occurring During the Freezing of Dilute Aqueous Solutions and Their Possible Relationship to Thunderstorm Electricity. Phys. Rev., Vol. 78, 1950, pp. 254-259.

105. Bredov, M.M. and I.Z. Kshemyanskaya. Electrification Detected After the Contact of Two Bodies. ZhTF, Vol. 27, No. 5, 1957, pp. 921-928.

106. Harper, W.R. The Generation of Static Charge. Advances in Physics. Quart. Suppl. Phil. Mag., Vol. 6, No. 24, 1957, pp. 365-417.

107. Fuks, N.A. Mechanics of Aerosols. Izd. AN SSSR, Moscow, 1961.

108. Levin, L.M. Issledovaniya po fizike grubodispersnykh aerozoley (Studies on the Physics of Coarsely Dispersed Aerosols). Izd. AN SSSR, Moscow, 1961.

109. Russel, A. The Coefficients of Capacity and the Mutual Attractions or Repulsions of Two Electrified Spherical Conductors When Close Together. Proc. Roy. Soc. (A), Vol. 82, 1909, pp. 524-531.

110. Grinberg, G.A. Izbrannyye voprosy matematicheskoy teorii elektricheskikh i magnitnykh yavleniy (Selected Questions of the Mathematical Theory of Electric and Magnetic Phenomena). Izd. AN SSSR, Moscow-Leningrad, 1948, pp. 120, 436.

111. Mikhaylovskaya, V.V. On the Design of Instruments for Measuring Particle Charges Inductively. Trudy GGO, No. 204, 1967, pp. 39-43.

112. Arabadzhi, V.I. On the Contact Potential Difference Between Water and Ice. DAN SSR, Vol. 60, No. 5, 1948, pp. 811-812.

113. Dinger, J. and R. Gunn. Electrical Effects Associated With a Change of State of Water. Terr. Magn. Atmos. Electr., Vol. 51, 1946, pp. 477-494.

114. Kampe, H.I. and H.K. Weickman. Trabert's Formula and the Determination of the Water Content in Clouds. J. Met., Vol. 9, No. 3, 1952, pp. 167-171.

115. Jaw Jeou-Jang. Statistical Theory of Precipitation Process. Tellus, Vol. 18, 1966, pp. 722-729.

116. Izmaylov, N.A. Elektrokhimiya rastvorov (Electrochemistry of Solutions). Kharkov University Press, 1959.

117. Saha, M.N. a) Ionization in the Solar Chromosphere. Philos. Mag. and J. Scien., Vol. 40, No. 238, 1920, pp. 472-488.
b) Elements in the Sun. Philosoph. Mag. and J. Scien. Vol. 40, No. 240, 1920, pp. 809-824

118. Granovskiy, V.L. Elektricheskiy tok v gaze (Electrical Current in a Gas). Gostekhizdat, Moscow-Leningrad, 1952, 1.

119. Krohn, V.E. Liquid Metal Droplets for Heavy Particle Propulsion. Ed. Langmuir D. Electrostatic Propulsion, Vol. 8, New York — London, Academic Press, 1961, pp. 73-80.

120. Tanner, R.L. and I.E. Nanevicz. Analysis of Corona-Generated Interference in Aircraft. Proc. IEEE, Vol. 52, No. 1, 1964, pp. 44-52.

121. Nanevicz, I.E. and R.L. Tanner. Some Techniques for the Elimination of Corona Discharge Noise in Aircraft Antennas. Proc. IEEE, Vol. 52, No. 1, 1964, pp. 53-64.

122. Tanner, R.L. A New Aircraft Static Discharger. Proc. IRE, Vol. 8, 1957, pp. 31-36.

123. Robinson, M. Movement of Air in the Electric Wind of the Corona Discharge. Communication and Electronics, No. 51, 1961.

SYMBOL LIST

Russian	English	Typed
зар	charge	ch
ф	fuselage	f
к	wing	K
з	charging	ch
с	signal	c
п	noise static	n
пр	threshold	th
М	lightning	M
Т	theoretical	T
ф	actual	act
эфф	effective	ef
а	atmosphere	a
кр	critical	cr
ср	average	av
макс	maximal	max
э	electric	e
в	helicopter	B
з	earth	e
ст	jet	CT
ст	glass	g
д	dural	D
з	gold	G
ист	true	tr
н	nickel plated	H
х	chromium	Cr
п	brass	Br
л	front	fr
ост	remaining	rem

Russian	English	Typed
с	airplane	apn
в	vertical	B
э	experimental	ex
щ	standard	st
р	discharger	p
к	collector	K
м	frontal	M
изм	measured	meas
к	contact	K
т	body	T
с	free	c
ш	sphere	sph
к	capacitor	K
с	system	c
рэк	recommended	rec
в	water	w
л	ice	i
равн	uniform	
д	diffusion	d
к	drop	K
п	total	t
ш	noise	n
д	dipole	di
р	loop	p
св	light	lt